INFORMATION TO USERS

This manuscript has been reproduced from the microfilm master. UMI films the text directly from the original or copy submitted. Thus, some thesis and dissertation copies are in typewriter face, while others may be from any type of computer printer.

The quality of this reproduction is dependent upon the quality of the copy submitted. Broken or indistinct print, colored or poor quality illustrations and photographs, print bleedthrough, substandard margins, and improper alignment can adversely affect reproduction.

In the unlikely event that the author did not send UMI a complete manuscript and there are missing pages, these will be noted. Also, if unauthorized copyright material had to be removed, a note will indicate the deletion.

Oversize materials (e.g., maps, drawings, charts) are reproduced by sectioning the original, beginning at the upper left-hand corner and continuing from left to right in equal sections with small overlaps.

ProQuest Information and Learning
300 North Zeeb Road, Ann Arbor, MI 48106-1346 USA
800-521-0600

ELECTROCHEMISTRY AND STOICHIOMETRY OF THIN FILM OXIDES ON NICKEL

by

Md. Abdus Sattar

A Thesis submitted in partial fulfillment

of the requirements for the degree of

Doctor of Philosophy

in the

Department of Chemistry
University of Ottawa,
Ottawa, Canada

July, 1968

B.E. Conway
Professor of Chemistry
Research Supervisor

Md. Abdus Sattar
Ph.D. Candidate

To my wife Ayesha Sattar for her patience and sacrifice to see this work completed.

PREFACE

The first alkaline storage battery based on the use of the higher oxides of nickel as the cathode material and cadmium as the anode material was made by W. Jungner in Sweden during the last decade of the 19th Century (U.S. Patent in 1899). About the same time Thomas A. Edison also invented, independently, the nickel-iron alkaline battery (1900). This invention initiated work on this electrode material and resulted in the subsequent publication of several hundred papers of fundamental and technological importance. In spite of the body of previously published work there are, however, a number of important matters which are still unsettled. It is known that hydrated $Ni(OH)_2$ is the electrochemically active material; in the "charged" state, this material is oxidised to higher oxides of nickel. Controversy exists, however, concerning the mechanism of oxidation and the state of oxidation of nickel in the charged material. Thus, it is not at all clear whether in the "charged" state the higher oxides exist in solid solution or in distinct mixed phases.

Although extensive work has been carried out on the mechanism of oxygen evolution on oxide surfaces using bulk or thick film nickel oxide as the electrode, little agreement has hitherto been reached with regard to the processes involved. Thin film nickel oxide electrode surfaces have

been used in only a few of these experiments.

The aims of the present work (see Chapter I, section 6) have therefore been to investigate some of the aspects of the behaviour of thin film nickel oxide electrodes and to compare the properties of this electrode with those of the silver oxide electrode.

In Chapter I, a number of matters involved in the present work have been reviewed in order to provide the necessary background to the problem and with respect to the discussion of the results obtained. This review material will also serve to place the original work in this thesis in perspective and demonstrate its connection with the earlier work carried out in this laboratory. In Chapter II, are presented the experimental techniques, and in Chapter III, the results. A detailed discussion of the present original results with regard to (a) the mechanism and kinetics of oxygen evolution on nickel oxides, (b) the associated self-passivation behaviour, (c) the stoichiometry of anodically formed nickel oxide in thin films and (d) hysteresis effects is given in Chapter IV.

The work presented in this thesis is in course of publication as indicated below:

(1) Charge, Discharge and Self-discharge Characteristics of Thin Film Nickel Oxide Electrodes - Proceedings

of the meeting of the Advisory Group of Aerospace Research Development, N.A.T.O., Liège, Belgium, June, 1967, (published June, 1968).

(2) Electrochemistry of The Nickel Oxide Electrode: Part V: Self-passivation Effects in Oxygen Evolution Kinetics - Electrochim. Acta, (accepted for publication).

(3) Electrochemistry of The Nickel Oxide Electrode: Part VI: Surface Oxidation of Nickel Anodes in Alkaline Solution - Electrochim. Acta, (accepted for publication).

(4) Electrochemistry of The Nickel Oxide Electrode: Part VII: Potentiostatic Step Method for Study of Adsorbed Intermediates - Electrochim. Acta, (accepted for publication).

(5) Electrochemistry of The Nickel Oxide Electrode: Part VIII: Stoichiometry of Thin Film Oxide Layers - J. Electroanal. Chem. (accepted for publication).

For convenience, chemical and mathematical equations in each section have been given numbers independent of those in other sections. However, figure numbers and table numbers are given in a serial order.

ACKNOWLEDGMENTS

The author wishes to express his sincere thanks to Professor B.E. Conway for his stimulating guidance, kind patience and enlightening discussions at every stage of the work. Professor Conway was always prepared to give freely of his time and advice whenever problems and difficulties arose. The author is also very grateful to Professor Conway for his help in the preparation of this thesis.

The author acknowledges discussions on scientific and other matters with Drs. D. Gilroy, J. Wojtowicz and H. Angerstein-Kozlowska. The author also wishes to thank Dr. Wojtowicz for use of the time-delay-relay (Figure 16) and Dr. Kozlowska for the original Figure 35, and for translating some scientific papers from Russian to English.

The author is thankful to the Canadian Commonwealth Scholarship and Fellowship Committee for the award of a scholarship from September, 1963 to August, 1967 and the Department of Chemistry, University of Ottawa for a studentship since September, 1967. The author also acknowledges the study-leave (with salary) from the Rajshahi University, Rajshahi, East Pakistan since September, 1963.

Grateful acknowledgment is made to the Defence Research Board, Department of National Defence, Canada for financial support to the author during part of the period of his studies.

TABLE OF CONTENTS

CHAPTER III

RESULTS

Page No.

LIST OF FIGURES

Page No.

Page No.

Page No.

Page No.

Page No.

Page No.

LIST OF TABLES

Page No.

ABSTRACT

The initial stages of electrochemical oxidation of nickel surfaces have been investigated with respect to (a) anodic formation and reduction characteristics of the thin oxide films; (b) chemical characterization of the films, e.g. determination of the active oxygen to nickel content and stoichiometry; (c) relation of the chemical and electrochemical properties of the oxide films to the kinetics of anodic oxygen evolution on the oxides; (d) investigation of the origin and significance of irreversibility in the processes of formation and reduction of the oxide films (hysteresis effects). Complementary comparative work has also been carried out on silver oxide electrodes where surface oxide films in at least two easily distinguishable valence states are involved, and at low temperatures the formation of a third oxide Ag_2O_3 is indicated.

Since electrochemical behaviour of an electrode depends significantly on the pre-history of the electrode and the nature of the surface oxide, much attention has been given to the preparation of electrodes in comparable states. This matter was found to be of particular importance in the studies on oxygen evolution kinetics at the oxidized nickel surfaces. The kinetic observations provided evidence in support of the ion-radical type of recombination step as rate-determining in oxygen evolution kinetics. This is in

agreement with the conclusions derived from studies on the behaviour of bulk oxide material studied previously in this laboratory.

The potentiostatic studies on the oxygen evolution reaction at nickel, oxidised nickel surfaces and at silver revealed inhibition effects (self-passivation) analogous to those found in anodic organic oxidations at the noble metals. Here, however, the inhibiting species, surface oxides, are directly involved in the overall reaction itself. A kinetic theory of the "self-passivation" effects is presented in general terms for various supposed oxidation states of the surface region of the electrode interphase.

In order to relate the nature of the surface oxides on nickel metal surfaces to the kinetics of oxygen evolution, various transient methods viz. potentiostatic step charging, potentiodynamic linear sweep and galvanostatic discharge methods have been applied. It is shown that higher nickel oxides are reduced in cathodic galvanostatic pulses only to $Ni(OH)_2$ and hydrogen commences to evolve on this latter oxide. A potentiostatic step (anodic) charging method was therefore developed for characterisation of the formation of the surface oxide at nickel in a progressive manner over small intervals of potential. A theoretical treatment for interpretation of results obtained by the step-

charging method has been developed.

The kinetics of growth of nickel oxides were investigated and it has been observed that the growth kinetics obey a simple logarithmic law. A theoretical formulation of a growth law logarithmic in time has been developed.

For the purpose of determining the stoichiometries of the surface oxides formed in the thin film at the metal surface, combined chemical and electrochemical methods were used. For determining micro-quantities of nickel in the thin film oxide layers, a new spectrophotometric method based on the principle of reductive stripping by aq. hydrazine has been developed. Stoichiometries of thin film layers (after allowance for self-discharge effects) are reported as a function of the formation potential.

The apparent extent of oxide reduction charge in the thin films, determined electrochemically by a fast galvanostatic reduction pulse, and the amount of nickel in the film determined chemically, pass through a maximum at ca. 0.9 V. This is shown to be connected with a change of the oxide layer to a more passive condition. This behaviour is closely connected with the self-passivation effect observed in the kinetics of the anodic oxygen evolution reaction at nickel oxide surfaces.

Hysteresis between the charge and discharge processes has been observed both at nickel and silver (similar effects also occur at more noble metals such as platinum, palladium, etc.). This phenomenon has been studied in some detail using potentiodynamic sweep and galvanostatic discharge techniques. It is proposed that hysteresis is an intrinsic thermodynamic effect and is possibly related to the change of state of the system arising from an irreversible rearrangement of the surface oxide during or after its formation.

CHAPTER I

INTRODUCTION

1. GENERAL REMARKS

The study of the nickel oxide electrode in alkaline solutions is of interest in regard to the fact that it is a convenient model material for consideration of some general characteristics of electrode processes occurring on oxide electrodes. Thus, it is believed that for anodic oxygen evolution on oxide electrodes, oxygen is generated on surface oxides (1) in which the metal may exist in various oxidation states depending on the anode potential (V). Some of these oxides, e.g. those of nickel, silver, etc. are semiconductors and hence the behaviour of such semiconducting materials when used as an electrode under the influence of an electric field will be of general importance in anodization phenomena.

Electrochemical investigations on the behaviour of the nickel oxide electrode are perhaps more generally of interest because bulk nickel oxide is used as the electrochemically active cathode material in nickel-cadmium and nickel-iron batteries which have gained wide applications in electrochemical technology.

A battery is an electrochemical energy converter where the chemical (free) energy of the reaction occurring in the system is converted directly into electrical energy

without going through intermediate steps of thermal and mechanical conversion; the well-known Carnot limitation is thus avoided. In electrochemical reactions (2), the theoretical efficiency of the energy conversion can be 100 per cent but kinetic limitations in one or more of the steps of the overall reaction (2) usually make the process less than ideally reversible for appreciable rates of energy conversion, so that the efficiency is less than the ideal figure.

From the point of view of the present work, the mechanism of charging, discharging and overcharging of these oxide electrodes is of greatest interest and presents features of fundamental theoretical importance with regard to solid state reactions and the nature of passivity.

Since the previous presentation of review material on nickel oxide electrodes (given in another thesis (1961) from this Department (3)) much new work has been done on the chemistry and electrochemistry of nickel oxides. Accordingly it will be necessary to examine this background material in some detail in order to put the original work in this thesis in perspective and to show its connection with the earlier work carried out in this laboratory.

2. THE NICKEL OXIDE ELECTRODE

(a) Nature of the Nickel Oxide Electrode

Although the nickel oxide electrode has been employed as the cathode material in nickel-cadmium and nickel-iron alkaline batteries since their invention by Jungner (1899) and Edison (1900), much remains uncertain about both the chemistry and the electrochemistry of the system. A number of different types of nickel oxide electrode have been used both in fundamental studies and in technological applications. This may perhaps account partly for the observed variations in the performance of various types of electrode because the behaviour of the electrode depends on its pre-history and physical construction; these factors then determine the current distribution and uniformity of electrolyte concentration within the electrode.

In previous fundamental studies in this laboratory, (3-7) porous sintered pure nickel plaques were employed (similar to those utilized in the nickel-cadmium battery) and were impregnated under vacuum with a saturated solution of cobalt-free nickel nitrate. Nickel hydroxide, $Ni(OH)_2$, was then precipitated in the sinter by immersion in 25% aqueous potassium hydroxide at 70°C for 10 minutes. The electrodes were then treated cathodically as described previously by Fleischer (8) for 30 minutes.

Other workers (e.g., 9-17, 19-21) used similarly prepared bulk nickel hydroxide electrodes for various types of physical and electrochemical studies in alkaline medium.

Thick films of nickel hydroxide can be prepared (i) by chemical attack of alkaline hypochlorite on nickel wire, foil or on electrochemically deposited nickel on platinum wire or (ii) by electrochemical precipitation of nickelous hydroxide by cathodic electrolysis at the surface of nickel or another inert basis metal (e.g. platinum) (22,23 cf. also ref. 18). Both the evolution of hydrogen (22,23) and the reduction of nitrate (24) have been used in this process; the former procedure usually involves periodic cathodic and anodic treatments and this usually results in films that are formed in at least a partly oxidized condition.

Thin nickel oxide films have been made by anodization of different crystal planes of single crystal and poly-crystalline nickel in potassium hydroxide solutions (25,26), and controlled potential methods have been employed in their study. Recently, Kronenberg (27) investigated the behaviour of thin film oxide material deposited on a nickel wire by controlled anodization in alkaline solution (9M KOH).

The electrodes used in alkaline storage batteries consist of finely divided, hydrated nickel oxide in intimate

contact with a conducting matrix (usually nickel metal or graphite) shaped in various ways. Since an extensive review on "The Nickel-Cadmium Cell" has recently been published (28) and in which is described the preparation of various types of the nickel oxide electrodes used for fundamental studies and technological purposes, further details on these preparative aspects will not be given here.

For whatever way the electrode is prepared, it is believed that in the reduced (discharged) state the active material is hydrated nickelous hydroxide* in very finely divided form; and in the oxidized (charged) state this becomes a higher valent hydrated oxide in which nickel has a mean formal valence of approximately three. Controversy concerning the stoichiometry of the electrolytic oxidation-reduction reaction was initiated in 1906 between Zedner (9-11) and Foerster (12-14) and despite numerous papers since that time, there is still by no means complete agreement on this subject.

However, recent determinations of the stoichiometries of the oxides (4,29-32), X-ray diffraction studies (15,33-35) and infrared absorption observations (20) on the oxides in the charged and discharged states of the electrode have helped

---

* Further discussion on the stoichiometry and nature of this material is given in a later section (2(d)) of this Chapter.

to elucidate some aspects of the mechanism of charging and discharging of the nickel oxide electrode.

(b) Oxidation States and Oxides of Nickel

Since the electrochemical behaviour of the nickel oxide electrode is closely connected with the chemistry of the oxides involved in the charged and discharged states of the electrode, it will be desirable first to review the inorganic chemistry of the materials involved.

(i) Oxidation States: Nickel is a moderately electropositive metal and dissolves readily in dilute mineral acids. In concentrated nitric acid, and also in sulphuric acid under anodic conditions, it passivates.

The electronic configuration for Ni $\{[Ar]3d^8 4s^2\}$ marks the end of the first "Transition series", but the d electrons are in energy states comparable with those of the succeeding 4s shell and even in the case of monatomic gas atoms, the $3d^9 4s^1$ state has roughly the same energy as the $3d^{10}$ state; that is, one of the d electrons may without difficulty be raised to the next higher s level. Because of this situation, a number of electrons may be removed by chemical oxidation. Hence nickel can exhibit various oxidation states. A table (36) of oxidation states of nickel with their respective co-ordination numbers, the geometrical shapes of known compounds exhibiting these

Table I (36)

Oxidation States and Stereochemistry of Nickel and Some Key Physical Properties of typical Compounds

Oxidation States	Co-ordination number	Geometry	Common Examples	Key Physical Properties
Ni(-1)	4 (?)	?	$[Ni_2(CO)_6]^{2-}$	-
Ni(0)	4	Tetrahedral	$Ni(CO)_4$, $Ni(PF_3)_4$	-
			$K_4[Ni(CN)_4]$, $K_4[Ni(C{\equiv}CH)_4]$	both unstable
Ni(I) (d^9)	4 (?)	Tetrahedral (?)	$K_4[Ni_2(CN)_6]$	Paramagnetic
Ni(II) (d^8)	4	Square planar	$NiBr_2(PEt_3)_2$, $[Ni(CN)_4]^{2-}$	-
		Tetrahedral	$[NiCl_4]^{2-}$	-
	6	Octahedral	NiO, $KNiF_3$,	-
			$Ni(dmg^*)_2$	-
Ni(III) (d^7)	-	-	$Ni_2O_3.2H_2O$(i.e. β-NiO.OH)	
	5	Square pyramid	$NiBr_3(PEt_3{}^{**})_2$	dipole moment 2.5 D
				mag. moment ~1.8 B.M.
	6	Octahedral	$NiCl_2(diars^x)_2Cl$	mag. moment ~1.9 B.M.
Ni(IV) (d^6)	6	Octahedral	K_2NiF_6	Diamagnetic (t_{2g}^6 state)
			$[Ni(diars^x)_2Cl_2](ClO_4)_2$	-

*dmg = dimethylglyoxime; **PEt_3 = triethylphosphine; x diars = O-phenylene-bis-dimethylarsine

oxidation states and the physical properties of these compounds is given in Table I.

Of the possible oxidation states of nickel, Ni(II) is the most stable and characterises much of the common chemistry of the element. Ni(-1), Ni(I) and Ni(0) compounds are very rare. Ni(III) and Ni(IV) states occur in certain oxide systems and in a few complexes. The constitution of the higher oxides of nickel has been the subject of much controversy. Towards the beginning of the century, the existence of Ni(III) was very much doubted; for example, Ni_2O_3 was considered to be either a mixture of Ni(II)O and Ni(IV)O_2 with water of hydration or a solid solution of these oxides (cf. ref. 12).

Recent studies have however removed doubts concerning the existence of Ni(III) and Ni(IV) oxidation states. Several complexes (Table I) of Ni(III) and Ni(IV) have already been identified and the oxidation states of the metal in them have been characterized by studying the magnetic properties of the complexes. Ni(III)-complexes (Table I) have been found to be paramagnetic; this shows the presence of one unpaired electron (magnetic moment $\sim$ 1.9 B.M.) in all of them.

(ii) Oxides: The divalent oxide and hydroxide of nickel are, of course, well known and well characterized.

The Ni(II)-oxide is prepared, in general, by thermal decomposition of the hydroxide, carbonate, oxalate or nitrate of nickel (II). The oxide may be prepared in stoichiometric form (in vacuo) by heating $Ni(OH)_2$ above 200°C in high vacuum (37), but pyrolysis of nickel nitrate yields the anhydrous oxide having oxygen in excess of the stoichiometric amount (38). Nickel (II) oxide is bright yellow in colour but turns brown when heated. When the oxygen is in slight excess, the colour is dark olive green becoming darker as the oxygen content increases (39). Nickel (II) oxide prepared at high temperatures is almost insoluble in acids and alkalies; however, the lower is the temperature of preparation, the more soluble it is, especially in hot nitric acid and ammonia (39). Nickel (II)-oxide has the rock salt structure.

Nickel (II)-hydroxide is precipitated from aqueous solutions of Nickel (II)-salts on addition of alkali metal hydroxides as a voluminous green gel which becomes (micro-) crystalline on prolonged standing (36). It is readily soluble in acids forming salts and also in aqueous ammonia owing to the formation of ammine complexes. In its freshly prepared form, nickel hydroxide usually contains some loosely bonded water in excess of that corresponding to $Ni(OH)_2$, but these water molecules are

readily lost by oven drying above 100°C (40,41). Pure Nickel (II)-hydroxide crystallizes with the hexagonal layer structure (42), an observation which is confirmed by infrared analysis (20). The infrared studies also show the absence of hydrogen bonding between hydroxyl groups in the crystalline state of the hydroxide (further discussion on this point will be deferred until a later section). Although reactions of the nickel oxide electrode are frequently written formally as though anhydrous nickel oxide NiO were involved, this material is not, however, electrochemically active (29,35)*. The hydroxide, on the other hand, can be oxidized electrolytically and, in fact, it is this compound which is used as the active material in the uncharged positive plates of the nickel-cadmium and the nickel-iron batteries.

Oxides in which nickel has a valency of three or more may be prepared by a variety of methods. Higher oxides cannot, however, be prepared by thermal oxidation of Ni(II)-compounds. When a suspension of $Ni(OH)_2$ in KOH solution is treated with a fairly mild oxidizing agent

---

* This is probably (35) because NiO_2, which has a face-centred cubic lattice of Ni^{2+} and O^{2-} ions, and is not hydrated, could only form the higher oxide by addition of OH^- or O^{2-} ions and extension or rearrangement of the lattice. Oxidation is therefore confined to the oxide/electrolyte interface and extension of the oxidation into the bulk phase is limited by the slowness of the solid diffusion process at room temperature. Oxidation of $Ni(OH)_2$ takes place by electron and proton transfer processes through the solid phase (see below).

such as Br_2 at a temperature $< 25^{\circ}C$, a black solid is obtained (39,40) which can be dried in vacuum or over concentrated H_2SO_4 to a composition of approximately $Ni_2O_3.2H_2O$. Any attempt to dry it further by heating causes decomposition with loss of oxygen to give NiO. When an alkaline suspension of $Ni(OH)_2$ is treated with strong oxidising agents, for example Cl_2, dark precipitates containing up to 1.9 g. atoms of oxygen per g.atom of nickel are obtained (cf. refs. 30,43). These solids do not appear to contain peroxide and are thus thought to be impure, possibly, hydrated NiO_2, or solid solutions of Ni(III) and Ni(IV) oxides. There is practically no direct evidence (cf. refs. 30,31) for the existence of pure $Ni(IV)O_2$ (42) nor is its constitution definitely known (35,44). These materials are unstable and are very strong oxidizing agents. Other methods of preparation of higher valent nickel oxides are peroxydisulphate ($K_2S_2O_8$) oxidation of $K_2Ni(CN)_4$ in alkaline medium (44,45), fusion of nickel with sodium peroxide (Na_2O_2) in the presence of excess sodium hydroxide (30,44) followed by careful hydrolysis, and electrolytic oxidation (44) of $NiSO_4$ in a solution pretreated with sodium acetate (CH_3COONa) at room temperature.

A considerable amount of work (e.g., 4,9-15, 20-22,24,29-35,43-51) has been carried out with the purpose

of elucidating the structures and/or compositions of the various hydrated oxides of nickel using analytical, calorimetric, X-ray diffraction, electron diffraction, infra-red spectroscopy, magnetic measurements and differential thermal analysis. As a result of this work, a variety of higher oxides of nickel have been reported some of which are listed in Table II.

The formulae given for these various oxides should not be taken very seriously since chemical analyses hardly support such ideal stoichiometries. It is usually found that either an excess or a deficiency of oxygen is present together with an excess of water, so it has become usual to explain the deviations from ideal stoichiometry by assuming that the end products are mixtures of various oxides. The results of X-ray diffraction experiments are also somewhat inconclusive since only a few diffuse lines appear. This is particularly true for oxides formed by electrolytic oxidation of nickel hydroxide where an almost amorphous condition of the material is indicated.

However, recent measurements on magnetic properties (30) of higher oxides of nickel formed by chemical oxidation of $Ni(OH)_2$ with sodium peroxydisulphate, hypochlorite or hypobromite give very interesting information. Thus, it has been shown that the transition from $Ni(OH)_2$

Table II

Higher Oxides of Nickel with details of their Preparation and Properties

Oxides	Preparative Methods	Properties and Evidence for Existence
$NiO_2.xH_2O$	1. Ni(II)-salt solution +KOH+Cl_2 (30,43) 2. Calorimetric titration (44,46) of alkaline $K_2S_2O_8$ solution with $Ni(NO_3)_2$ solution.	Evidence in calorimetric studies (44,46). Higher oxygen content. Amorphous to X-rays (15,35,44). Diamagnetic (30).
α-NiO.OH	1. $K_2S_2O_8$ + KOH + $K_2Ni(CN)_4$ (44,45)	Identified by X-ray diffraction (44).
β-NiO.OH	1. Ni(II)-salt solution or a suspension of $Ni(OH)_2$ + KOH + Br_2 (40). 2. Solution of $NiSO_4$ + CH_3COONa - electrolysis at a temperature below 25°C (44). 3. $K_2S_2O_8$ + KOH + $Ni(NO_3)_2$ (44).	Identified by X-ray diffraction (44). Paramagnetic (30).
γ-NiO.OH	1. Metallic Ni + Na_2O_2 + NaOH - fusion, followed by careful extraction with ice water (30,44). 2. Anodic oxidation of α-$3Ni(OH)_2.2H_2O$ (overcharging) (21).	Identified by X-ray diffraction. (Black lustrous hexagons or needles). Paramagnetic (30).

$NiO_{1.07-1.22} \cdot xH_2O$	1. $K_2S_2O_8$ + KOH + $Ni(NO_3)_2$ (44). 2. Anodic oxidation of $NiSO_4$ + CH_3COONa solution (44).	Identified by X-ray diffraction.
$Ni_3O_2(OH)_4$	1. $Ni(NO_3)_2$ solution + KOH + Br_2 at 50-100°C (44). 2. Solution of $NiSO_4$ + CH_3COONa at 50-60°C - electrolysis (44).	Identified by X-ray diffraction. Crystalline (hexagonal) "Double layer lattice". On heating to 140°, it decomposes to NiO.

to β-NiO.OH takes place within the same phase, and consequently, NiO.OH is formed in the normally developed $Ni(OH)_2$ structure (44). A magnetic study (30) of the reaction with sodium peroxydisulphate showed a progressive oxidation to Ni(III)- and Ni(IV)-oxides, while the hypochlorite, hypobromite and electrochemical treatments caused simultaneous oxidation to the higher states in proportions which could be calculated from the magnetic susceptibility and the observed degree of oxidation. Although the hydroxides do not obey the Curie-Weiss law rigorously, thermomagnetic studies showed that Ni(III)- and Ni(IV)-oxides has 1 and 0 unpaired electrons, respectively.

(c) Electrochemical Behaviour of the Nickel Oxide Electrode (Bulk and Thick Film Oxide)

(i) Mechanism of Electrolytic Oxidation and Reduction of Nickel Oxide (Charge-Discharge Mechanism): In contrast to the case of the lead oxide electrode (52), there is evidence that the oxidation of nickel hydroxide occurs directly in the solid phase. Kuchinskii and Ershler (1) showed that oxidation and reduction of the oxide does not take place by solution of the oxide followed by reaction at the metal-solution interface and subsequent deposition of the product. A solid-state mechanism of oxidation is further supported by the fact that

only divalent nickel has been observed in solution. In recent experiments, however, it was shown (25) that no nickel ion could be detected (25) by X-ray fluorescence (limit $\sim$ 0.1 p.p.m) in the residue obtained by evaporating the electrolyte in which a nickel electrode had been subjected to a cyclic potentiodynamic programme for 2 hours. Also apart from the complexes mentioned previously, oxides appear to provide the only medium in which the tri- and quadrivalent ions are capable of existing, for no simple salts of these valence states have so far been reported. Also Tuomi (53) recently observed by X-ray and microscopic examination that $Ni(OH)_2$ which was initially microcrystalline remains microcrystalline and, correspondingly, macrocrystalline material remains macrocrystalline over long periods of "cycling". This strongly supports the view that the oxidation-reduction reactions take place primarily in the solid-state and not through a solution-precipitation mechanism. Since the oxide layer apparently remains "in situ" throughout oxidation and reduction, reaction between the oxide and the electrolyte can take place only at the interface between the two (29). Consequently, oxidation and reduction can proceed into the bulk from the surface oxide layer only if at least one of the phases in contact with the substrate metal is electronically conducting, a property usually associated with the presence of metal ions in two valency states.

Various views on the mechanism of charging and discharging the nickel oxide electrode in alkaline medium have been proposed. According to Foerster (12,13) and Glemser et al. (47), during the charging process $Ni(OH)_2$ is first oxidised to a tetravalent nickel compound "NiO_2" and this material subsequently reacts with more $Ni(OH)_2$ to give a trivalent compound Ni_2O_3 or β-NiO.OH, or spontaneously decomposes with loss of oxygen to form Ni_2O_3 or β-NiO.OH (cf. ref. 30); during the discharging process direct reduction of the trivalent nickel compound, β-NiO.OH to the divalent $Ni(OH)_2$ was envisaged.

Quite recently, Wynne-Jones and co-workers (29,35) suggested the following simple mechanism for the charging and discharging processes in the nickel oxide electrode:

$$Ni(OH)_2 + OH^- \underset{\text{discharging}}{\overset{\text{charging}}{\rightleftharpoons}} NiO.OH + H_2O + e \quad I$$

The phase change $Ni(OH)_2 \rightleftharpoons$ NiO.OH is facilitated by the fact that $Ni(OH)_2$ and β-NiO.OH have related hexagonal layer lattices (of course, the lattice of $Ni(OH)_2$ must become disordered and distorted during charging in order to accommodate the greater relative proportion of oxygen) and because, for charging, a simple process equivalent to the joint removal of an electron and a proton is necessary.

Since this process of oxidation can only occur at the interface between the grains of oxide and the electrolyte, it is necessary in order that oxidation can spread through the bulk of the oxide, for proton diffusion to occur through the solid phase. This process sets up a concentration gradient of the various oxidation states of Ni in the solid phase. It has also been suggested (29,35) that some oxidation of NiO.OH to NiO_2 is necessary in order to give the oxide electronically conducting properties. The latter situation is required if oxidation is to proceed within the bulk of the oxide. However, there is no evidence that the Ni(IV) state proposed by Wynne-Jones *et al.* is really necessary for good electronic conducitivity. A solid solution of Ni(II) and Ni(III) oxides would also be expected to have a good electronic conductivity. Recently Bockris *et al.* (54) deduced that the passive oxide layer on Ni having a non-stoichiometric composition $NiO_{1.5-1.7}$ has good electronic conductivity.

Lukovtsev and Slaidin (16,55,56) recently proved experimentally that during the charging and discharging process, diffusion of protons through the solid oxide phase does actually occur. Protons diffuse towards the oxide-electrolyte interface from the bulk during charging and in the opposite direction on discharge. By adding impurity

ions, e.g. Li^+, Zn^{2+}, Al^{3+}, MoO_3 or WO_3, to the electrolyte (55,56) and studying the effects of their adsorption at the interface on proton diffusion and oxygen overvoltage, they also were able to show indirectly the presence of "NiO_2" (an n-type semiconductor) in small quantity at the oxide-electrolyte interface. This material was formed through the reaction

$$NiO.OH + OH^- \longrightarrow "NiO_2" + H_2O + e. \quad II$$

Incorporation of lower valent (< 4) impurity ions (Li^+, Zn^{2+} or Al^{3+}) into the Ni^{4+} lattice of the oxide will tend to decrease the electric conductivity and increase the proton concentration. Hence a decrease in the proton concentration gradient in the film results. The opposite will be the case when W^{6+} (supposedly from WO_3) is incorporated into the Ni^{4+} oxide lattice (56). These results therefore indicate that there is a concentration gradient of various oxidation states of Ni through the solid oxide phase. At the metal-oxide interface, $Ni(OH)_2$ predominates whereas "NiO_2" tends to characterise the oxide-electrolyte interface region (55,56).

Moreover, oxygen evolution succeeds the initial stages of the formation of the oxide and hence must take place at the oxide-electrolyte interface (1,4,6,16,29, 53,56,57,77,122) rather than at the metal surface (i.e. metal-oxide interface); hence it may be presumed that higher oxides

(viz. "NiO_2") tend to be formed at the oxide-electrolyte interface and the lower ones near the metal surface.

An interesting observation was made by Kuchinskii and Ershler (58) in an experiment in which the oxidation and reduction of a single grain of nickel hydroxide was observed microscopically in alkaline solution. When current was passed through the grain, it darkened next to the anode (but not at the contact point between the wire and the grain) and darkening gradually proceeded throughout the whole grain. The darkening was obviously due to the oxidation of $Ni(OH)_2$ to species containing excess active oxygen, viz. NiO.OH or higher oxides having good conductivity. Complete reduction of this material by cathodic polarization was found to be impossible because the cathodic end of the grain became an insulator when it lost its active oxygen; in other words, by cathodic polarization, an insulating layer of $Ni(OH)_2$ was interposed between the oxidized material and the metal contact so that the remaining material became electrically isolated.

(ii) Mechanism and Kinetics of Self-discharge: One of the features of interest in the study of the nickel oxide electrode is the loss of charge of the electrode when it is left standing in pure alkaline solution on open-circuit. This is actually the limiting factor in "Shelf-life" of a

charged accumulator. The loss of charge is always accompanied by oxygen evolution and decay of e.m.f. of the cell.

Some of the earliest work on the self-discharge process was carried out by Foerster (12) who observed that a fully charged nickel oxide electrode on open-circuit would continue to evolve oxygen at a visible rate for as long as 24 hrs. after cessation of the charging current. The initial rate is very rapid and slows down after an initial period but continues for many days before eventually becoming negligible. Foerster's e.m.f. results are in good agreement with those obtained recently by Pitman and Work (59) and by Conway and Bourgault (4) using modern procedures and more refined and elegant techniques. However, Foerster (12) reported that the loss of electrical charge, as measured coulombically by electrical discharge, was greater than that which could be accounted for on the basis of the oxygen gas collected. This was probably due to the fact that the measurements on the volume of gas were made on a complete nickel-iron battery unit (using "pocket" type electrodes) in which the presence of hydrogen, liberated from the negative plates and the presence of readily oxidizable iron complicated the measurements of the net quantity of oxygen evolved.

Foerster suggested that the initial drop of electrode potential corresponded to the decomposition of

"NiO_2" present in small quantities at the end of charging, after which the potential became stabilized at the characteristic potential of Ni_2O_3.

Foerster's results, however, were insufficient to lead to any definite conclusion on the effects of KOH or water activity on the rate of self-discharge and this led Pitman and Work (59) to measure the rate of oxygen evolution on open-circuit, following polarization, as a function of electrolyte concentration using a nickel-cadmium battery unit. They concluded that the rate of self-discharge (in terms of oxygen evolved) was proportional to the square root of the water activity (cf. ref. 29). This conclusion was not without ambiguity, however, since it was based on the total amount of oxygen evolved over a 13 hr. period on open-circuit following polarization at a given fixed current density; no account was taken of the potential of the electrode or its state of oxidation at any time during this decay; nor was it realised, apparently, that the rate of self-discharge must vary considerably during this period of time as the electrode potential falls (since the rate of self-discharge is a function of electrode potential (4)).

Pitman and Work (59) also observed correctly that the decay of e.m.f. of the nickel oxide electrode on

open-circuit was approximately logarithmic in time and that dV/dlog[rate of oxygen evolution] is 0.105 V for the higher potential region and 0.035 V for the lower region. The value 0.035 V is in relatively good agreement with values found by others (see section 3) for anodic oxygen evolution on nickel oxide. These authors (59), however, inspite of the significance of this agreement with the value of the Tafel slope*, concluded that the oxygen evolution partial reaction was not the rate-determining process in the coupled self-discharge process (cf. ref. 4); they preferred the explanation that the electrochemical reduction of adsorbed oxygen on β-NiO.OH (step I) was rate-determining:

$$(\beta\text{-NiO.OH})_2O_{ads.} + H_2O + 2e \longrightarrow 2\ \beta\text{-NiO.OH} + 2OH^- \qquad \text{I}$$

$$2OH^- \longrightarrow H_2O + \tfrac{1}{2}O_2 + 2e \qquad \text{II}$$

Wynne-Jones et al. (29) observed that the rate of potential decay on open-circuit during self-discharge of the charged electrode was at first rapid but gradually became slower until eventually a virtually linear "arrest" at potential ca. 0.4 V (vs Hg/HgO) was reached. It was

---

* The Tafel slope, b is defined as dV/dlog[i] where V is the electrode potential and i is the current density.

during this period when potential decayed very slowly, that most of the electrochemical charge was lost. The charge loss during the steep fall of potential was negligible. This was indicated by the active O:nickel ratios at different time intervals. The behaviour was, however, found to depend on the layer thickness and KOH concentration. The thin film oxide electrode discharged more rapidly than the thick film one. When the rate of self-discharge was determined by measuring the total time required for completion of self-discharge of the electrode in different concentrations of KOH, it was observed that the rate of self-discharge increased in an approximately linear manner with increasing KOH concentration (it is to be noted that the dependence of self-discharge rate on the KOH activity, according to these authors, is in the opposite sense to that found by the authors of ref. 59). Based on these observations, Wynne-Jones et al. (29) concluded that local cell action at the metal/oxide interface (and not spontaneous decomposition of the oxides (except possibly initially)) was responsible for self-discharge of the nickel oxide electrode (cf. refs. 4,6). This idea was further substantiated by the fact that (A) the active material when detached from the electrode surface was more stable in KOH solution than when it was at the electrode surface and (B) the rate of self-discharge is dependent on

KOH concentration and hence a corresponding interaction between oxide and electrolyte solution was involved. Further, the possibility of a disproportionation reaction between the nickel metal and the oxide was discarded because the layers undergo self-discharge as readily on a Pt substrate as on Ni.

Conway and Bourgault (4,6) from the results of rigorous kinetic analyses came to the conclusion that the self-discharge must proceed by a mechanism analogous to that of electrochemical corrosion of a metal (cf. ref. 29), i.e. anodic and cathodic reactions are occuring simultaneously at a common mixed potential at the oxide/electrolyte interface (cf. ref. 29). According to these authors, the following scheme of reactions involving a mixed Ni(III) and Ni(IV) non-stoichiometric hydrated oxide lattice may represent the self-discharge process:

$$Ni^{4+}.2O^{2-}_{(surf.)} + OH^- \longrightarrow Ni^{4+}.2O^{2-}_{(surf.)} + OH_{(ads.)} + e_{(latt.)} \qquad III$$

$$Ni^{4+}.2O^{2-}_{(surf.)} + e_{(latt.)} \xrightarrow[\text{(fast)}]{\text{electron transfer}} Ni^{3+}.2O^{2-}_{(surf.)} \qquad IV$$

$$Ni^{3+}.2O^{2-}_{(surf.)} + H_2O \xrightarrow{\text{proton transfer}} Ni^{3+}.O^{2-}.OH^-_{(surf.)} + OH^- \qquad V$$

Due to electronic and protonic mobility in the lattice, $Ni^{4+}.2O^{2-}$ can be regenerated at the surface of the oxide by the reaction:

$$Ni^{3+}.O^{2-}.OH^{-}_{(surf.)} + Ni^{4+}.2O^{2-}_{(bulk)} \xrightarrow[\text{transfer}]{e,H^{+}}$$

$$Ni^{4+}.2O^{2-}_{(surf.)} + Ni^{3+}.O^{2-}.OH^{-}_{(bulk)} \qquad \text{VI}$$

The discharge of OH^{-} ions (III) can then continue to occur in the double-layer region until all lattice Ni^{4+} ions are converted to Ni^{3+}; similarly self-discharge of the $Ni^{3+}.O^{2-}.OH^{-}$ phase to $Ni^{2+}.2OH^{-}$ can also occur over a range of lower potentials. The processes (IV and VI) involving electron transfer in the lattice will be very fast and could not be rate-determining. Again, since self-discharge rates are increased substantially by increasing KOH activity (see also ref. 29), the process (V) is unlikely to be rate-determining because, with increasing KOH activity from 0 to 15M, the water activity falls from unity to about 0.2. Thus, these authors (4,6) concluded that the rate of the self-discharge process is controlled by some step (for example VII below) in the anodic oxygen evolution partial reactions (see also section 3, this chapter), rather than the cathodic one of reduction of nickel oxide in the bulk or in the surface phase as suggested by Pitman and Work (59)

(reaction I, p. 23): thus, e.g.

$$OH_{(ads.)} + OH^- \xrightarrow[\text{determining}]{\text{rate}} O_{(ads.)} + H_2O + e \qquad \text{VII}$$

$$2\,O_{(ads.)} \longrightarrow O_2\,(g). \qquad \text{VIII}$$

On the basis of the identity of oxygen evolution rate (on open-circuit) and the steady-state anodic d.c. polarization Tafel slopes [2.3 x 2RT/3F to 2.3RT/F] for O_2 evolution observed experimentally, these authors (6) also pointed out that the self-discharge process in the over-charge region is <u>not</u> a non-electrochemical decomposition (cf. ref. 12,43) or a desorption from the surface phase at the interface of the nickel oxide particles but, rather unambiguously, an electrochemical one similar to that occurring at the partially charged material. Further convincing evidence opposing the idea of "non-electrochemical decomposition" (12,43) and the "cathodic reduction" (59) of the charged nickel oxide during the "self-passivation" process given by these authors (6) was the observation of an "inverse H_2O/D_2O isotope effect" on the rate of the oxygen evolution reaction. Both for the open-circuit decay process and the d.c. anodic polarization behaviour, the H_2O/D_2O isotope effect on the rate of oxygen evolution is an <u>inverse</u> one having a magnitude of about $^1/_5$, the reaction in the

D-solvent being the faster at a given oxygen overpotential. The identity of the direction of the isotope effects for self-discharge on open-circuit and d.c. polarization shows that the rate-controlling process is likely to be the same in the two cases and is hence associated with oxygen evolution. The direction of the isotope effect observed is also important negative evidence that the cathodic reduction step involving proton transfer viz.

$$NiO.OH \xrightarrow{H^+, e} Ni(OH)_2 \qquad IX$$

which must occur in self-discharge, is not rate-determining, as had been suggested by Pitman and Work (59). Recently Tuomi (53) confirmed that there is a relationship between ease of formation of Ni(IV) species and the rate of the self-discharge process.

(iii) Effect of Additives: Casey and co-workers (17) recently summarised the known effects of additives (anions and cations) on the charge-discharge behaviour of the nickel oxide electrode. They (17) observed no appreciable effect of carbonate on the coulombic capacity of the nickel hydroxide electrode at 25°C. However, at low temperatures, for example, at -18°C and -40°C, the loss in capacity due to carbonate was found to be larger for plates which contained a greater amount of active material. This was explained

(17) as originating because of the formation of a nickel hydroxy-carbonate as an intermediate in the process of electrochemical reduction. At -40°C, the carbonate effect observed is fairly small until the carbonate content becomes sufficiently high that the electrolyte becomes glassy (at about 60 equiv. % CO_3^{2-}), when the rate of transport of water needed for the discharge reaction

$$H_2O + e + NiO.OH \rightarrow Ni(OH)_2 + OH^- \qquad I$$

falls practically to zero.

Addition of Li^+, Ag^+, Sb^{3+}, Al^{3+}, Bi^{3+}, etc. to the electrolyte has effects on capacity and charge-retention of cycled nickel oxide electrodes, and the effect of addition of Li^+ to the electrolyte has been studied exhaustively. Addition of LiOH to KOH gives an increased coulombic capacity and a longer life to the positive electrode. The increase in electrode potential observed with a lithiated electrolyte has been interpreted as an increase in the oxygen over-voltage permitting higher nickel oxidation states to be reached on charge (17,60). This hypothesis is substantiated by oxygen over-voltage measurements on nickel plates (55,56,60).

According to the view proposed recently by Tuomi (53), the presence of LiOH in the electrolyte

eliminates the formation of the so-called α-phase (53) (a tetravalent nickelate) at the electrode surface (cf. ref. 4) during charging of the nickel oxide electrode. In the mixed electrolyte, although the α-phase is formed initially, it disappears after several cycles; the final "charged" material is the β-phase (Ni III). On the other hand, in a pure aqueous KOH electrolyte the α-phase is formed at the surface region of the electrode and this phase contributes to the electrochemical capacity if the discharge rate is sufficiently slow. If the current density is too large, however, it is stated that the α-phase does not cycle and it is believed to function as an inert material* decreasing the effective amount of active material and hence the effective coulombic capacity. Thus the increased capacity which is attainable in the lithiated electrolyte can be attributed to the elimination of the rate-sensitive, low density α-phase, which is not efficiently cycled at normal current densities. The elimination of the α-phase also permits ready oxidation of $Ni(OH)_2$ (in the discharged condition of the oxide) throughout the compacted layers to trivalent nickel species (β-phase).

---

* This appears to be a controversial point and seems inconsistent with the properties of electrodes formed under the most strongly anodic conditions.

(iv) Hysteresis in the Charge-Discharge Processes: A process is said to exhibit hysteresis if, when the direction of change of an independent variable x is reversed, a dependent variable y fails to retrace the values through which it passed in the forward process; the dependent variable "lags behind" in its attempt to follow the changes in the independent variable. In some systems the size of the hysteresis loop depends upon the speed with which the loop is traversed and, hence, upon the frequency of the oscillation of the independent variable.

In the nickel oxide-KOH system two kinds of hysteresis have been observed: (A) kinetic hysteresis and (B) hysteresis of a more fundamental kind in the charge-discharge process. Kinetic hysteresis in the O_2 evolution process has been observed in the present and other work (61-63). In general, kinetic hysteresis is due to "sluggishness" of some step in the ascending (change to more positive potentials) or descending polarization processes. Commonly it arises in exothermic adsorption processes, where the activation energy for adsorption is much less than that for desorption. Kinetic hysteresis is exhibited strongly by the nickel oxide electrode doped with lithium (61,62).

Hysteresis in the processes of charge and discharge of the nickel oxide electrode is an important and well-known phenomenon but differs from the kinetic hysteresis in O_2 evolution at nickel oxide. In this case, a certain potential separation (Δ V) between the charging and the discharging curves exists. This is because when the independent variable, potential, is changed in the reverse direction (discharge), the change of the dependent variable, charge, lags behind as the changes in potential are impressed on the electrode. The result is a hysteresis loop. Although this phenomenon is well known, no satisfactory explanation has hitherto been given. It will be considered further in this thesis.

Two different kinds of general explanations for the occurrence of hysteresis have been given. First, according to Foerster (12-14), and Glemser and Einerhand (47), the separation of potential between the curves of the charging and discharging processes is due to the fact that a higher electrode potential is required for charging the nickel oxide electrode than is required for discharge. Thus, the idea was advanced that charging (cf. ref. 30) of $Ni(OH)_2$ takes place through the initial formation of a tetravalent nickel compound "NiO_2" which then gives the trivalent nickel compound, NiO.OH by reacting with more $Ni(OH)_2$ or by decomposing

spontaneously to NiO.OH, whereas during the discharging process, direct reduction of NiO.OH to $Ni(OH)_2$ is involved, i.e. there is an intrinsic irreversibility of the process (except at the equilibrium potential).

Secondly, Wynne-Jones et al. (29) have suggested that the potential separation between the curves for the charging and discharging processes is due to the concentration gradient set up with respect to variously oxidized species (viz. Ni^{2+}, Ni^{3+}, Ni^{4+}) within the solid phase. This then introduces, during the charging process, a certain amount of "iR" polarisation (ohmic overpotential across the solid oxide phase) into the measured electrode potential, while during discharge "iR" is reduced or eliminated (as on open-circuit discharge). According to these authors (29), concentration polarization of the electrolyte (i.e. when the KOH concentration in the immediate vicinity of the electrode differs from that in the bulk) will also make a contribution to the observed "potential separation", although probably this would be a rather small effect. Neither of these explanations for the occurrence of hysteresis seems to be very satisfactory.

Conway and Gileadi (7) experimentally determined the quasi-equilibrium potential E^o for the reaction

$$Ni(OH)_2 + OH^- \rightleftharpoons NiO.OH + H_2O + e \quad I$$

and found it to be equal to 0.523 V vs NHE; Foerster (12), assuming that during charging $Ni(OH)_2$ is oxidised to "NiO_2" according to the reaction

$$Ni(OH)_2 + 2OH^- \rightleftharpoons NiO_2 + 2H_2O + 2e, \quad II$$

found E^o for this latter reaction to be equal to 0.49 V vs NHE. The E^o value for this reaction cannot be calculated theoretically* with any degree of accuracy because the free energy of formation of "NiO_2" is not known accurately since "NiO_2" has never been prepared in a well characterised state. From the closeness of the two E^o values, both the reactions forming β-NiO.OH and NiO_2 are to be expected to occur simultaneously. This has, in fact, been observed by Labat (30) by means of magnetic susceptibility measurements.

---

* The value given in Latimer's tabulations (64) is based on the e.m.f. of battery electrode materials, and is quoted for the reaction involving "NiO_2" and the standard H_2 electrode process. However, this result begs the question, since it was, and still is not known what is the exact condition of the higher oxide present in the anodically formed material. The potential and formal degree of oxidation attainable depend, in fact, very much on KOH concentration and temperature. Further studies on the latter matter are presented in this thesis.

(d) Stoichiometry and States-of-charge of Nickel Oxide in the Charged Material (Bulk Oxide and Thin Film Oxide Materials)

Various types of chemical and physical methods have been applied in a complementary way to electrochemical studies on this electrode material in order to determine the stoichiometry of the oxide in the charged state and then the state-of-charge of electrodes under other conditions. Much of the early work, in particular that of Zedner (9-11) and Foerster (12,13), was concerned with establishing the stoichiometry of species involved in the oxidation and reduction reactions. Although different conclusions regarding the nature of the overall reactions were reached, these workers agreed that water was liberated during the charging reaction and consumed during the discharging reaction but disagreed regarding the stoichiometric amount of water involved, as well as the degree of hydration of both the oxidized and reduced products. More complete studies of stoichiometry of bulk oxides in the charged and discharged states at the electrodes have been made recently, e.g. by chemical methods (29,33,51,53), combined chemical and electrochemical methods (Conway and Bourgault, 4,6), by chemical and magnetochemical procedures (Labat, 30,31) and by chemical and differential thermal analysis (DTA)

(Aia, 32). In most of these studies, bulk nickel oxide was used but Jones et al. (29) used both thin and thick films of electrochemically or chemically deposited nickel oxide on a basis metal such as nickel wire or foil, or platinum.

In the "fully-discharged" state of the electrode material, there is usually found a certain quantity of cathodically determinable residual charge. The quantity of this residual charge (i.e. equivalents per Ni above the Ni(II) state) depends on the nature of the electrode material: it is least ($\sim$0.0) when thin oxide film material is used. With bulk or thick film oxides, the residual charge may sometimes become quite appreciable (29). When thin film oxides are used, the nickel valency in the discharged material tends to a value of +2 (29). Therefore the "discharged" electrode material is essentially $Ni(OH)_2$. In relation to the constitution of oxides present in the discharged nickel oxide battery cathode, it is to be noted that a new bivalent hydrated nickel oxide α-$3Ni(OH)_2.2H_2O$ has recently been characterised (21). According to Bode and co-workers (21), in strong KOH and at high temperatures this hydrated oxide is converted to β-$Ni(OH)_2$ which on electrochemical oxidation gives β-NiO.OH.

On charging the nickel oxide electrode, it has been observed (29) that the "active oxygen", [O]* content increases with increasing potential and at the highest potential the final product has a mean stoichiometry "$NiO_{1.8}$". Conway and Bourgault (3-6), using precipitated nickel hydroxide in sintered plaque electrodes in various concentrations of KOH, observed that the electrode could be oxidized to the formal state "$NiO_{1.57}$" in the strongest solution (14.6 M) of KOH at 25°C and to smaller extents in more dilute solutions and/or higher temperatures.

Aia (32) found with mixed Ni/Co oxide electrodes that as the charging of the sintered oxide electrode in 7M KOH solution progresses from the "over-discharged" state containing mostly $Ni(OH)_2$, the mole ratio [O]/[Ni+Co] gradually increases and the mole ratio $[H_2O]$/[Ni+Co] gradually decreases. The mole ratio [O]/[Ni+Co] was observed to vary from 0.1 for the "over-discharged" state

---

* Active oxygen, [O] may be defined chemically as the oxidizing equivalents of the nickel oxide which are determinable by release of iodine from acid solutions of iodide. This oxygen is thus determinable iodometrically. It is also (see Chapter II, section 9) the quantity of [O] beyond that corresponding to the divalent state of nickel in the oxide and is thus determinable by other suitable reductants. "Active oxygen" content in the charged state of the electrode is thus a measure of the available electrochemical charge (or capacity) of the electrode (30-32).

of the material to 0.55 for the 100% charged material and the mole ratio $[H_2O]/[Ni+Co]$ was found to vary from 1.20 to 0.70 for the above two states of the electrode material. The highest O:Ni stoichiometry attained by the charged material prepared by Aia (32) was "$NiO_{1.81}$" reached in a (formally) "660%" charged state of the electrode. Bode et al. (21) observed that the electrochemical oxidation of α-$3Ni(OH)_2.2H_2O$ yields an oxide having a formula $[Ni_4O_4(OH)_4]O_{1.5}(OH)_{0.5}K$ with nickel valency of 3.62. Tuomi (53) observed that the maximum oxidation state attained by nickel in the over-charged state was between 3.34 and 3.48 depending on concentration, purity of the electrolyte, temperature and the nature of the initial nickel hydroxide electrode material. Bro and Cogley (65) recently prepared a high valency oxide (Ni valency $\sim$ 3.6) by hypochlorite oxidation (cf. refs. 22,29,30,35) of $Ni(NO_3)_2$.

From results on the stoichiometry of nickel oxide in the charged and discharged states, it is usually found that a freshly charged positive electrode always contains more "active oxygen" than that corresponding to the formula Ni_2O_3 or NiO.OH. One group of co-workers (4,6,9-12,29,35,47,53),

has sought to explain this result in terms of the presence of "NiO_2" (or a tetravalent nickelate (53)) with Ni_2O_3 or β-NiO.OH (or a trivalent nickelate (53)) in the form of a solid solution in the charged state of the electrode; a second group (15,48,49,59) has suggested the presence of adsorbed atomic oxygen associated with the charged oxide material, i.e. $Ni_2O_3(O)_{ads.}$ or β-NiO.OH$(O)_{ads.}$. X-ray evidence cannot give any information about the presence of such adsorbed oxygen or of atomic oxygen in an electrochemically active form (35). "NiO_2" has never been identified as such by X-ray diffraction in the charged material of the electrode, even when the electrode is overcharged (15,35 cf. ref. 53). This is probably because "NiO_2" is an amorphous material. However, the presence of "NiO_2" (i.e. Ni(IV) oxide) in the charged oxide material has been demonstrated in the magnetic measurements of Labat (30) (Ni(IV) is diamagnetic) and indirectly by Lukovtsev et al. (55,56) (cf. the X-ray diffraction measurements (53) of Tuomi).

The question of formation of a β-phase nickelate rather than a higher oxide of nickel upon charging of the $Ni(OH)_2$-phase has been considered recently by Tuomi (53) using X-ray diffraction analysis. He noted that although the intense X-ray diffraction line for the β-phase formed

in aq. LiOH and KOH mixtures at a diffraction angle of 19° (=2Θ) was practically coincident with that for the $Ni(OH)_2$ (001) plane reflection, the complete X-ray diffraction pattern for this phase was more closely related to that of $LiNiO_2$ (66) than to that of $Ni(OH)_2$. This author hence suggested that the β-crystalline phase is a trivalent nickelate (viz. $KNiO_2$, $LiNiO_2$ etc.) rather than a trivalent nickel oxide (viz. NiO.OH like lepidocrocite) (cf. ref. 67 and 204). It has, however, been observed by X-ray diffraction (15,35,53) that electrochemically deposited thin film oxide material has, in the charged state, a structure distinctly different from that of the β-phase obtained by anodization of well crystallized bulk $Ni(OH)_2$ material.

In concentrated KOH solutions, the β-phase can be further oxidized giving the α-phase $(K_2Ni^{3+}_{2(1-y)}\ Ni^{4+}_{y}\ O^{2-}_{(4-y)}$ where y = 0.5 to 1), a tetravalent nickelate having an appreciable solid state solubility for trivalent nickel. This α-phase differs from the β-phase in having an intense diffraction line at 12.5° (=2Θ) instead of the line at 19° (=2Θ) characteristic (see above) of the β-phase. The formation of α-phase nickelate is accelerated in highly concentrated solutions of KOH or NaOH and at low temperatures. The presence of LiOH in the electrolyte tends to eliminate, however, the formation of the α-phase but in the absence of

LiOH there is always some tendency for formation of the α-phase at the β-phase-electrolyte interface. In order to account for the incorporation of various cations in the oxidized phase and the propagation of an oxidation front throughout the bulk phase during charging, Tuomi (53) proposed a series of complex reactions which are believed to occur at the oxide-electrolyte and β-phase-nickel hydroxide interfaces.

An observation confirming the incorporation of alkali cations into the lattice of nickel oxide as the latter becomes charged has recently been made by Kober and Lublin (68). These authors observed by potassium X-ray scanning that in the charged state the nickel oxide electrode contains a high concentration of potassium which is distributed non-uniformly throughout the whole mass. After discharge, the potassium concentration in $Ni(OH)_2$ is found to decrease to a low value.

Absorption of KOH and H_2O by charged nickel oxide and their release upon discharge was also observed semi-quantitatively by Ershler et al. (69) and Kornfeil (70) and more quantitatively by Conway and Bourgault (5) and Aia (32). However, Aia's results contradict the idea of formation of a nickelate proposed by Tuomi (53). Aia observed (32) that much less Li^+ could be detected in the

charged oxide species whereas quite appreciable amounts of K^+ were present. Moreover, recent observations by Uflyand *et al.* (67) showed that "$NaNiO_2$" is electrochemically inactive so that the nickelate could not possibly act as a reversible cathode material in the battery. Therefore, it seems that the nature and bonding of K^+ ions and their effect on the structure of the charged material requires further investigation. It is possible that K^+ ions occupy cation defect sites or are bound between layers of oxygen octahedra (as in mica) or are substituted for protons on hydroxyl sites. If the alkali metal cations go into Ni^{2+} sites (cation defect positions) then it would be expected, on the basis of ionic radii considerations, that Li^+ ions would more favourably replace Ni^{2+} ions than would K^+ ions. However, the contrary is observed.

More recently Kober (20) using high resolution infra-red spectroscopy re-examined the states of nickel hydroxide in the charged and the discharged condition of the electrode. The spectrum of the oxide in the charged state is characteristically different from that in the discharged state on account of the absence of the hydroxyl band at 3650 cm^{-1}. This band is replaced by a broad diffuse absorption centred at *ca.* 3450 cm^{-1}, while in the far infra-red, charging results in a broadening and shift

of the band at 535 cm^{-1} to a higher energy (575 cm^{-1}). Other changes on charging are associated with the disappearance of the $Ni(OH)_2$ combination band (interaction of the Ni-O stretching with the OH lattice libration mode) at 350 cm^{-1}, accompanied by a broadening of the Ni-O stretching fundamental at 450 cm^{-1}. In the charged form, it is concluded that "free" (non-hydrogen bonded) hydroxyl groups which are characteristic of the discharged state, are not present. A hydrogen bonded structure is on the other hand developed in the charged state. During discharge of the higher oxide, $Ni(OH)_2$ is formed continuously with a corresponding gradual disappearance of hydrogen bonds as indicated by the progressive shift in the librational water band from 575 to 535 cm^{-1}. If the discharge process involved the formation of solid solutions, "solute-solvent" types of interaction should be observed in the spectra, i.e. either a shift or broadening of the hydroxyl band or the appearance of combination bands in the region of 3650 cm^{-1} due to these interactions should arise. Since these interactions were not observed, an important conclusion, which differs from earlier deductions (cf. refs. 7, 15, 34,48,53) based on X-ray crystallographic and electrochemical evidence (continuity of charging curves, and quasi-equilibrium potential behaviour in a limited range of total charge

(10-50%)) is that the Ni(II)-hydroxide forms mixtures (distinct phases) with the charged species as opposed to continuous solid solutions (7,15,34,48,53). Both Salkind et al. (34) and Falk (15) consider, however, the X-ray diffraction behaviour where some $Ni(OH)_2$ lines disappear and others appear as implying a solid solution phase transformation between $Ni(OH)_2$ and the β-phase (see also ref. 35). Tuomi (53), however, suggested that the observed coincidence of the X-ray diffraction patterns for the β-phase and $Ni(OH)_2$ reflects a coincidence of $LiNiO_2$ and $Ni(OH)_2$ diffraction lines rather than indicating a solid solution of trivalent nickel in the $Ni(OH)_2$ crystal lattice. Thus, Tuomi disputes that the phase transformation can be viewed as a simple proton migration out of the $Ni(OH)_2$ lattice to form a solid solution of the higher valent oxide, since the alkali metal cation is an essential component of the oxidized phases. The formation of mixtures of Ni(II)- and Ni(III)-oxides as opposed to solid solutions during charge and discharge was also proposed on the basis of X-ray diffraction results by Wynne-Jones et al. (29,35) as mentioned previously. However, other work (4,9-13,29,35,47) indicates that their results do not necessarily disprove the possibility of formation of a solid solution of several higher oxides when the electrode material is in its charged state (4,9-13,29,35,47).

The principal experimental feature for which the solid solution model offers no satisfactory explanation is the essentially rate-independent separation between the charge and discharge potentials (see section above on hysteresis). This cannot be accounted for in a simple fashion on the basis of any of the kinetic treatments of charge-transfer reactions which require that rates of a process in either direction can only be increased by application of increasing potential of appropriate sign (electrochemical Arrhenius equation). It is, of course, conceivable that the departures from equilibrium are sufficient that the mechanisms of the forward and reverse reactions are different under the usual experimental conditions; with such a supposition, a more complex kinetic treatment might be able to account for the observed behaviour. This matter is treated further in the original aspects of the present work to be reported in a later section.

3. NICKEL METAL OXIDATION AND THE MECHANISM OF OXYGEN EVOLUTION DURING OVERCHARGE

Many workers have reported studies on oxidation of metallic nickel and subsequent anodic oxygen evolution on nickel oxide in alkaline solutions. However, it seems that there is no wide agreement amongst the kinetic results

of various workers. For example, values of the Tafel slope, b, characterising log(current density)-potential plots, on the basis of which probable reaction mechanisms may in some cases be proposed, have been reported for the high current density (c.d.) region ($i > 10^{-3}$ amp. cm^{-2},) as ca. 0.09-0.13 V per decade of c.d. by Elina et al. (71) and by Gantman and Lukovtsev (72) and as 0.13-0.14 V by Sato and Okamoto (73); in the low c.d. region ($i < 10^{-3}$ amp. cm^{-2}), on the other hand, values close to 0.03-0.04 V have been reported by Fiseiskii and Tur'yan (74), and by Elina et al. (71) for alkaline solutions. Using "bare" nickel electrodes, Volchkova and Krasil'shchikov (75) in the case of KOH solutions and Tsinman (76), in the case of NaOH solutions, observed $b \doteqdot 2.3(2RT/3F)$. Tsinman (76) using an electrochemically oxidised nickel electrode, also observed a slope close to 2.3 RT/2F at low c.d. in NaOH solutions and 2.3(2RT/3F) in KOH solutions. Conway and Bourgault (4,6) and Tsinman (76) noted the dependence of Tafel slopes on concentration of KOH solutions, but according to the latter author b was almost constant in NaOH solutions. Sato et al. (73) working at lower c.d. in alkaline sulphate solutions observed that b was between 0.055 and 0.076 V and was dependent on pH of the solution. The latter workers proposed a mechanism for the oxygen evolution reaction ("o.e.r"), at

the nickel surface in alkaline sulphate solutions as follows (cf. ref. 77):

(a) at high c.d. with b = 0.13 - 0.14 V,

$$H_2O \xrightarrow{r.d.s.} OH_{(ads.)} + H^+ + e \qquad I$$

followed by other steps involving reaction with $OH_{(ads.)}$ leading to oxygen evolution, and

(b) at low c.d., with b = 0.055 - 0.076 V,

$$OH^- \longrightarrow OH_{(ads.)} + e \qquad II$$

$$OH_{(ads.)} + OH^- \xrightarrow{r.d.s.} O_{(ads.)} + H_2O + e \qquad III$$

$$2\,O_{(ads.)} \longrightarrow O_2(g). \qquad IV$$

Based on his own and earlier experimental findings, Krasil'shchikov (78) gave a modified mechanism for the o.e.r. on oxidised nickel surfaces as (cf. refs. 4,6):

$OH^- \longrightarrow OH + e$	$b = 2.3(2RT/F)$	when r.d.s.	V
$OH + OH^- \rightarrow O^- + H_2O$	$= 2.3(RT/F)$	"	VI
$Ni_2O_3 \longrightarrow Ni_2O_2 + O$	$= 2.3(2RT/3F)$	"	VII
$Ni_2O_4 \longrightarrow Ni_2O_3 + O$	$= 2.3(RT/2F)$	"	VIII
$O + O \longrightarrow O_2$	$= 2.3(RT/4F)$	"	IX

Several groups of workers (e.g. refs. 1,3-7,10-14,16, 22,29,35,47) have studied the evolution of oxygen during overcharge in alkaline solution directly at the nickel-oxide (battery material) electrode surface prepared in various ways. The interpretation of the electrochemical o.e.r. on the bulk oxide material can be quite complex owing to the semiconducting behaviour of these oxides and the various valence states in which the oxide can exist depending on anode potential. In an elegant experiment, Lukovtsev and Slaidin (16) showed that proton diffusion (first suggested by Wynne-Jones and Jones (29)) in the hydroxide was an important step in the mechanism of oxidation of $Ni(OH)_2$ to NiO.OH:

$$Ni(OH)_2 + OH^- \underset{-10}{\overset{10}{\rightleftharpoons}} NiO.OH + H_2O + e \qquad X$$

oxygen evolution occurred at the electrode simultaneously with step 10 by the process:

$$4OH^- \longrightarrow 2H_2O + O_2 + 4e, \qquad XI$$

Weininger and Breiter (25,26) investigated the effect of crystal orientation on the anodic oxidation of nickel in alkaline solution by a linear sweep method, using single crystals of nickel as electrodes. They suggested the following mechanism for oxidation of nickel in KOH solution:

(c) from -0.30 to -0.10 V vs H_2/H^+ (i.e. -1.226 to -1.026 V vs Hg/HgO in the same solution): hydrogen evolution with the rate-determining step:

$$Ni + H_2O + e \longrightarrow Ni/H + OH^- \qquad XII$$

(d) above -0.10 V vs H_2/H^+ (i.e. -1.026 V vs Hg/HgO): removal of adsorbed H or electrochemical adsorption of OH:

$$Ni/H + OH^- \longrightarrow Ni + H_2O + e \qquad XIII$$

or

$$Ni + OH^- \longrightarrow Ni/OH + e \qquad XIV$$

(e) above 0.10 V to 0.60 V vs H_2/H^+ (i.e. -0.826 to -0.326 V vs Hg/HgO) formation of $Ni(OH)_2$ by

$$Ni + 2OH^- \longrightarrow Ni(OH)_2 + 2e \qquad XV$$

Beyond this region, the rate of reaction falls owing to mobility of Ni(II) ions through the hydroxide surface layer.

(f) from 0.60 to 1.20 V vs H_2/H^+ (i.e. -0.326 to + 0.274 V vs Hg/HgO) oxidation of $Ni(OH)_2$ to NiO.OH takes place: (cf. refs. 16,29):

$$Ni(OH)_2 + OH^- \rightleftharpoons NiO.OH + H_2O + e \qquad X$$

Simultaneously and in a consecutive relation with this step occurs the process

$$Ni + 2OH^- \longrightarrow Ni(OH)_2 + 2e \text{ (see e above)} \qquad XV$$

and it is supposed that both $Ni(OH)_2$ and NiO.OH can exist in this region in a quasi-solid solution (cf. ref. 20 and the discussion given in the previous section).

(g) from 1.20 to 1.50 V vs H_2/H^+ (i.e. 0.274 to 0.574 V vs Hg/HgO): Nickel is directly converted to NiO.OH.

(h) Above 1.5 V vs H_2/H^+ (0.574 V vs Hg/HgO): Oxygen evolution commences together with further oxidation of Ni(III) to Ni(IV) in the oxide layer.

Conway and Bourgault (4,6) observed that the same Tafel slopes characterised both the oxygen evolution reaction which occurs during self-discharge and the anodic d.c. polarization reaction. Detailed interpretations were given in terms of mechanism and coverage of surface oxide sites and indicated the basic identity of the reactions involved in both types of process.

Owing to the differing kinetic results obtained by various workers, it was felt desirable to study, further, this aspect of the electrode process on nickel under conditions where thin oxide films were involved and could be characterised chemically and electrochemically. Such investigations form an important aspect of the present work reported in following sections.

4. ELECTROCHEMICAL BEHAVIOUR OF THE SILVER OXIDE ELECTRODE

The silver oxide electrode was also studied for the purpose of comparison of its behaviour with that of the nickel oxide electrode. Silver oxide is used as the cathode material in Ag-Zn alkaline cells. However, the high electrical resistance of pure Ag_2O (79) and its solubility in alkaline solutions (80) limit its effectiveness as an active material in alkaline batteries.

It is almost universally agreed that during charging, metallic Ag is oxidised first to Ag_2O and then Ag_2O is oxidised to AgO. Oxygen evolution then commences on the AgO oxide surface. These three distinct stages in oxidation are revealed by the three distinct potential plateaus in galvanostatic charging and discharging curves (79,81,83-85), and also by potentiodynamic sweep transients (86,87). The electrochemical formation of Ag_2O can be represented by the equation

$$2\,Ag + 2OH^- \longrightarrow Ag_2O + H_2O + 2e \qquad I$$

The variation of E_{Ag-Ag_2O} with OH^- ion concentration is in agreement (86) with the above equation.

The mechanism of oxidation of Ag_2O to AgO is disputed, but the equilibrium condition is commonly represented by the equation (83,36)

$$Ag_2O + 2OH^- \longrightarrow 2AgO + H_2O + 2e \qquad II$$

Hickling and Taylor (81) suggested that the oxidation of Ag_2O to AgO occurs via an intermediate step involving Ag_2O_3 species according to the following scheme

$$Ag_2O + 4OH^- \longrightarrow Ag_2O_3 + 2H_2O + 4e \qquad III$$

$$Ag_2O + Ag_2O_3 \longrightarrow 4\ AgO \qquad IV$$

The high potential is necessary to form some "Ag_2O_3" nuclei. This potential requirement for the formation of Ag_2O_3 ultimately gives rise to the observed "peak" in the galvanostatic charging potential-time transient. This mechanism is consistent with that suggested by Yost (82) for the oxidation of Cr(III) by persulphate ion to Cr(VI) in the presence of Ag(I) as catalyst. However, this mechanism cannot explain the "iR-drop" in the oscilloscopic open-circuit decay curve (83).

Jones et al. (84), Dirkse et al. (83) and Cahan et al. (79) suggested that Ag_2O is directly oxidized to AgO. The observed peak or "overshoot" in the galvanostatic transient has been ascribed by Jones et al. (84) to the difficulty associated with nucleation of AgO in the lattice of Ag_2O and by Dirkse et al. (83) to the high resistance of the Ag_2O film. The peak was regarded by Cahan et al. (79) as

being produced by concentration of the current into small localised areas where the conversion of Ag_2O to AgO could proceed. Recently Yoshizawa et al. (88) ascribed the "peak" to the difficulty in diffusion of Ag^+, Ag^{2+} and O^{2-} ions through the oxide film.

One group of workers (85,89) proposed that during oxidation of Ag to its oxides the cubic arrangement of the Ag atoms or ions is distorted or destroyed due to penetration of the O^{2-} ion into the Ag metal lattice but another group of workers (90,91) regarded oxidation of silver as taking place by migration of Ag atoms through the oxide layer. A third group of workers (92), however, believe that the oxides are formed at the electrode surface through a recrystallization process and not through a modification of the existing Ag lattice. It has been claimed (93) that the kinetics of oxidation of Ag to its oxides is controlled by diffusion of O^{2-} ions across the Ag_2O-AgO interface.

However, the question of the existence of AgO at all is disputed. The paramagnetism of AgO as measured by Klemm (94) and Noyes et al. (95) supports the existence of Ag(II)O ($4d^9$) with an unpaired electron but the diamagnetic behaviour observed by Neiding et al. (96) and by Scatturin et al. (97), supported by the results of neutron diffraction analysis (97), suggests that AgO is a mixture of Ag(I)

($4d^{10}$) and Ag(III) ($4d^{8}$)-oxides. Recently, however, Gorodetskii (98) and Casey et al. (99) claimed to have observed a new potential plateau corresponding to the formation of Ag_2O_3 at higher electrode potentials. Wales and Burbank (92) were, on the other hand, unable to detect any oxide higher in degree of oxidation than that corresponding to AgO even when a prolonged anodic polarization was carried out at a potential 0.3 V above the reported AgO-Ag_2O_3 potential. Three oxides have been detected in the present work at low temperatures.

5. NATURE OF THIN OXIDE FILMS ON METALS: THEIR ROLE IN PASSIVATION AND AS CATHODE MATERIALS (OXIDATION AND REDUCTION BEHAVIOUR)

The thin film oxide material on nickel behaves not only as an interesting oxidation-reduction system but also as a passivating layer (100) at the interface. Since the latter aspects of the behaviour of these films is also closely related to the present work, the origin of passivity will be briefly discussed.

(a) Anodic Passivation and the Nature and Role of Oxide Films in Passivation

Experimentally, passivation is indicated in galvanostatic current-potential curves by transition regions

where there is a relatively abrupt change of the current-potential relation from one Tafel region to another; in potentiostatic determinations, it is indicated by limiting currents with reversal of the direction of the current-potential relation.

Although there is a little agreement concerning the details of the mechanism of passivation amongst various schools, the basic reason for passivation is the formation of oxide film (oxide "skin" (101)) on the metal surface. Faraday (101) realised the importance of the oxide film in relation to corrosion and passivation and commented on the passivity of iron as follows:

> "My strong impression is that the surface of iron is oxidized, or that the superficial particles of the metal are in such relation to the oxygen of the electrolyte as to be equivalent to an oxidation, and that having their affinity for oxygen satisfied and not being dissolved by the acid.....there is no renewal of the metallic surface....."

Thus Faraday conceived the critical role of the surface oxide in determining the stability of a metal in a corrosive environment. Moreover, he distinguished two possible modes of interaction between oxygen and the reactive metal surface (viz. oxidation and an oxygen-metal relationship equivalent to surface oxidation).

Recently, important work in the field of metal dissolution and passivation has also been carried out on the

reactor metals, viz. U, Zr, Ti and their alloys (102-104). Leach and co-workers (102-104) observed that the different semiconducting properties of the oxides (corrosion products) influenced the corrosion behaviour in an important way. They (102) found that in the case of reactor metals, the rate of corrosion increases with increasing cathodic polarization, and is simply related to the hydrogen activity at the oxide-electrolyte interface over a wide range of potentials. These authors (103) also established that the corrosion of uranium and uranium-zirconium alloys in alkaline solutions differs significantly from the corrosion in acid solution and this difference in behaviour is ascribed to the formation of oxides other than UO_2 in solutions of high pH.

Inhibition of metal dissolution is variously attributed to blocking of active sites (105,106) by chemisorbed oxygen species or by a non-porous monolayer of oxide (107-110) having good electronic conductivity (54). Thicker layers are involved in many cases, e.g. at Pb or Fe.

Recently ellipsometric studies have shown (54) that one of the essential causes of passivation is an increase in electronic conductivity of the multilayer oxide at a critical potential and stoichiometry of the film. In the case of Ni in sulphuric acid (54), prior to passivation

a thick (> 45 Å), 3-dimensional, pre-passive oxide layer of $Ni(OH)_2$ is formed on the metal surface by a dissolution-precipitation mechanism (111) at a potential distinctly cathodic to the passivation potential. This film is then converted to a more consolidated semiconducting film at the passivation potential. The development of electronic conductivity then prevents further high-field ion transport occurring through the film and thus further oxidation of the metal becomes inhibited. In another view (112,113) regarding passivation of nickel, it is the conversion of a thick porous NiO layer to a non-porous Ni_3O_4 layer which is responsible for the passivity of the metal (112,113) in sulphuric acid. Kinetic aspects (114,115) have also been considered.

(b) Role of Thin Oxide Films as Battery Electrode Materials

In usual practice, bulk nickel oxide is used as the battery cathode material and is impregnated in pores of thin nickel sinters or plaques or in admixture with graphite in pockets in a nickel metal structure.

During discharge of bulk material or thick oxide layers (29), the full theoretical charge cannot usually be withdrawn. This effect is more pronounced at higher discharge rates and therefore results in a lower available capacity. On the other hand, if a thin film oxide electrode

is used as cathode, the apparent oxidation state for nickel in the reduced films (after discharge) is observed to be approximately +2 (e.g. in the present work and ref. 29) so that the local isolation of reducible material on discharge is avoided.

With respect to the upper state of oxidation, it has been observed that the highest apparent valency of nickel reached, electrochemically, is about 3.7 (29), this occurring with film electrodes. The highest states of oxidation reached when bulk oxide materials were used have been 3.14 (4,6) and 3.62 (32) in the overcharge region.

From these considerations, it is seen that a larger quantity of charge can be withdrawn (even at high rates) from the thin oxide film electrodes than from the thick layer or the bulk oxide electrodes. Therefore the thin film oxide can possibly be used as cathode material for batteries operating under pulsed charge and discharge conditions (116) where high rate, short duration electrical fluxes are involved. Furthermore, when the bulk oxide is used as electrode material, the ohmic overpotential effect which results from clogging of pores due to increase in volume of the material after charging, becomes of greater importance. Also internal concentration polarization effects which may also arise with respect to the two or more

states of oxidation of Ni[Ni(II), Ni(III), Ni(IV)] in the bulk oxide material, become comparatively more important than in the thin film oxide material. Therefore it is suggested that thin film electrodes may show superior performance in certain battery applications.

6. AIMS OF THE WORK

Studies on the anodic formation of oxide films at metallic nickel in alkaline solution are of special interest in regard to (a) the mechanism of surface oxide formation and reduction in relation to solid state proton and electron transfer reactions; (b) the mechanism of self-passivation; (c) the examination of this electrode as a model for studying oxygen evolution reaction mechanisms where it is believed that oxygen is evolved on surface oxides which may exist in various oxidation states depending on potential; (d) the initial stages of development and rearrangement of thin oxide films on metals. Finally, (e) considerable interest is attached to the possibility of using thin, electrochemically-active oxide films at nickel in special battery electrode configurations where high-rate, pulsed discharge may be required.

Previous work in this laboratory has been concerned with the electrochemical behaviour of bulk nickel oxides so it was considered desirable to examine in some detail the properties of thin film oxides under somewhat similar conditions. Metallic nickel electrodes were therefore studied in the following ways:

(a) thin oxide films were formed and studied by a potentiostatic step charging method. The theory of the method is based on the treatment of Gerischer and Mehl (117) for steady-state kinetic processes but is developed here for examining the change of coverage by adsorbed species on the electrode in relation to the rate of overall reaction involving such species, e.g. as in the o.e.r. at Ni. The results obtained by this method were compared with those obtained by the galvanostatic discharging and the potentiodynamic (triangular wave) sweep methods.

(b) the degrees of surface oxidation in the steady-state (i.e. stoichiometries and "active oxygen" contents of thin oxide films)were determined. A suitable method for reductive stripping of the oxide in the thin film from metal surface was developed.

(c) The possibility of using the thin film oxide as a battery material was investigated.

(d) the mechanism and kinetics of oxygen evolution at the oxidized nickel electrode surface were studied by a potentiostatic steady-state method. Here the influence of addition of Li^+ ion to the electrolyte was observed. Self-inhibition effects were observed and are treated theoretically in terms of surface coverage and a passivation mechanism.

It was felt that it would be of interest to compare the electrochemical behaviour of the nickel oxide electrode with that of the silver oxide electrode.

Hysteresis between potential ranges for oxidation and reduction (i.e. charge and discharge) processes at many metal electrode surfaces (viz. Pt, Ir, Rh, Ni, Ag etc.) are commonly observed: hence the occurrence and origin of this type of phenomenon at Ni and Ag metal electrodes as models were investigated in some detail; a treatment in terms of a two-dimensional irreversible phase transition is given.

CHAPTER II

EXPERIMENTAL

1. INTRODUCTION

In general, the formation, nature and role of thin oxide films on metal surfaces must be studied complementarily by a number of related but independent methods. However, the interpretation of results obtained by different methods sometimes becomes complicated since the behaviour of the electrode is usually sensitive to experimental conditions and its pre-history. The particular electrochemical behaviour when studied by different methods must therefore be investigated as far as possible under identical conditions. The following three classes of approach may be employed: (a) electrochemical, (b) analytical and (c) optical, and in the present work the first two have been used.

Optical methods employ the principles of (i) interference and diffraction; (ii) light absorption or (iii) ellipsometry (polarization and refraction).

In the present work, the formation of thin films of nickel oxide was studied by a non-steady state potentiostatic step charging procedure (117), the experimental and mathematical bases for which were in part developed in the present work. The results obtained with this method have been compared with those obtained by the non-steady-state potentiodynamic

"triangular" voltage sweep method (118,119) and the galvanostatic discharge method (cf. ref. 120).

The stoichiometry of the thin film oxide was determined by a combined electrochemical and analytical procedure. An analytical method based on chemical reductive stripping of the oxide from the metal surface was developed and its reliability investigated.

The kinetics of oxygen evolution on the thin film oxide surfaces were studied by potentiostatic steady-state measurements. The latter method was preferred to the galvanostatic procedure because potentiostatically the detailed structure of any transition region can be discerned in a way which is not accessible under galvanostatic conditions due to instability of potential in regions of reversal of direction of the current-voltage relation (passivation) or in regions where limiting currents arise.

The measured electrode potential was corrected for any ohmic overpotential (iR) contributions where necessary by an open-circuit e.m.f. decay technique.

In the present chapter, the above experimental procedures will be described in some detail but first a general account of the essential experimental technique for preparation and purification of electrolyte solutions, preparation of electrodes, purification of gases, control of temperature,

etc. will be given.

2. SOLUTIONS:

(a) Preparation of Potassium Hydroxide Solutions (Standard method)

The electrolyte solutions used in the experiments were made up from potassium hydroxide at various concentrations. The solutions were prepared by dissolving Baker analytical grade* potassium hydroxide in triply distilled water, distilled directly on to the caustic potash crystals in a calibrated dilution flask which was connected with a line from which purified nitrogen could be drawn; connections were also provided to the experimental cell. The solution was made homogeneous by bubbling purified nitrogen gas and was then transferred to the previously cleaned experimental cell (Fig. 3) under pressure of the nitrogen. The solution was never open to atmospheric contamination.

The triply distilled water was made by redistilling "once distilled" water distilled from alkaline permanganate in a still provided with three spray traps. This "second

---

*Since impurities are sometimes of importance in electrochemical processes the assay of this material is recorded below:

"Baker analyzed" reagent meeting A.C.S. specification: Nickel 0.0003%; sodium 0.03%; Potassium carbonate 0.3%; chloride 0.005%; nitrogen compound 0.0005%; phosphate 0.0002%; sulphate 0.001%; heavy metals 0.0004%; iron 0.0002%.

Figure 1. Schematic diagram of the KOH crystallizing bath for high purification.

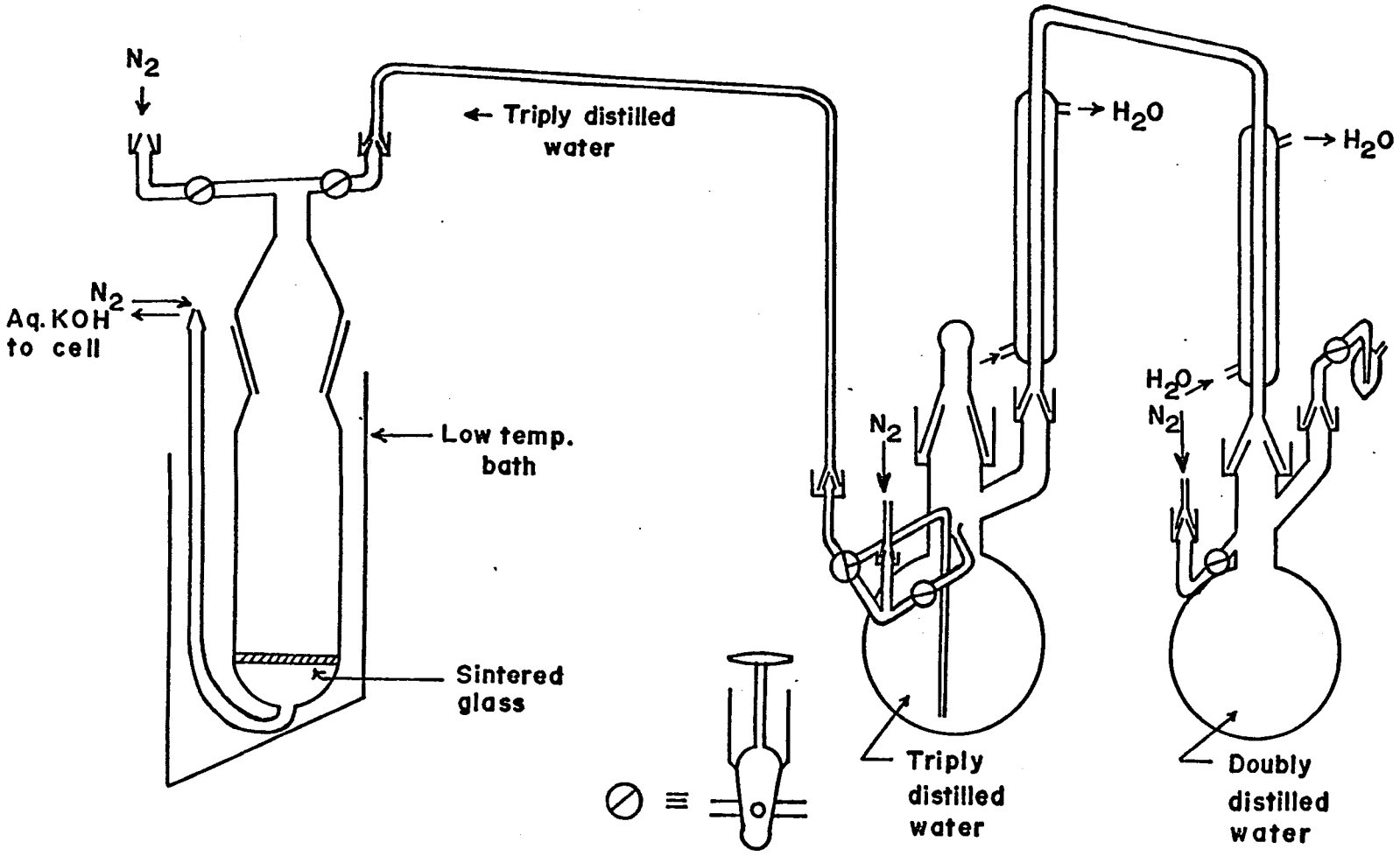
N_2
Aq. KOH to cell
N_2
← Triply distilled water
→ H_2O
→ H_2O
← Low temp. bath
N_2
H_2O
N_2
Sintered glass
Triply distilled water
Doubly distilled water

distilled" water was then refluxed in a stream of the purified nitrogen (the procedure for nitrogen purification is described below) for at least 0.5 hr. in a small glass distillation unit in order to degass it and then "redistilled" for the second time on to the potassium hydroxide crystals in the dilution flask.

(b) High Purification Technique for Potassium Hydroxide

Baker analytical grade potassium hydroxide was initially recrystallized (cf. ref. 121) at -40°C from a 10 M aq. solution in triply distilled water in an all-glass vessel provided with a sintered glass plug (Fig. 1) for filtering off KOH crystals from the solution in the absence of air (CO_2). When an appreciable quantity of the potassium hydroxide hydrate crystals had been precipitated out at the low temperature, the mother liquor containing any trace impurities was forced out through the sintered disc under pressure of the purified dry nitrogen. Doubly distilled water was then distilled a third time and transferred from the reservoir flask onto the crystals to form the desired electrolyte solution which was subsequently forced over into the previously cleaned experimental cell. The strong KOH solutions were kept for the shortest time in contact with glass in order to minimize dissolution of silicate ions.

(c) Potassium Hydroxide-Lithium Hydroxide Solutions

In certain experiments solutions containing Li^+ were required. These were prepared as follows. The required amount of A.C.S. grade potassium hydroxide was taken in the dilution flask and the solution was made up in the way described under (a) above. The solution was standardised and then the required amount of A.C.S. grade lithium hydroxide was added and the solution made homogeneous by bubbling purified nitrogen.

(d) Standardisation of Solutions

The concentrations of the electrolyte solutions were determined by standardisation against hydrochloric acid solution of known strength using an indicator; standardizations were carried out both before as well as after the runs.

(e) Purification of the Electrolyte by Pre-electrolysis

The electrolyte solutions thus prepared may still have contained traces of dissolved impurities. Since the behaviour of electrodes is often sensitive to even traces of electrodepositable or adsorbable impurities (122,131,152), the electrolyte in the cell was always further purified by prolonged anodic pre-electrolysis (131) (ca. 24 hrs.) before experimental runs, using a large sacrificial platinum or nickel electrode maintained in the working compartment, and

operating at a current density of approximately 20 ma. cm^{-2}. This electrode was withdrawn from the solution before the experimental test measurements were commenced.

In a few experiments, where investigations by the steady-state potentiostatic technique was carried out below the oxygen evolution region (< 1.23 V. vs H_2/H^+) the electrolyte was subjected first to prolonged potentiostatic cathodic pre-electrolysis prior to the runs, following galvanostatic anodic pre-electrolysis (above). A separate sacrificial large platinum electrode was used to remove dissolved oxygen, and its potential was so adjusted that no hydrogen was evolved.

During pre-electrolysis, purified nitrogen was continuously bubbled around the electrodes in order to facilitate diffusion of impurity ions to the electrode; it also carried off any evolved gas.

3. ELECTRODES

(a) Working Electrodes

(i) Nickel: Electrodes were prepared from spectroscopic grade, polycrystalline nickel wire of diameter 0.254 mm. supplied by Johnson Matthey and Mallory Co. The wire was first degreased by keeping it under reflux in benzene and benzene vapour for 24 hrs. A piece of wire

Figure 2. Schematic diagram of the electrode annealing train.

A Liq. air cooled trap

B High vac. stop-cock

C Stop-cock

D Spherical joint (vac. sealed)

E Graded seal (quartz-pyrex)

F Quartz tube furnace

G Glass bulb for sealing-in electrode.

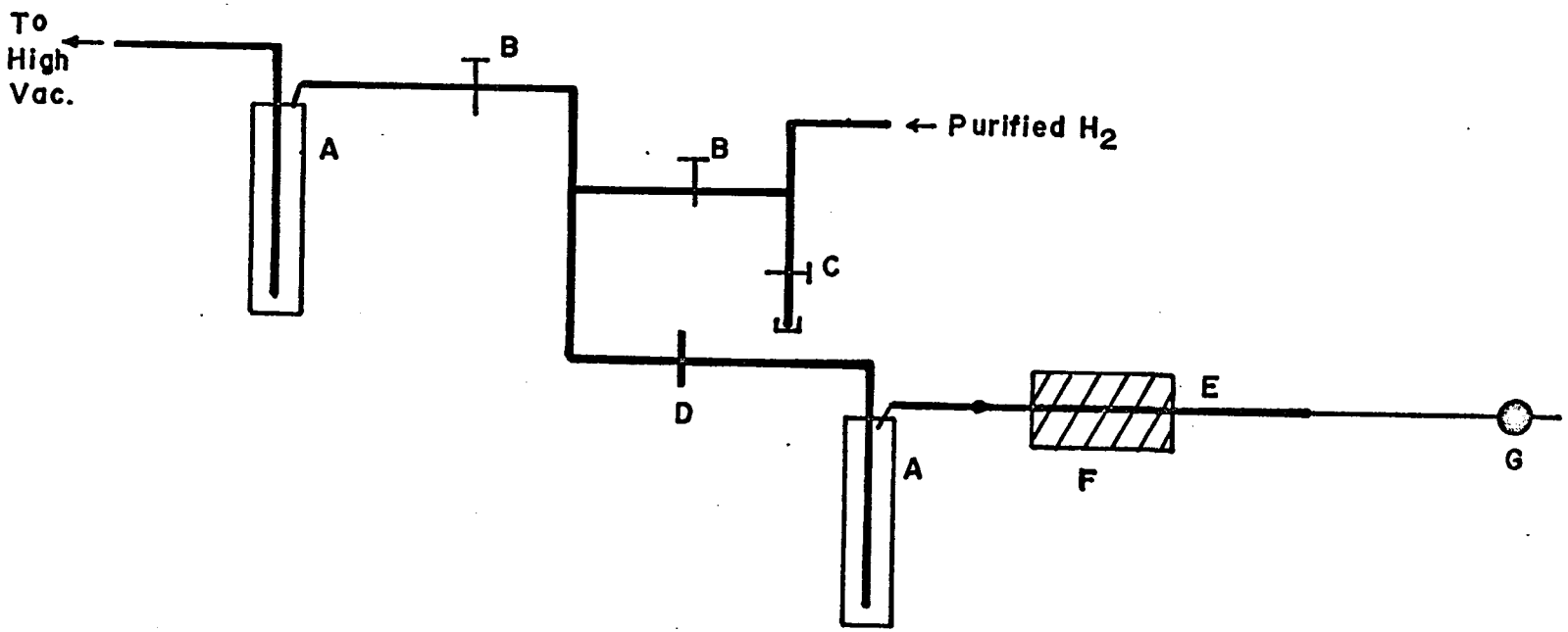

2 cm. in length was then annealed for 1 hr. in a quartz-tube furnace maintained at 600°C in a stream of dry purified hydrogen. At the other end of the furance tube was sealed a clean and dry glass tube in which a thin walled bulb had been previously blown. After annealing, the wire was sealed into the tube in a dry hydrogen atmosphere with about one cm. length of the wire projecting into the bulb. The bulb was then sealed at the other end, and connected to a sliding glass tube as described previously elsewhere (124). Some of the nickel electrodes were annealed in vacuum (ca. 10^{-6} mm. Hg) at 600°C in the quartz-tube furnace for 1 hr. In this case, when the furnace was cold, the electrode wire was pushed into the furnace tube, the thin bulb was sealed and then the whole system was flushed with dry purified H_2 for 15 mins. to drive out air; finally, after sealing the farther end of the bulb and closing the hydrogen line, the whole system was slowly opened to the high vacuum line and annealing was commenced (Fig. 2). Finally, after vacuum annealing, the wire was sealed in the bulb as described above. Two liquid air traps were provided before the quartz-tube furnace in order to remove any condensible impurities that might otherwise contaminate the wire.

Nickel electrodes prepared under these controlled conditions gave satisfactory and very reproducible kinetic

results which, over certain ranges of potential, were virtually superimposable from one run to another. The behaviour of electrodes prepared in the above two ways was also almost identical in the oxygen evolution region.

Several electrodes were annealed for 0.5 hr. at 600°C in a stream of carbon dioxide-free oxygen, for comparison. The results obtained with these electrodes were, however, not so reproducible.

Chromic acid cleaning of the electrode (123) was not considered desirable, owing to a possible pre-passivating effect of adsorbed chromate ions (25,26). In some measurements, the electrodes were, however, pre-conditioned electrochemically as described in later sections.

The annealing temperature was measured by means of a chromel-alumel thermocouple* covered by high temperature fibre glass (Type: HGHG 22-CT). The e.m.f. and hence the temperature was measured on a Pyrometer (Fischer Scientific Co., model 32-J) (external resistance ≒ 0.5 ohm.) which was recalibrated against a standardized Honeywell Potentiometer (model No. 2704).

---

*Accuracy quoted: ± 4°F from 0 → 530°F

± ¾% from 530 → 2300°F.

The residual pressure associated with the vacuum was measured by a Phillips ionization gauge.

(ii) Silver: In the comparative work on silver electrodes, first a piece of spectroscopic grade silver wire of 0.254 mm. diameter and 1 cm. in length was cut and fused, end-to-end, with a 0.5 cm. long platinum wire (of the same diameter) in a blowpipe flame. The electrode was then degreased in the manner described above and sealed in a thin glass bulb in a stream of purified hydrogen after annealing the electrode for 1 hr. at 600°C in dry purified hydrogen in the manner described above (3(a), (i)). Special care was taken in completing the metal-to-glass seal to avoid any "leak" and also to avoid melting the silver; these were common troubles in the initial stages of working with silver.

In practice, the platinum wire was directly sealed in the glass up to the platinum-silver joint and then the joint was covered further by glass down the silver wire over a short distance. This method was satisfactory for obtaining leak-proof seals with silver (cf. ref. 124). The platinum end was used for electrical contact.

The direct sealing of silver wire in pyrex glass is not possible owing to the proximity of the melting points of silver and pyrex glass and because of the different coefficients of thermal expansion. The use of lead glass

for sealing silver was not considered desirable owing to the probable dissolution of lead from the glass in alkaline solution.

In all cases, the electrodes thus prepared in the bulbs were then sealed to ground-glass sliding tubes bent at an angle near the bulb in a way convenient for adjusting the position of the electrode to optimum proximity to the "Luggin" capillary communicating with the reference electrode.

(b) Reference Electrode

The potentials of the working electrodes were measured against a mercury-mercuric oxide reference electrode prepared in the same solution as that used for the experimental run. The reference electrode compartment was separated by a grease-free, solution-sealed, closed stop-cock which inhibited any diffusion of traces Hg^{2+} ions into the working electrode compartment. The concentration of Hg^{2+} is in any case very low. The reference electrode was freshly prepared for each set of runs from purified redistilled mercury and the yellow allotropic form (3) of mercuric oxide (A.C.S. grade). The reference electrode may be represented as

(Pt) Hg/HgO, KOH (aq.).

Platinum wire is used only for electrical contact and special care must be taken to ensure that it does not, under any

circumstances, come in contact with the electrolyte otherwise an incorrect reference potential would, of course, be obtained. This electrode is uniquely the most well-behaved of all the oxide electrodes.

The E^{o} value of this electrode measured against the reversible hydrogen electrode was found by Ming Chow (125) to be extremely reproducible with a value of 0.92640 $\pm$ 0.00006 V at 25°C and 0.9268 V by Mujamoto (126). Lewis and Randall (127) recalculated the value of E^{o} at 25° using data of Brønsted and obtained 0.9265 V. Taking the mean of all the results corrected to zero concentration, Hamer and Craig (128) obtained E^{o} at 25°C equal to 0.92581 $\pm$ 0.00036 V with a temperature coefficient at 25° of $-0.0002878\ V.{}^{o}C^{-1}$. This is in excellent agreement with the value of 0.92575 V calculated from critically selected thermodynamic data by Latimer (129).

For the purpose of electrode kinetic work where reproducibility of overpotential values rarely exceeds 5 mV, the behaviour of this electrode is more than adequate.

In order to specify electrode potentials with reference to the potential of the reversible hydrogen electrode, 0.926 V must be <u>added</u> to the electrode potentials reported (Stockholm convention) with reference to the mercury-mercuric oxide (Hg/HgO) electrode in this thesis. Unless otherwise

mentioned, all the potential values quoted in this thesis are reported with reference to the Hg/HgO electrode in the same experimental solution.

The advantages of using this electrode are that (i) no special precautions except those needed to secure components of reasonable purity are necessary for setting it up: cadmium and tin are, for example, harmful contaminants in mercury (174), and (ii) no disturbing effects can arise due to the presence of other valence states of the oxide because mercurous oxide does not exist (130). A disadvantage, however, is that this electrode cannot, of course, be used in acidic solutions. For such cases the Hg/Hg_2SO_4 or Hg/Hg_2Cl_2 half-cells are satisfactory.

(c) Counter or Auxiliary Electrode

A platinum gauze or sometimes a platinum-rhodium gauze containing 95% of platinum and having very large surface area was used as the counter electrode.

4. GASES

(a) Nitrogen

During pre-electrolysis and also during the experimental runs, purified nitrogen was bubbled near the working electrode and also near the counter electrode in the cell.

Nitrogen gas was purified (cf. refs. 131,132) by passage through dehydrating agents, a Linde molecular sieve material, magnesium perchlorate-calcium chloride mixture and then through a furnace containing copper turnings maintained at a temperature of about 350°C for removal of oxygen and then through traps cooled in liquid air, through glass wool filters and finally by bubbling through a presaturator containing the same electrolyte (KOH solution) as that in the experimental cell. Presaturators were used to avoid change of composition of the electrolyte during prolonged runs. The KOH also absorbed residual traces of CO_2, if any, present in the stream of nitrogen gas.

When the copper turnings in the nitrogen purification furnace became oxidised after prolonged use, they were regenerated by passing a stream of hydrogen gas, instead of nitrogen, through the tube while the furnace was still maintained at about 350°C. During this procedure, the experimental cell was disconnected.

(b) Oxygen

In the runs where the steady-state kinetics of anodic oxygen evolution on the electrode surface were of the main interest, purified oxygen gas was bubbled around the working electrode in the cell instead of nitrogen. In principle, there was no difference in behaviour of the

Figure 3. Photograph of the experimental cell.

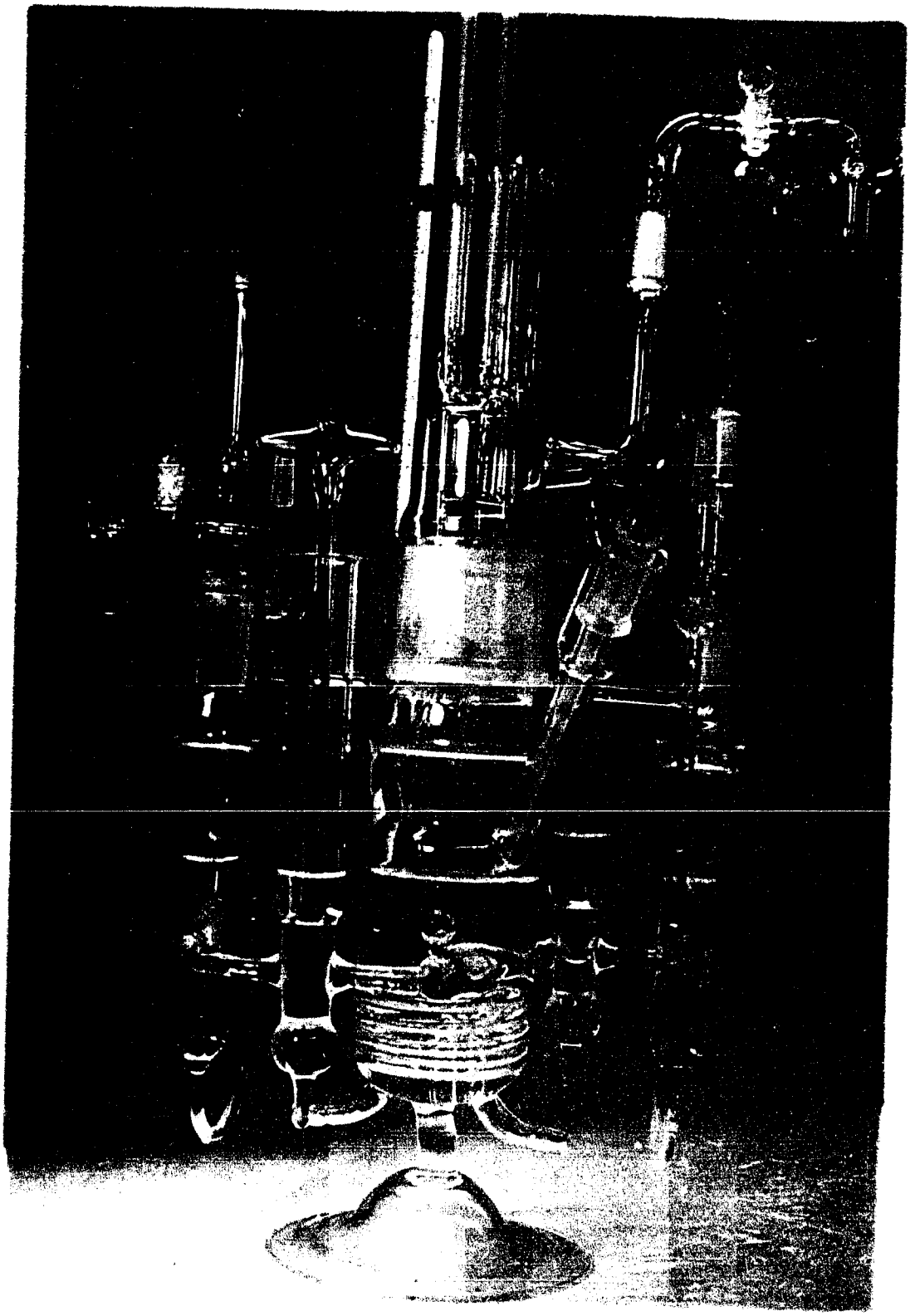

electrode with respect to oxygen evolution kinetics between that when oxygen or that when nitrogen was bubbled.

Bourgault (3) observed that special purification of oxygen was not necessary and that oxygen gas could be used directly from the cylinder. In the present experiments, however, the oxygen gas used was freed from CO_2 by passage through a series of CO_2 absorbers, viz. soda lime, pellets or crystals of KOH and then finally through the pre-saturators mentioned above.

(c) Hydrogen

Purified hydrogen gas was used for annealing the electrode as described previously under 3(a), (i). The hydrogen purification train consisted of the same stages with the same materials as those in the nitrogen purification train, except that the former did not have any pre-saturator. A furnace tube of palladized asbestos operating at 400°C was provided for catalytic removal of any traces of oxygen.

5. CELL

A three-compartment pyrex glass cell (Fig. 3) of the type described previously (132) was used. The middle compartment containing six working electrodes was provided with a glass coil through which fluid could be circulated from a thermostat for maintaining the electrolyte at any

temperature from ca. 5 to 90°C. The temperature was read from a built-in thermometer situated near the Luggin capillary. For low temperature studies (down to -30°C) a similar three compartment cell but smaller in size, which could be placed in a Dewar flask (9" - 12" diam.) was used. In this case only one electrode could be used at a time.

6. CLEANING OF GLASSWARE

The cell and electrode bulbs were cleaned first with chromic-sulphuric acid mixture followed by rigorous washing with tap water and then distilled water. Finally, the cell and the electrodes were washed several times with doubly-distilled water and soaked in doubly-distilled water for 24 hrs., washed once or twice again with doubly-distilled water and then finally with triply-distilled water. Very rigorous washing was carried out to remove any adsorbed chromate ion which might have remained on the glass surface.

7. TEMPERATURE CONTROL

(a) Temperatures above Room Temperature

For electrochemical studies at and above room temperature (viz. up to 90°C), a heating fluid from a thermostat was circulated through the glass heat exchanger coil built into the cell. The temperature of the thermostatic

bath was controlled to ± 0.1°C by a mercury thermoregulator.

(b) Low Temperatures

For studies at temperatures down to -30°C, a small three-compartment cell which could be placed inside a 12" diameter Dewar flask, was used. The cell containing the electrodes and electrolyte solution was placed in the Dewar and a cooling mixture was then poured in the flask. The level of the electrolyte in the cell was kept below that of the cooling mixture. . The gas which was bubbled through the electrolyte solution, ensured uniformity of temperature throughout the electrolyte solution and minimization of concentration gradients. At least 15 mins. or more (depending on the temperature difference) were allowed for thermal equilibration with the bath.

Cooling mixtures for different temperatures were prepared from various mixtures of dry ice and acetone. The temperature could be regulated to within ± 0.5°C by adding more dry ice as necessary.

8. INSTRUMENTATION AND TECHNIQUE

(a) Instruments

Potentials were controlled by a Wenking short rise-time potentiostat and measured on a Radiometer pH-mV meter (Model PHM 4c). In the programmed potentiodynamic

and potential step operations, the necessary signal-function was fed to the reference input of the potentiostat. In other cases, the reference input was shorted so that the working electrode could be made anodic or cathodic with respect to the counter electrode. Linear sweep potentiodynamic measurements were made using a "Servomex" function generator Type L.F. 141 for single and repetitive sweeps. For potentiostatic step charging, a manual step-function switching arrangement was used. For a source of constant current a conventional divided resistance arrangement was made. A 90-120 V. D.C. Power supply (Model 22-110, Dressen-Barnes Corp.) with excellent voltage stability characteristics was used as the source of power.

The steady-state currents were measured on a "Sensitive Research" milliammeter (Model S) connected in series with the counter electrode. A Keithley Electrometer (Model 600 A) was also sometimes used, particularly for measuring very small currents. Transient currents in potentiodynamic and potential step experiments were measured by leading the current through an accurately known resistance R and then recording the resulting potential difference (E = iR) created across the resistance on an oscilloscope or a Moseley high impedance X-Y recorder (Model 2D-2AM).

Figure 4. View of the experimental set-up showing various apparatus.

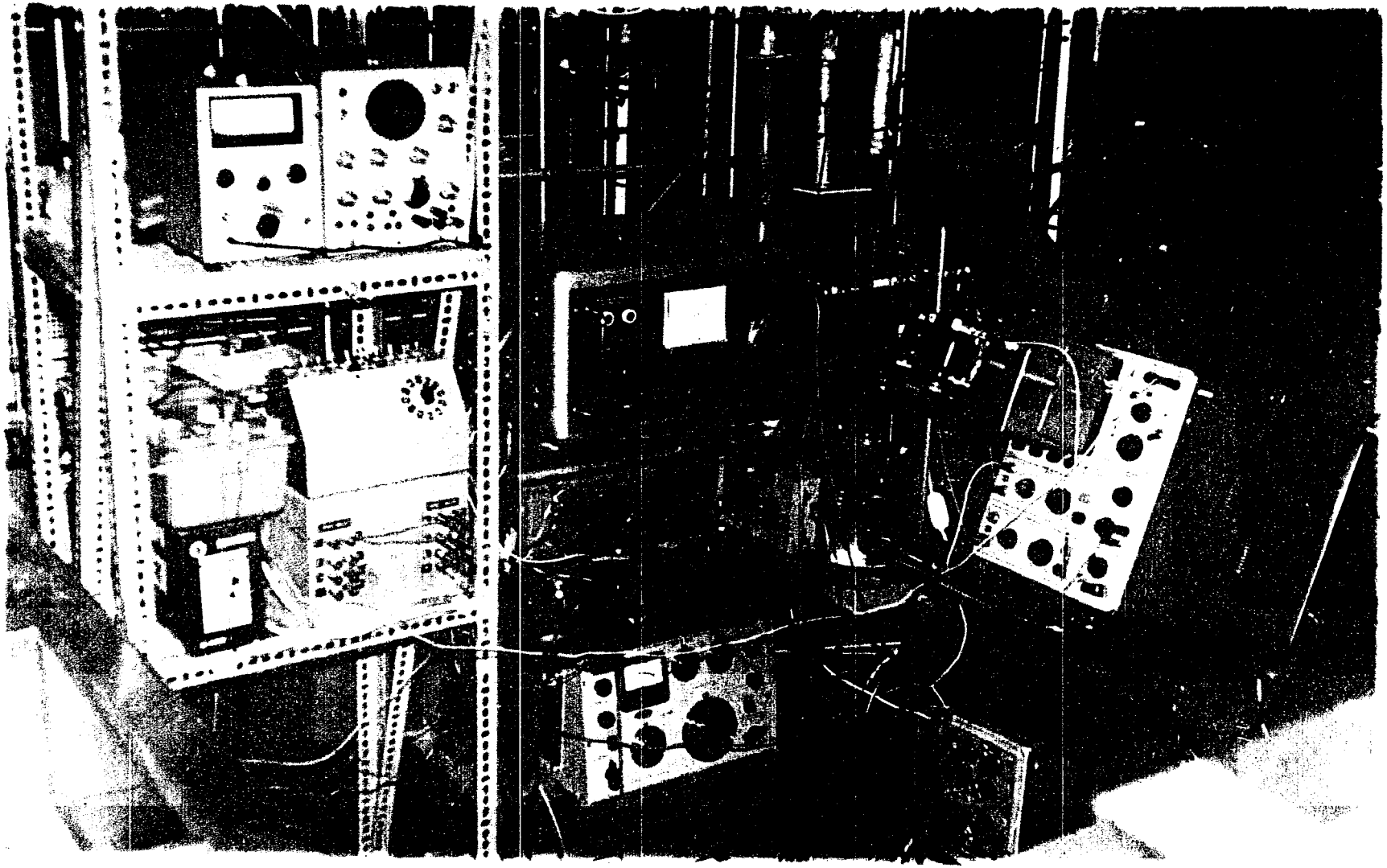

Figure 5. View of the experimental set-up showing the cell and other glass apparatus.

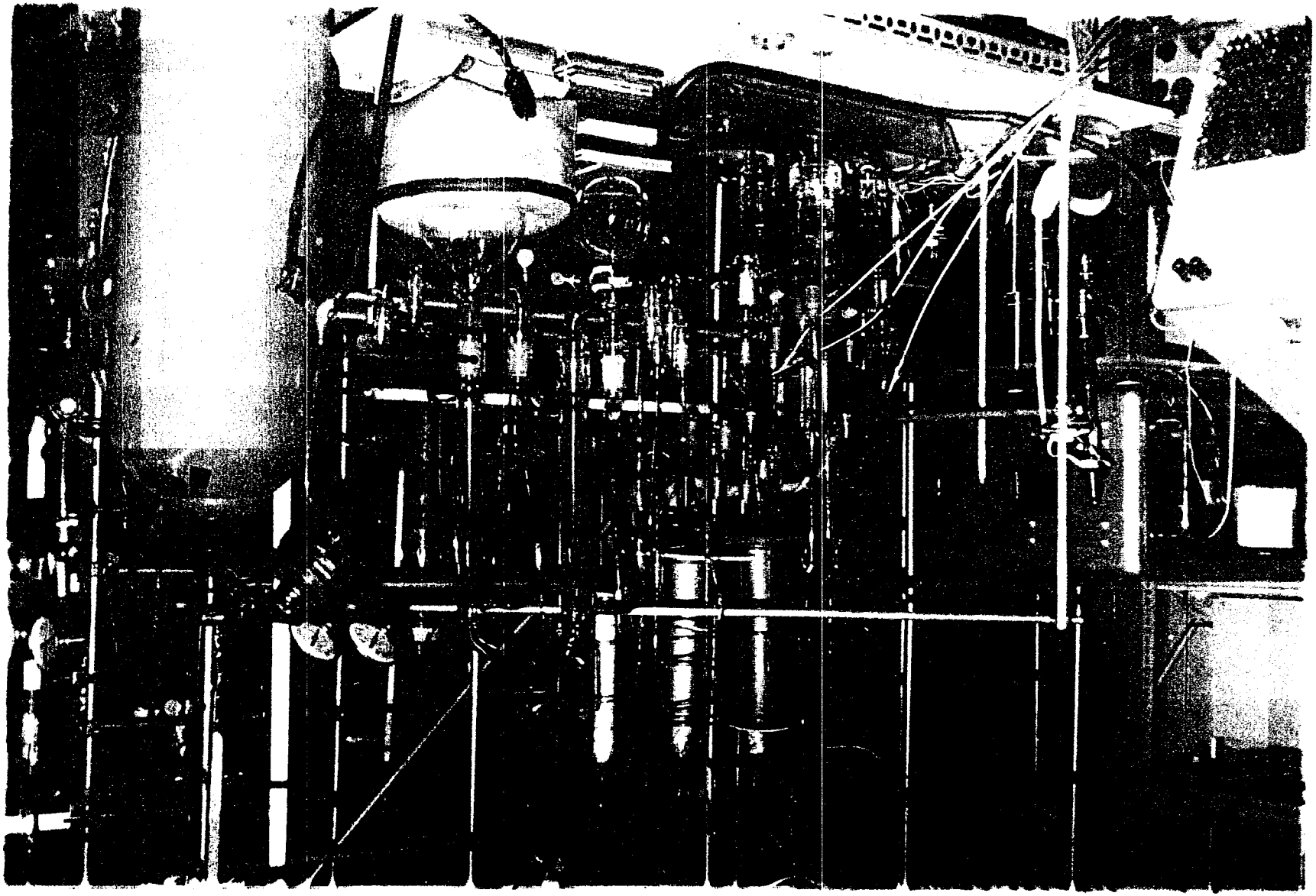

Figure 6. Schematic circuit diagram for steady-state potentiostatic anodic polarisation.

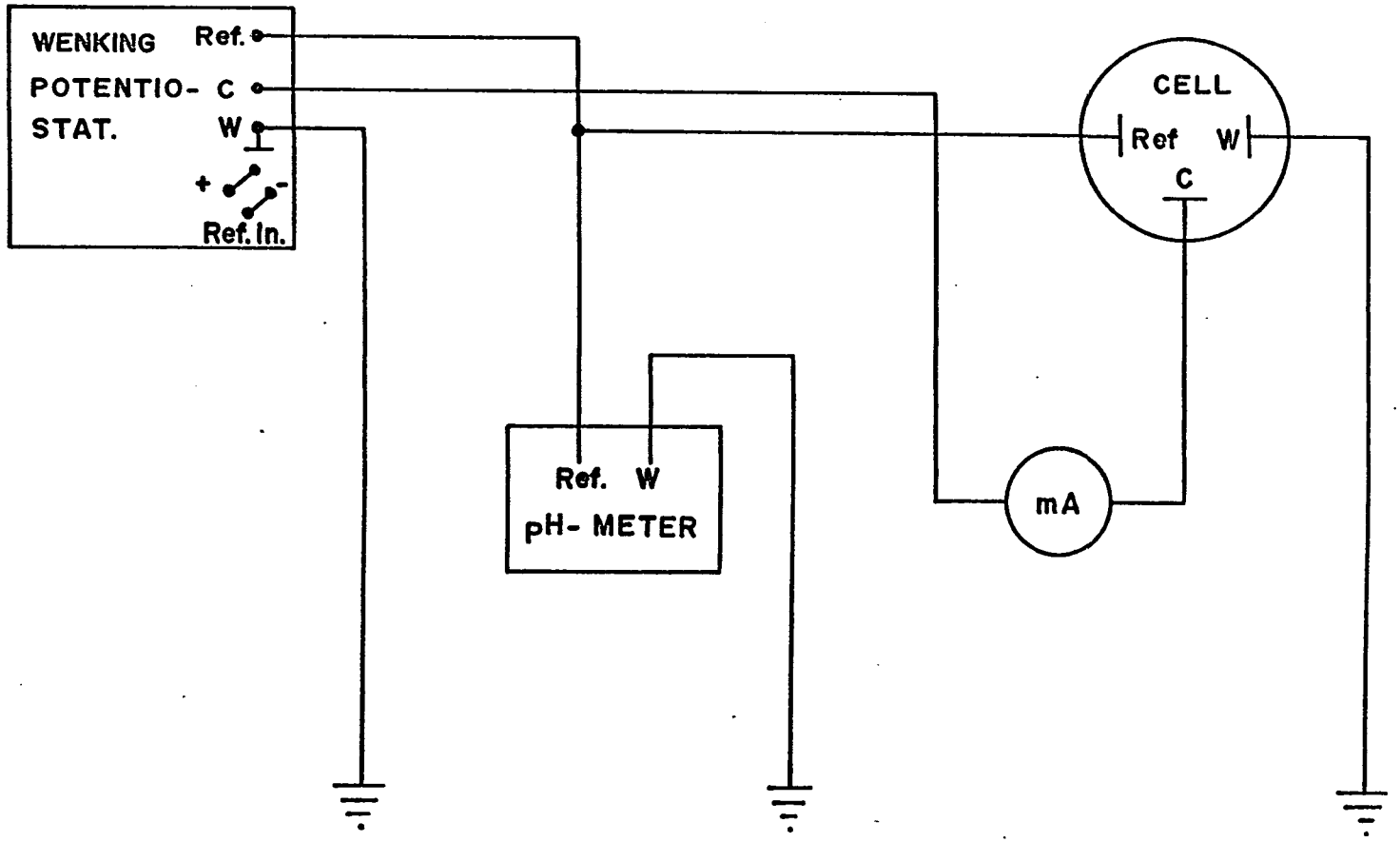
WENKING
POTENTIO-
STAT.
Ref.
C
W
+
-
Ref. In.
Ref. W
pH- METER
CELL
Ref W
C
mA

All transients (viz. potential-time, current-potential or current-time) arising from galvanostatic, open-circuit e.m.f. decay, potentiodynamic sweep or potentiostatic step charging methods were photographed from a Tektronix dual-beam oscilloscope (Type 502) using a 35 mm reflex camera or were recorded on the Moseley X-Y recorder. For comparatively slow transients (< 0.25 V.sec^{-1}), the X-Y recorder was usually used. The electrode potential signal was passed through a Tektronix type "O" operational amplifier before feeding it to the oscilloscope or the recorder. The type "O" operational amplifier provided both a differentiating and a high input impedance (cathode follower) stage. The overall view of the experimental apparatus is shown in Figs. 4 and 5.

(b) Electrochemical Procedures

(i) Potentiostatic Steady-state Kinetic Measurements: The circuit shown in Fig. 6 was used for potentiostatic polarization of the electrode. In the experimental arrangement, the working electrode which was grounded, was made the anode with respect to the counter electrode by shorting the reference input of the potentiostat appropriately. In several runs, when it was required that the working electrode be polarized cathodically with respect to the Hg/HgO reference electrode, a Weston standard cell was

interposed between the reference electrode and the reference terminal of the potentiostat to provide an opposing bias voltage.

Steady-state potentiostatic polarization runs were conducted using a fresh electrode for every run. Polarization was commenced just after breaking the bulb under the solution by means of a glass probe and placing the electrode as close as possible to the "Luggin capillary". During polarization, purified and pre-saturated nitrogen gas was bubbled around the working and the counter electrodes. Each current measurement was taken one minute after the potential had been set on the potentiostat. Point by point delineation of the log[i]-V relation for all conditions was made first in the direction of ascending (more anodic) potentials and then in the descending direction at intervals of 0.02-0.04 V. Although these conditions do not represent an absolutely steady-state behaviour, (due to long time effects), the anodic currents measured were almost steady. Under these "standardised" conditions, the nature of the log[i]-V relation is found to be adequately representative of the steady-state behaviour and indeed the reproducibility of the results from one electrode to another, and from one solution to another of the same concentration, was found to be excellent.

Figure 7. Schematic circuit diagram for studying open-circuit decay of e.m.f.

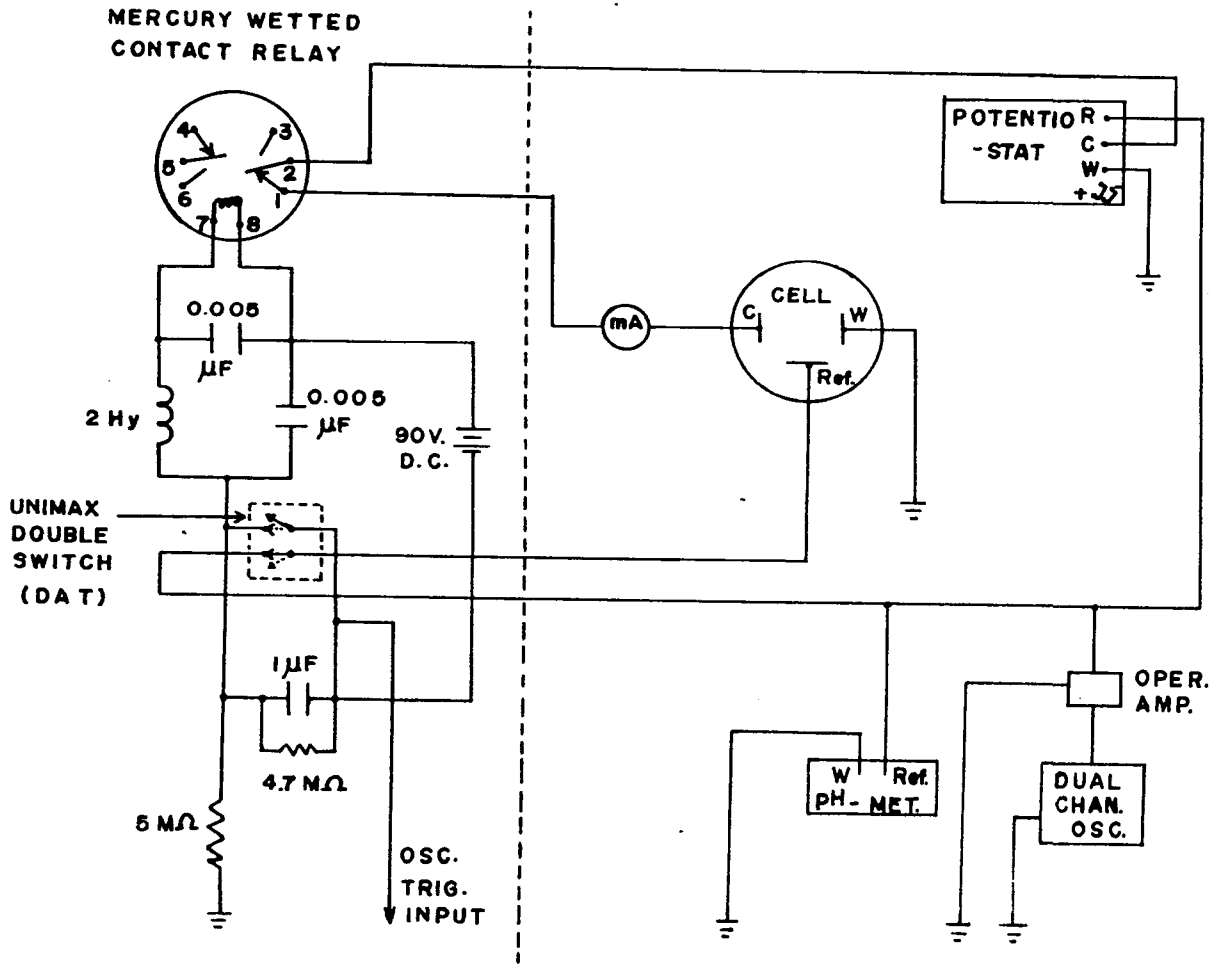
MERCURY WETTED
CONTACT RELAY
4
3
5
2
6
1
7
8
0.005
μF
2 Hy
0.005
μF
90V.
D.C.
UNIMAX
DOUBLE
SWITCH
(DAT)
1μF
4.7 MΩ
5 MΩ
OSC.
TRIG.
INPUT
mA
CELL
C
W
Ref.
POTENTIO
-STAT
R
C
W
+25
OPER.
AMP.
W
Ref.
PH-MET.
DUAL
CHAN.
OSC.

(ii) Correction of Measured Potential for iR drop (Ohmic Overpotential, ΔV_R): In the steady-state kinetic runs, the electrode was polarised potentiostatically into the region of current density where ohmic potential drops between the electrode and the Luggin capillary could be significant. Moreover, curves which appeared to exhibit "inhibition" behaviour, an effect that might in fact have arisen from iR error, were being investigated so that it was of some importance to establish the magnitude of any iR effects at high anodic currents. "iR" corrections were therefore made in all the high c.d. measurements by observing the virtually instantaneous initial drop of potential ΔV_R when the electrode was put on open-circuit decay. The open-circuit decay transient was photographed on an oscilloscope by running the time base fast (< 0.1 msec. cm^{-1}) and applying the electrode p.d. through a high input impedance stage with small rise-time (Tektronix type "O" operational amplifier in cathode follower configuration). ΔV_R was determined from the picture after appropriate enlargement.

The conventional circuit diagram for open-circuit decay measurements is shown in Fig. 7. The electrode was first polarized potentiostatically to a potential V and then by operating a fast micro-switch the electrode was put on open-circuit and the e.m.f. decay

recorded. In this arrangement, the reference electrode was also disconnected by the relay system at the same moment that the working electrode was put on open-circuit.

(iii) Potentiostatic Step Charging Technique: The potentiostatic step charging method is similar, in principle, to Eigen's (133) relaxation methods developed by him for kinetic studies of very fast reactions. In this method, if a single step equilibrium is disturbed by changing an external parameter (viz. temperature, pressure or electrical field intensity) which influences the equilibrium of the system, the new equilibrium state will be reached at a rate characterised by the relaxation time τ (Langevin time). The constraint applied may be changed (A) periodically (harmonic oscillation), (B) in a single impulse having some characteristic form, e.g. a linear sweep, or (C) in a rectangular step. Various applications of these principles have been used in electrochemistry (117,134-140) including studies of the kinetics of surface oxidation of Pt (137).

In the present work, the experimental and theoretical bases for the potentiostatic step charging method for calculation of the adsorption pseudo-capacitance of an electrode have been further developed. The theoretical principles will be discussed in Chapter IV.

For potentiostatic (rectangular) step charging,

Figure 8. Programme for pre-conditioning of the electrode prior to potentiostatic step charging, with following steps and reduction transient shown.

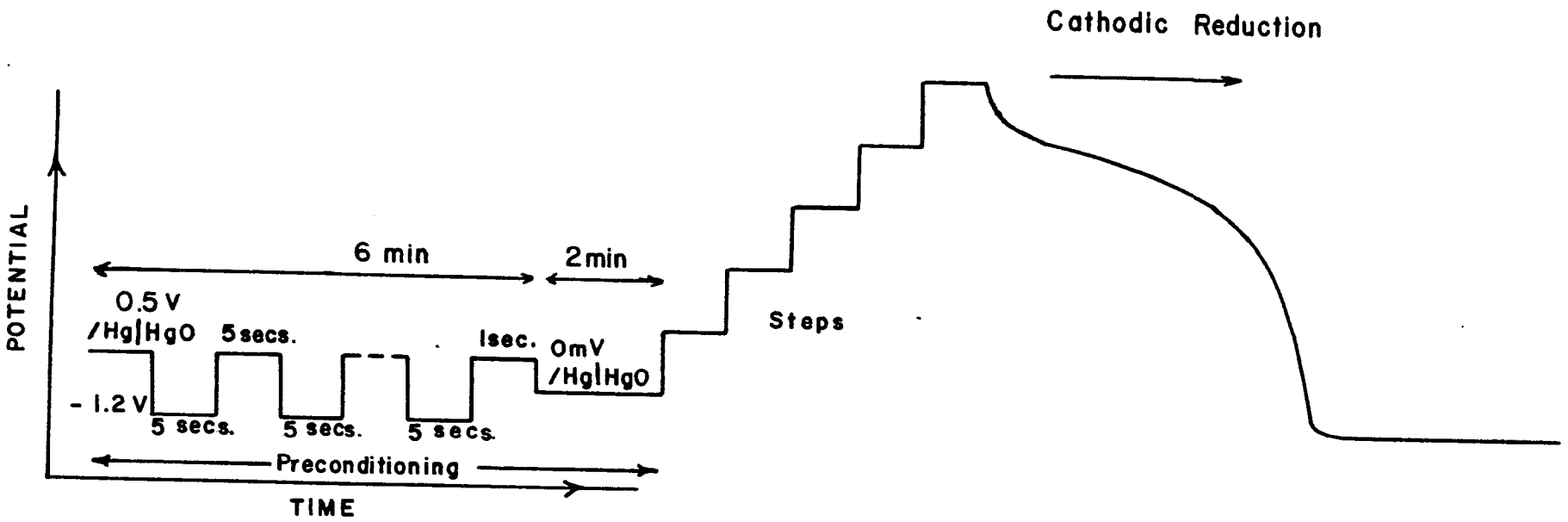
Cathodic Reduction
POTENTIAL
6 min
2min
0.5 V
/Hg|HgO
5secs.
1sec.
0mV
/Hg|HgO
Steps
- 1.2 V
5 secs.
5 secs.
5 secs.
Preconditioning
TIME

Figure 9. Manual step-function switching circuit using two Honeywell slide-wire potentiometers.

STAIRCASE POTENTIAL FUNCTION

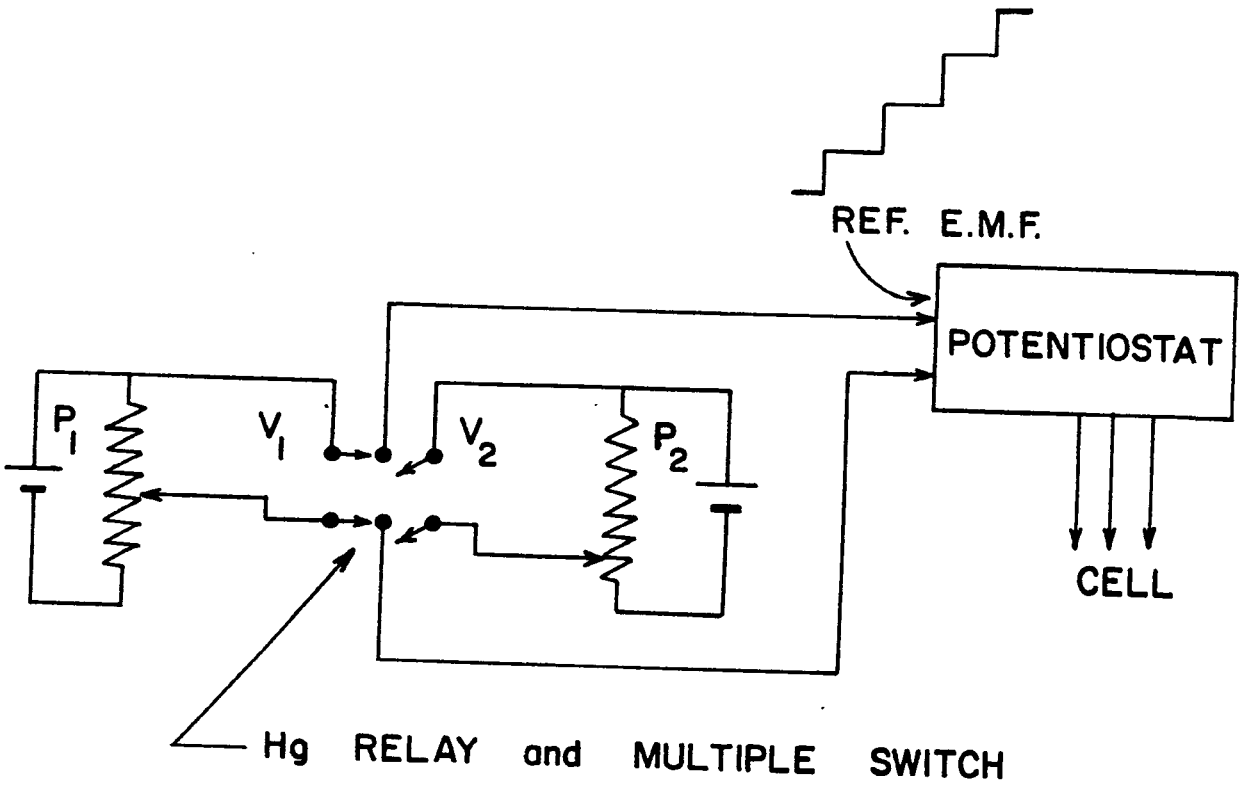

freshly annealed metallic nickel electrodes (prepared as described under section 3(a), (i) of this Chapter) as well as electrochemically pre-conditioned electrodes were used. With fresh electrodes, potentiostatic step charging was commenced just after breaking the bulb under the solution and placing the electrode close to the Luggin capillary. In other cases, the electrodes were pretreated electrochemically according to the conditioning programme shown in Fig. 8. Nitrogen was bubbled around the electrodes.

The principle of the potentiostatic (rectangular) step charging method* is illustrated in Fig. 9. The electrode is polarised to a certain potential V_1 by switching on the potentiometer P_1. When a steady-state condition is reached, the potentiometer P_2 with a preset higher value of potential V_2 is switched in, replacing P_1 and its potential V_1, through a fast acting mercury vacuum relay; the resulting oscilloscopic current-time transient is recorded photographically. In the meantime, another higher potential V_3 is set on P_1 and is then switched in, replacing the previous potential on P_2. This process is continued

---

*It is analogous electrochemically to the temperature jump method employed in kinetics of fast homogeneous reactions. A relaxation current flows in response to the step in the intensive variable, potential.

Figure 10. Circuit diagram for the potentiostatic (rectangular) step function (manually operated).

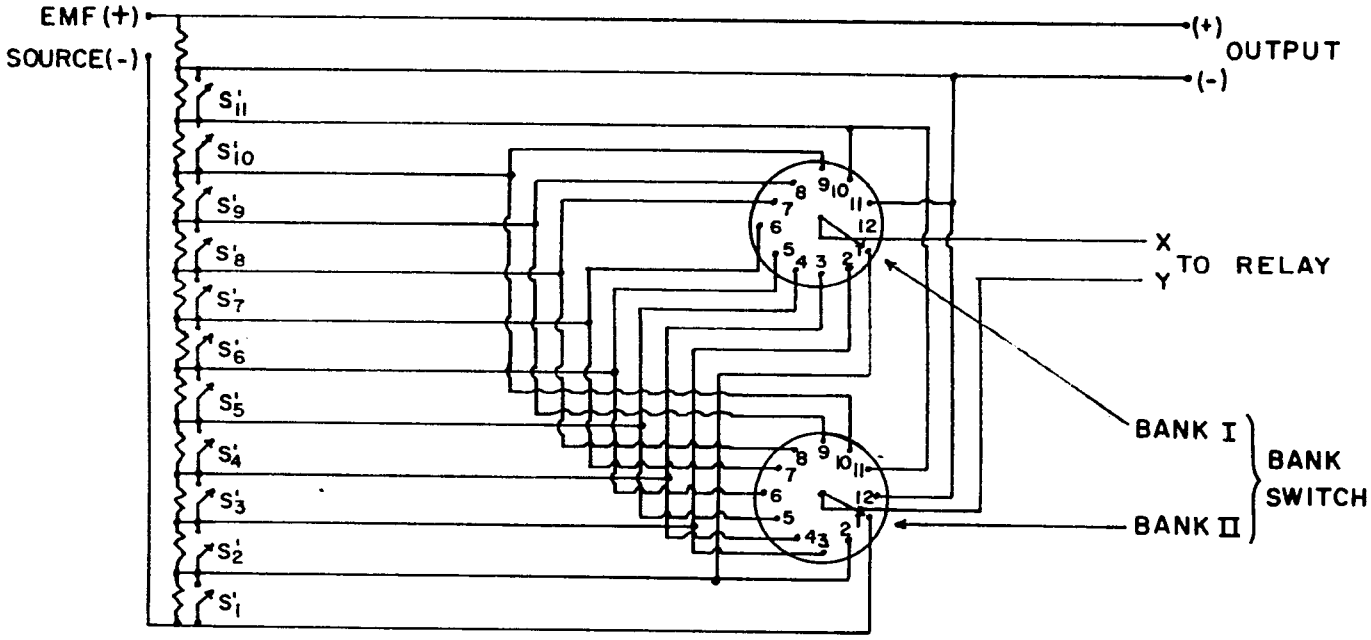

POTENTIAL STEP FUNCTION SWITCH SYSTEM

Figure 11. Schematic circuit diagram for potentiostatic step charging technique (including the additional circuit for galvanostatic discharging transients following potentiostatic step polarisation).

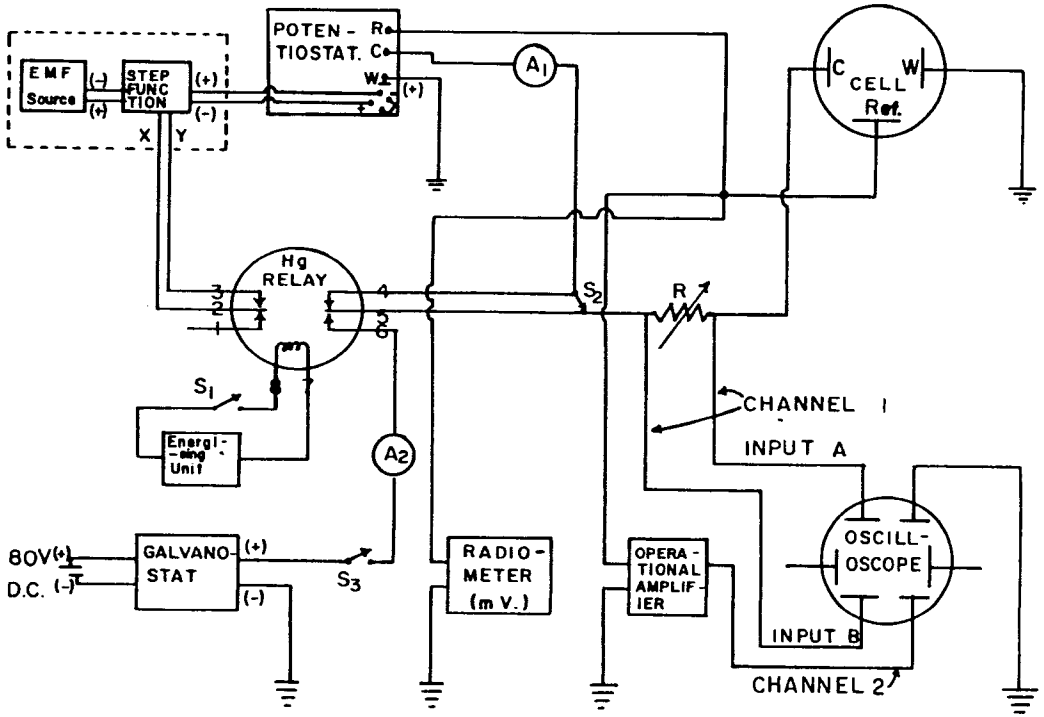

FOR POTENTIOSTATIC STEP CHARGING: SWITCH S_2 - "ON" AND SWITCH S_3 "OFF"

FOR GALVANOSTATIC REDUCTION: SWITCH S_2 - "OFF" AND SWITCH S_3 "ON"

OPERATION CARRIED OUT BY OPERATING SWITCH S_1

RELAY CONNECTION SHOWN IN "UNENERGISED" CONDITION

until the electrode is polarised up to the highest potential under study in a "staircase" manner of potential increase. All potential increments are applied for controlled measured times. The current-time transients for all the steps can be recorded photographically and the steady-state currents at all potentials can also be measured on a "Sensitive Research" milliammeter connected in series with the counter electrode.

In the present experiments, the electrode was polarised in steps using the circuits shown in Figs. 10 and 11. At the bottom step, all switches S'_1 to S'_{11} (Fig. 10) were in the off position (i.e. open) and the "Bank Switch" (Fig. 10) was set in position 1 and the potentiometer of the potentiostat was at the zero position. By operating the switch S_1 (Fig. 11), the terminals across S'_1 (see Fig. 10) were shorted through the relay switch via the Bank switch and hence the output voltage across the step-function generator was higher and thus the input voltage, externally fed to the potentiostat, was raised to a higher value. Since the shorting was achieved momentarily through the fast acting mercury relay, the potential of the polarised working electrode was also raised virtually instantaneously. The current-time transient was photographed from the oscilloscope. Keeping the relay switch closed, switch S'_1

was then closed and the relay switch was then re-opened, with the electrode potential remaining constant. The "Bank Switch" was then shifted to position 2 and again, by operating S_1, the potential of the electrode was raised in a rectangular step and the current-time transient was recorded, as above. By carrying out similar repetitive operations, the working electrode was polarised in potentiostatically controlled steps from the lowest potential to approximately 0.9 V with respect to the Hg/HgO reference electrode. The values of potential at each step and the corresponding steady currents were also recorded.

The charge and hence change of degree of surface oxidation at the electrode interface was calculated for each potential step from the respective experimental current-time transients in the manner described in Chapter IV.

In order to achieve the best accuracy in the integration of areas under the curves, photographs were taken on 35 mm. negatives and traced on metric graph paper at an enlargment of about eight times.

(iv) Potentiodynamic Repetitive and Single Sweep Experiments: The potentiodynamic linear sweep method was originally employed by Sevčik (141) and later used by Delahay and Perkins (142) for diffusion controlled processes. This method has been extensively

Figure 12. Schematic circuit diagram for the potentiodynamic triangular (linear)sweep method.

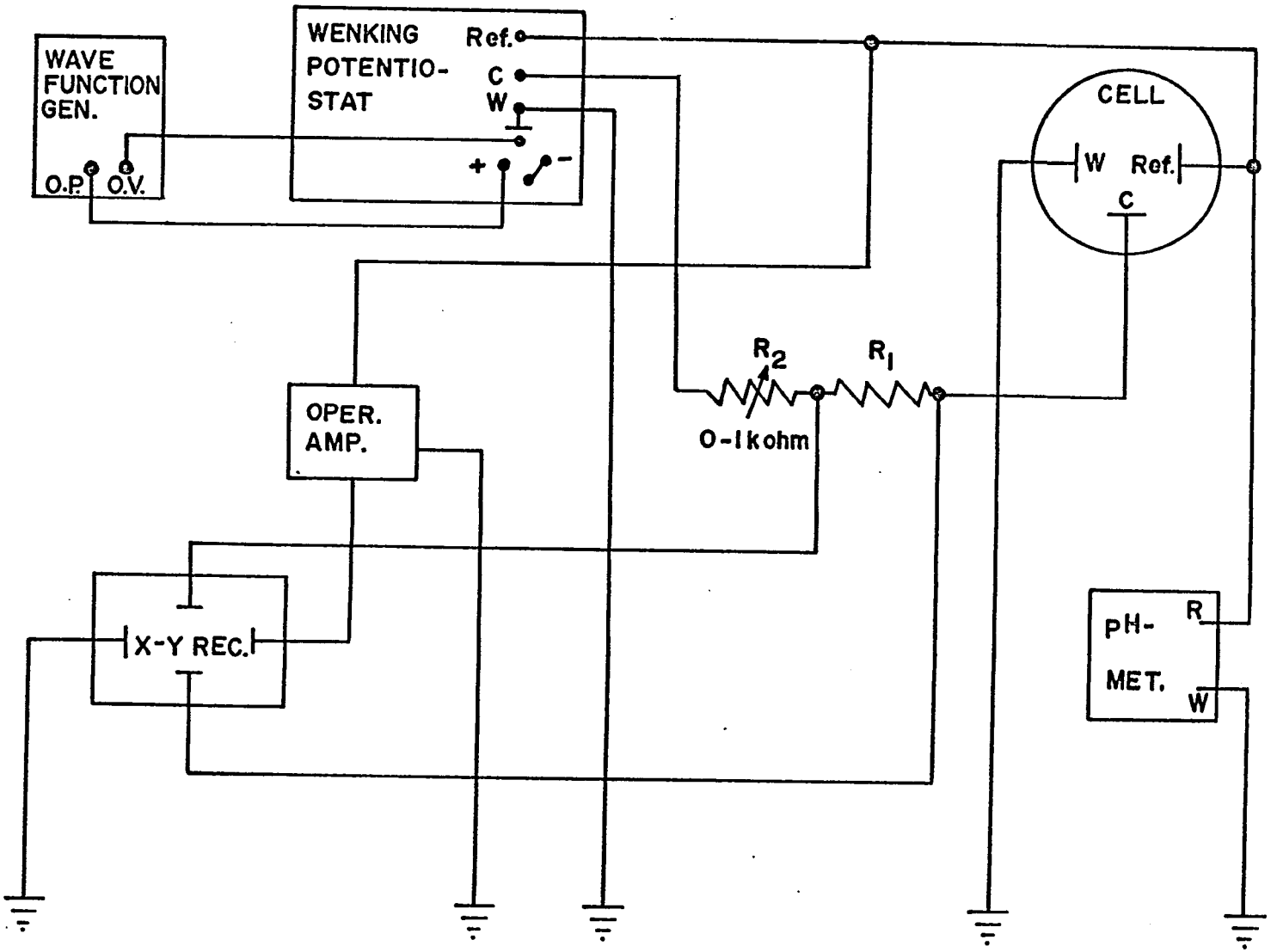
WAVE
FUNCTION
GEN.
O.P
O.V.
WENKING
POTENTIO-
STAT
Ref.
C
W
+
-
CELL
W
Ref.
C
R2
R1
0-1kohm
OPER.
AMP.
X-Y REC.
pH-
MET.
R
W

used by Will and Knorr (118) and Breiter (25,26,119) for studying both diffusion and activation controlled processes.

The circuitry (Fig. 12) used for potentiodynamic sweep measurement is a modification of the one used for the steady-state measurements (cf. Fig. 6). Here the desired programmed reference signal (viz. triangular, sinusoidal, rectangular etc.) drawn from the output of a "Servomex" wave function generator is fed to the reference input (control) of the potentiostat. The potential of the working electrode (vs. the reference electrode potential) then varies according to the selected programmed signal and is fed through a high impedance amplifier stage to the X-axis input of the oscilloscope or the X-Y recorder. Therefore, the X-axis is driven externally by the operation of the function generator. A calibrated decade resistance R_1 is connected in series with the counter electrode. When current passes through the cell, a potential difference is developed across this resistor. This potential difference is then fed to the Y-axis input of the oscilloscope (to the A and B inputs) or the recorder (signal not grounded) on which it is displayed as a function of time (or potential). Thus the transient current $i_{(t)}$ passing through the cell at a given moment arising from the programmed change of electrode potential is measured as a potential difference

$\Delta V_{(t)}$ ($\Delta V_{(t)} = i_{(t)} \cdot R_1$) developed across the resistor. Any noise in the Y-axis signal is suppressed by using an input filter (Hewlett Packard Model 17106 A) and any auto-oscillation is damped by a resistance R_2 in series with the counter electrode. The shape of the current-time (or potential) transient depends on the nature of the potential programme and on the electrochemical behaviour of the process under investigation. A satisfactory display of the current is obtained by suitably selecting the value of the resistance R_1 for an appropriate sensitivity of the Y-axis of the oscilloscope or the recorder. A minimum value of the resistance R_1 with the maximum sensitivity of the Y-axis is preferred. For optimum results, the working electrode, the operational amplifier and the oscilloscope are grounded.

The range of potential (amplitude) over which the electrochemical process is to be investigated is adjusted by appropriate settings on the potentiostat and the function generator. During setting, the extreme end potentials of the wave are first roughly read on the meter on the potentiostat. The final adjustment of the potential range is, however, always made by taking readings on the potentiometer.

In the present potentiodynamic charging and discharging experiments on nickel and silver, a symmetrical triangular wave-form was used. The current-time (or current-voltage) transients were recorded on the X-Y recorder

for slow sweep rates and on the oscilloscope for faster sweeps. Single pulse, single cycle and repetitive cycles could be used.

The oxide formation and reduction peak potentials were investigated on nickel and silver as a function of sweep rate over a constant range of potential. The surface oxidation and reduction processes were also investigated as a function of the range of potential scanned, starting from a fixed cathodic potential at a constant sweep rate.

(v) Galvanostatic Charging or Discharging Procedure: In the galvanostatic charging method (various procedures are reported in refs. 143-147), a pulse of constant anodic current is instantaneously imposed on the electrode under investigation whereas in the galvanostatic discharge technique, the electrode is first polarised anodically to a steady-state with a potentiostat and then a constant cathodic current is superimposed instantaneously after switching off the anodic current in order to force the reverse of the charging reaction to occur. In both cases the time dependence of the potential is followed on a recording instrument. In these experiments, N_2 gas was at all times bubbled around the electrodes.

In the present work, the charge for electrochemical reduction of the surface oxide on the nickel

Figure 13. Schematic circuit diagram for the galvanostatic discharge method.

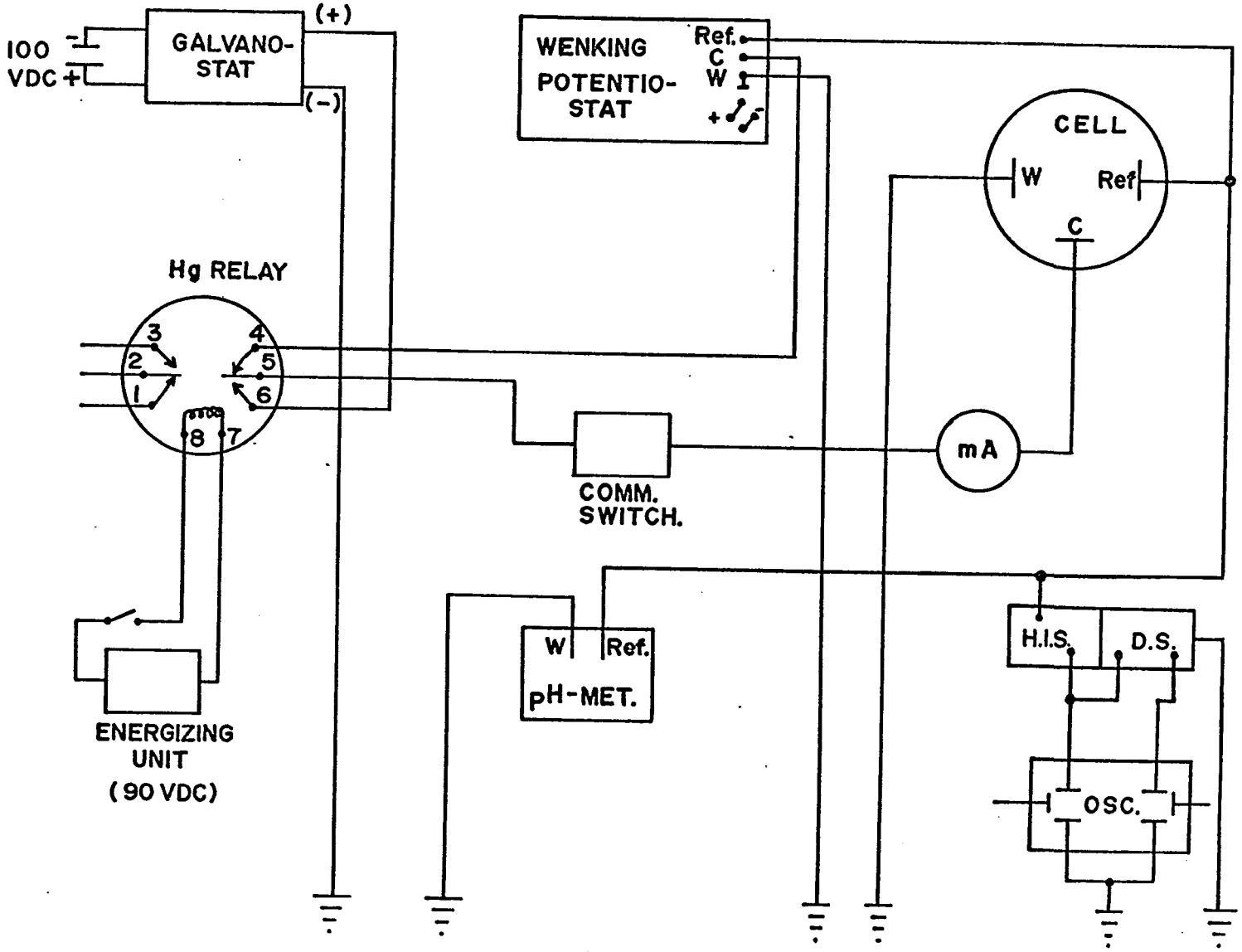
100 VDC
GALVANO-STAT
(+)
(-)
WENKING POTENTIO-STAT
Ref.
C
W
CELL
W
Ref
C
Hg RELAY
1
2
3
4
5
6
7
8
mA
COMM. SWITCH.
ENERGIZING UNIT (90 VDC)
W
Ref.
pH-MET.
H.I.S.
D.S.
OSC.

Figure 14. Schematic electrochemical pre-treatment programme (galvanostatic).

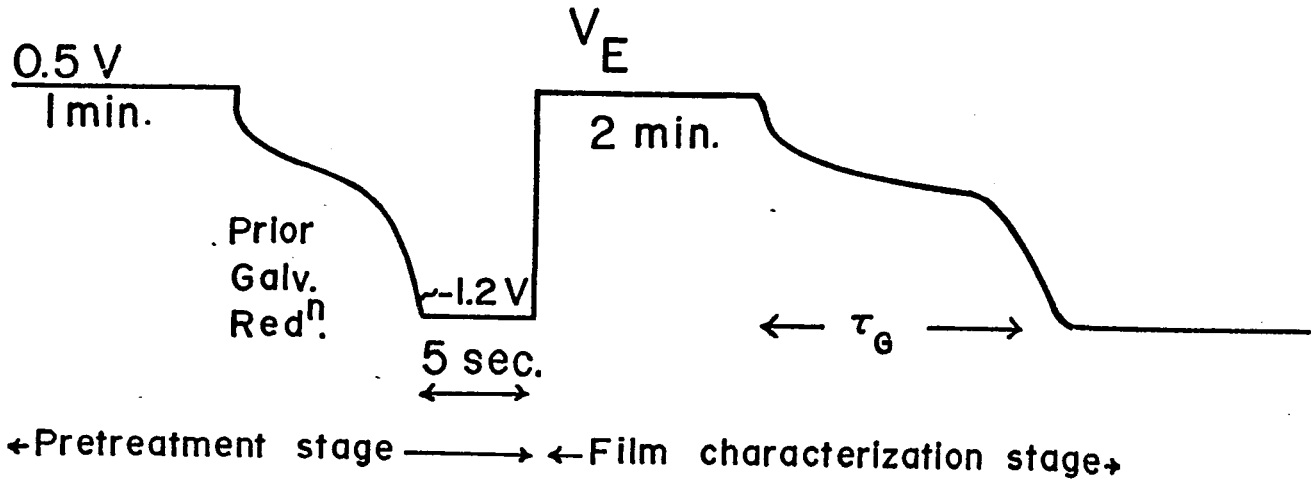
0.5 V
1 min.
Prior
Galv.
Red^{n}.
~-1.2 V
5 sec.
V_E
2 min.
τ_G
←Pretreatment stage——→
←Film characterization stage→

electrode was determined by the fast differential galvanostatic discharge method of Kozlowska and Conway (120). The circuit used in this method is shown in Fig. 13. In the unenergised condition of the mercury relay, the galvanostatic circuit through the relay is open whereas the anodic polarizing circuit of the potentiostat is closed. When the microswitch is closed, the mercury relay switch is energised causing the galvanostatic circuit to be closed and the potentiostatic circuit to be opened simultaneously. A reversed current is then imposed on the working electrode causing the reverse reaction to commence at the electrode. A single milliammeter could be used for measuring both the anodic and the cathodic currents by changing the polarity with a commutator switch.

In this part of the work, the electrode was potentiostatically polarised first to 0.5 V for 1 min. to form an oxide. Then to obtain a clean metal surface this oxide was reduced in a cathodic galvanostatic pulse and the following stage of reduction by hydrogen, and the clean electrode was again polarised potentiostatically for a controlled time (2 min.) to the experimental potential (V_E) from which the oxide reduction charge was to be determined (Fig. 14); the potentiostatic polarising circuit was then opened by pressing the microswitch and a constant-current reduction pulse (0.5 - 1 a. cm^{-2}) was applied simultaneously. The direct galvanostatic potential *vs* time transient and

Figure 15. Circuit diagram for suppression of noise in the differential of the discharge transient.

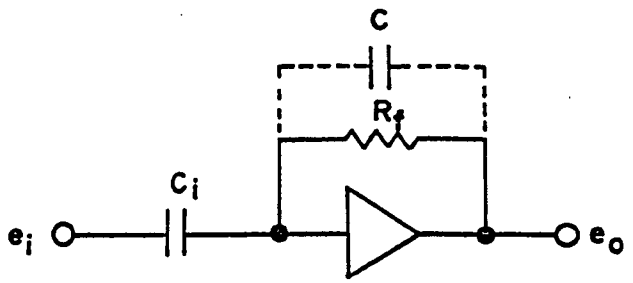

$$e_o = -R_f C_i \frac{de_i}{dt}$$

For noise suppression, $C = C_i / 100$

OR

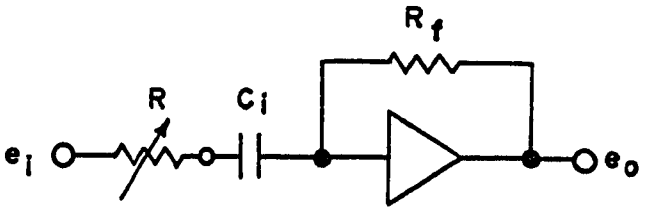

For noise suppression, R = 0 - 10 k ohm.

its electronically differentiated form were recorded on a dual-beam oscilloscope. From the "transition time" (i.e. the time interval between the occurrence of the differential peaks for double-layer charging and for complete reduction of oxide) and the known magnitude of the constant cathodic current, the charge associated with oxide reduction could be calculated.

Under certain conditions, the differentiated signal becomes noisy. In this case (Fig. 15) a noise suppression capacitor may be placed in the feedback circuit or a resistor (0 - 10 kohm) in the input circuit to limit the high-frequency response above the signal frequency.

(vi) Determination of Loss of Charge on Open-Circuit E.m.f. Decay: It is well known that the charged nickel oxide electrode suffers an internal loss of electrochemically active material when it is left standing in alkaline solution on open-circuit. In order to investigate this behaviour further, experiments were performed in which the electrode was polarized potentiostatically to a certain potential for a definite period of time, after the usual pre-conditioning programme; the electrode was then kept on open-circuit for various controlled periods of time (τ_D), after the lapse of which, a fast galvanostatic cathodic pulse was automatically applied. The potential-time transients

Figure 16. Circuit diagram of the time-delay-relay (J. Wojtowicz and B.E. Conway).

MERCURY WETTED
CONTACT RELAY
MODEL JM2 110-22

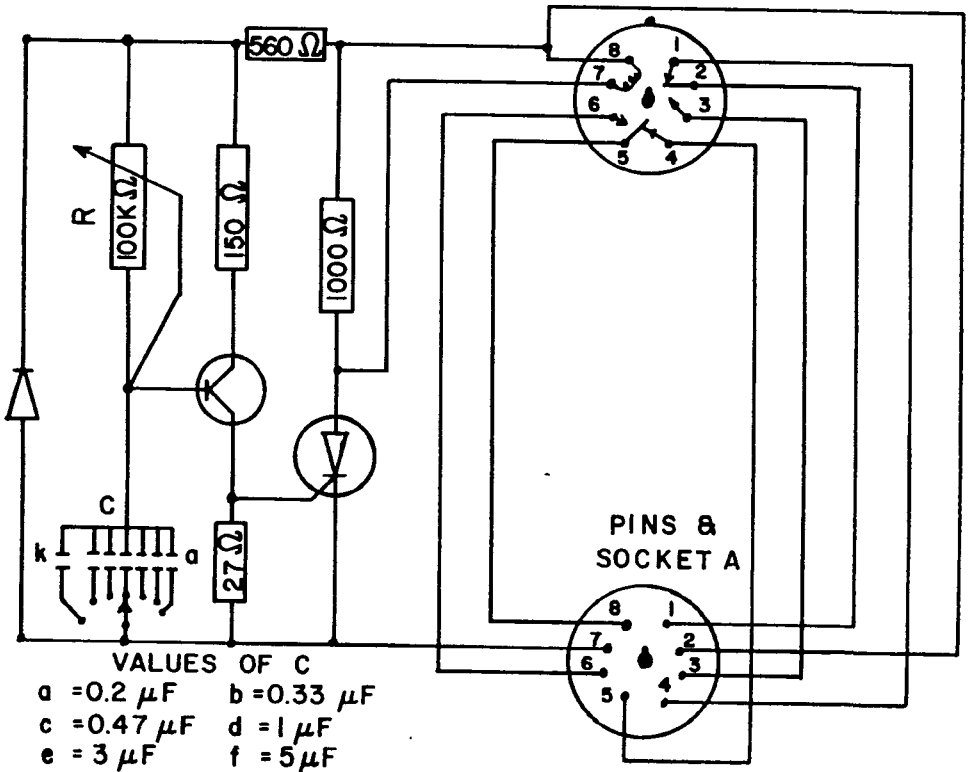

VALUES OF C

a = 0.2 μF	b = 0.33 μF			
c = 0.47 μF	d = 1 μF			
e = 3 μF	f = 5 μF			
g = 10 μF	h = 20 μF			
i = 50 μF	j = 68 μF	k = 100 μF		

TIME DELAY, $\tau[m.s] \doteq 1.3R[K\Omega] \times C[\mu F]$

Figure 17. Schematic circuit diagram for galvanostatic discharge with prior open-circuit decay of e.m.f. for controlled time.

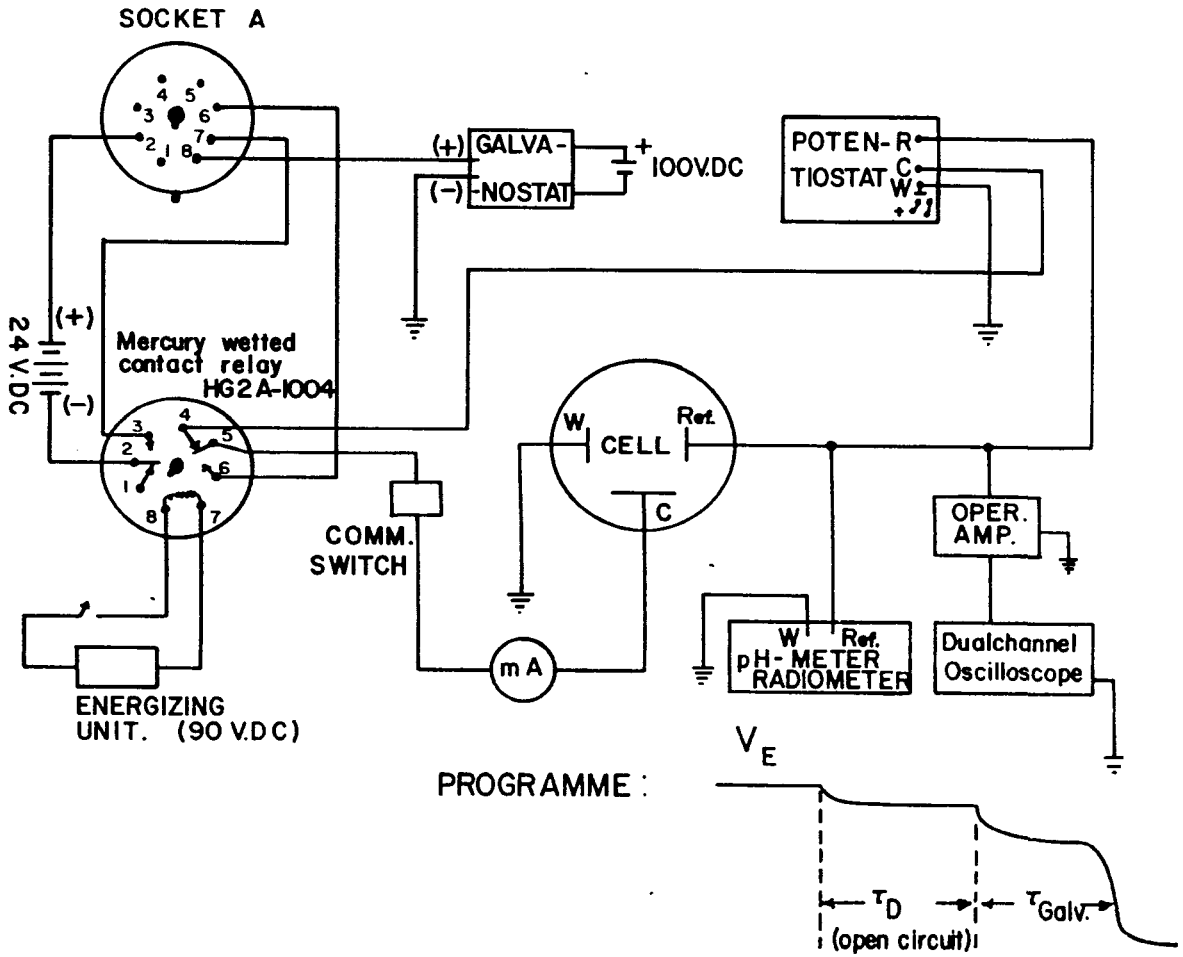
SOCKET A
(+) GALVA-
(-) -NOSTAT
+
100V.DC
POTEN-R
TIOSTAT C
W
24 V.DC
(+)
(-)
Mercury wetted
contact relay
HG2A-1004
W
CELL
Ref.
C
COMM.
SWITCH
OPER.
AMP.
mA
W
Ref.
pH-METER
RADIOMETER
Dualchannel
Oscilloscope
ENERGIZING
UNIT. (90 V.DC)
PROGRAMME :
V_E
τ_D
(open circuit)
$\tau_{Galv.}$

with their differential coefficients were photographed. The oxide reduction charge passed in the cathodic pulse was determined as above (under 8(b), (v)) and hence the amounts of electrochemically reducible material remaining after various τ_D were deduced. Both the length of the period τ_D and the moment of application of the galvanostatic cathodic pulse after the time τ_D were regulated electronically by a "time delay relay", the circuit of which is shown in Fig. 16. The general experimental circuit which is shown in Fig. 17 is in fact a modification of the one used for the galvanostatic discharge measurements (cf. Fig. 13).

Purified N_2 gas was bubbled around the working and the counter electrodes during all these experiments.

(vii) Potentiostatic Step Charging Procedure with Following Galvanostatic Discharge: The results from the step charging method were compared with those from the fast galvanostatic reduction method. After the electrode had been polarised in steps up to the highest potential, the total charge associated with (electrochemically reducible) oxide species at the electrode was also estimated by a single fast galvanostatic reduction transient. The essential principle is shown schematically in Fig. 8.

The diagram of the circuit used in this experiment is shown in Fig. 11. By keeping the switch

S_2 "closed" and S_3 "open", the electrode could be charged potentiostatically in steps in the manner described in section 8 (b), (iii) of this chapter. After stepwise polarization up to the highest potential, the switch "S_2" was opened and "S_3" was closed and then by operating "S_1", the galvanostatic cathodic reduction pulse was imposed simultaneously with the opening of the potentiostatic polarizing circuit. The current-time transient was recorded on one channel and the galvanostatic potential-time transient on the second channel of the oscilloscope.

(viii) Kinetics of Growth of Nickel Oxide: In this part of the work, the electrode was first electrochemically pre-conditioned according to the scheme shown in Fig. 14, and then kept potentiostatically at the experimental potential V_E for a controlled period of time, t. At the end of this period, a fast galvanostatic cathodic pulse was applied as described above (section 8(b), (v)) in order to determine the charge required for reduction of the active "O" in the oxide film. Amounts of oxide formed at constant potential for various lengths of time could hence be determined.

9. ANALYTICAL PROCEDURE

(a) Search for a Suitable Method

For determining the stoichiometry of nickel oxide

in the form of thin films at the metal electrode surface, methods were sought which would give a complete and rapid stripping of the oxide film without appreciable continuing attack of the metal. Two reagents were employed in separate types of experiment: aq. KCN for complexation of the Ni (148); aq. N_2H_4 for reduction of the oxide and complexation of the Ni. The latter reagent was employed first in a chemical method for determination of the "active" oxygen. Dimethylglyoxime was also investigated as a reagent for the Ni determination. The quantities of Ni were, however, too small for gravimetric determinations to be satisfactory and the colorimetric procedure with this reagent is less accurate than that using KCN to form the $[Ni(CN)_4]^{2-}$ complex which has a strong absorption in the u.v.

Method (i): The amount of nickel metal oxidized in the formation of the anodic film was determined by dissolving off the oxide film from the metal in a known volume of 0.5% KCN solution which was previously deoxygenated by bubbling purified N_2 gas. The absorbance of the complex, $[Ni(CN)_4]^{2-}$ was measured at 268 mμ (148) and the amount of nickel present was calculated from a Beer-Lambert calibration plot. Corrections for any dissolution of pure metallic nickel in the 0.5% KCN solution were introduced into the final calculation for the amount of nickel present in the oxide

film. From knowledge of the amount of nickel and the "active" oxygen content of the film, determined electrochemically, the stoichiometry of the oxide can be deduced.

Method (ii): In the second method, the electrode was polarised as described above, and the oxide was then reductively dissolved in a known volume of standard (0.02M) hydrazine solution (or ammoniacal hydrazine to complete the dissolution of the Ni in the film) which was first deoxygenated by bubbling pure nitrogen in order to prevent oxidation of hydrazine by atmospheric oxygen and to minimize oxidation of metallic nickel. All the experiments with hydrazine were carried out in an atmosphere of purified nitrogen. Hydrazine reduces higher valent nickel in the oxide to the divalent state which becomes complexed as follows:

$$4\ NiOOH + N_2H_4 \rightarrow 4Ni(OH)_2 + N_2 \qquad I$$

or

$$2\ NiO_2 + N_2H_4 \rightarrow 2\ Ni(OH)_2 + N_2 \qquad II$$

with

$$Ni(OH)_2 + x\ N_2H_4 \rightarrow [Ni(N_2H_4)_{x=2,3}]^{2+} + 2OH^- \qquad III$$

Theoretically, if no other side reactions occur leading to a loss of hydrazine (see below), then determination of the amount of hydrazine reacted, enables the quantity of available "active" oxygen, [O], to be calculated using the

following equation:

$$N_2H_4 + 2[O] \rightarrow N_2 + 2H_2O \qquad IV$$

Hydrazine can be quantitatively estimated before and after the experiment by determination with iodate (149) and a number of experiments were carried out by this procedure.

For an alternative estimation of nickel, a small portion of the original solution, after reductive complexation of the oxides with hydrazine, was evaporated to dryness in a dish on a water bath and the residue dissolved in a known volume of 0.5% KCN solution. Since the CN group is one of the strongest ligands, it replaces NH_2NH_2 from the $[Ni(N_2H_4)_{x=2,3}]^{2+}$ complex to form $[Ni(CN)_4]^{2-}$. Hence the nickel content of the sample can be determined by measuring the absorbance of the solution at 268 mμ as before, using 0.5% KCN as the reference solvent.

The u.v. spectrum of $[Ni(CN)_4]^{2-}$ solution determined against 0.5% aq. KCN as reference is shown in Fig. 49 (Chapter III) and, for comparison, the spectrum of $[Ni(CN)_4]^{2-}$ prepared from $[Ni(N_2H_4)_{x=2,3}]^{2+}$ and measured against the same reference is superimposed.

This method (ii) was first tested using precipitated nickelic oxide, NiO.OH (Ni^{2+} + KOH with potassium

hypobromite (150)) in order to determine both the Ni (by KCN) and the active oxygen by means of hydrazine. The results were encouraging (see Fig. 51, Chapter III) in so far as at relatively short treatment times (up to 30 min.) a constant value of the active oxygen : nickel ratio (= 0.5, corresponding to "Ni_2O_3" or NiO.OH) was obtained. However, after longer times (see Fig. 51 (b) Chapter III) a substantial increase of this value became evident. It is known that hydrazine decomposes to N_2 and NH_3 through the reaction

$$3\ N_2H_4 \longrightarrow N_2 + 4\ NH_3\ , \qquad V$$

a process which is catalysed in the dry state by NiO (151); the high apparent values of the O:Ni ratio may hence arise because some of the N_2H_4 becomes lost by catalytic decomposition, in addition to loss by reaction with active "O".

Application to large area oxidized nickel gauze electrodes gave the results shown in Table VIII (Chapter III) where again the chemically determined active "O" is much larger than the electrochemically determined values, based on the cathodic reduction transients. Here some of the loss of N_2H_4 may be due to catalytic decomposition by the underlying metal once the oxide film is stripped. Hence, it was concluded that the oxidative loss of N_2H_4 cannot be used reliably as a method for determination of the active

"O" at nickel electrodes. Cathodic reduction (see Section 8(b), (v)) must therefore remain the preferred method, since reaction with iodide in acid media would be relatively unsatisfactory for thin film oxide. However, in order to use the cathodic reduction method for accurate determination of the active "O", it is first necessary to ascertain the extent of reduction of the oxide in a cathodic pulse (see below, (b) (iii)).

(b) Experimental Procedure

(i) Preparation of Test Electrodes: Two types of electrodes were used: (A) Wire electrodes as described in section 3(a), (i) above and (B) Commercial pure nickel wire gauze; the latter was formed into large area electrode of cylindrical shape and cleaned in an aq. ammonia-hydrazine mixture and then washed in distilled water several times until it was free from hydrazine.

(ii) Determination of Electrochemically Reducible Oxide ("Active" oxygen [O] content): The charge for electrochemical reduction of the oxide film was measured by the fast differential galvanostatic cathodic transient method (120) described above.

Before dissolving the oxides in the course of the subsequent analytical operations for determination of the amount of nickel oxidized in the formation of the

anodic film, the charge for electrochemical reduction of the active "O" for each electrode and for each potential was determined in six separate experiments; the data were then averaged to obtain a final mean value. For each potential, a different electrode was used.

(iii) Extent of Reduction of Higher Valent Nickel Oxides in a Fast Galvanostatic Pulse: A series of experiments was carried out to investigate if higher valent nickel oxides are reduced to the Ni(II) state in a fast galvanostatic reduction pulse (cf. refs. 27,54) and if hydrogen gas evolves on the lower valent oxide ($Ni(OH)_2$) itself. The electrode was polarized for 2 mins. at a certain potential in the usual manner and the reduction charge was determined galvanostatically. Just after the end of the cathodic reduction pulse, the electrode was removed and the oxide was stripped in 0.5% aq. KCN and the amount of nickel (from the oxide) complexed was determined spectrophotometrically. Another electrode was polarized at the same potential for 2 mins. in an identical manner but without discharging it; the oxide was then stripped in 0.5% aq. KCN solution and the amount of nickel again determined. Experiments were carried out at three potentials and the results are given in Table IX (Chapter III).

(iv) Analytical Determination of the Amount of Nickel in the Oxide Film: The amount of nickel oxidized in the controlled formation of the thin oxide film was determined by dissolving the film in a known volume of deoxygenated 0.5% aq. KCN solution or in 0.02M NH_2NH_2 solution as described above. The oxide electrode was kept in the complexing solution for controlled times in the range 2-5 mins. during which period the oxide film dissolved completely giving a bright nickel surface. The reaction was carried out in an atmosphere of purified nitrogen.

When 0.5% KCN solution was used as the complexing agent, the resulting homogeneous solution was directly used for measuring the absorbance at 268 mμ using 0.5% aq. KCN as the reference solution. When 0.02 M NH_2NH_2 solution was used, the procedure described on p.95 was employed.

(v) Corrections for Corrosion of Nickel: The amount of nickel resulting from the dissolution of the oxide was corrected for the microquantity of nickel which also

dissolves on account of corrosion of the metal itself in deoxygenated 0.5% KCN solution and also in NH_2NH_2 solution (see Fig. 52). The corrections were made as a function of the time ($\tau_{dis.}$) for which the electrode was kept in the solution (see Fig. 52). The complexing solution was first deoxygenated by bubbling purified nitrogen for 15 min. while the electrode in the glass bulb was kept in the solution. The bulb was then broken beneath the level of the solution and the electrode was kept in solution for various times $\tau_{dis.}$ in the presence of nitrogen, after which the electrode was removed and the amount of nickel dissolved by corrosion was determined spectrophotometrically.

CHAPTER III

RESULTS

1. POTENTIOSTATIC STEADY-STATE KINETICS: EVOLUTION OF OXYGEN

The formation of oxide films at nickel is closely connected with the kinetics of anodic oxygen evolution at nickel since the intermediates in the latter reaction constitute the surface species on the oxide film. The same applies to silver, also considered in the present work. While the study of the formation and properties of such films constituted the main aspect of the work reported in this thesis, it will be logical and convenient to present first the results for the oxygen evolution behaviour, since the formation of oxides in various states of oxidation can then be related to potential in terms of the framework of kinetic processes in oxygen evolution and intermediates that may be involved in that reaction.

In the steady-state method for the study of reactions occurring at electrode surfaces, the rate of reaction is measured directly in terms of current, i, as a function of potential, V. In certain favourable cases, the reaction mechanism(s) can be elucidated by determining the values of the Tafel slope, b (=dV/dlog i) (4,6,77,122,154), the stoichiometric number, γ (155-158) (which can be calculated from the quantity $\frac{4F}{RT}\left(\frac{1}{b_a} - \frac{1}{b_c}\right)^{-1}$ where b_a and b_c are the

anodic and the cathodic Tafel slopes (122,159)) or the reaction order, $[\delta \ln i / \delta \ln c]_V$ (160-161). These three different but related approaches have, in a number of favourable cases, been used complementarily for elucidation of reaction mechanisms.

In the present work, the Tafel slope has been considered and in the potentiostatic steady-state kinetic analysis, log[i]-V curves for ascending and descending directions of potential change have been constructed for nickel metal electrodes and also for silver electrodes for comparative purposes. The current-potential graphs shown in the following pages were based on 30 to 50 points in each direction but for convenience of presentation, the individual points have been shown on only two of the graphs (Fig. 21a and b).

All current densities considered in the results are referred to the apparent geometrical area since real area measurements based on internal H accommodation factors cannot be made on Ni as they can on the more noble metals. Determination of true current densities at Ag electrodes is more difficult than at Ni electrodes because the silver oxides (Ag_2O, AgO etc.) formed during oxidation are appreciably soluble in aq. KOH and, consequently, the real geometrical area of the electrode can change during the runs.

(a) Kinetics of Evolution of Oxygen at Nickel Electrode Surfaces

(i) Effects of Purification of the Potassium Hydroxide Solution: In two or three steady-state kinetic measurements at 25°C, highly purified KOH

Figure 18. Comparison of steady-state potentiostatic log[i]-V relations for nickel electrodes in 0.122 M aq. KOH (25°C) prepared according to (a) the high purification technique and (b) the standard method.

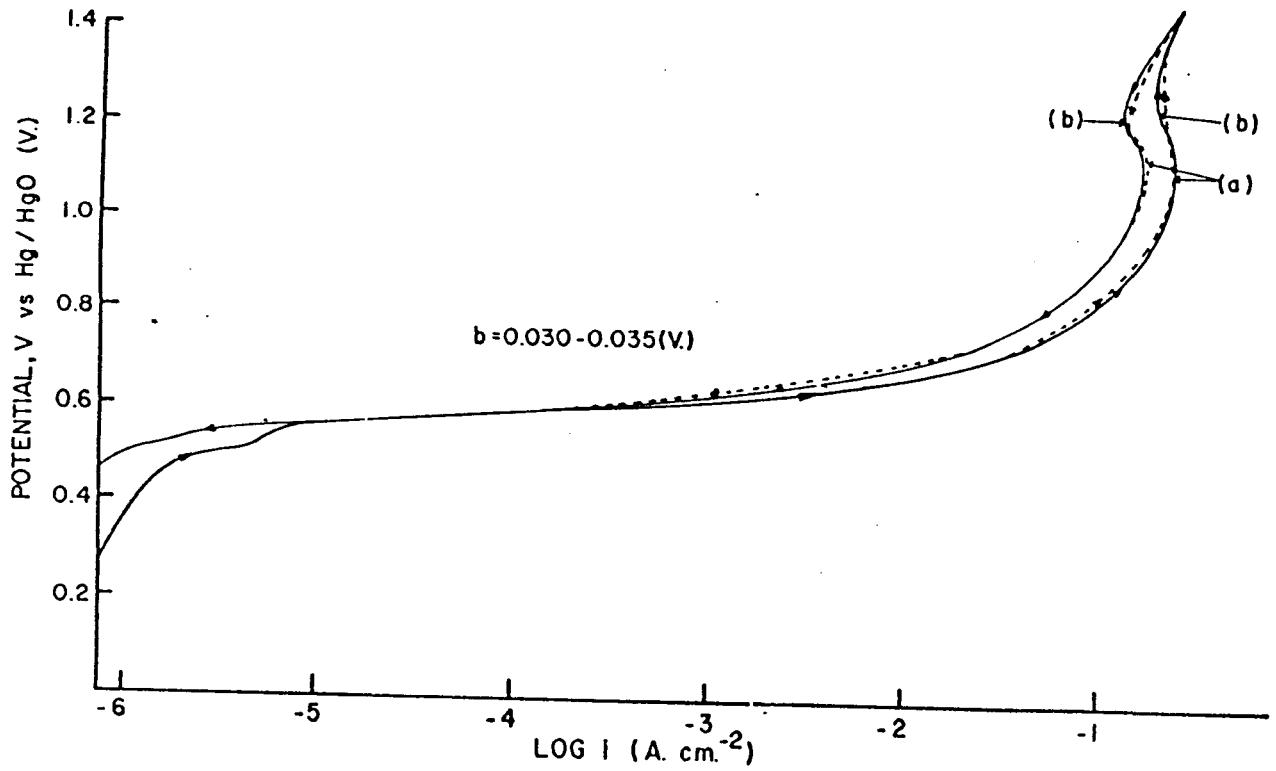
1.4
1.2
1.0
0.8
0.6
0.4
0.2
POTENTIAL, V vs Hg / HgO (V.)
b=0.030-0.035(V.)
(b)
(b)
(a)
-6
-5
-4
-3
-2
-1
LOG I (A. cm.$^{-2}$)

Figure 19. Comparison of log[i]-V relations for nickel electrodes in (a) H_2 and in (b) vacuo (2.05 M KOH, 25°C).

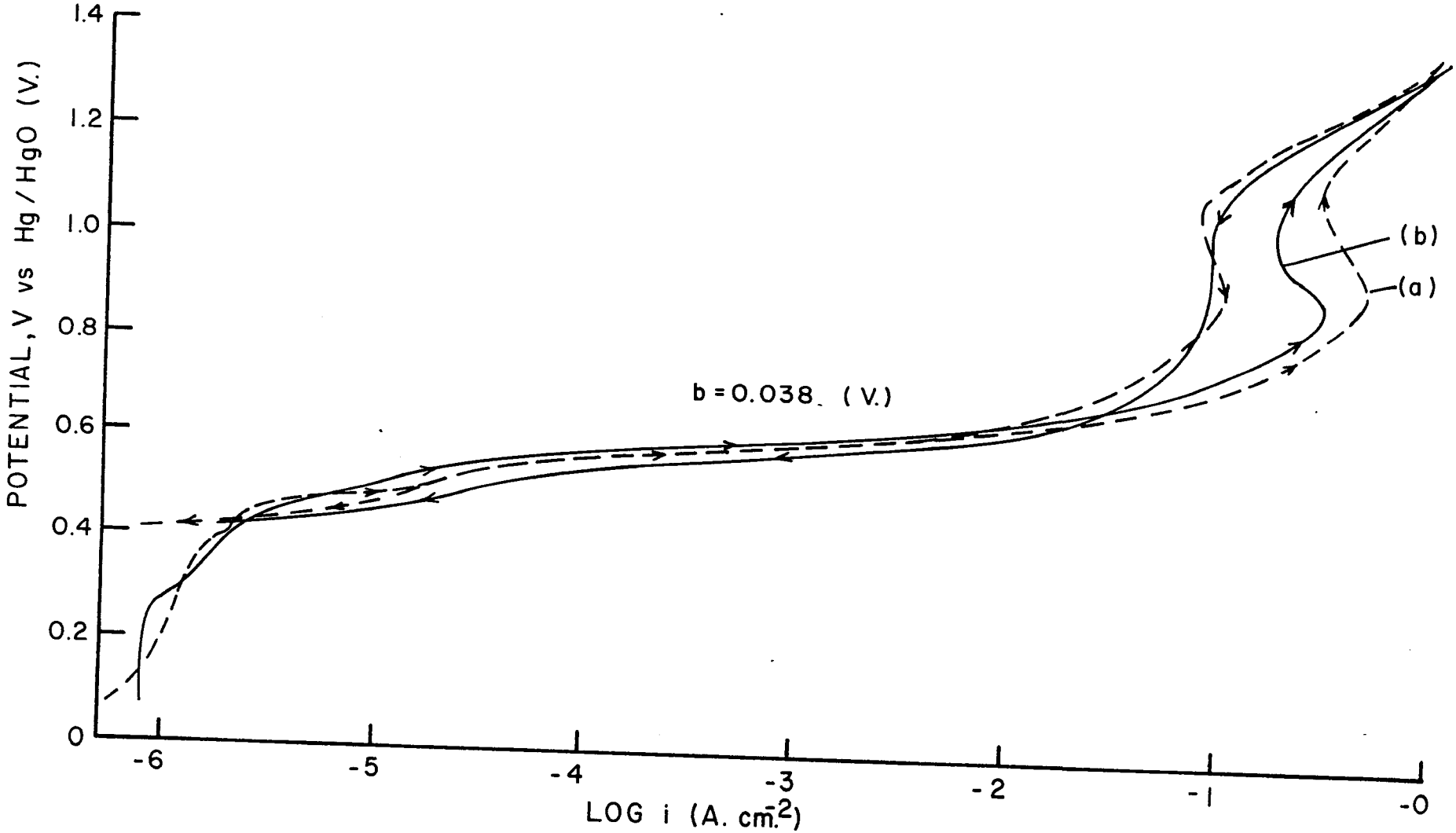
POTENTIAL, V vs Hg / HgO (V.)
1.4
1.2
1.0
0.8
0.6
0.4
0.2
0
b = 0.038 (V.)
(b)
(a)
-6
-5
-4
-3
-2
-1
-0
LOG i (A. cm⁻²)

Figure 20. Steady-state potentiostatic log[i]-V relations for nickel annealed in oxygen 2M KOH, 30°C (results are less reproducible from one electrode to another than in the case of annealing in vacuo or in H_2).

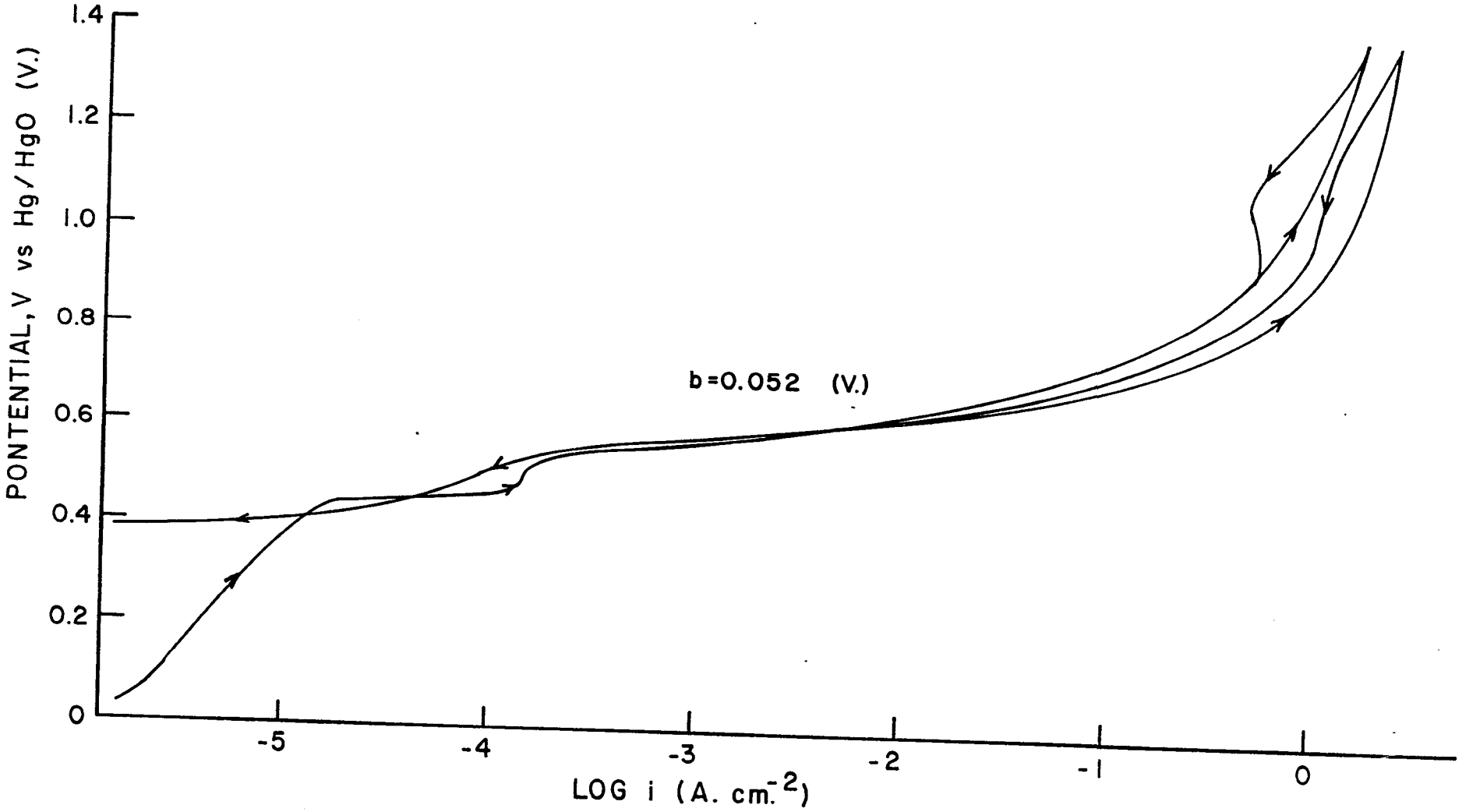
1.4
1.2
1.0
0.8
0.6
0.4
0.2
0
POTENTIAL, V vs Hg/HgO (V.)
b=0.052 (V.)
-5
-4
-3
-2
-1
0
LOG i (A. cm.$^{-2}$)

solutions were used; however, no appreciable difference in the kinetic behaviour of nickel electrodes in the anodic oxygen evolution region was noticeable in comparison with that for solutions made according to the standard method (Fig. 18). The latter procedure was therefore used for all other experiments with KOH solutions.

(ii) Effects of Variation in the Method of Preparation of the Electrodes: Nickel electrodes were prepared in three different ways. Potentiostatic steady-state log[i]-V curves for ascending and descending directions of potential change were obtained for 2.05 M aq. KOH at 25°C using electrodes annealed in hydrogen, in vacuum and (for 2 M aq. KOH at 30°C for electrodes) in oxygen. The results are shown in Figs. 19 and 20, and indicate that there is no substantial difference between the kinetic behaviour of electrodes annealed in hydrogen and those treated in vacuum. The results for electrodes annealed in oxygen are, however, less reproducible from one electrode to another, and different Tafel slopes (see Fig. 20) are observed.

(iii) Effects of Concentration and Temperature of The Electrolyte: Steady-state kinetic runs were carried out at various concentrations and temperatures of the electrolyte using electrodes annealed in hydrogen and in vacuum. The log[i]-V plots for ascending and descending

Figure 21. Steady-state potentiostatic log[i]-V relations for nickel annealed in vacuo:

(a) 0.122 M KOH, 25°C ;

(b) 2.05 M KOH, 25°C ;

(c) 7.3 M KOH, 30°C ;

(d) 14.3 M KOH, 25°C.

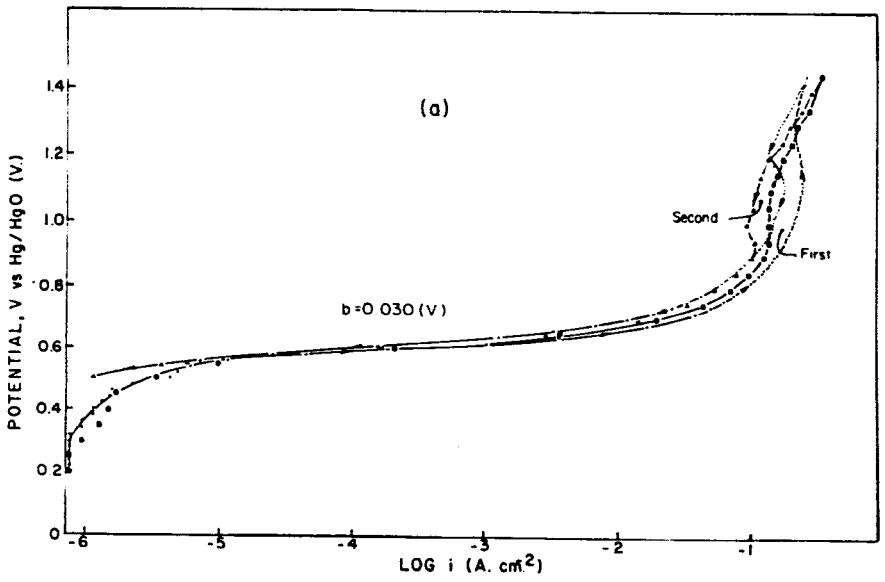
(a)
Second
First
b=0.030 (V)
POTENTIAL, V vs Hg/HgO (V.)
LOG i (A. cm⁻²)

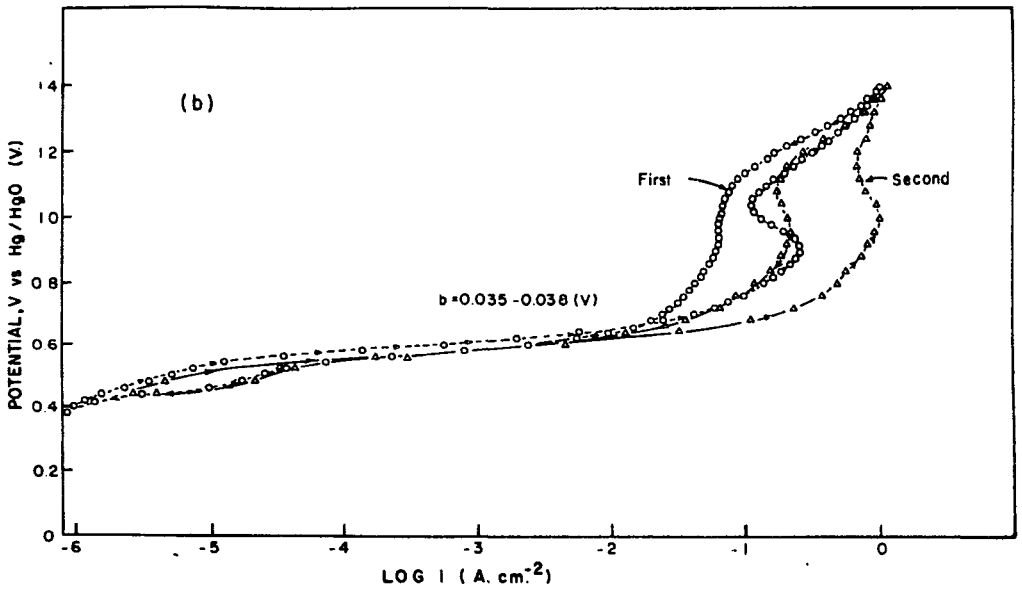
(b)
First
Second
b=0.035 -0.038 (V)
POTENTIAL, V vs Hg/HgO (V)
LOG I (A. cm⁻²)

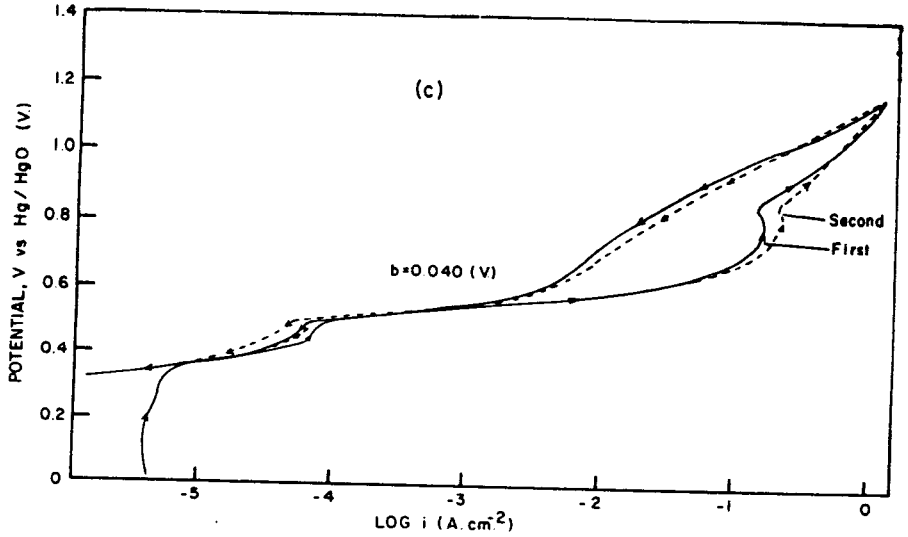
(c)
Second
First
b=0.040 (V)
POTENTIAL, V vs Hg/HgO (V.)
LOG i (A.cm⁻²)

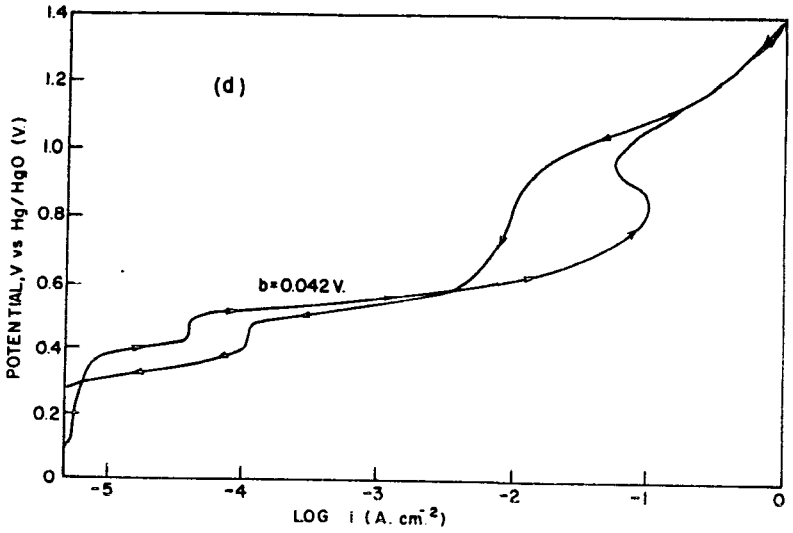
(d)
b=0.042 V.
POTENTIAL, V vs Hg/HgO (V.)
LOG i (A. cm⁻²)

Figure 22. Steady-state potentiostatic log[i]-V relations for nickel annealed in vacuo:

(a) 14.3 M KOH, 60°C;

(b) 14.3 M KOH, 89°C.

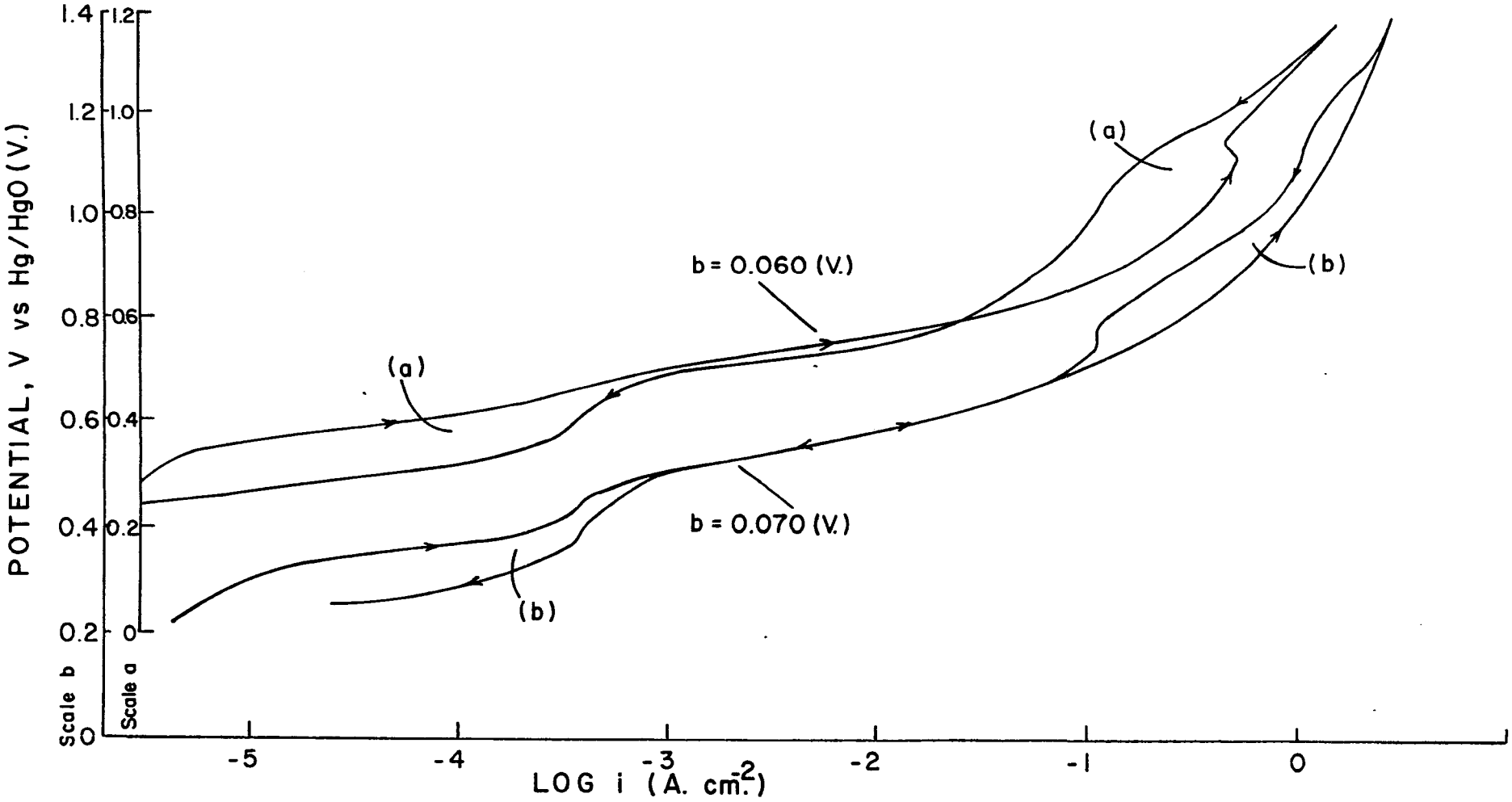
POTENTIAL, V vs Hg/HgO (V.)
Scale b
Scale a
1.4
1.2
1.0
0.8
0.6
0.4
0.2
0
1.2
1.0
0.8
0.6
0.4
0.2
0
-5
-4
-3
-2
-1
0
LOG i (A. cm.-2)
(a)
(b)
b = 0.060 (V.)
b = 0.070 (V.)
(a)
(b)

Figure 23. Steady-state potentiostatic log[i]-V relations for nickel annealed in vacuo: 7.3 M KOH, -30°C.

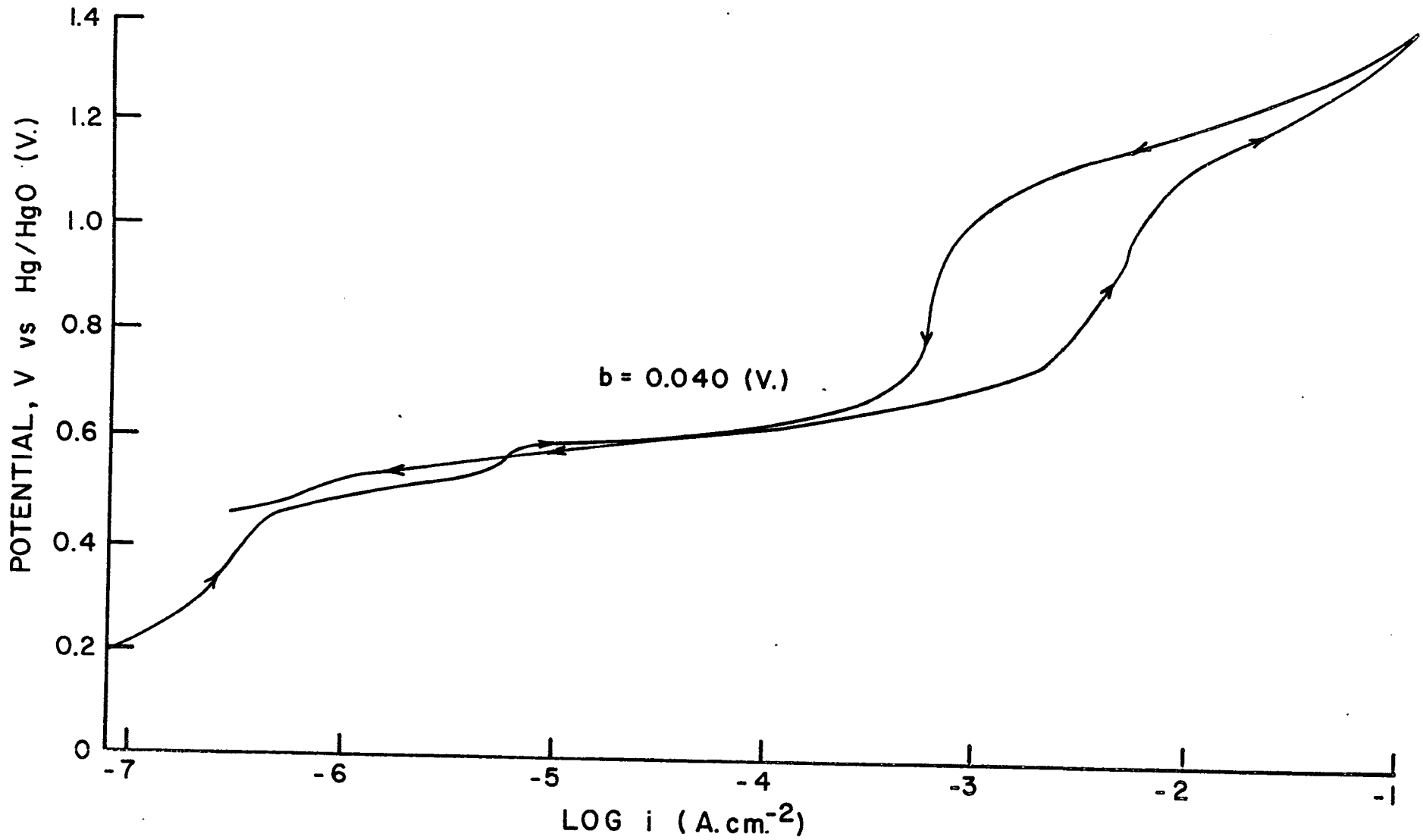
1.4
1.2
1.0
0.8
0.6
0.4
0.2
0
POTENTIAL, V vs Hg/HgO (V.)
b = 0.040 (V.)
-7
-6
-5
-4
-3
-2
-1
LOG i (A.cm.-2)

Figure 24. Steady-state potentiostatic log[i]-V relations for nickel annealed in H_2:

(a) 2.05 M KOH, 30°C ;

(b) 2.05 M KOH, 60°C ;

(c) 2.05 M KOH, 83°C.

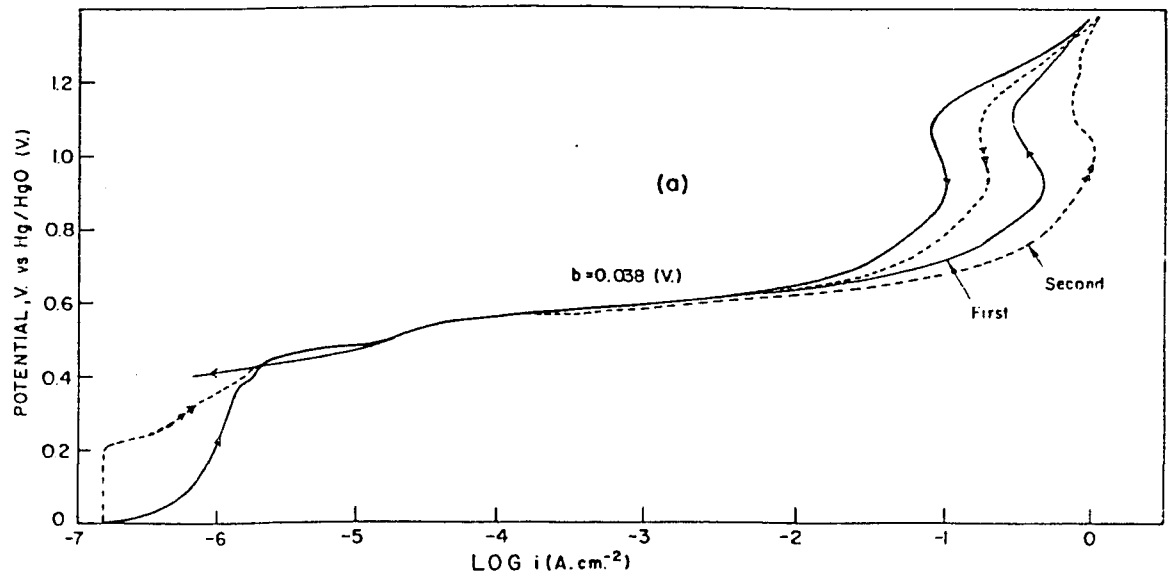
(a)
b=0.038 (V.)
First
Second
POTENTIAL, V. vs Hg/HgO (V.)
LOG i (A.cm.-2)

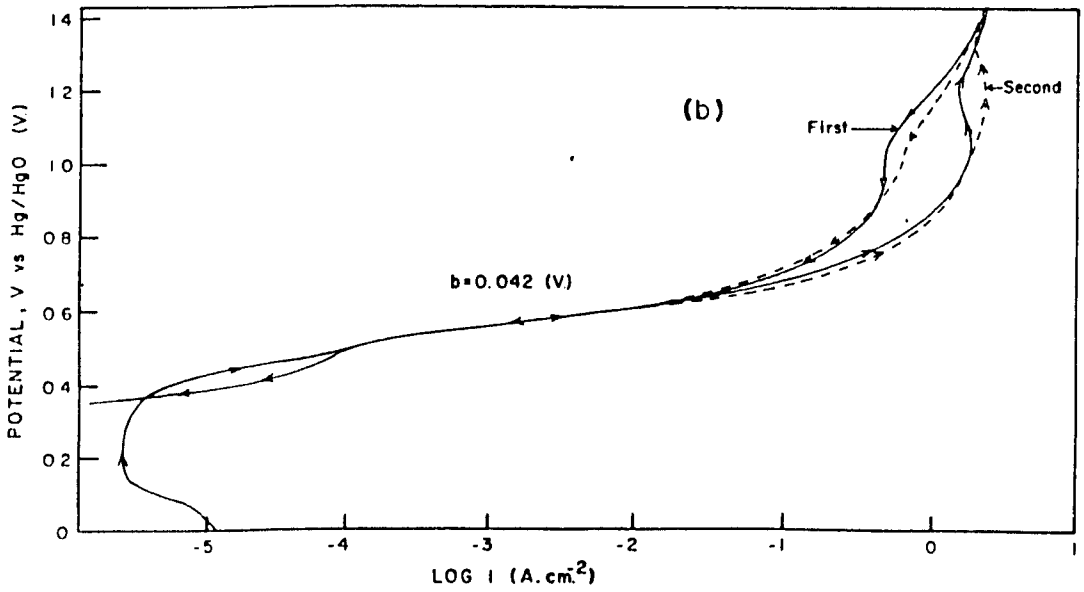
(b)
First
Second
b=0.042 (V.)
POTENTIAL, V vs Hg/HgO (V.)
LOG I (A.cm.-2)

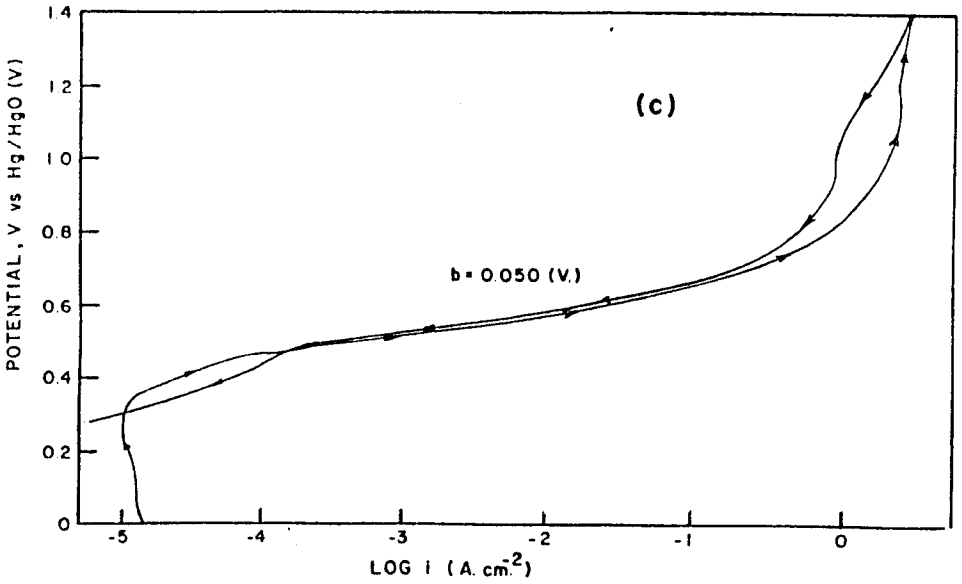
(c)
b = 0.050 (V.)
POTENTIAL, V vs Hg/HgO (V.)
LOG I (A.cm.-2)

Figure 25. Steady-state potentiostatic log[i]-V relations for nickel annealed *in vacuo*: 1.62 M KOH with 0.46 M LiOH at 25°C.

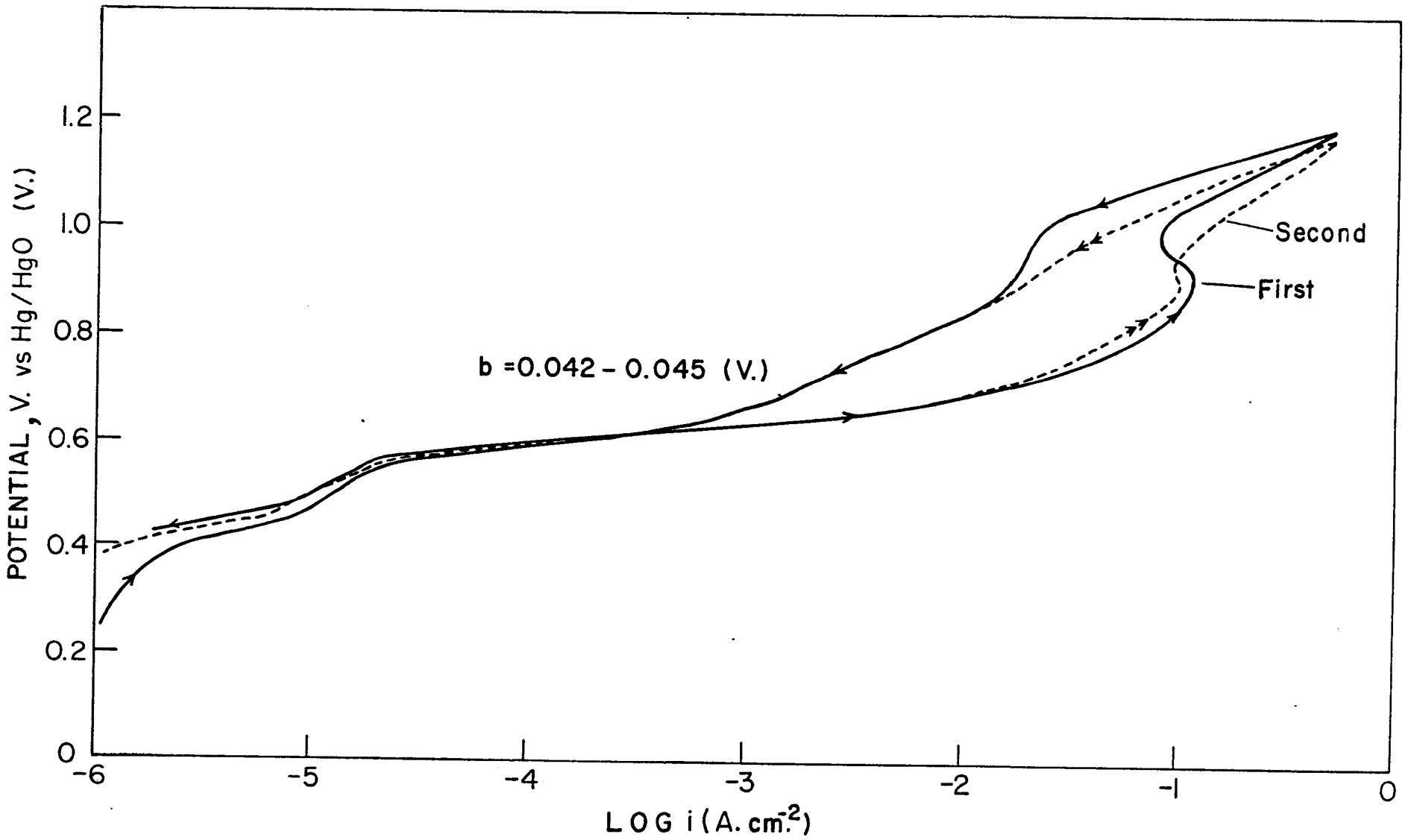
POTENTIAL, V. vs Hg/HgO (V.)
1.2
1.0
0.8
0.6
0.4
0.2
0
-6
-5
-4
-3
-2
-1
0
LOG i (A. cm.-2)
b =0.042 - 0.045 (V.)
Second
First

directions of potential change are shown in Figs. 21-24.

(iv) Effects of Addition of Li^+ ions to the Electrolyte: Effects of addition of LiOH to aq. KOH in regard to the steady-state oxygen evolution kinetics at 25°C at a nickel oxide electrode are shown in Fig. 25. The electrolyte solution consisted of 1.62 M aq. KOH and 0.46 M aq. LiOH.

(v) Notable Features of the Steady-state Kinetic Results: It has been found in the present work that in the o.e.r. at nickel studied under steady-state potentiostatic conditions, the log[i]-V relation is linear over about 2-3 decades; a particular point of interest is that this linear Tafel region is followed by a region of reversal ("self-passivation" effect (115)) of the direction of the current-potential relation at ca. 0.95 V. The Tafel slopes in the linear region (> ca. 10^{-4} a.cm^{-2}) have values given by b = ca. 2.3 (2RT/3F) for electrolyte solutions of concentrations 0.122 M, 2.05 M and 7.3 M at each of the temperatures 25°, 30°, 60° and 83°C and for 7.3 M aq. KOH at -30°C and for 14.3 M aq. KOH at 25°C; the Tafel slopes for 14.3 M aq. KOH at 60° and 89°C have values close to 2.3 RT/F. A short transition region between the potentials 0.40 and 0.50 V is observed. Below 0.4 V to 0.5 V, a very short linear log[i]-V region is apparent: the extrapolated values of the

Tafel slopes for this region ($< 10^{-4}$ a.cm^{-2}) are ca. 2.3 (2RT/F) (cf. ref. 18). The coordinates of the self-passivation region for the o.e.r. at Ni, and the Tafel slopes for the kinetic behaviour in electrolytes of various concentrations and at various temperatures, are summarised in Table III.

Increase in temperature up to 83°C diminishes the tendency for the passivation type of effect to occur and the hysteresis between ascending and descending log[i]-V curves at high c.d. becomes smaller and only an approach to a region of rather higher Tafel slopes is evident. In the Tafel region, the slopes become higher with temperature, as expected, and the results for ascending and descending potentials are in excellent agreement (Figs. 21-24).

Up to about 0.2-0.4 V, a rapid ascent into the foregoing transition region occurs and this appears to be connected with initial oxidation of the nickel surface.

The presence of Li^+ ions in the KOH solution had significant effects on the self-passivation behaviour (Fig. 25): thus, the limiting current is somewhat diminished in comparison with that observed in 2.05 M KOH (25°C) and the hysteresis between the ascending and descending curves is enhanced. This is in agreement with general observations on bulk oxide material (17,55,56,60,61,200).

Table III

Tafel Slopes and Coordinates of the Self-Passivation Region for the o.e.r. at Nickel Electrodes in KOH solutions of different Concentrations and Temperatures

Electrodes annealed in	Concentration and temp. of KOH	i_{max} ($a.cm^{-2}$)	V_{max} vs Hg/HgO (V)	Tafel slopes (V), (> 0.5V; > 10^{-4} $a.cm^{-2}$)	Extrapolated Tafel slopes (V) for ascending poln. (< 0.5V; < 10^{-4} $a.cm^{-1}$
vac.	0.122 M				
	25°C	0.23(1st poln.)	1.12(1st poln.)	0.03	-
vac.	2.05 M				
	25°C	0.26(1st poln.) 1.0 (2nd poln.)	0.91(1st poln.) 1.0 (2nd poln.)	0.035-0.038	0.110-0.120
H_2	2.05 M				
	30°C	0.49(1st poln.) 1.10(2nd poln.)	0.93(1st poln.) 1.0 (2nd poln.)	0.035-0.038	0.040
	60°C	1.75(1st poln.) 2.25(2nd poln.)	1.04(1st poln.) 1.20(2nd poln.)	0.042	0.060-0.090
	83°C	2.4 (inflection)	1.14(inflection)	0.050	0.080-0.140
vac.	7.3 M				
	-30°C	0.0049(inflect.)	0.93(inflection)	0.040	0.080
	30°C	0.155(1st poln.) 0.22 (2nd poln.)	0.82(1st poln.) 0.82	0.040	0.080

Table III (Cont'd)

vac.	14.3 M				
	25°C	0.10	0.86	0.042	0.070-0.090
	60°C	0.15	0.91	0.060	0.050-0.055
	89°C	broad inflection	broad inflection	0.070	0.055
vac.	2.0 M (LiOH+KOH)				
	25°C	0.11(1st poln.)	0.91(1st poln.)	0.042-0.045	0.120
		0.10(2nd poln.)	0.91(2nd poln.)		
O_2	2.0 M				
	30°C	-	-	0.052	-

Figure 26. Typical current density [i] vs ohmic overpotential [iR] plot.

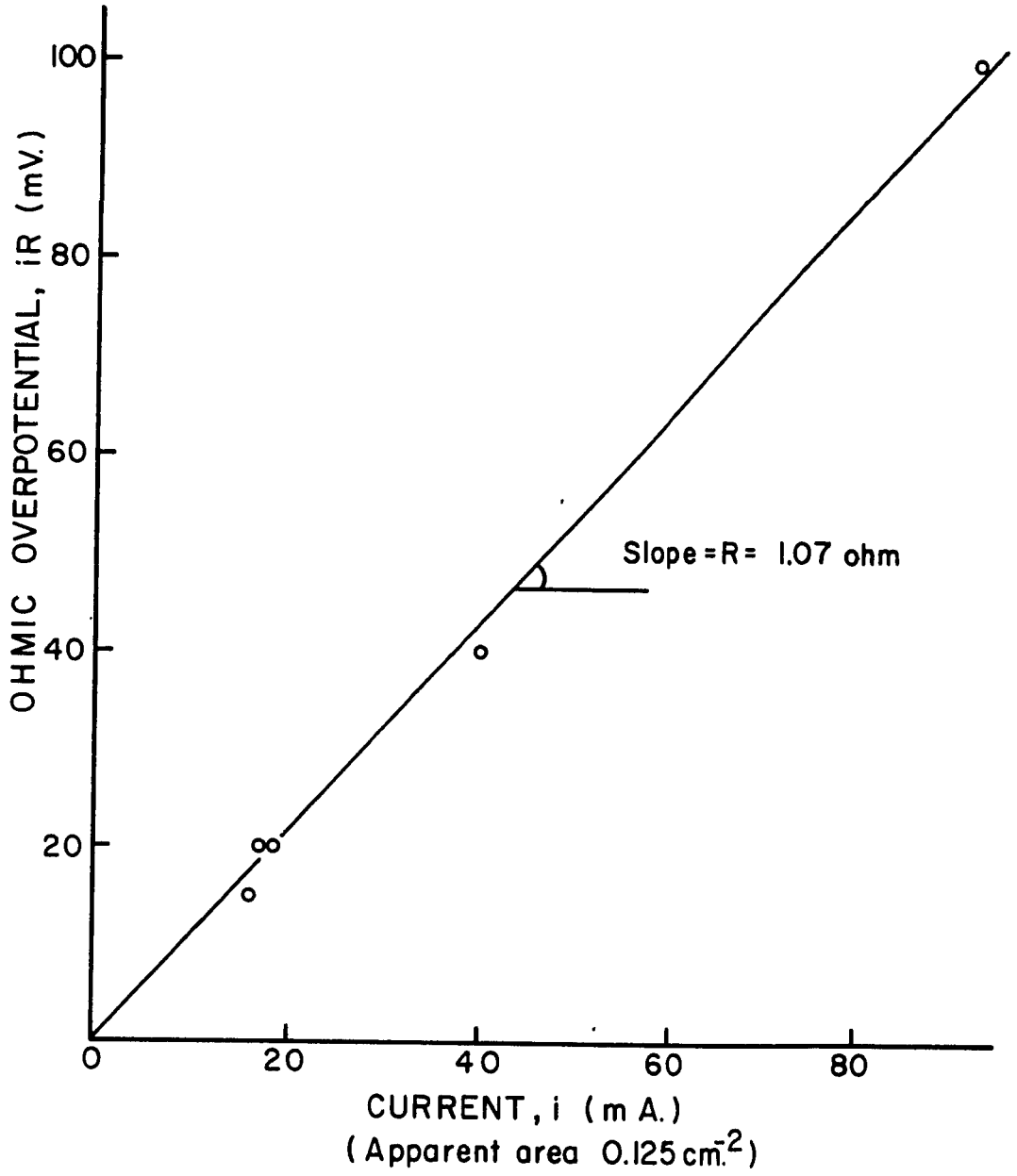
OHMIC OVERPOTENTIAL, iR (mV.)
100
80
60
40
20
0
20
40
60
80
Slope = R = 1.07 ohm
CURRENT, i (m A.)
(Apparent area 0.125 cm.⁻²)

It is observed that if proper control of the time factor in the measurements is made, the log[i]-V curves from one run to another in the same solution but with different electrodes were virtually superimposable. Runs in different solutions, but of the same concentration, were also excellently reproducible (cf. the similar conclusions of MacDonald and Conway (132) and Barnartt (162) regarding the kinetics of the o.e.r. at Au and Au-Pd alloys). However, in most of the runs, the first steady-state scan of ascending and descending potentials usually gave somewhat lower currents than did the second and subsequent scans of potential in anodic and cathodic directions.

(vi) Corrections for Resistance Error (iR) Effects: It is observed from the above results that at high c.d.'s, there is a tendency for the direction of the log[i]-V relation to become reversed (passivation effect) or for log[i] to approach a limiting value. Since at high c.d.'s the ohmic overpotential contribution may be significant, the measured potentials at high c.d.'s were corrected for iR-drop where necessary. iR-drops determined from open-circuit transients were first plotted against i for several potentials; the iR-drops for other potentials were then calculated by interpolation from this plot. A representative i vs. iR plot is shown in Fig. 26 for one typical kinetic run.

Figure 27. Steady-state potentiostatic log[i]-V relations for silver annealed in H_2:

(a) 2M KOH, 25°C ;

(b) 2M KOH, 60°C.

(Potentiodynamic cyclic charging and discharging curves are represented on the same potential axis).

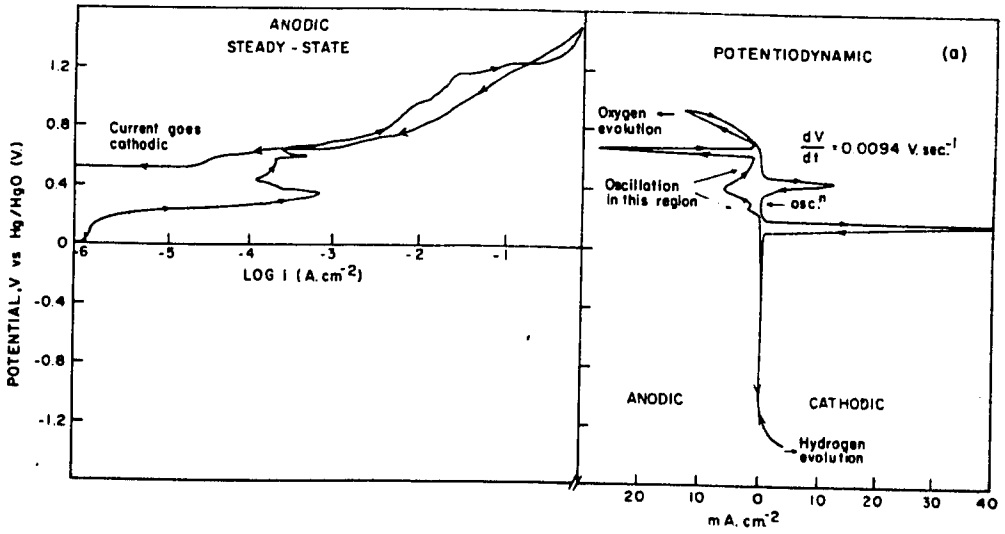
ANODIC
STEADY - STATE
Current goes cathodic
LOG I (A.cm⁻²)
POTENTIODYNAMIC
(a)
Oxygen evolution
dV/dt = 0.0094 V.sec⁻¹
Oscillation in this region
osc.ⁿ
ANODIC
CATHODIC
Hydrogen evolution
mA.cm⁻²
POTENTIAL, V vs Hg/HgO (V.)

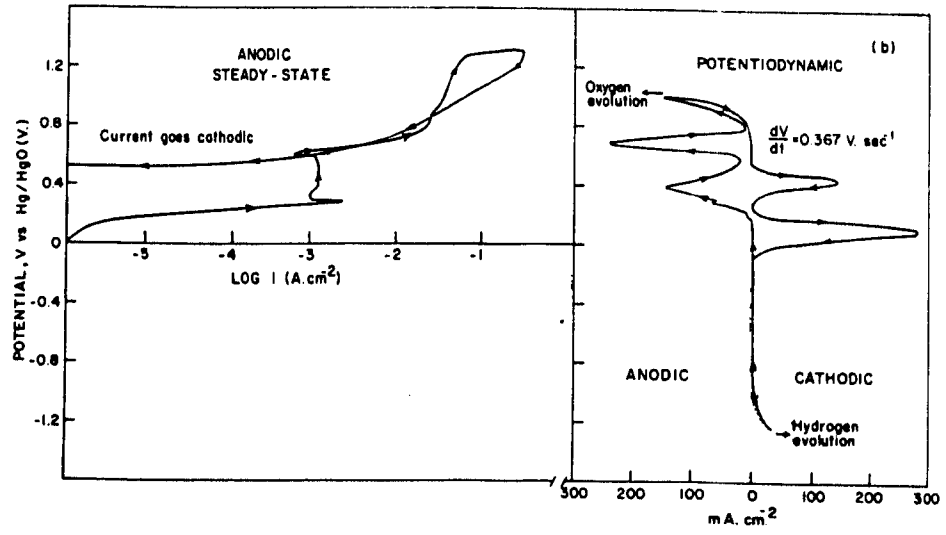
ANODIC
STEADY - STATE
Current goes cathodic
LOG I (A.cm⁻²)
POTENTIODYNAMIC
(b)
Oxygen evolution
dV/dt = 0.367 V. sec⁻¹
ANODIC
CATHODIC
Hydrogen evolution
mA.cm⁻²
POTENTIAL, V vs Hg/HgO (V.)

All the kinetic log[i]-V plots shown above have, where necessary, been iR corrected* in the high c.d. region by the procedure described above. It is clear that the inversions of the Tafel relations and the approaches to limiting currents cannot be ascribed to iR effects since (A) the latter would not, in fact, lead to inversions or "passivation effects"; (B) such behaviour is also observed at high KOH concentrations where the effects of ohmic p.d.'s are negligible, and (C) hysteresis in the upper potential regions would not occur if only iR effects were involved.

(b) Kinetics of Evolution of Oxygen at Silver Electrode Surfaces

In order to compare the steady-state oxygen evolution kinetic behaviour at nickel electrodes with that at the silver and also to clarify further the mechanism of oxidation of silver, steady-state potentiostatic studies were also carried out at the latter metal. Results are shown for 2 M aq. KOH at 25°C and 60°C in Fig. 27.

The results show (Fig. 27) that at first the current increases logarithmically with increase of potential

---

*i.e. also allowing for the fact that in potentiostatic experiments, the iR effect modifies the reference electrode potential input to the potentiostat and hence the effective potential to which the potentiostat adjusts itself.

and the electrode then undergoes a passivation type of effect at a potential ca. 0.3 V. The current again increases very slowly with increase of potential after the second oxidation process has commenced at a potential ca. 0.4 V. When a potential of ca. 0.6 V is reached, a large increase of anodic current accompanied by O_2 evolution is observed. It is also found that the anodic currents for the descending direction of potential change are greater than those for ascending potentials in the oxygen evolution region.

2. NON-STEADY-STATE MEASUREMENTS

(a) Estimation of Formation Charge (and Pseudo-Capacitance) Associated with the Adsorbed Oxide Species

(i) Potentiostatic Step Charging at Nickel Metal Electrodes: Applications of the potentiostatic anodic step charging method (based on principles to be described in Chapter IV) were made to the study of the development of surface oxide species in the oxygen evolution reaction at nickel electrodes in alkaline solution. The potential range covered included a region where faradaic oxygen evolution can occur. Under these conditions, a method based on the principles to be described in Chapter IV must be adopted since currents of both a faradaic (for the overall reaction) and a pseudo-faradaic (for the surface charging process)

Figure 28. Typical experimental current-time transients for potentiostatic step charging at nickel in aq. KOH.

(a) At low coverage (i.e. at low potentials) and in absence of appreciable faradaic current.

(b) At intermediate coverage and with appreciable faradaic co-current (O_2 evolution).

(c) at full coverage with no appreciable charging.

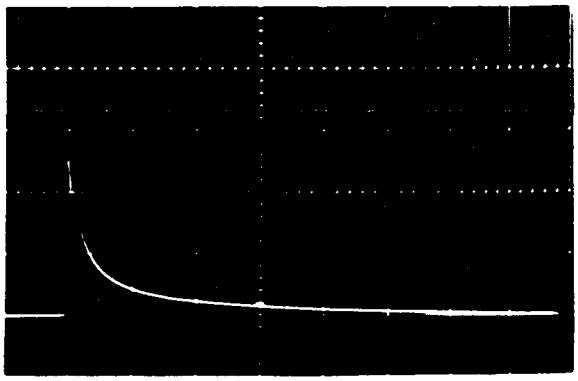

(a)

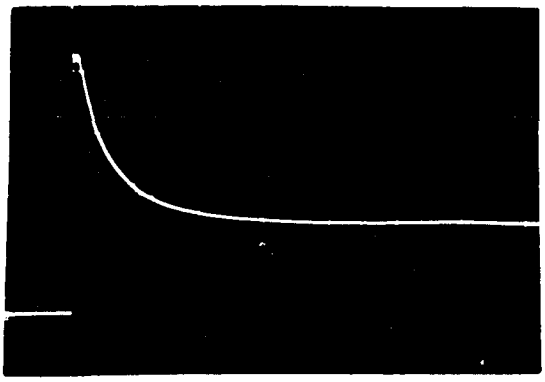

(b)

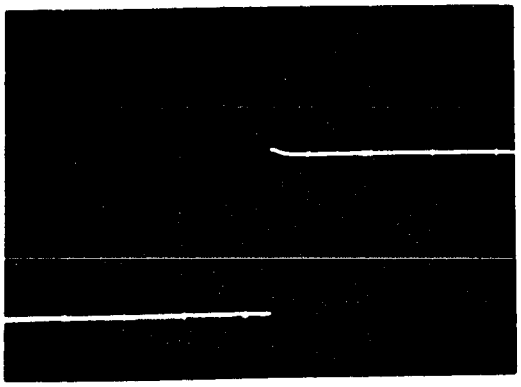

(c)

origin pass in a common range of potentials. Under these conditions, the analysis of linear anodic sweep results can become very complex (163). A method for the study of the formation of the surface oxide layer in the anodic direction is also desirable because cathodic galvanostatic reduction of the oxide at nickel is found to be incomplete (see section 3 (f) of this Chapter) as also indicated in other work (54). Similar effects are observed in fast reductions of the bulk nickel (III) oxide when the underlying layers tend to become relatively insulated by a less conducting $Ni(II)(OH)_2$ layer.

The step charging method also enables studies of successive degrees of oxidation of the surface (or of an already existing surface oxide) to be made from one potential to another, while the galvanostatic method gives the overall degree of surface oxidation established at the electrode at a given prior, potentiostatically maintained potential.

The current-time transients for all the potential steps were recorded photographically and the steady-state currents at all potentials were measured on a milliammeter in series with the counter electrode. Several typical current-time transients are shown in Fig. 28.

The charge passed, and hence the change of degree of surface oxidation at the electrode interface, was

Figure 29. Charge,Q,for potentiostatic step charging as a function of potential, V, for various concentrations of potassium hydroxide, and temperatures:

(1) 2.05 M KOH, 30°C;

(2) 2.05 M KOH, 60°C;

(3) 13.1 M KOH, 30°C;

(4) 13.1 M KOH, 60°C;

(5) 13.1 M KOH, 89°C;

(6) 6.7 M KOH, -30°C.

(The electrodes were pre-conditioned as in Fig. 8).

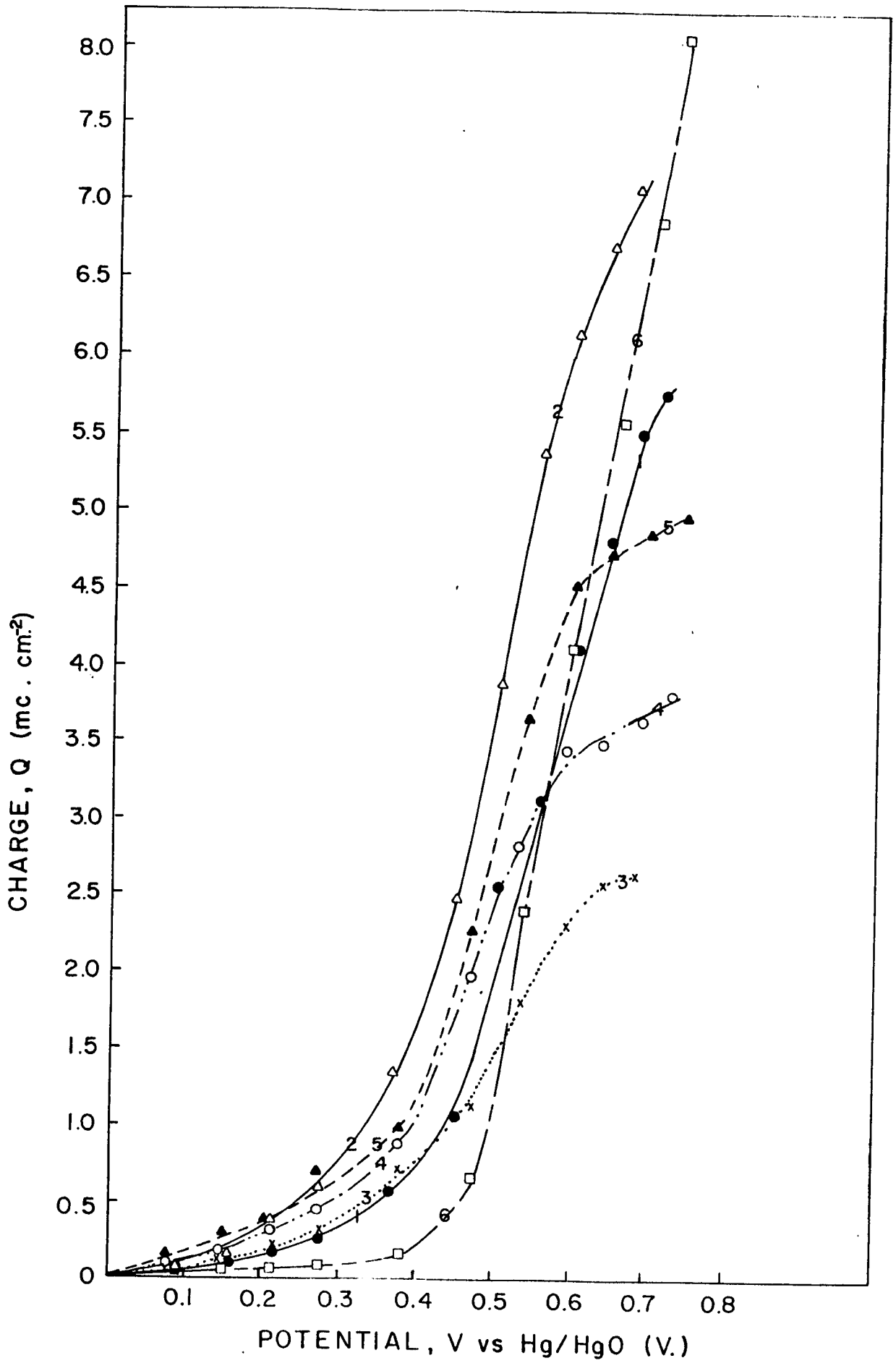
8.0
7.5
7.0
6.5
6.0
5.5
5.0
4.5
4.0
3.5
3.0
2.5
2.0
1.5
1.0
0.5
0
CHARGE, Q (mc. cm.-2)
0.1
0.2
0.3
0.4
0.5
0.6
0.7
0.8
POTENTIAL, V vs Hg/HgO (V.)
1
2
3
4
5
6

Figure 30. Pseudo-capacitance, C, as a function of potential, V, obtained by differentiation of the relations in Fig. 29

(1) 2.05 M KOH, 30°C;

(2) 2.05 M KOH, 60°C;

(3) 13.1 M KOH, 30°C;

(4) 13.1 M KOH, 60°C;

(5) 13.1 M KOH, 89°C;

(6) 6.7 M KOH, -30°C.

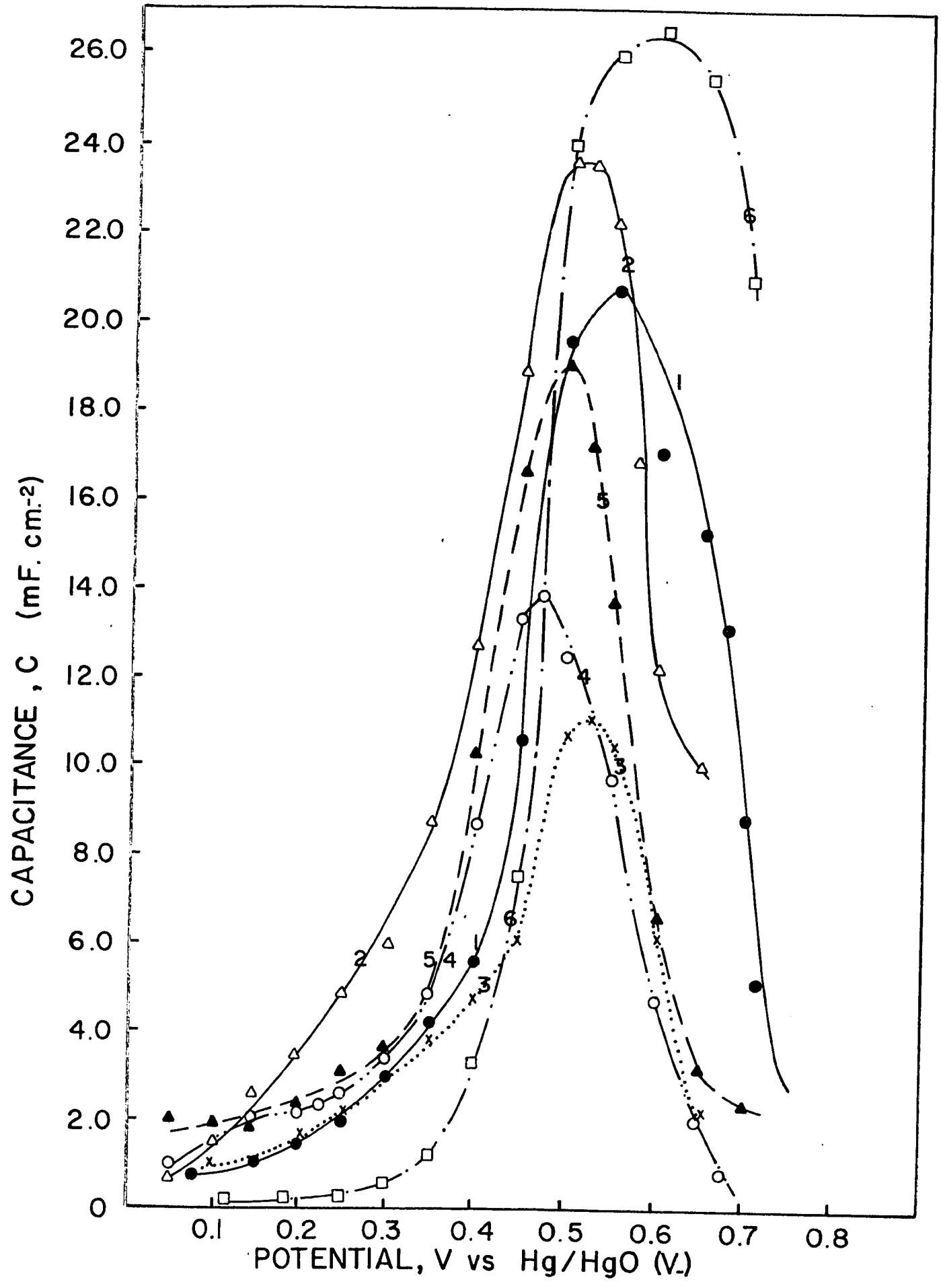
CAPACITANCE , C (mF. cm.-2)
26.0
24.0
22.0
20.0
18.0
16.0
14.0
12.0
10.0
8.0
6.0
4.0
2.0
0
0.1
0.2
0.3
0.4
0.5
0.6
0.7
0.8
POTENTIAL, V vs Hg/HgO (V.)
1
2
3
4
5
6

Figure 31. Charge,Q,for potentiostatic step charging as a function of potential, V using bare nickel electrodes: (The electrodes were annealed *in vacuo* but not pre-conditioned as in Fig. 8)

(1) 2.02 M KOH, 30°C;

(2) 14.4 M KOH, 30°C.

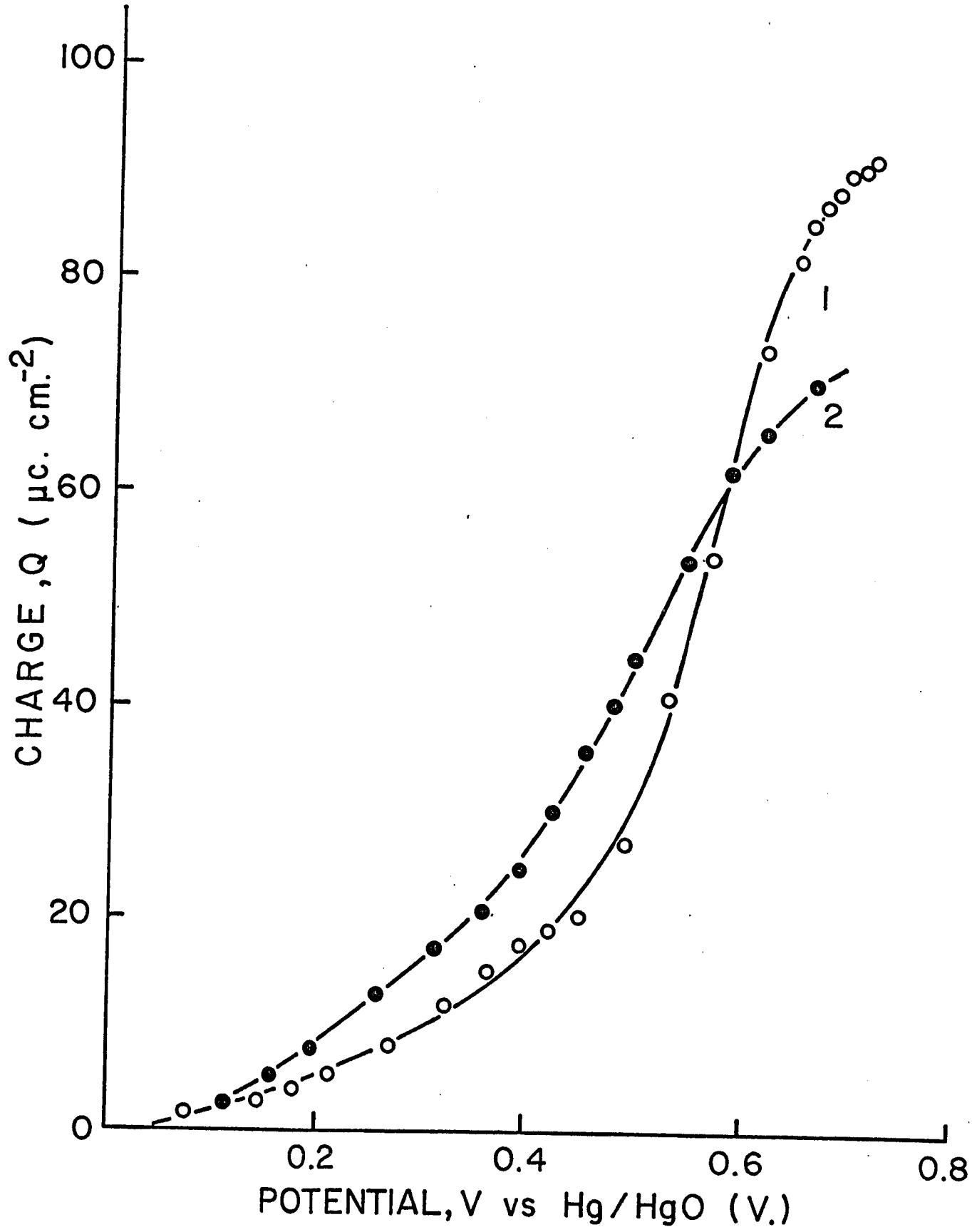
100
80
60
40
20
0
CHARGE, Q (μc. cm.-2)
0.2
0.4
0.6
0.8
POTENTIAL, V vs Hg/HgO (V.)
1
2

Figure 32. Charge, Q, for potentiostatic step charging as a function of potential, V, in 2.0 M KOH at 30°C when polarisation was commenced E_{HgO} = -0.92 V in the same solution using "fresh" electrode. (The electrode was annealed in H_2 but not pre-conditioned as in Fig. 8).

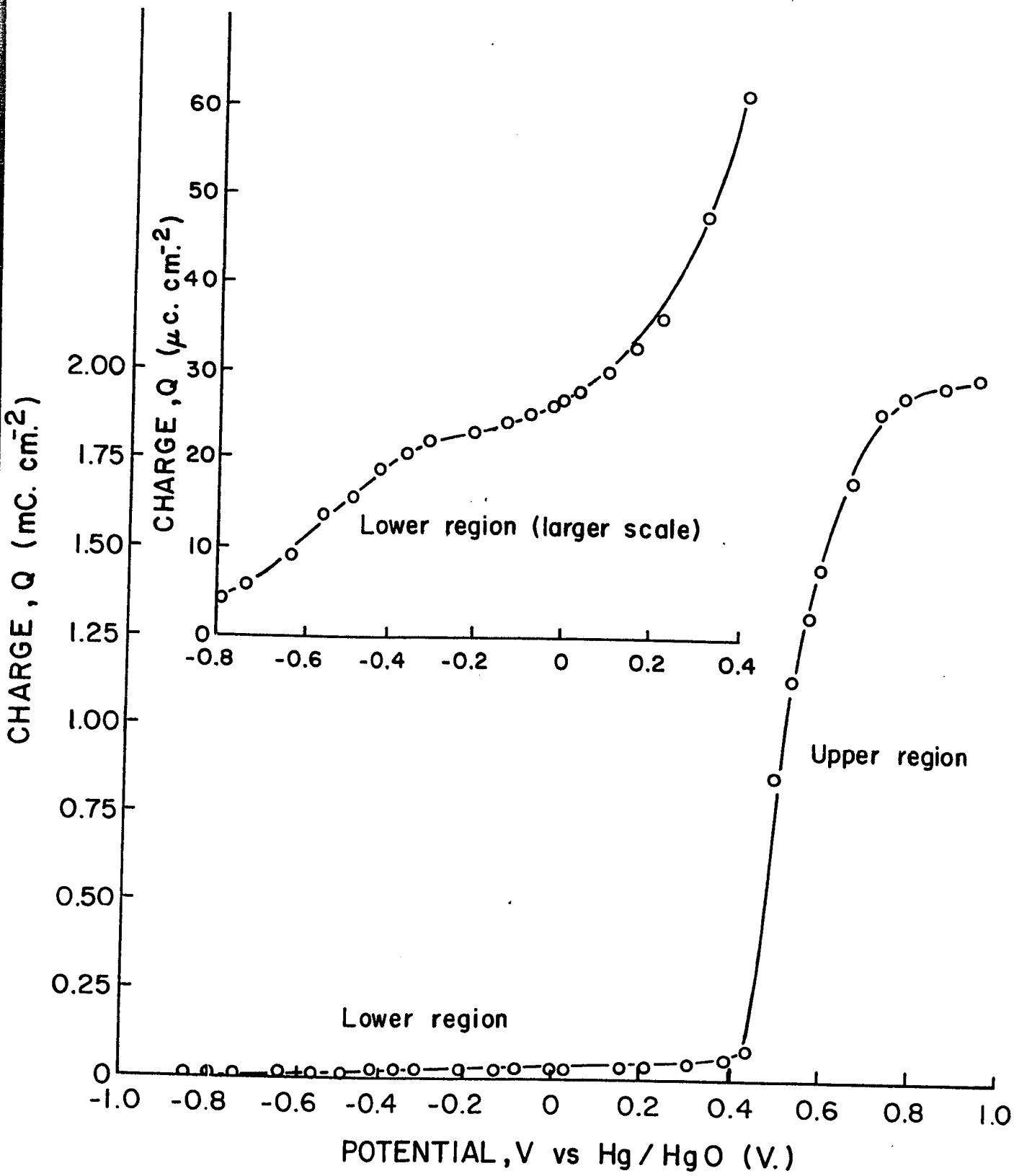
CHARGE , Q (mC. cm.$^{-2}$)
2.00
1.75
1.50
1.25
1.00
0.75
0.50
0.25
0
-1.0
-0.8
-0.6
-0.4
-0.2
0
0.2
0.4
0.6
0.8
1.0
POTENTIAL , V vs Hg / HgO (V.)
Lower region
Upper region
CHARGE , Q (μc. cm.$^{-2}$)
60
50
40
30
20
10
0
-0.8
-0.6
-0.4
-0.2
0
0.2
0.4
Lower region (larger scale)

Figure 33. Pseudo-capacitance, C as a function of potential, V, obtained by differentiation of the relations in Fig. 32.

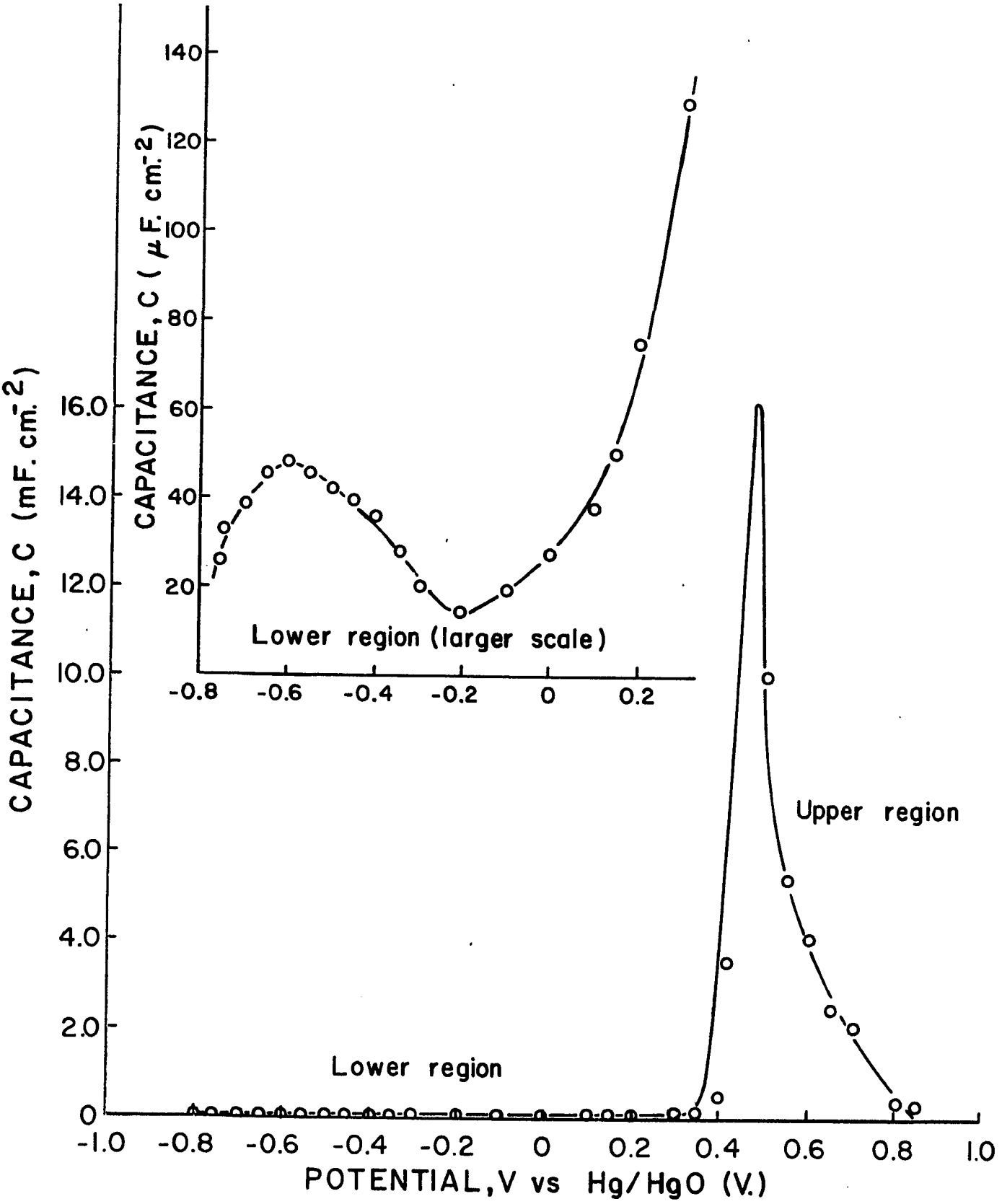
CAPACITANCE, C (mF. cm.-2)
16.0
14.0
12.0
10.0
8.0
6.0
4.0
2.0
0
CAPACITANCE, C (μF. cm.-2)
140
120
100
80
60
40
20
Lower region (larger scale)
-0.8 -0.6 -0.4 -0.2 0 0.2
Upper region
Lower region
-1.0 -0.8 -0.6 -0.4 -0.2 0 0.2 0.4 0.6 0.8 1.0
POTENTIAL, V vs Hg/HgO (V.)

calculated for each potential step from the experimental current-time transients in the manner to be described in Chapter IV. Addition of the charge increments gave the total charge, Q, *vs.* potential, V, profile shown in Fig. 29. Differentiation gave the pseudo-capacitance, C (= dQ/dV) profile which is almost symmetrical about a potential of *ca.* 0.5 V (Fig. 30): the exact value depends on temperature and electrolyte concentration. The above results (Figs. 29 and 30) were obtained for KOH solution at concentrations of 2.05 M (30 and 60°C), 13.1 M (30°, 60° and 89°C) and 6.7 M (-30°C) using the electrochemically pre-conditioned nickel wire electrodes (see Chapter II).

Measurements were also made at fresh *bare* electrodes (annealed *in vacuo* and in H_2) (Figs. 31 and 32). In one set of measurements, polarization was commenced in 2M KOH solution at 30°C in potentiostatic steps from -0.92 V up to about +0.9 V (Fig. 32). Much less charge was involved in oxidation of the fresh bare electrode than that in oxidation of an electrochemically preconditioned electrode (Figs. 29, 31 and 32). Differentiation of the relation in Fig. 32 gave a pseudo-capacitance profile exhibiting two preaks (Fig. 33), one at a potential *ca.* -0.6 V and the other at *ca.* +0.5 V (cf. Fig. 34 a,c).

The results from the potentiostatic step charging method were compared with those from the fast galvanostatic reduction method. After the electrode had been polarised in steps up to the highest potential, the total charge associated with (electrochemically reducible) oxide species at the electrode was also estimated by a fast galvanostatic reduction transient (Fig. 8). The maximum charge for reduction at the highest potential, estimated by the step method, was found to be about 20% less than that by the galvanostatic method. This discrepancy may arise because oxide was continuing to grow significantly between consecutive steps. The results are given comparatively in Table IV.

(ii) Potentiodynamic Linear Repetitive Sweep Method: As mentioned in Chapter II, the potentiodynamic sweep measurements involve the use of an electronically programmed "triangular" wave signal applied to the electrodes in order to obtain the i-V (or t) relations.

In a potentiodynamic run, the aim is to obtain an i-V relation in which charging and discharging peaks associated with adsorption and desorption of intermediates on the electrode surface can be observed in a well-defined and reproducible manner. The peak potentials are related to the free energies of adsorption and desorption of the

Table IV

Charges Q Determined by the Step Charging and the Galvanostatic Discharging Methods at Nickel Electrodes in aq. KOH

Concentration and temp. of the Electrolyte	Potential vs Hg/HgO (V)	Charges determined by Step Charging method (mc. cm^{-2})	Charges determined by Glav. discharge (mc. cm^{-2})
2.0 M, 30°C	0.59	5.5	7.0
6.7 M, -30°C	0.738	8.0	9.5
13.1 M, 30°C	0.685	2.7	3.7

Figure 34. Repetitive potentiodynamic triangular sweep at nickel electrodes in KOH solutions for various concentrations and temperatures:

(a) 2.05 M KOH, 30°C;

(b) 2.05 M KOH, 30°C; shorter potential range.

(c) 12.45 M KOH, -15°C;

(d) 7.0 M KOH, -30°C.

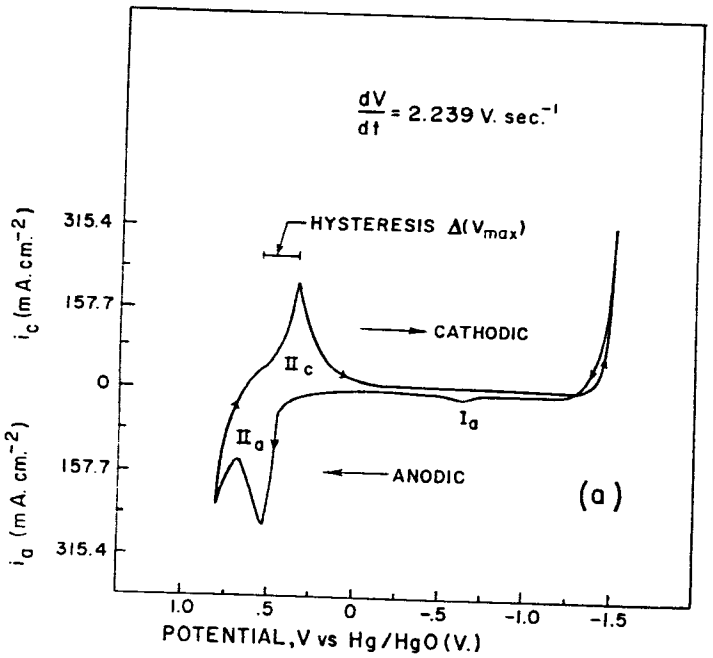
dV/dt = 2.239 V. sec.⁻¹
HYSTERESIS Δ(V_max)
CATHODIC
ANODIC
II_c
II_a
I_a
i_c (mA.cm⁻²)
i_a (mA.cm⁻²)
315.4
157.7
0
157.7
315.4
1.0
.5
0
-.5
-1.0
-1.5
POTENTIAL, V vs Hg/HgO (V.)
(a)

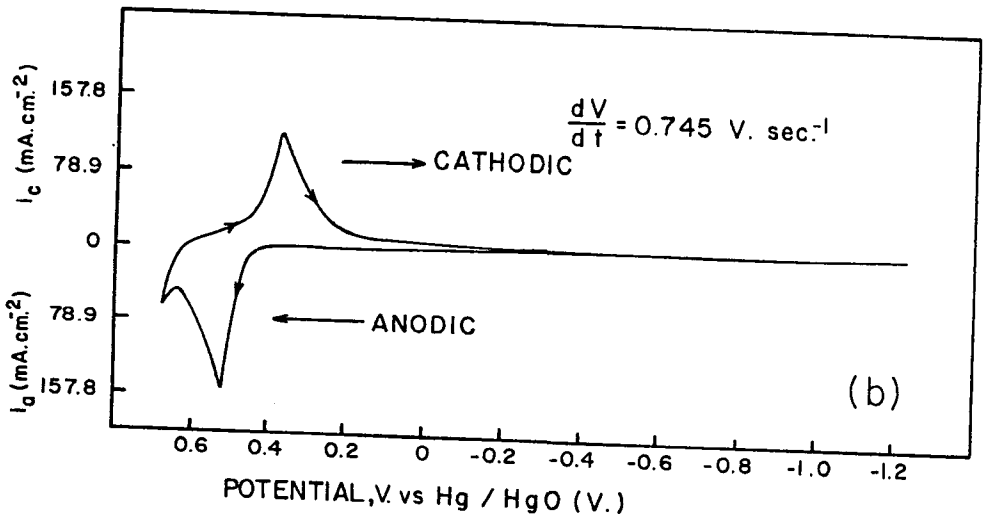
dV/dt = 0.745 V. sec.⁻¹
CATHODIC
ANODIC
i_c (mA.cm⁻²)
i_a (mA.cm⁻²)
157.8
78.9
0
78.9
157.8
0.6
0.4
0.2
0
-0.2
-0.4
-0.6
-0.8
-1.0
-1.2
POTENTIAL, V. vs Hg / HgO (V.)
(b)

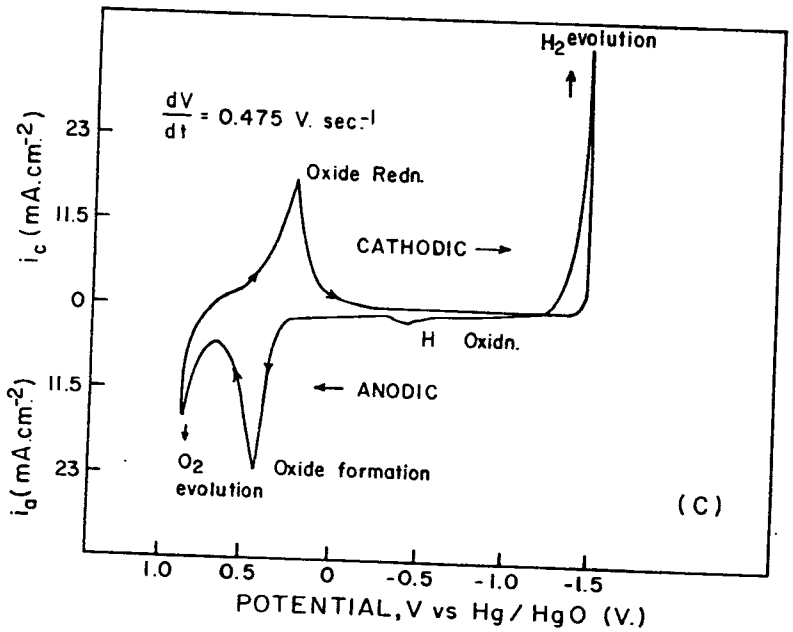
dV/dt = 0.475 V. sec.⁻¹
H₂ evolution
Oxide Redn.
CATHODIC
H Oxidn.
ANODIC
O₂ evolution
Oxide formation
i_c (mA.cm⁻²)
i_a (mA.cm⁻²)
23
11.5
0
11.5
23
1.0
0.5
0
-0.5
-1.0
-1.5
POTENTIAL, V vs Hg / HgO (V.)
(C)

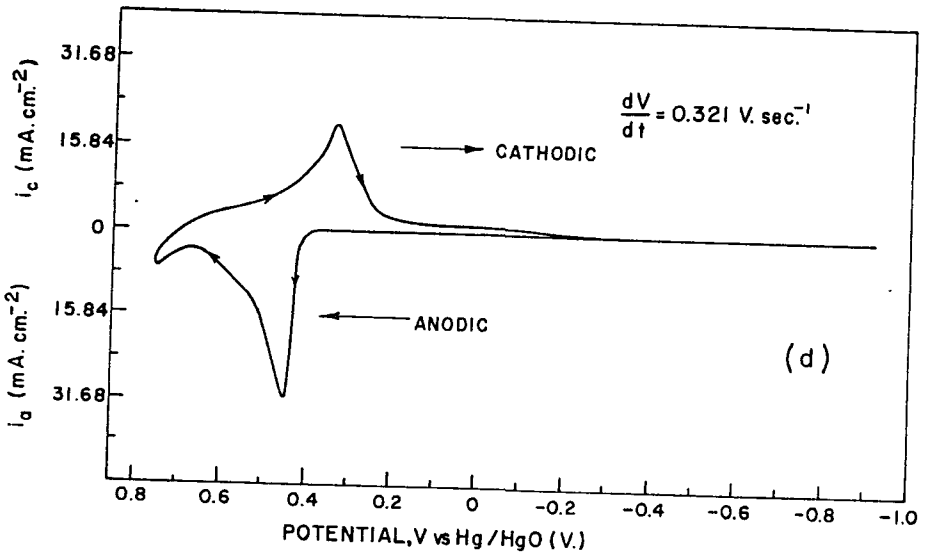
dV/dt = 0.321 V. sec.⁻¹
CATHODIC
ANODIC
i_c (mA.cm⁻²)
i_a (mA.cm⁻²)
31.68
15.84
0
15.84
31.68
0.8
0.6
0.4
0.2
0
-0.2
-0.4
-0.6
-0.8
-1.0
POTENTIAL, V vs Hg/HgO (V.)
(d)

various species at the electrode surface (163-165). The amounts of charge passed in the formation and desorption of the species can be calculated by estimating the areas under the corresponding peaks. In the case of symmetrical peaks, the potentials of the maxima correspond to half-reduction or half-oxidation of the surface.

In some cases where more than one species is formed at the electrode surface over ranges of potential which are not well-separated, the peaks overlap partially or completely depending on the separation in peak potentials. In such cases, it is difficult to interpret the results obtained and this difficulty becomes more important at higher sweep rates where the peak potentials can become shifted due to polarization effects.

In the absence of Faradaic currents, the current-potential relation obtained from a linear sweep (dV/dt = constant) experiment is equivalent to a pseudo-capacity-potential relation because, in the absence of an appreciable faradaic current, the pseudo-capacity $C = i/\frac{dV}{dt} = i \times \text{constant}$.

(A) Nickel Electrodes: Potentiodynamic i-V profiles were obtained at nickel electrodes for various concentrations and temperatures of the KOH solutions. Typical i-V profiles are given in Fig. 34, and for comparison,

Figure 35. Repetitive potentiodynamic triangular sweep at platinum electrodes in (a) 1M H_2SO_4 and (b) in 1M KOH solutions.

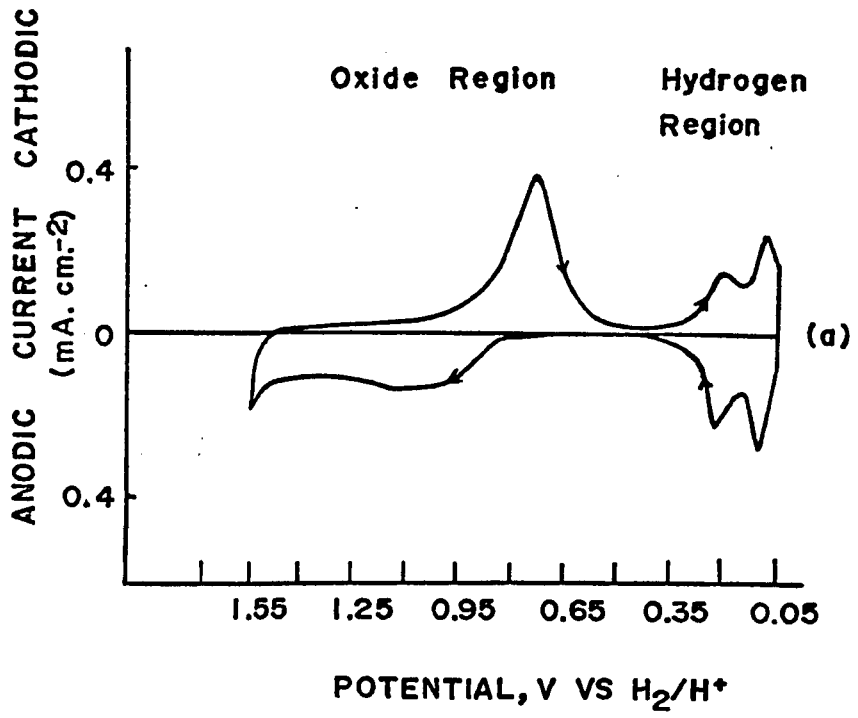

(a) Pt/H_2SO_4 ; $dV/dt = 0.1$ V. sec.-1

(b) Pt/KOH ; $dV/dt = 0.1$ V. sec.-1

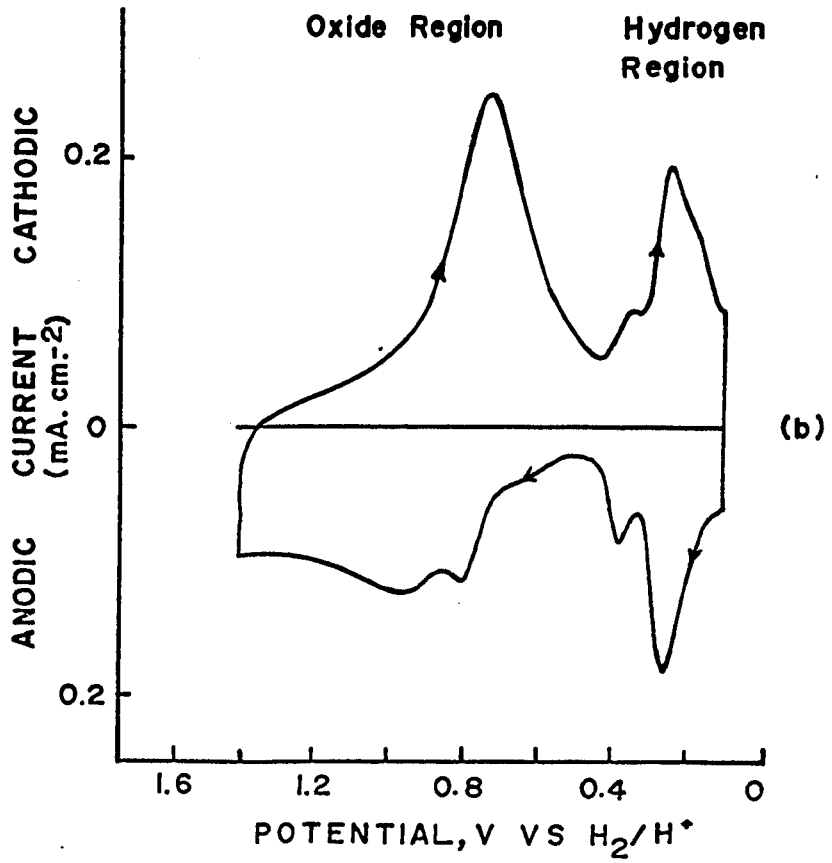

the corresponding behaviour at Pt in H_2SO_4 and KOH solutions is also shown (Fig. 35). The difference between the i-V relation for nickel electrodes and that for platinum electrodes in KOH solution is obvious: unlike the case of platinum electrodes, no H adsorption and desorption peaks are observed for nickel electrodes; also two anodic peaks are observed at nickel (Fig. 34 a,c) whereas only one broad oxide formation region arises in the case of platinum electrodes in acid. In the cathodic direction of scanning, one oxide reduction peak is observed for both the nickel and platinum electrodes in slow transients.

In some runs with nickel electrodes, measurements were also made for different ranges of the scanning potential. Thus, if the end potential in the cathodic direction is such that there is no hydrogen production at the electrode surface, then it is found that the first small peak for oxide formation which usually occurs at a potential of ca. -0.6 V disappears (cf. Fig. 34 b,d).

The second anodic oxide formation peak occurs at a potential of ca. +0.5 V but the exact value of the peak potential depends on the concentration and temperature of the electrolyte, and the sweep rate. The peak potential for the reduction of the oxide species formed at a potential of ca. 0.5 V is observed to occur at a potential of ca. 0.35 V.

An appreciable hysteresis between the processes of oxidation and reduction of the lower valent oxide species (viz. $Ni(OH)_2$) at the electrode surface therefore arises. This phenomenon is also observed at both platinum and silver electrode surfaces in KOH solution (see also sub-section (b), below).

A small hysteresis loop is also observed in the cathodic region for evolution of hydrogen on the oxide surface and on the free (?) metal surface (Fig. 34, a,c). However, this aspect of hysteresis was not studied specially in the present work.

The charges Q passed for the formation of the oxide and for its reduction were calculated from the areas under the respective peaks for various sweep rates, and various concentrations and temperatures of the KOH solution. Charge balance was also checked. The results are summarised in Table V. It is seen that Q depends significantly on the sweep rate. This effect may arise because the oxide grows at the electrode surface with time; alternatively, the observed peaks may be associated with currents both of pseudo-faradaic and a faradaic origin. Under such conditions, the slower the sweep rate the greater will be the contribution of the faradaic charge (e.g. here for O_2 evolution) to the total charge. From the charge ratio

Table V

Values of Charges Q_{anodic} and $Q_{cathodic}$ as a function of dV/dt at Nickel Electrodes in aq. KOH

Concentration and temp. of the Electrolyte	Potential range vs Hg/HgO (V.)	Scanning rate (V. Sec^{-1})	Anodic Charge (mc. cm^{-2})	Cathodic Charge (mc. cm^{-2})	Ratio $\frac{Q_{anodic}}{Q_{cathodic}}$
2.0 M, 30°C	-1.426 to +0.812	0.448	29.15	31.23	0.93
		0.895	30.88	31.94	0.97
		2.239	25.77	21.86	1.18
		4.477	26.33	20.06	1.31
	-1.196 to +0.676	0.372	20.96	21.27	0.99
		0.745	21.8	25.43	0.86
		1.862	17.14	19.68	0.87
		3.724	14.03	16.60	0.85
	-0.695 to +0.826	1.521	14.28	13.38	1.07
		3.042	13.38	12.74	1.05
		6.084	9.38	10.64	0.89
7.3 M, -30°C	-0.853 to +0.750	0.321	10.25	10.48	0.98
		0.641	9.55	9.32	1.03

Figure 36. Repetitive potentiodynamic triangular sweep at silver electrodes in KOH solutions for various concentrations and temperatures:

(a) 2.0 M KOH, 25°C;

(b) 2.0 M KOH, 60°C;

(c) 2.0 M KOH, 27.5°C; shorter potential range;

(d) 7.0 M KOH, -32 to -42°C; shorter potential range:

(1) -32°C; (2) -34°C; (3) -36°C; (4) -38°C; and (5) -42°C.

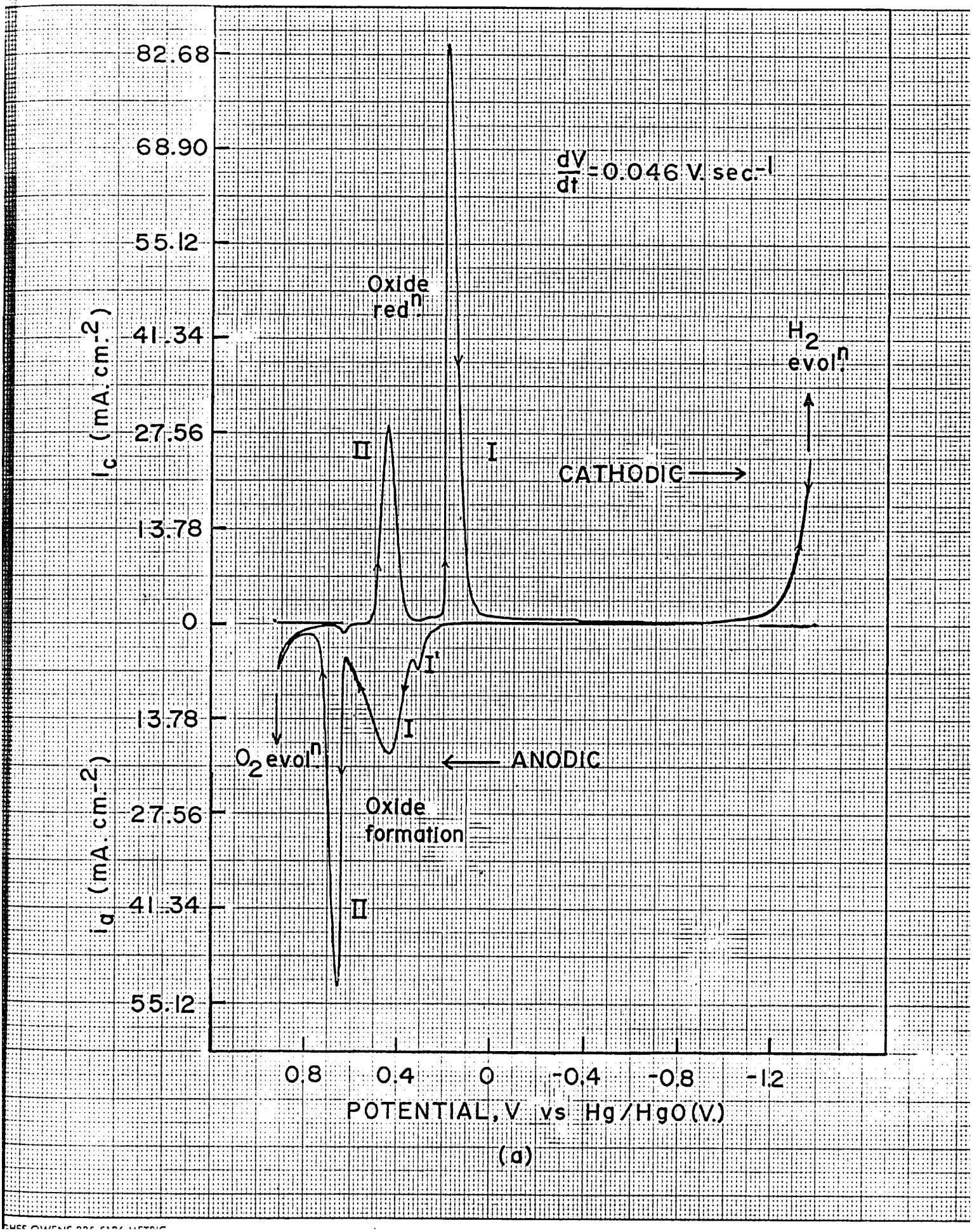
82.68
68.90
55.12
41.34
27.56
13.78
0
13.78
27.56
41.34
55.12
i_c (mA. cm.$^{-2}$)
i_a (mA. cm.$^{-2}$)
$\frac{dV}{dt}$ = 0.046 V. sec.$^{-1}$
Oxide red^{n}.
H_2 evol^{n}.
II
I
CATHODIC ⟶
I'
I
O_2 evol^{n}.
⟵ ANODIC
Oxide formation
II
0.8
0.4
0
-0.4
-0.8
-1.2
POTENTIAL, V vs Hg/HgO (V.)
(a)

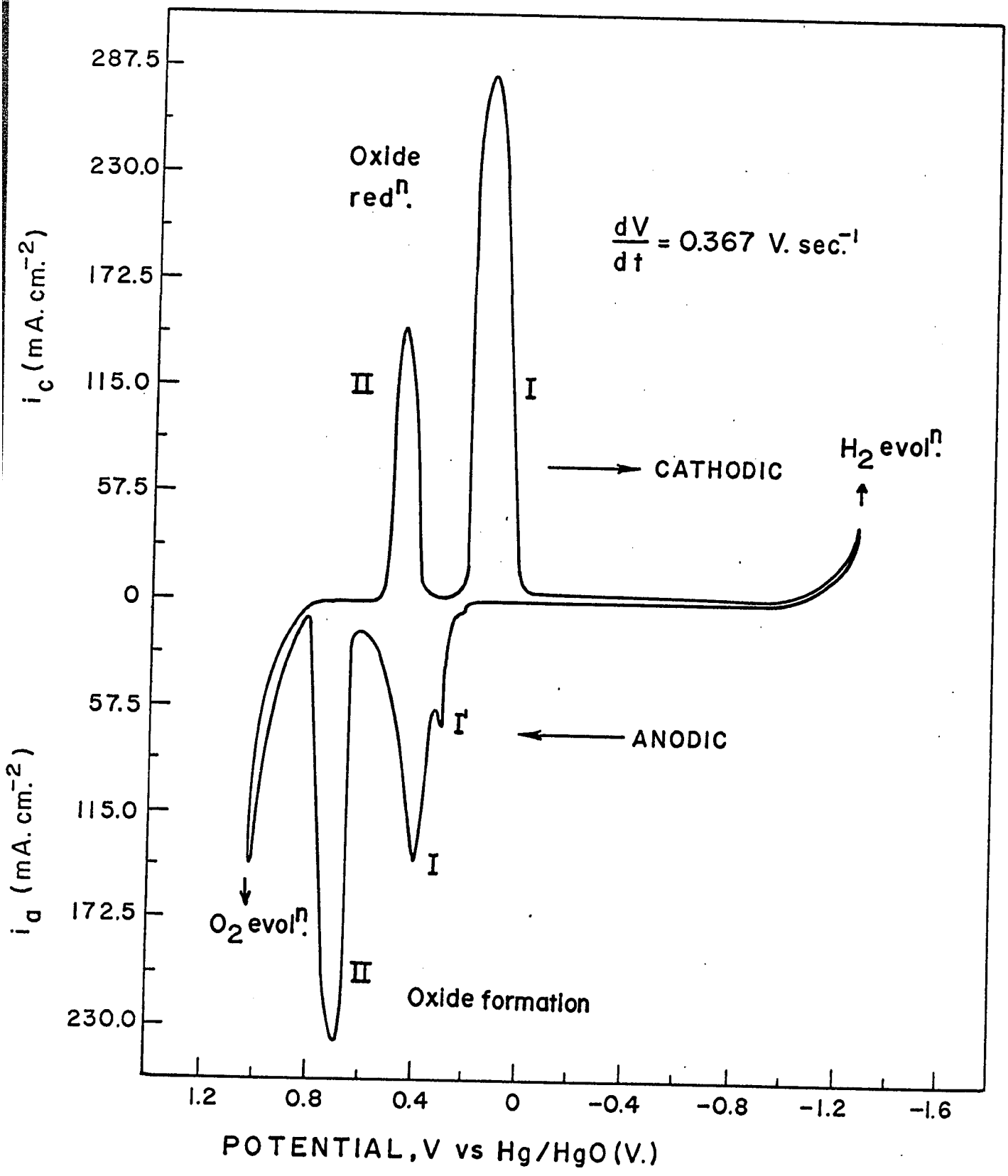
287.5
230.0
172.5
115.0
57.5
0
57.5
115.0
172.5
230.0
i_c (mA. cm.$^{-2}$)
i_a (mA. cm.$^{-2}$)
Oxide red^n.
$\frac{dV}{dt}$ = 0.367 V. sec.$^{-1}$
II
I
CATHODIC
H_2 evol^n.
I'
ANODIC
I
O_2 evol^n.
II
Oxide formation
1.2
0.8
0.4
0
-0.4
-0.8
-1.2
-1.6
POTENTIAL, V vs Hg/HgO (V.)

(b)

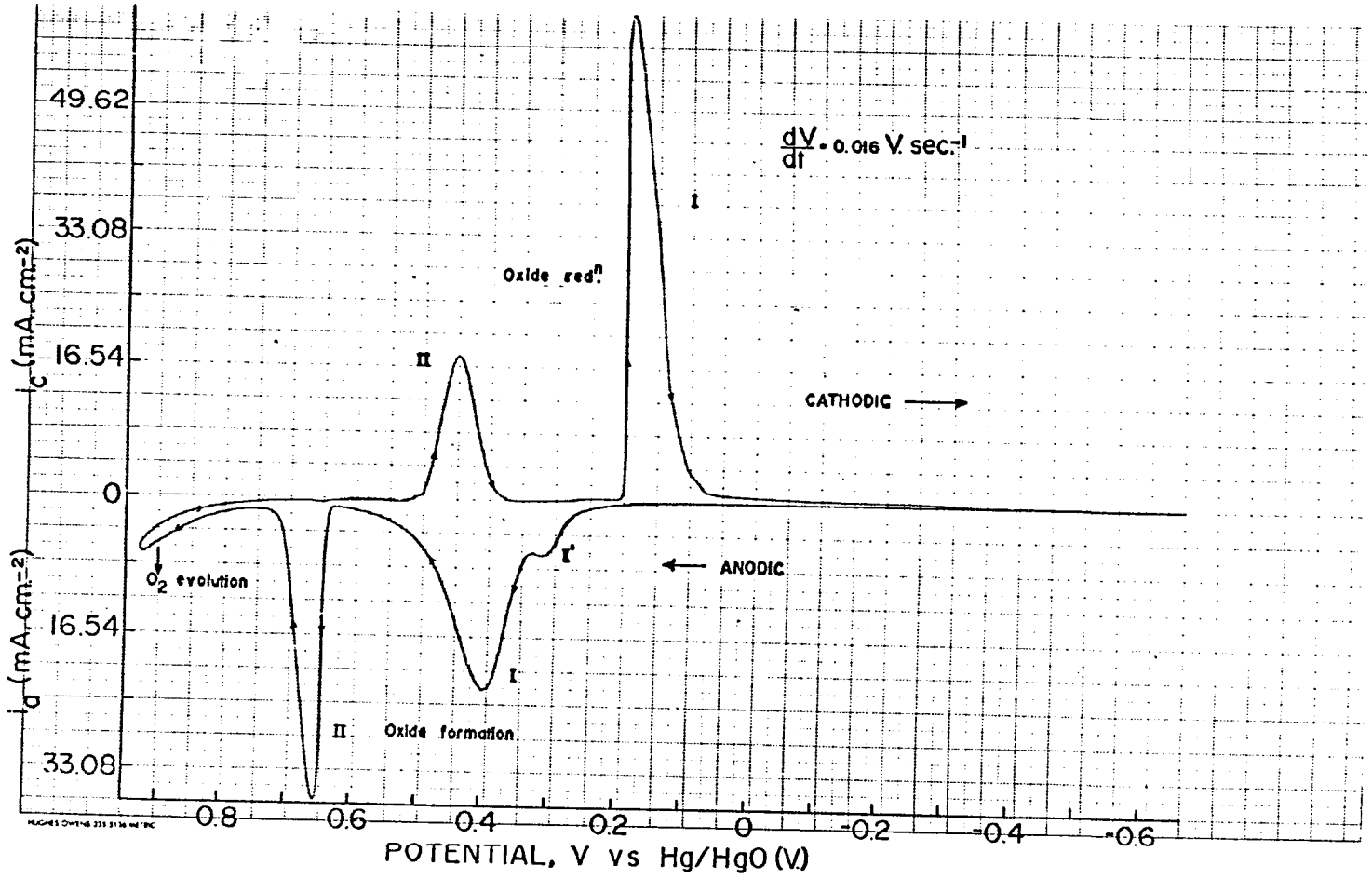
49.62
33.08
16.54
0
16.54
33.08
i_c (mA.cm^{-2})
i_a (mA.cm^{-2})
$\frac{dV}{dt}$ = 0.016 V. sec^{-1}
I
II
Oxide red^{n}
CATHODIC
ANODIC
O_2 evolution
I'
I
II
Oxide formation
0.8
0.6
0.4
0.2
0
-0.2
-0.4
-0.6
POTENTIAL, V vs Hg/HgO (V)

(c)

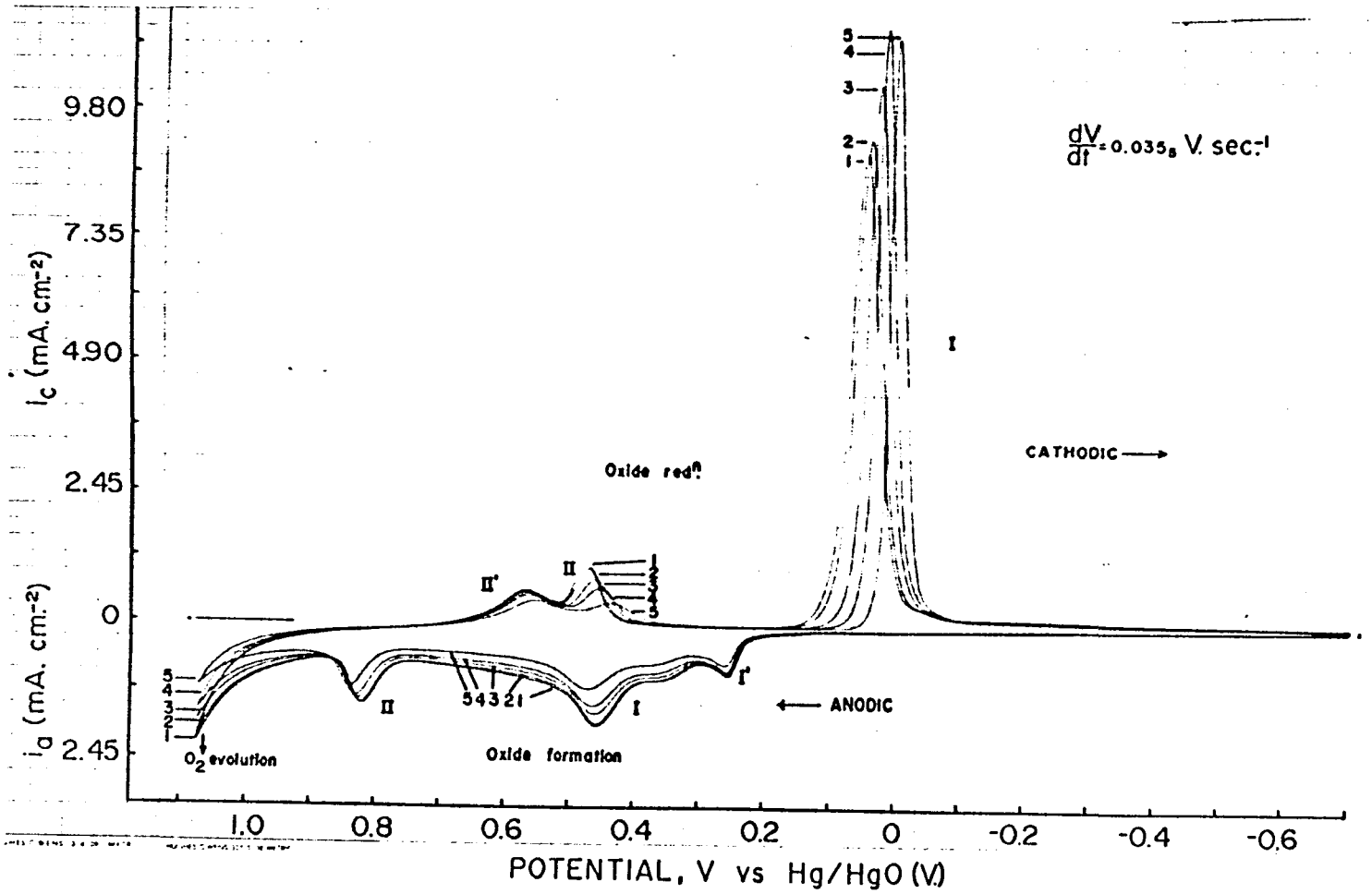
9.80
7.35
4.90
2.45
0
2.45
i_c (mA. cm^{-2})
i_a (mA. cm^{-2})
$\frac{dV}{dt}$ = 0.035$_8$ V. sec^{-1}
5
4
3
2
1
I
CATHODIC ⟶
Oxide red^n.
II'
II
I'
5 4 3 2 1
⟵ ANODIC
O_2 evolution
Oxide formation
1.0
0.8
0.6
0.4
0.2
0
-0.2
-0.4
-0.6
POTENTIAL, V vs Hg/HgO (V)

(d)

(Column 6, Table V) it may, however, be concluded that the contribution of charge due to an overall faradaic process is negligible.

(B) Silver Electrodes: Potentiodynamic i-V profiles at silver metal electrodes in 2.0 M aq. KOH at 30°C and 60°C and in 7.0 M aq. KOH at -30°C to -40°C were obtained for the purpose of comparison with the behaviour observed at nickel electrodes. Typical i-V profiles are shown in Fig. 36.

Two well-defined oxide formation peaks and two corresponding oxide reduction peaks occur in the i-V curves. A third small and ill-defined peak (I') appears at the beginning of the first anodic peak at and above room temperature: this peak becomes more prominent in runs conducted at low temperatures (Fig. 36d). Under such conditions (viz. at -30°C) the first anodic oxidation peak broadens and a new oxide reduction peak (II') appears (Fig. 36d).

The peak potentials themselves and the potential range of separation between the corresponding oxidation and reduction peak potentials were found to depend significantly on the sweep rate and the temperature (cf. Fig. 45).

Figure 37. Typical galvanostatic potential vs time transient (charging).

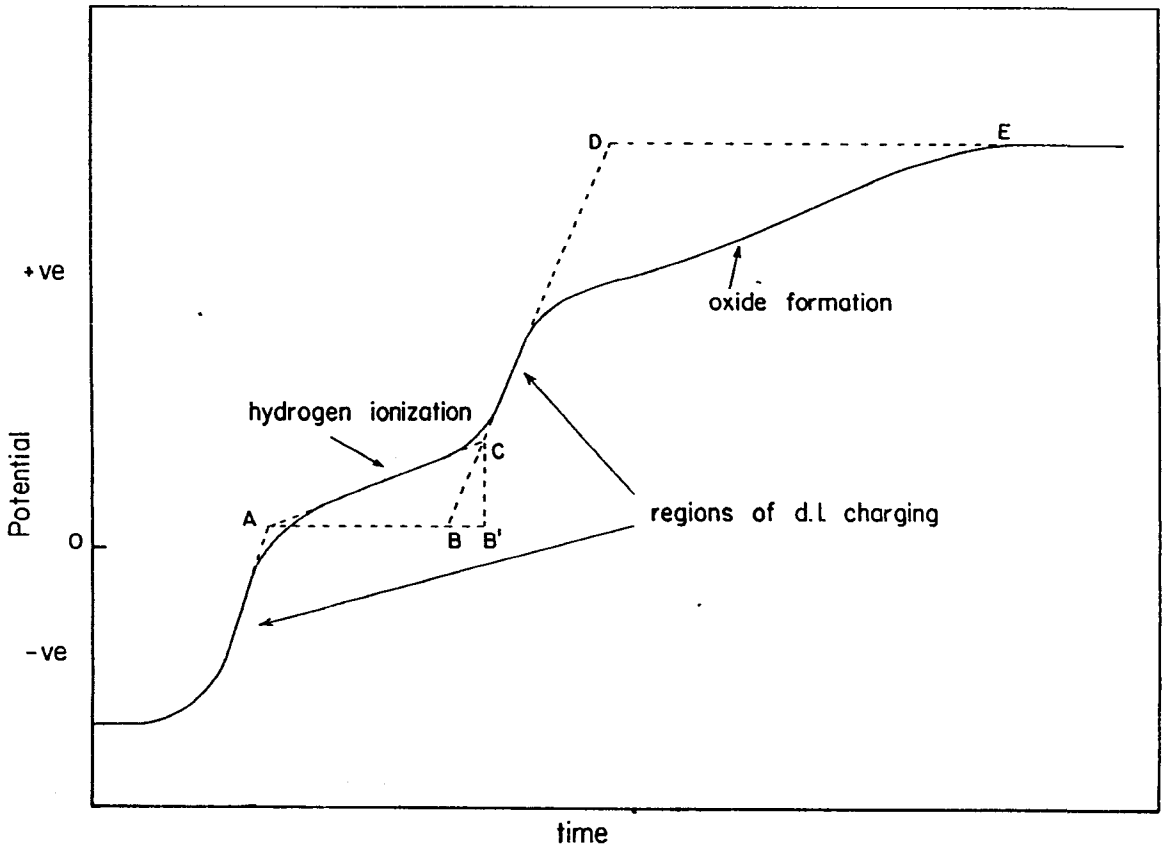
+ve
0
-ve
Potential
time
A
B
B'
C
D
E
hydrogen ionization
oxide formation
regions of d.l charging

As at Ni, no H- adsorption or desorption peaks are observed at silver.

Oscillations of both currents and/or potentials were frequently observed at silver electrodes during the formation of the first oxide and in the potential region between the two cathodic reduction peaks (viz. Fig. 36). However, at higher temperatures (60°C), the oscillations were eliminated.

The charges Q passed for formation and reduction of the oxides were calculated as a function of sweep rate for 2.0 M aq. KOH at 30°C and 60°C, and for 7.0 M aq. KOH at -40°C. A charge balance was also made; results obtained are summarised in Table VI.

(iii) Results of Fast Galvanostatic Discharge Experiments:

(A) Principles Involved and the Determination of the Electrochemically Available Charge: A typical galvanostatic charging (or discharging) transient (cf. Fig. 37) has usually two regions corresponding to high adsorption pseudo-capacity where the rate of change of potential, V, with time, t, at constant current, i, is relatively small (i.e. "arrests" are observed in the transient). These are separated by a low capacity region corresponding to a change of charge in and configuration of the ionic

Table VI

Values of Charges Q_{anodic} and $Q_{cathodic}$ as a function of dV/dt at Silver Electrodes in aq. KOH

Concentration and temp. of the Electrolyte	Potential range vs Hg/HgO (V)	Scanning rate ($V.\ Sec^{-1}$)	Anodic Charge ($mc.\ cm^{-2}$)		Cathodic Charge ($mc.\ cm^{-2}$)		Ratio $\frac{Q_{anodic}}{Q_{cathodic}}$
			I+1'	II	I	II	
2.0 M, 25°C	-1.380 to +0.929	0.0092	122.78	93.42	140.14	72.07	1.02
		0.023	118.51	96.63	168.16	69.40	0.91
		0.0462	118.26	104.78	206.39	43.66	0.89
		0.0693	81.03	111.11	195.12	34.39	0.84
		0.0924	58.21	99.87	164.69	34.07	0.80
	-0.572 to +0.930	0.006	136.30	92.00	158.45	77.52	0.97
		0.030	76.41	53.49	90.55	42.03	0.98
		0.060	82.11	56.64	117.09	36.12	0.91
2.0 M, 60°C	-1.269 to +1.025	0.046	91.27	81.27	121.9	52.51	0.99
		0.367	60.65	69.57	123.65	37.52	0.81
		0.459	52.51	62.51	88.77	32.51	0.95
7.0 M, -40°C	-0.920 +0.960	0.0188	17.42	3.23	16.84	2.31	1.08

I and II refer to the two well separated regions of oxidation and reduction at Ag. 1' refers to the small peak overlapping the peak I. At -40°C, the charges at peaks II and II' are summed up.

double layer. One of the high capacity regions corresponds (at noble metals) to ionization of hydrogen atoms chemisorbed on the electrode surface and the second to the formation of a surface oxide or a layer of adsorbed oxygen. Thus the presence of adsorbed electro-active species at the electrode surface is indicated by "arrests" in the galvanostatic V-t transients.

A typical galvanostatic V-t transient would represent directly a Q (or θ) vs V profile provided that most of the current passed is of a pseudo-faradaic origin, i.e. currents of non-faradaic (for double-layer charging) and faradaic origins (for the overall reaction) are relatively small. Hence, the first derivative (dV/dt) of the relation represented by the V-t transient would give a $\frac{1}{C}$ vs. V profile, directly. Since the galvanostatic V-t transients themselves usually show only ill-defined inflections from which it is difficult to calculate capacitances graphically with satisfactory accuracy, the direct differential method of Kozlowska and Conway (120) was used. This method has the advantage of giving directly the detailed form of the potential-dependence of the capacitance associated with the charging (or discharging)processes and can indicate the presence of two or more intermediates at the electrode surface in more complex reactions.

Figure 38. (a) Typical potential vs. time transient and its differential coefficient obtained in a fast galvanostatic reduction pulse.

(b) Typical potential vs. time transient and its differential obtained in a fast galvanostatic reduction pulse following an open-circuit decay for a controlled time (τ_D).

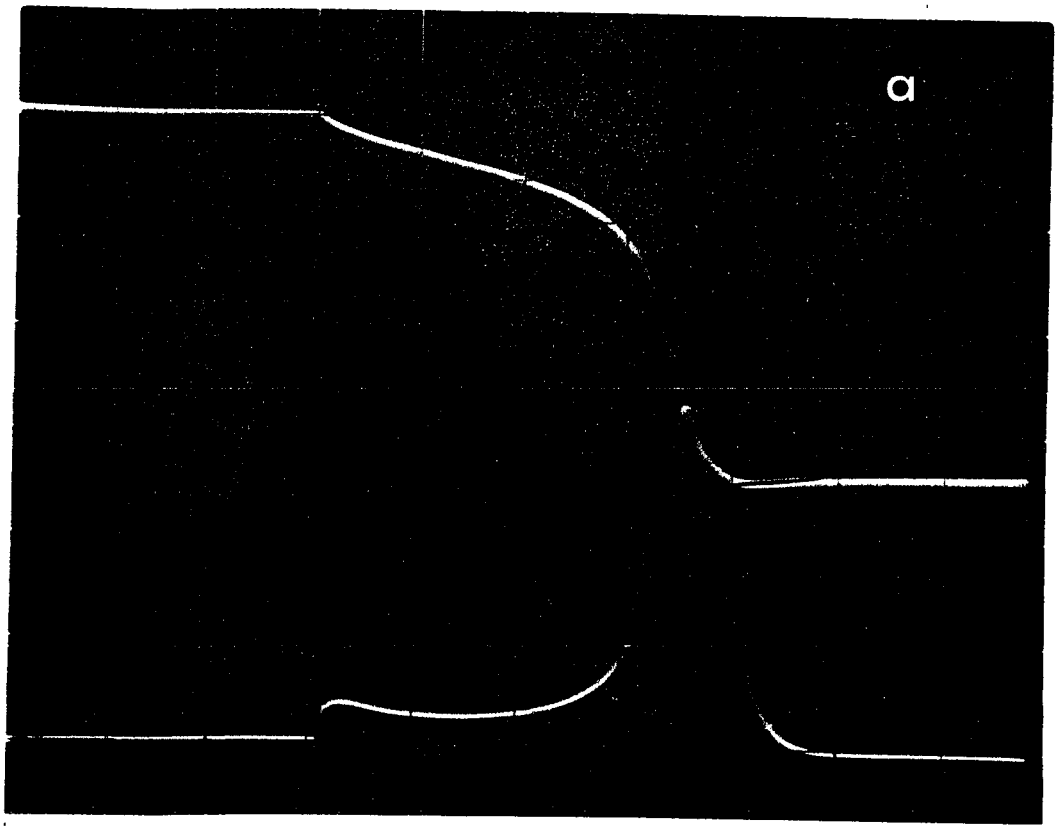
a

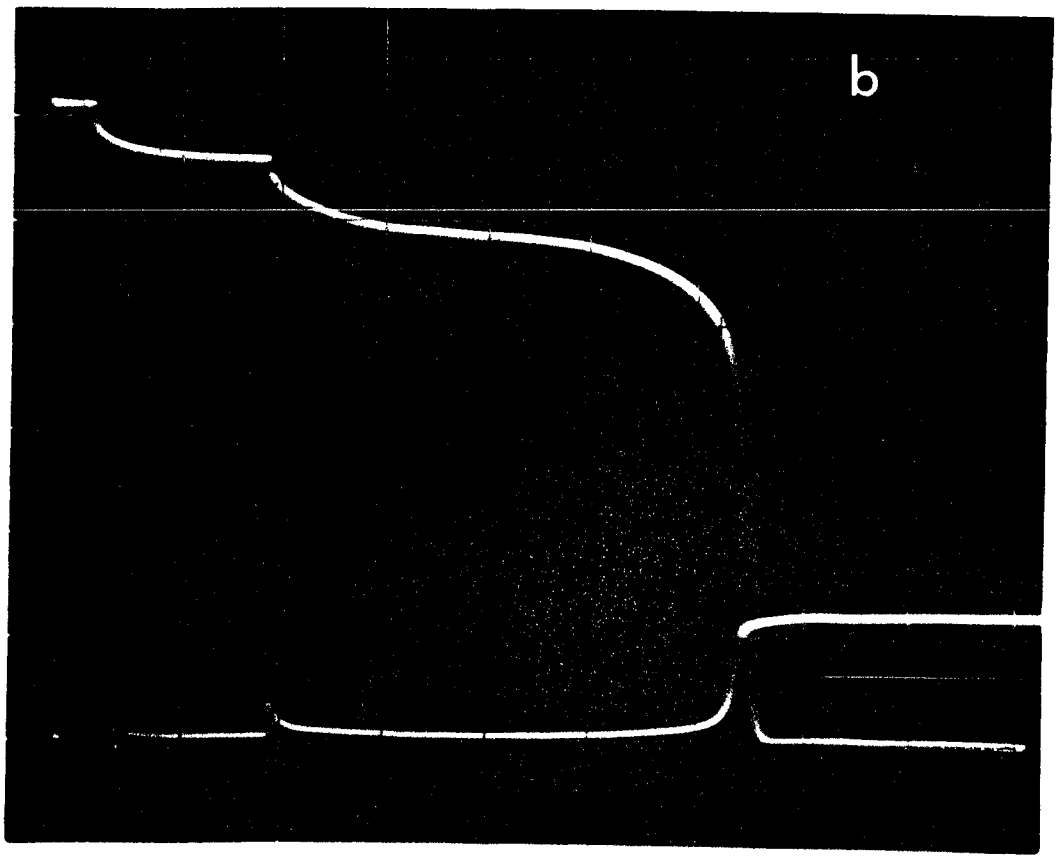
b

Figure 39. Oxide charge, Q, for the nickel oxide electrode (reducible in a fast galvanostatic reduction pulse) as a function of electrode potential, for various concentrations of KOH and temperatures:
(a) 2.05 M KOH, (1) 30°C, (2) 60°C, (3) 83°C;
(b) 13.1 M KOH, (1) 30°C, (2) 60°C, (3) 89°C, (4) -15°C in 12.45 M KOH, and
(c) 6.7 M KOH, (1) -30°C and (2) 30°C.

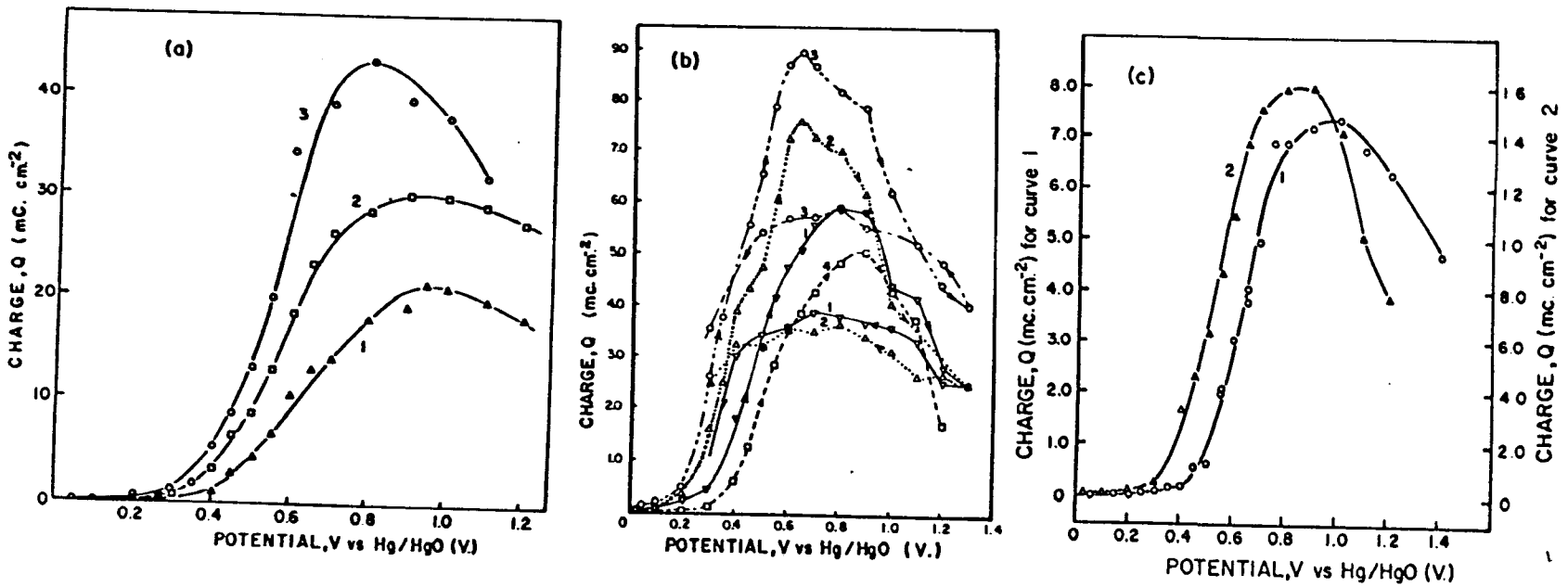
(a)
CHARGE, Q (mC. cm^{-2})
POTENTIAL, V vs Hg/HgO (V.)
(b)
CHARGE, Q (mc. cm^{-2})
POTENTIAL, V vs Hg/HgO (V.)
(c)
CHARGE, Q (mc. cm^{-2}) for curve 1
CHARGE, Q (mc. cm^{-2}) for curve 2
POTENTIAL, V vs Hg/HgO (V.)

Figure 40. Relation between inflections in kinetic log[i]-V curves and the potential-dependence of charge for oxide film reduction at similar nickel electrodes:

(a) 2.05 M KOH, 25°C;

(b) 2.05 M KOH, 60°C.

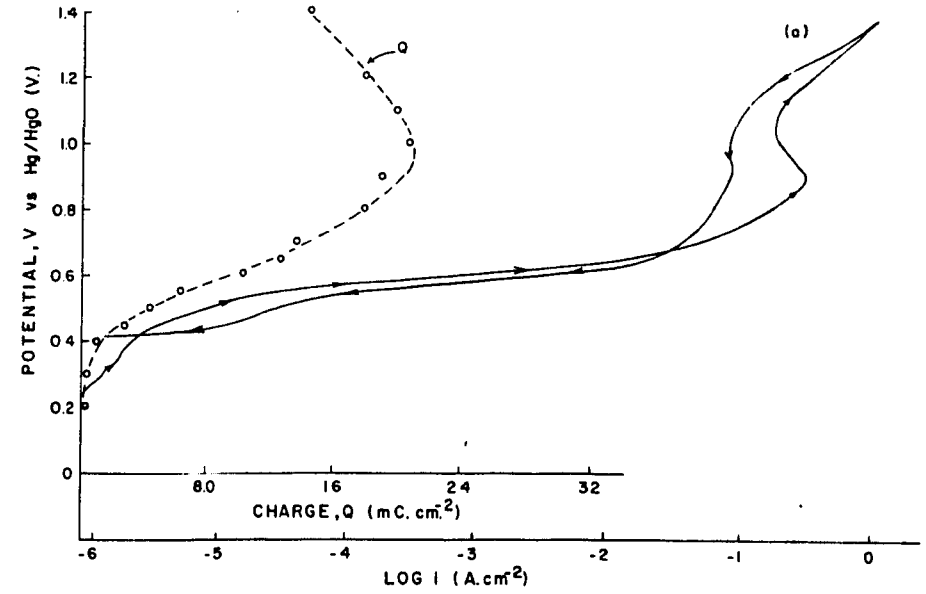
(a)
Q
POTENTIAL, V vs Hg/HgO (V.)
1.4
1.2
1.0
0.8
0.6
0.4
0.2
0
8.0
16
24
32
CHARGE, Q (mC. cm⁻²)
-6
-5
-4
-3
-2
-1
0
LOG I (A.cm⁻²)

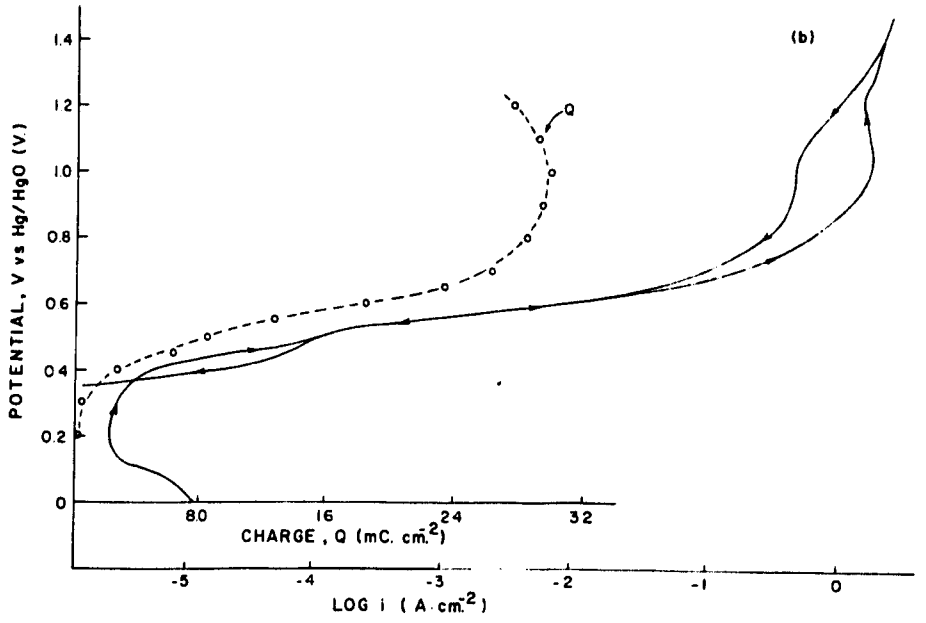
(b)
Q
POTENTIAL, V vs Hg/HgO (V.)
1.4
1.2
1.0
0.8
0.6
0.4
0.2
0
8.0
16
24
32
CHARGE, Q (mC. cm⁻²)
-5
-4
-3
-2
-1
0
LOG i (A.cm⁻²)

In the present work, the amounts of the charge associated with reduction of oxygen-containing species in the thin film oxide layers at the electrode surface in KOH solution were determined by fast galvanostatic reductions (Chapter II) from controlled anodic potentials at 0.05 V intervals using a constant high current (see below). A typical fast discharge transient for a nickel oxide electrode is shown in Fig. 38a together with its time-dependent differential coefficient.

In this way, the charges required for reduction of the oxide layer at the nickel electrode in KOH solutions at various concentrations (2.05 to 13.1 M) and temperatures (from -30°C to +89°C) could be calculated. The results are given in Fig. 39. It is observed that the charge, Q, vs. potential, V, profile has a maximum around 0.8 V. Comparison with the steady-state log[i]-V plots (for example, Fig. 40) shows that in the region where self-passivation occurs, the quantity of cathodically reducible oxide gradually decreases, and the chemically determinable amount of nickel oxidised also decreases (see section 3 (g) of this Chapter).

Up to the potential at which the charge maximum occurs (see Fig. 39), the Q vs. V profile has the same shape as that observed in a V-t transient (Fig. 38 a)

Figure 41. Dependence of oxide charge, Q, for the nickel oxide electrode (reducible in a cathodic galvanostatic pulse) on the galvanostatic reduction current density.

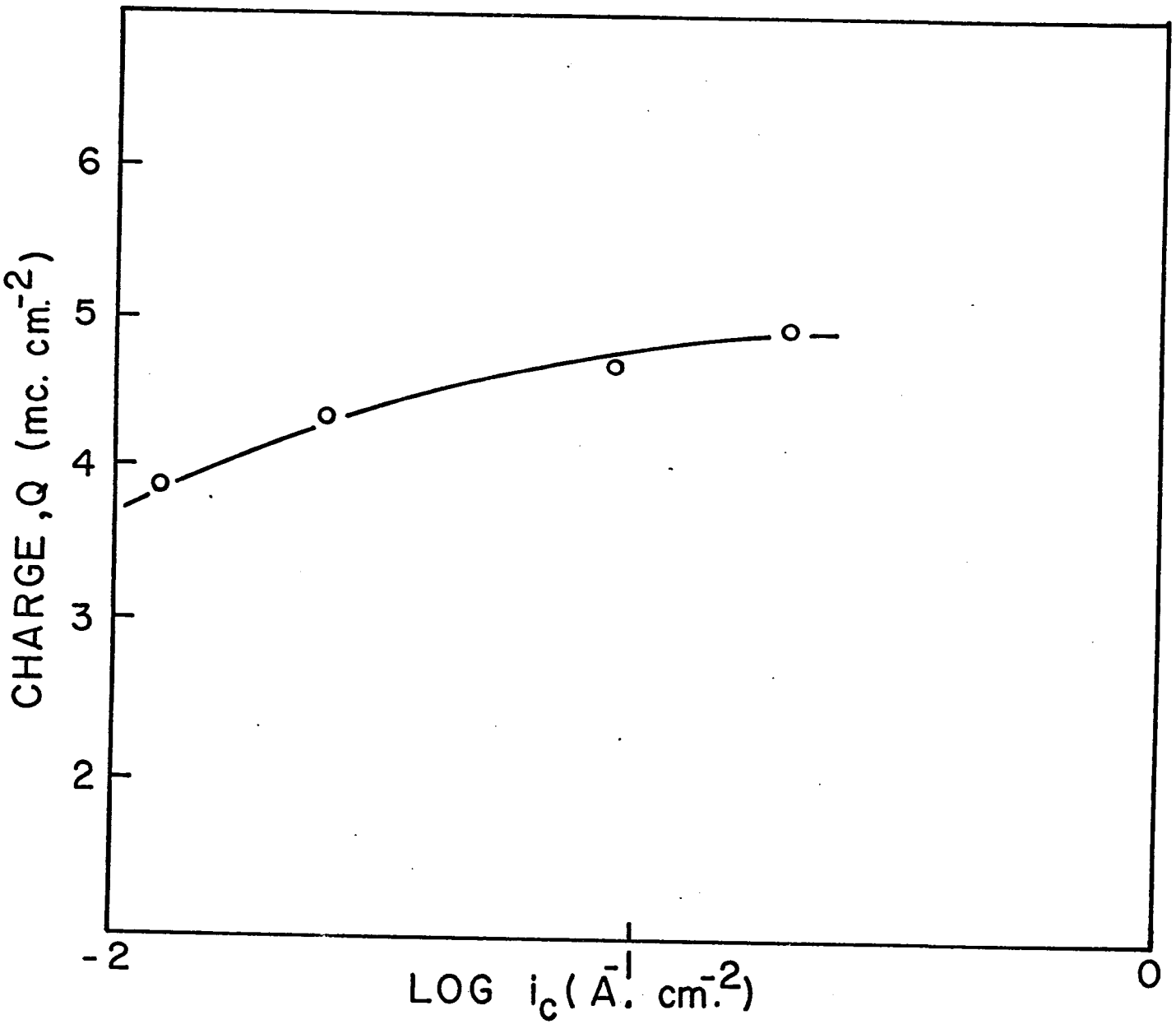
CHARGE, Q (mc. cm.$^{-2}$)
6
5
4
3
2
-2
-1
0
LOG i_c (A. cm.$^{-2}$)

from a galvanostatic pulse, as would be expected in the absence of an appreciable faradaic current (163,164).

(B) Dependence of Charge for Oxide Reduction on the Galvanostatic Reduction Current Density, i.e. Rate of Reduction: Here the charge associated with reduction of oxygen-containing species at the electrode surface in KOH solution at a certain electrode potential was determined as above, but varying intensities of the galvanostatic reduction current density were employed. The results are given in Fig. 41. It is observed that as the cathodic current density is increased, Q increases to an extent of ca 20%. This is due to self-discharge effects to be discussed in the following section.

(C) Loss of Oxide Charge at the Nickel Oxide Electrode during Open-circuit E.m.f. Decay: The apparent decrease of charge with increase of potential (cf. Fig. 39) (i.e. occurrence of the maximum) may be due in part to a self-discharge process which occurs at high potentials simultaneously with the electrochemical reduction during determination of oxide charge in a fast galvanostatic cathodic pulse. In order to account for this loss of oxide charge, experiments were performed in the manner described in Chapter II, section 8(b), (vi). A typical potential-time transient with its differential coefficient

Figure 42. (a) Self-discharge at thin film nickel oxide electrodes at a potential 1.0 V in 2.0 M KOH at 28°C.

(b) Self-discharge at thin film nickel oxide electrodes in 2.0 M KOH at 27°C from various anodic potentials:

(1) V_i = 0.5 V

(2) V_i = 0.7 V.

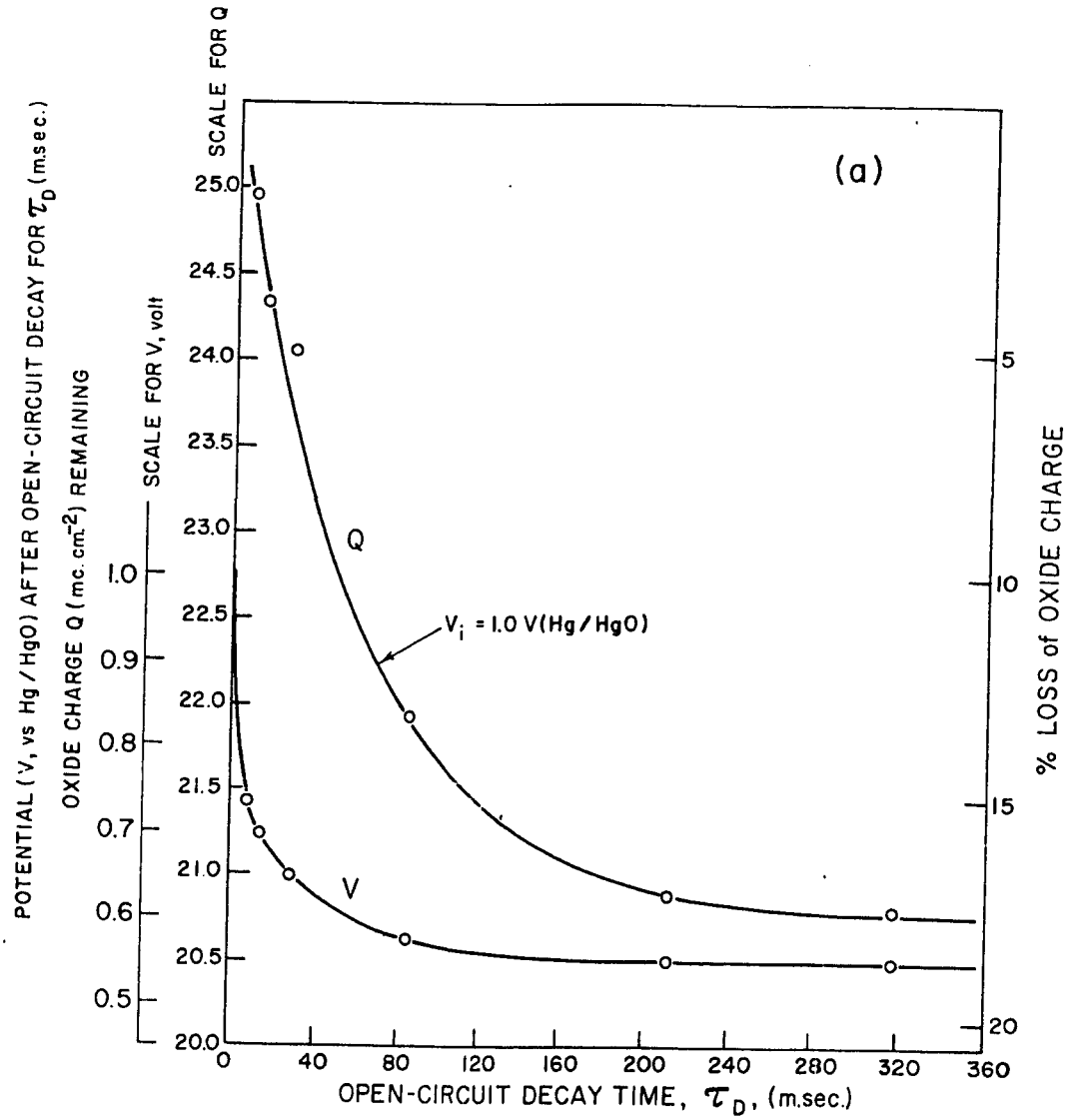
(a)
SCALE FOR Q
SCALE FOR V, volt
POTENTIAL (V, vs Hg/HgO) AFTER OPEN-CIRCUIT DECAY FOR τ_D (m.sec.)
OXIDE CHARGE Q (mc.cm^{-2}) REMAINING
% LOSS of OXIDE CHARGE
Q
V
V_i = 1.0 V(Hg/HgO)
OPEN-CIRCUIT DECAY TIME, τ_D, (m.sec.)

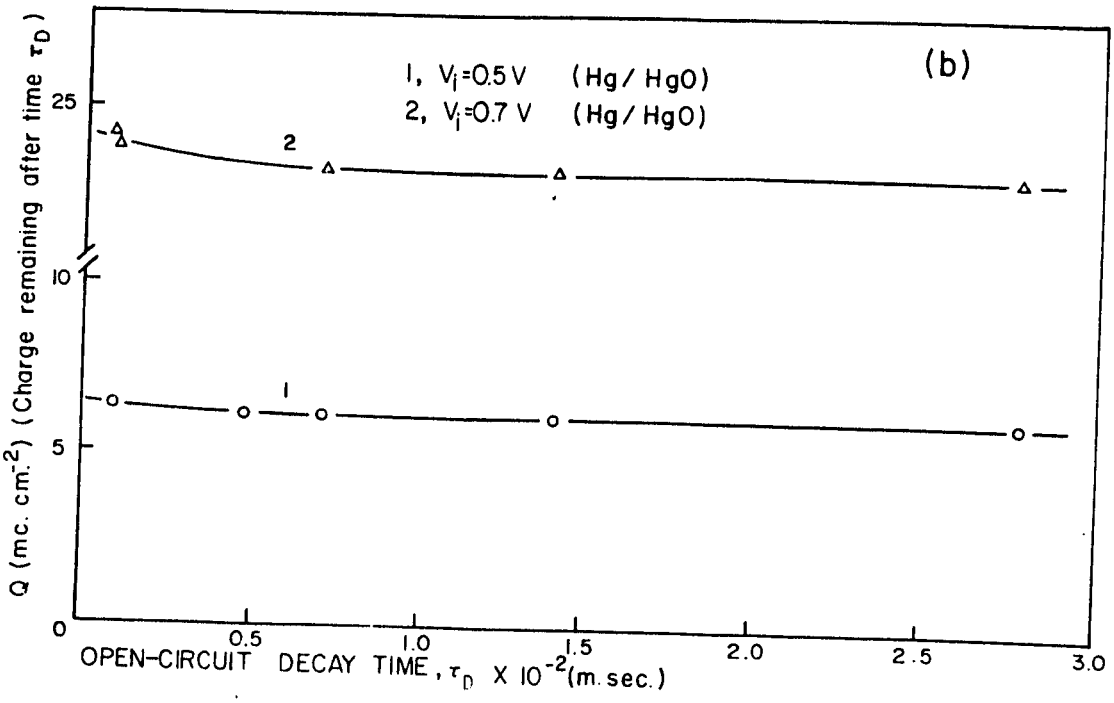
(b)
1, V_i=0.5 V (Hg/HgO)
2, V_i=0.7 V (Hg/HgO)
Q (mc. cm^{-2}) (Charge remaining after time τ_D)
OPEN-CIRCUIT DECAY TIME, τ_D X 10^{-2}(m.sec.)

Figure 43. Increase of oxide charge for nickel oxide electrodes (determined by galvanostatic reduction) with time at various indicated potentials in aq. KOH solution of various concentrations and temperatures:

(a) 2.0 M KOH, 30°C;

(b) 2.0 M KOH, 60°C;

(c) 13.1 M KOH, 30°C and 60°C.

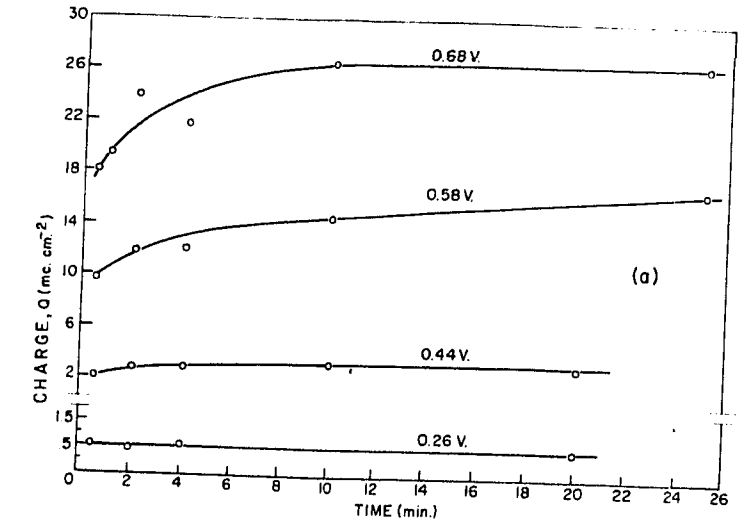
0.68 V.
0.58 V.
0.44 V.
0.26 V.
(a)
CHARGE, Q (mc. cm⁻²)
TIME (min.)

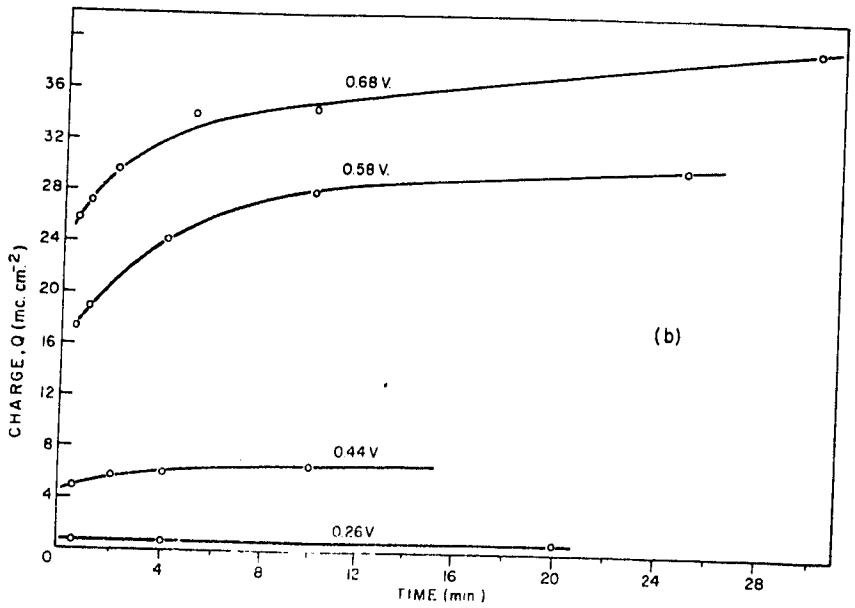
0.68 V.
0.58 V.
0.44 V
0.26 V
(b)
CHARGE, Q (mc. cm⁻²)
TIME (min.)

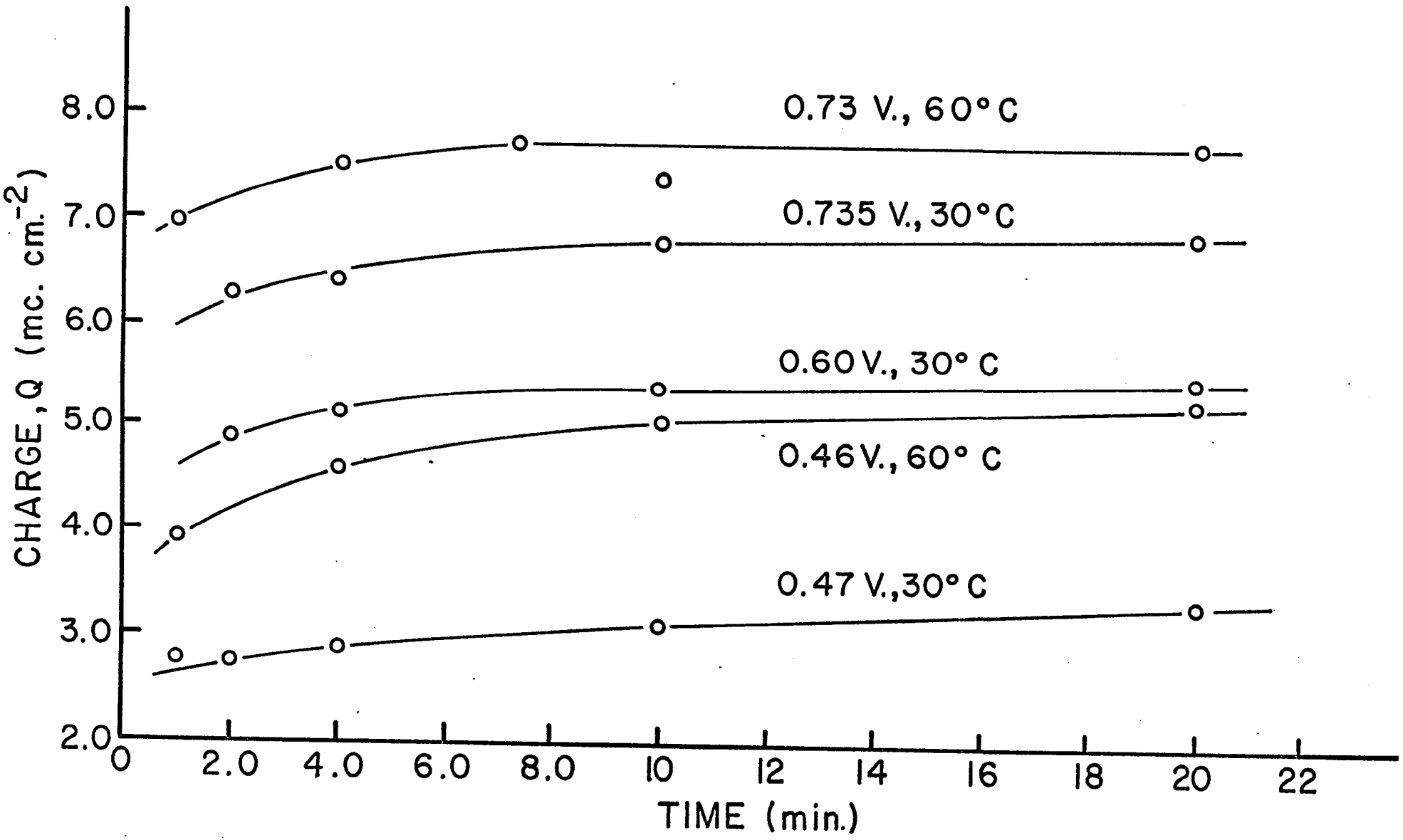
8.0
7.0
6.0
5.0
4.0
3.0
2.0
CHARGE, Q (mc. cm.$^{-2}$)
0.73 V., 60° C
0.735 V., 30° C
0.60 V., 30° C
0.46 V., 60° C
0.47 V., 30° C
0
2.0
4.0
6.0
8.0
10
12
14
16
18
20
22
TIME (min.)

(c)

is shown in Fig. 38 b. The charge for oxide reduction passed in the cathodic pulse was determined as described in Chapter II, section 8(b), (v) and hence the amounts of electrochemically reducible material remaining in thin layers of oxide after various short open circuit (delay) times τ_D were deduced. A plot of charge Q vs τ_D was made (Fig. 42 a) from which the amounts of electrochemically reducible material that would have been present had self-discharge been negligible could be estimated by extrapolation (Fig. 42 a). It was found that the extent of loss of cathodically reducible material is potential-dependent (Fig. 42) (as expected) and that the loss is up to ca. 20% (Fig. 42 a).

(D) Kinetics of Growth of Nickel Oxide Films at The Nickel Metal Electrode Surface: In order to study the apparent rate of growth of oxide (i.e. in terms of material determinable by measurements of the charge required for oxide reduction) at the nickel metal electrode surface in KOH solution, experiments were carried out in the manner described in Chapter II, section 8(b), (viii). Results showing the rate of increase of charge for oxide reduction at various potentials in 2.0 M KOH solution at 30°C and 60°C are shown in Fig. 43 from which it is apparent that the charge for oxide reduction increases approximately logarithmically with time (see also Fig. 64).

(b) Kinetic Behaviour and Hysteresis in the Charge-Discharge Processes at Nickel and Silver Electrodes

Two important general aspects of the behaviour of surface oxide materials are connected with: (i) the kinetics of their formation and reduction; and (ii) any intrinsic irreversibility of a more fundamental thermodynamic kind associated with phase transformation of thin layer materials during or after their anodic formation.

In the present work, attention has been given to these two matters by examining anodic and cathodic charging processes for thin layer materials formed at nickel and silver under potentiodynamic conditions.

Kinetic effects were examined in two ways: (A) by observation of the shape and peak potentials for the oxide formation and reduction peaks in potentiodynamic sweep experiments. The peak potentials were evaluated as a function of sweep rate (dV/dt) using the principles discussed by Conway, Gileadi and Kozlowska (163); (B) by observation of the dependence of inflection potential, V_{inf} (determined from the differentiated charging curve profiles), in cathodic

Figure 44. (a) Typical repetitive potentiodynamic triangular sweeps at nickel as a function of dV/dt within a constant potential range (2.0 M KOH, 22°C):

(1) 0.0059 V sec^{-1}; 0.164 $mA.cm^{-2}$/10 mm;

(2) 0.0117 V sec^{-1}; 0.204 $mA.cm^{-2}$/10 mm;

(3) 0.0234 V sec^{-1}; 0.327 $mA.cm^{-2}$/10 mm;

(4) 0.059 V sec^{-1}; 0.545 $mA.cm^{-2}$/10 mm;

(5) 0.117 V sec^{-1}; 0.818 $mA.cm^{-2}$/10 mm.

(b) Peak potentials for anodic and cathodic sweeps at nickel as a function of dV/dt (potential range -1.426 to +0.812 V, 2M KOH, 30°C).

(c) Peak potentials for anodic and cathodic sweeps at nickel as a function of dV/dt (potential range -1.196 to +0.676 V, 2M KOH, 30°C).

(d) Peak potentials for anodic and cathodic sweeps at nickel as a function of dV/dt (for various potential ranges and at slow sweep rates: 2.0 M KOH, 22°C).

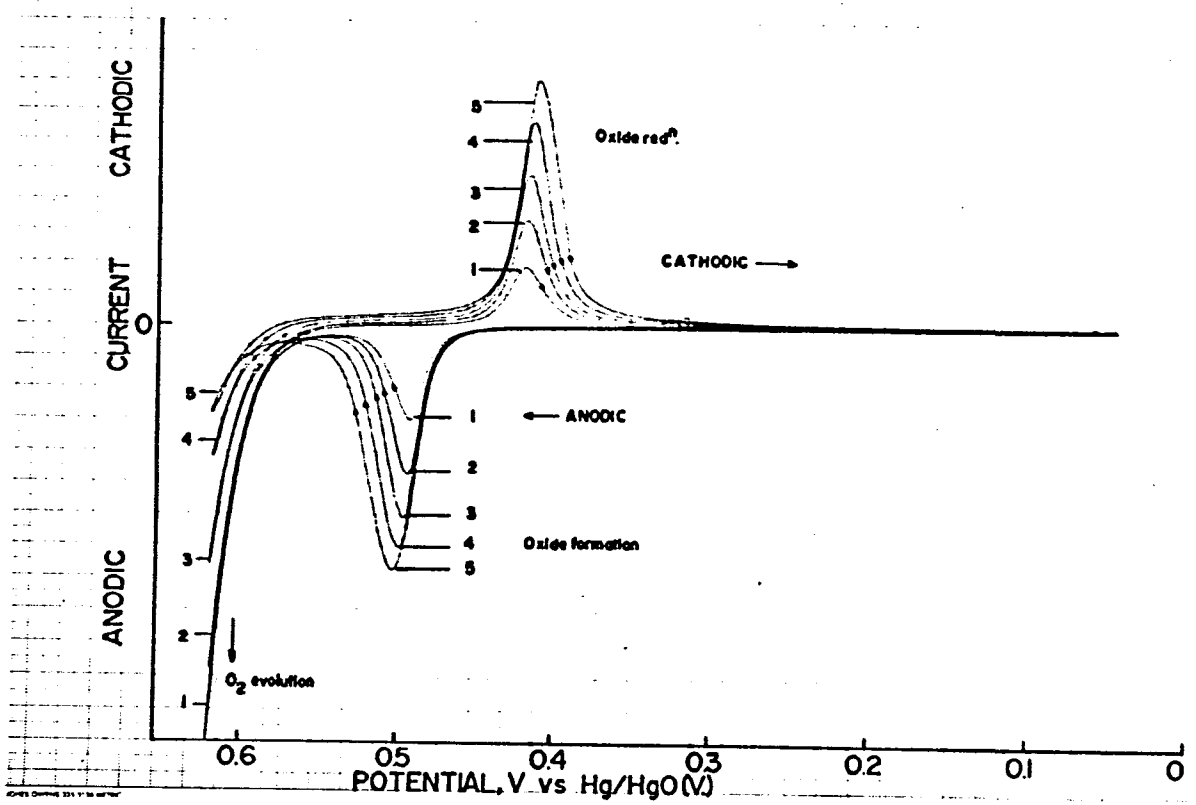
CATHODIC
CURRENT
0
ANODIC
5
4
3
2
1
Oxide red^n.
CATHODIC
ANODIC
Oxide formation
O_2 evolution
0.6
0.5
0.4
0.3
0.2
0.1
0
POTENTIAL, V vs Hg/HgO (V)

(a)

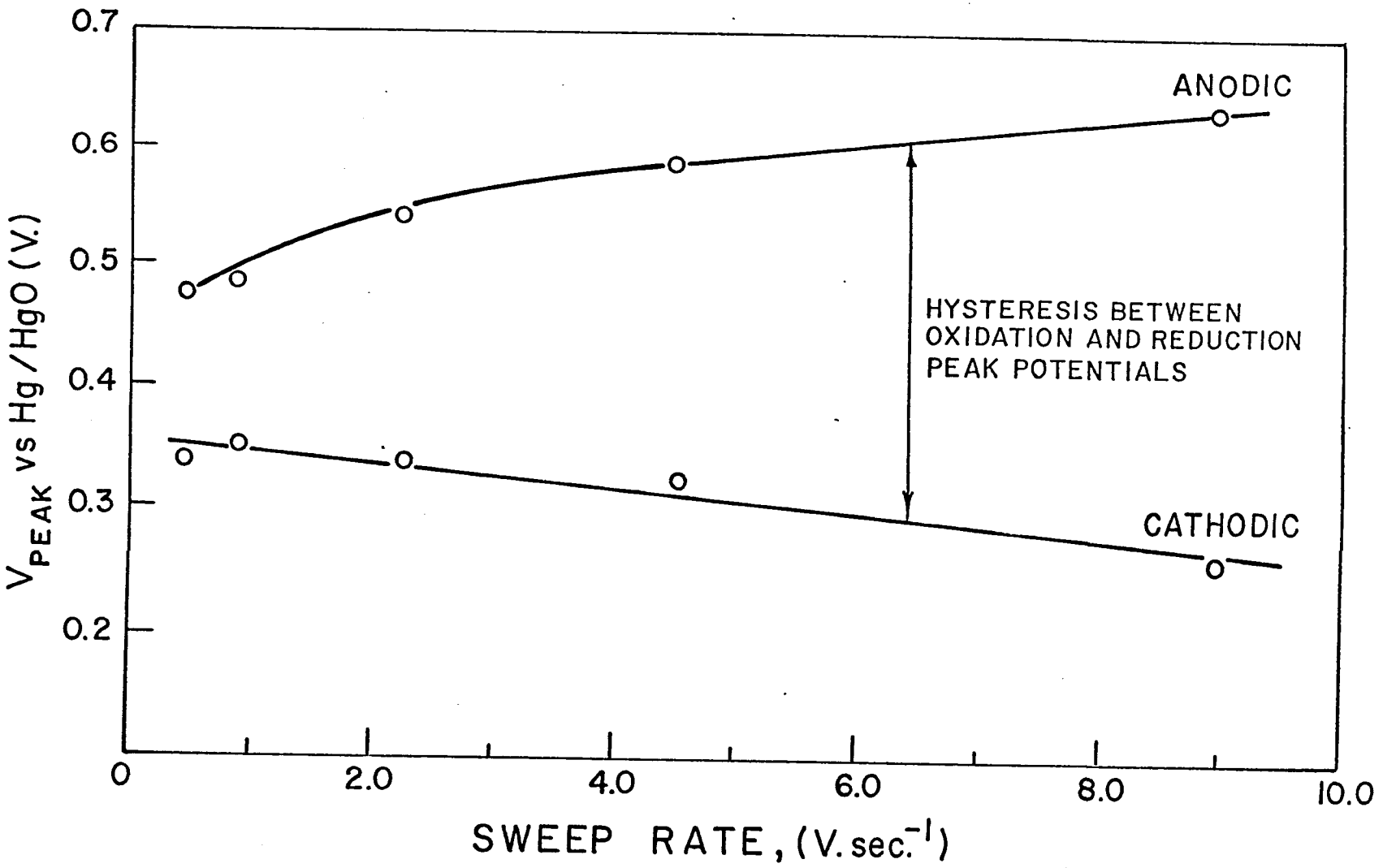
0.7
0.6
0.5
0.4
0.3
0.2
V_{PEAK} vs Hg/HgO (V.)
ANODIC
HYSTERESIS BETWEEN
OXIDATION AND REDUCTION
PEAK POTENTIALS
CATHODIC
0
2.0
4.0
6.0
8.0
10.0
SWEEP RATE, (V. sec.$^{-1}$)

(b)

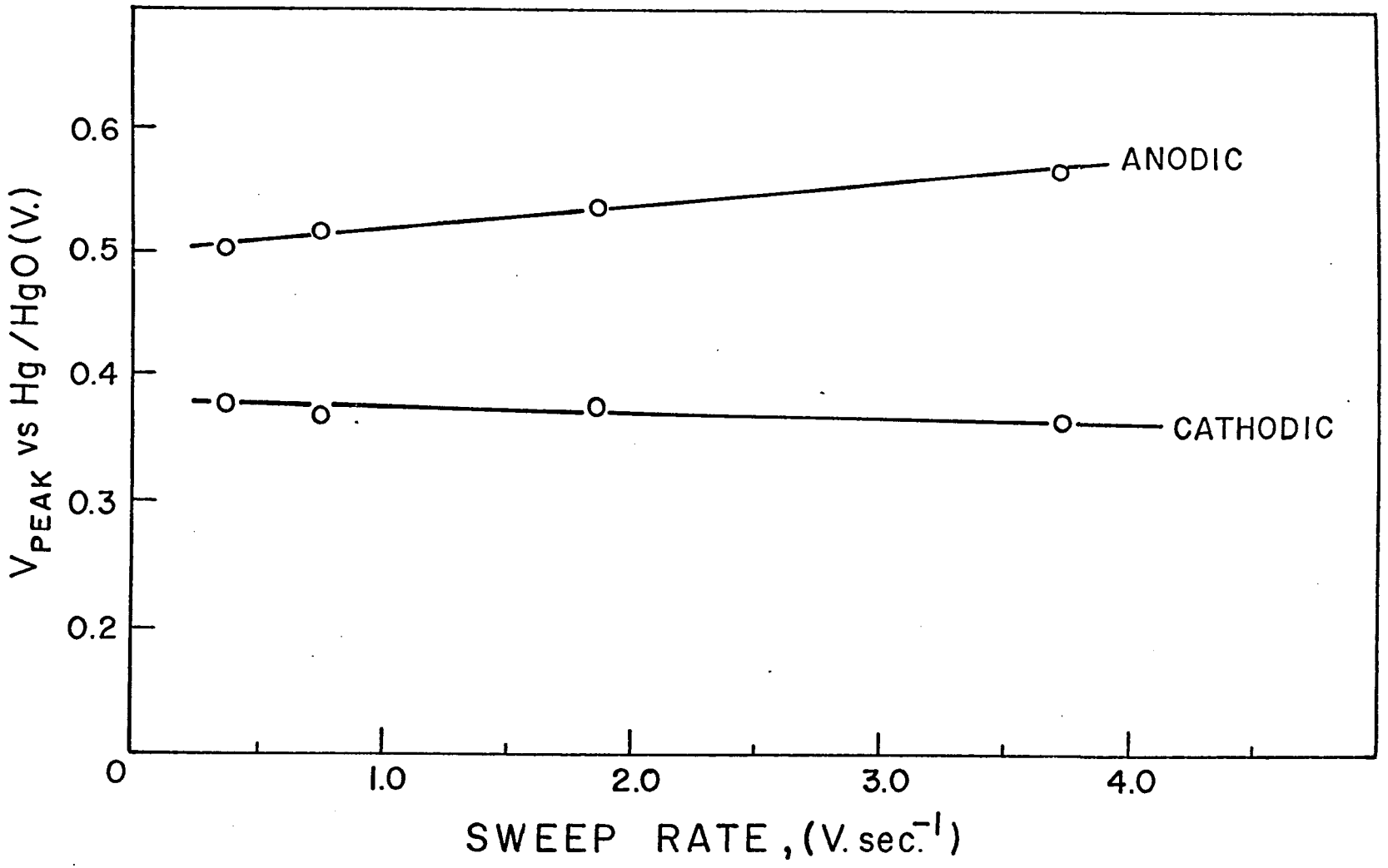
0.6
0.5
0.4
0.3
0.2
0
1.0
2.0
3.0
4.0
ANODIC
CATHODIC
V_{PEAK} vs Hg / HgO (V.)
SWEEP RATE, (V. sec.$^{-1}$)

(c)

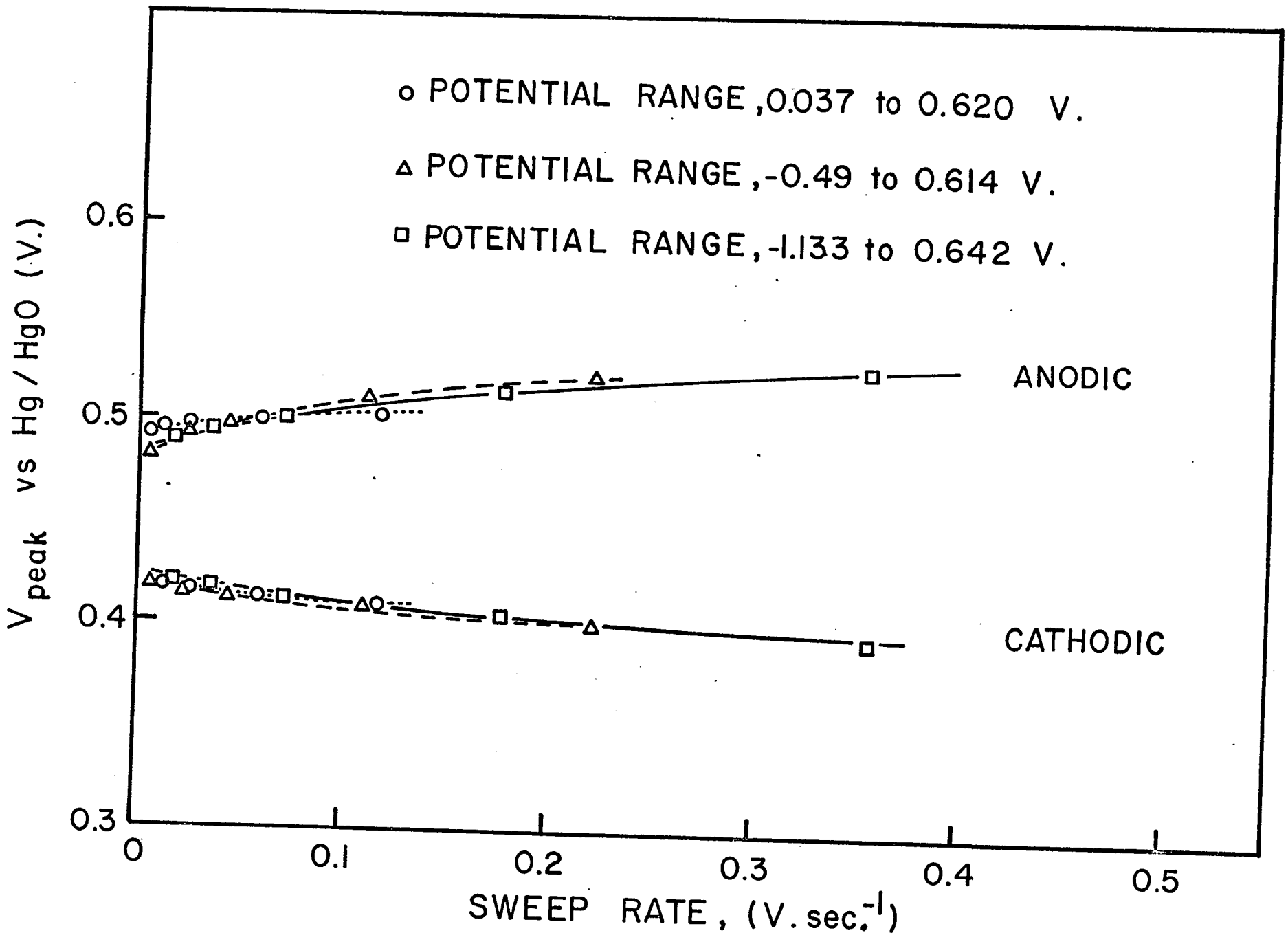
o POTENTIAL RANGE, 0.037 to 0.620 V.
Δ POTENTIAL RANGE, -0.49 to 0.614 V.
□ POTENTIAL RANGE, -1.133 to 0.642 V.
ANODIC
CATHODIC
V_{peak} vs Hg / HgO (V.)
0.6
0.5
0.4
0.3
0
0.1
0.2
0.3
0.4
0.5
SWEEP RATE, (V. sec.$^{-1}$)

(d)

discharging curves as a function of cathodic discharge rate* (cf. 163).

The results for method (A) based on the potentiodynamic sweeps are shown in Fig. 44 for cathodic-going and anodic-going sweeps. The polarisation in the charging and discharging process is indicated by the dependence of V_{peak} on dV/dt. Somewhat more polarisation is evidently indicated in both Figures for the anodic than the cathodic process; it will include any internal "iR" polarisation associated with the oxide film. "External" solution iR effects were negligible. The separation between the potentials V_{peak} for the anodic and cathodic current maxima is a measure also of the hysteresis (see below) between the potentials for formation and reduction of the surface oxide, a situation which is also observed on most other metals e.g. Pt, Pd (63,153) and Ag (see below). For comparative purposes, analogous results were obtained at silver and are shown

---

* The dependence of peak potentials V_{peak} on dV/dt or of inflection potentials (V_{inf}) on current density give almost equivalent information on polarisation (irreversibility) effects in the charging or discharging process (oxide formation or reduction), depending to what extent the oxide redox pseudocapacity depends on charging or reduction rate. At V_{peak}, the charging current is $C_{max} \cdot (dV/dt)$ and kinetic effects at this potential should ideally be equivalent to those arising in a galvanostatic experiment at an appropriate charging rate (163). In general, the displacement of capacity maximum potential is an indication of polarisation in the kinetics of the charging process. In a galvanostatic experiment, V_{inf} will, correspondingly, vary with reduction current as shown in the present work.

Figure 45. (a) Peak potentials for anodic and cathodic sweeps at silver as a function of dV/dt (potential range -1.380 to +0.929 V, 2M KOH, 25°C). (1) First anodic peak; (2) Second anodic peak; (3) First cathodic peak; (4) Second cathodic peak.

(b) Peak potentials for anodic and cathodic sweeps at silver as a function of dV/dt (potential range -1.269 to +1.025 V; 2M KOH, 60°C). (1) First anodic peak; (2) Second anodic peak; (3) First cathodic peak; (4) Second cathodic peak.

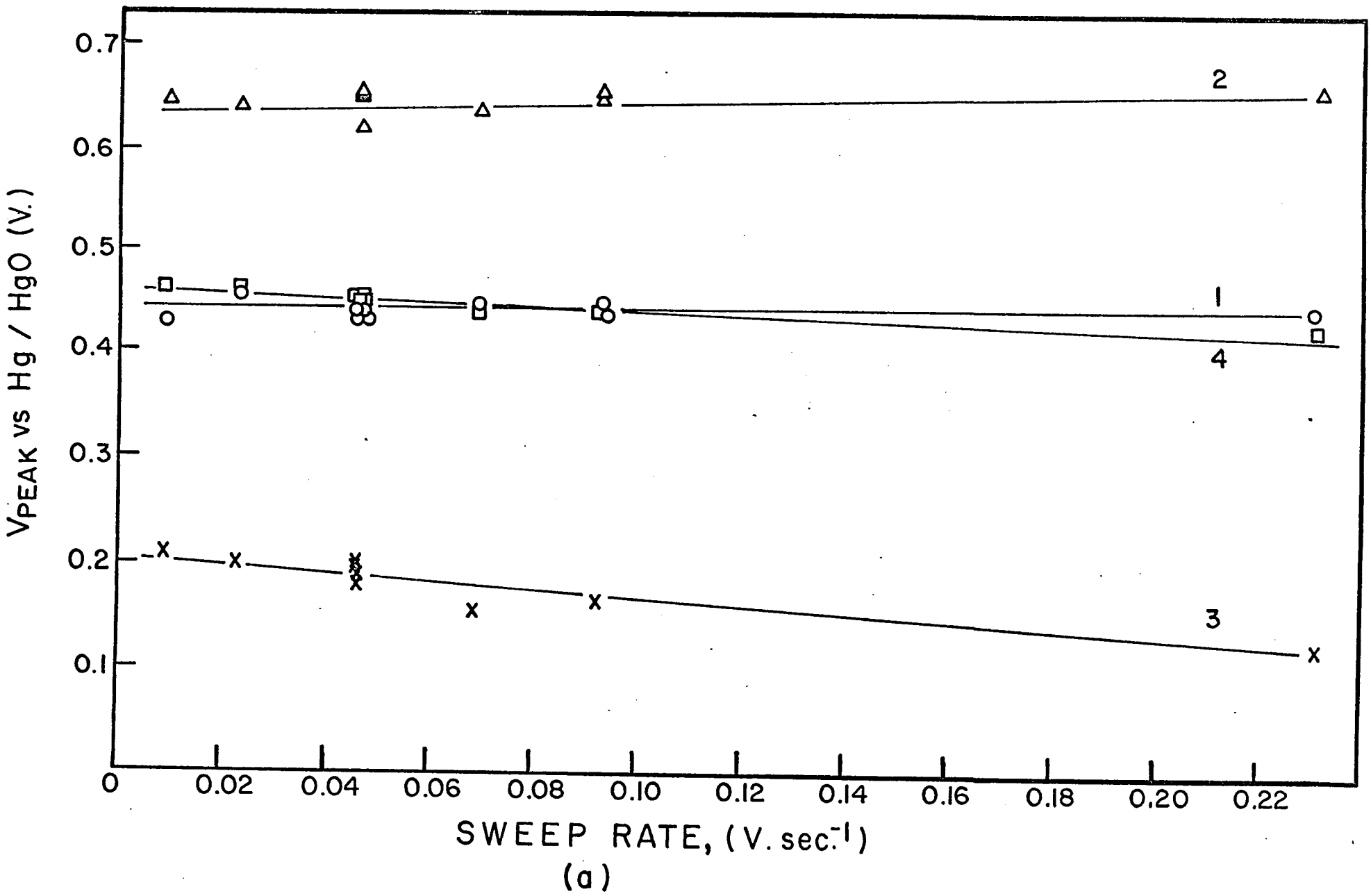
0.7
0.6
0.5
0.4
0.3
0.2
0.1
0
0.02
0.04
0.06
0.08
0.10
0.12
0.14
0.16
0.18
0.20
0.22
2
1
4
3
V_{PEAK} vs Hg / HgO (V.)
SWEEP RATE, (V. sec^{-1})

(a)

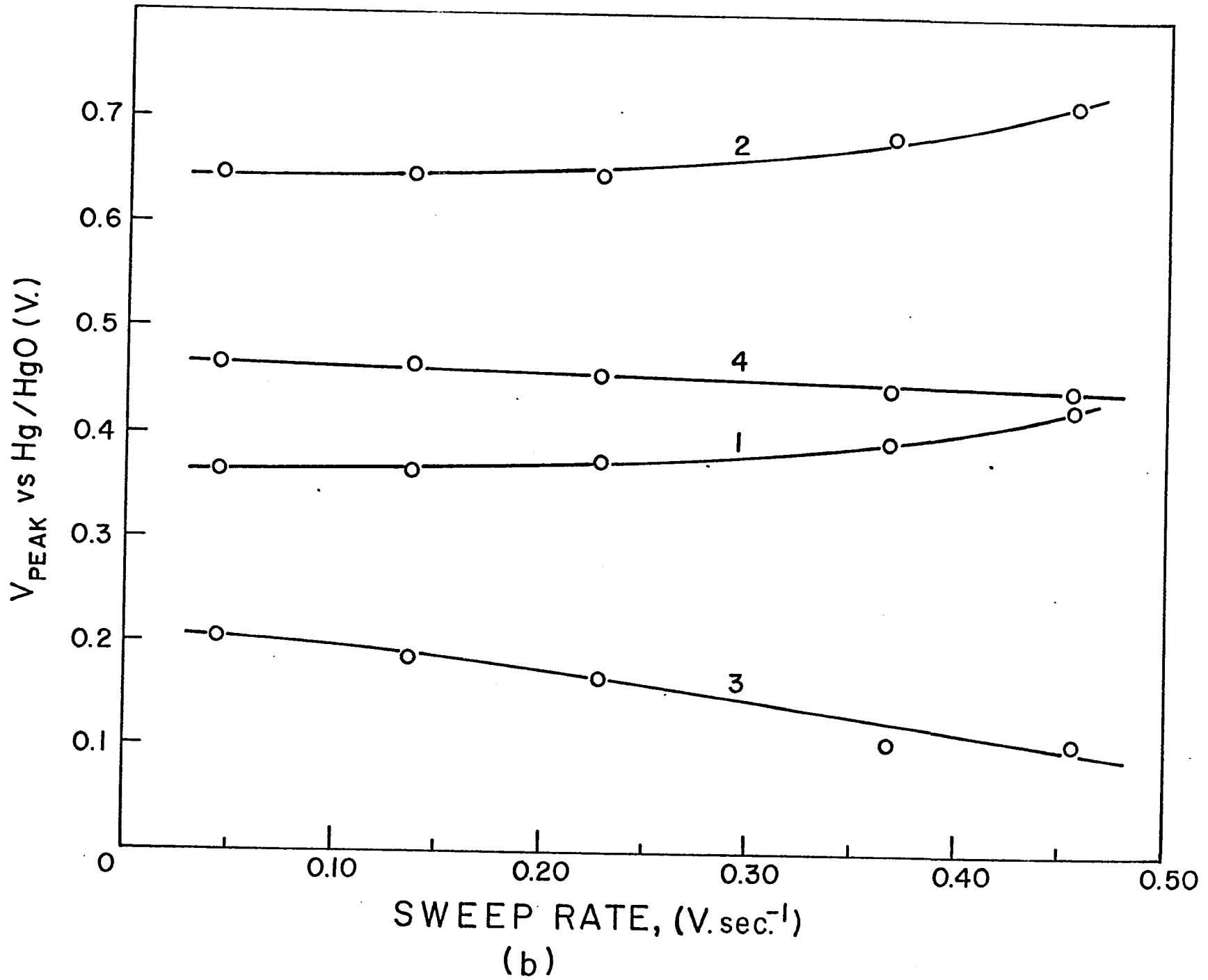
0.7
0.6
0.5
0.4
0.3
0.2
0.1
0
V_{PEAK} vs Hg/HgO (V.)
2
4
1
3
0.10
0.20
0.30
0.40
0.50
SWEEP RATE, (V. sec.$^{-1}$)

(b)

Figure 46. Inflection potential, $V_{inf.}$ (at capacity maximum in discharging curve - see Fig. 38 a) as a function of cathodic current density, i_c in galvanostatic reduction of surface oxide at nickel (2M KOH, 30°C) for various initial anodic potentials, V_i (vs Hg/HgO):

(1) V_i = 0.5 V....o and V_i = 0.6 V.... □

(2) V_i = 0.7 V.... Δ

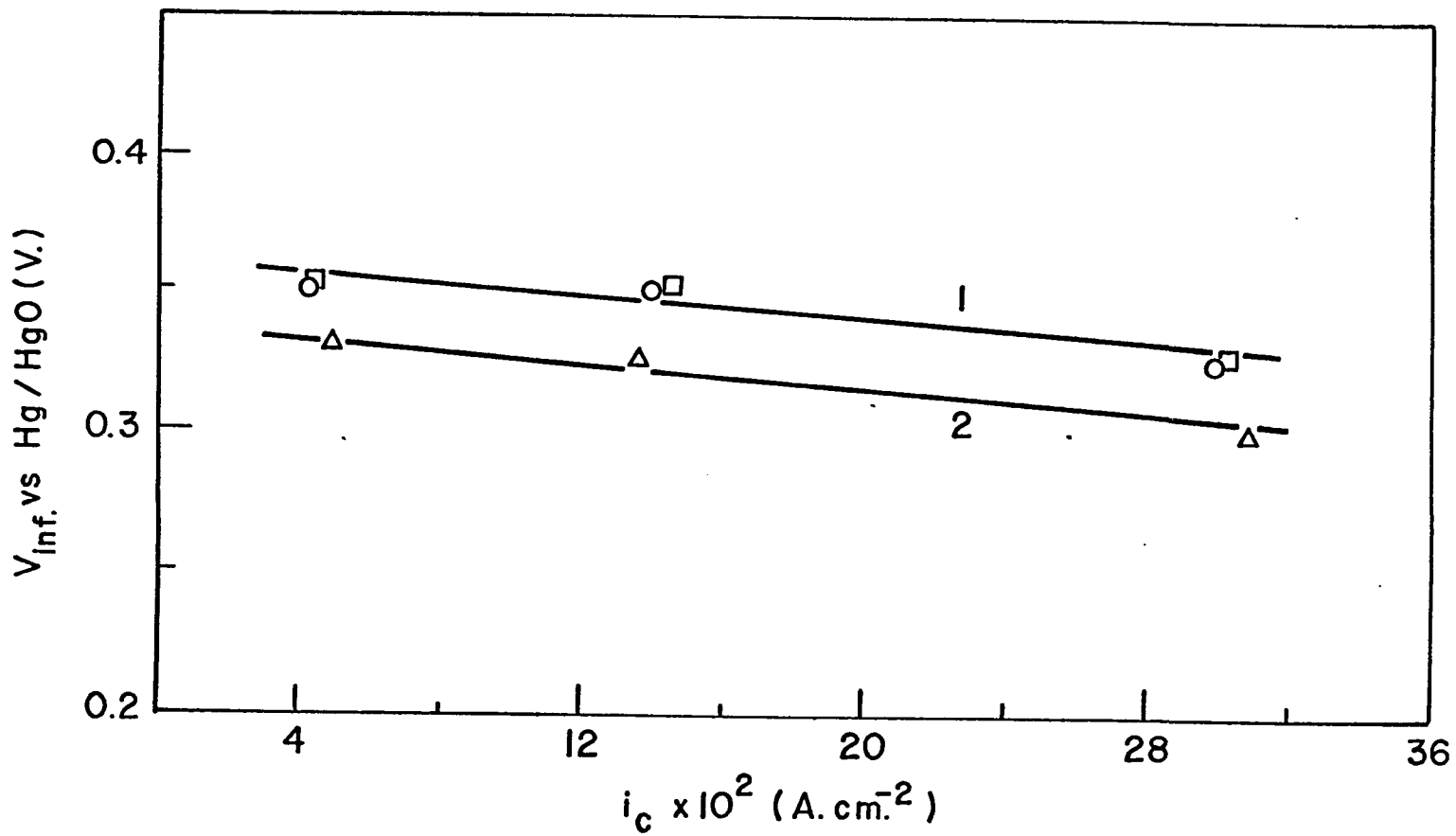
0.4
0.3
0.2
$V_{Inf.}$ vs Hg / HgO (V.)
1
2
4
12
20
28
36
$i_c \times 10^2$ (A. cm.$^{-2}$)

Figure 47. Inflection potential, $V_{inf.}$ at a constant reduction current at nickel ($i_c = 3 \times 10^{-1}$ a.cm^{-2}) as a function of prior anodic polarisation potential, V_i (pretreatment sequence shown in inset); (nickel in 2M KOH, 30°C).

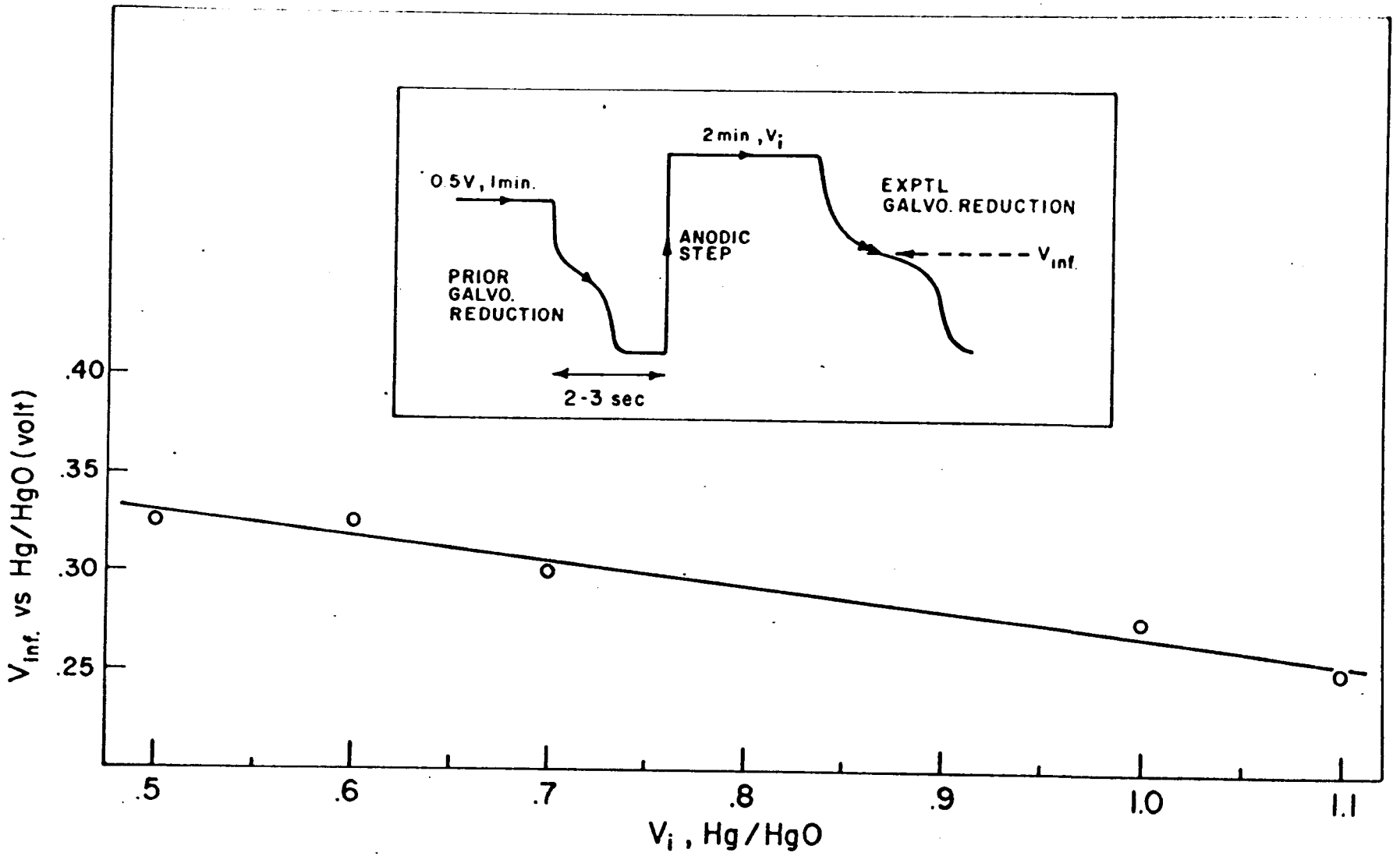
2 min , V_i
0.5V, 1min.
EXPTL
GALVO. REDUCTION
ANODIC
STEP
$V_{inf.}$
PRIOR
GALVO.
REDUCTION
2-3 sec
.40
.35
.30
.25
$V_{inf.}$ vs Hg/HgO (volt)
.5
.6
.7
.8
.9
1.0
1.1
V_i , Hg/HgO

in Fig. 45. In these results, it should be noted that two oxidation peaks and two reduction peaks are well separated, and correspond to the well-known two principal oxides of silver which have been characterised electrochemically in earlier work.

The data obtained by method (B) are shown in Fig. 46 (based on transients such as those for nickel) and a similar polarisation in cathodic reduction is observed. Although the range of reduction rates investigated was not large, the effect is reproduced for reduction of the oxide from three prior anode polarisation potentials (see below, Fig. 47).

In Figure 47 is shown the effect of prior anodic polarisation potential, V_i on the inflection potential, V_{inf} (see Fig. 38 a) for nickel surface oxide reduction in galvanostatic transients taken at $i_c = 3 \times 10^{-1}$ a.cm^{-2}. The inflection in the (dis)charging curve appears at potentials which are more <u>cathodic</u> the more <u>anodic</u> is the prior steady-state polarisation (see pretreatment conditions indicated in inset to Fig. 47). This somewhat surprising result is, however, not uncommon; for example, at platinum (63), the peak for oxide reduction occurs quite generally at more cathodic potentials the higher is the upper limit of potential for prior anodic polarisation in the oxide formation process.

The effect is again connected with hysteresis in formation and reduction of the surface oxide. A similar situation is found with regard to the surface oxide formed at platinum in the Kolbe reaction in aqueous media (166), where as higher anodic polarisations are reached, oxide is formed which is reduced only at correspondingly lower cathodic potentials.

At Pt and Pd, it is well known that the anodic oxide film formation occurs over a broad range of potentials while reduction does not occur until a potential is reached which is just lower than the lowest potential required for commencement of oxide film formation in the anodic direction of potential change (cf. Fig. 35). The reduction occurs however with an almost symmetrical current peak having an half-width of ca. 0.24 V corresponding to an almost ideal simple redox process for the surface atoms of Pt, considered with respect to a corresponding oxide "PtOH" or "PtO" (63) and reduced sites "Pt".

At nickel, well defined cathodic and anodic charging current peaks II_{cath}, II_{an} arise* but are not symmetrical (cf. Fig. 34). At silver, two well-separated anodic and two cathodic peaks are observed, I_{an}, I_{cath}, and II_{an} and

---

* A very small but reproducible anodic peak I is also seen at lower potentials and may be associated with oxidation of adsorbed or occluded hydrogen.

Figure 48. Potentiodynamic scanning curves for an oxidation and reduction process exhibiting hysteresis (at a constant dV/dt):

(a) at nickel in 2.0 M KOH at 22°C ;

(b) at silver in 2.0 M KOH at 27.5°C and

(c) at silver in 7.0 M KOH at -41°C.

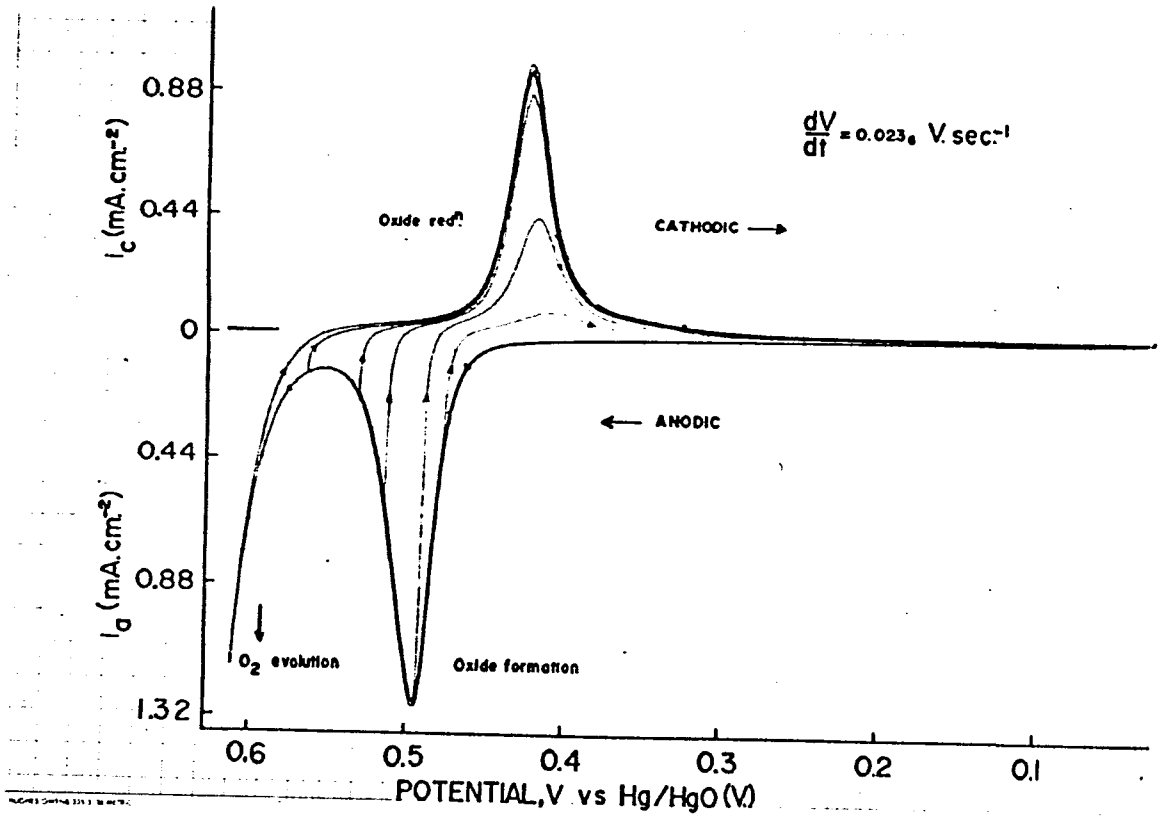
0.88
0.44
0
0.44
0.88
1.32
I_c (mA.cm^{-2})
I_a (mA.cm^{-2})
$\frac{dV}{dt}$ = 0.023$_6$ V. sec^{-1}
Oxide red^n
CATHODIC
ANODIC
O_2 evolution
Oxide formation
0.6
0.5
0.4
0.3
0.2
0.1
POTENTIAL, V vs Hg/HgO (V.)

(a)

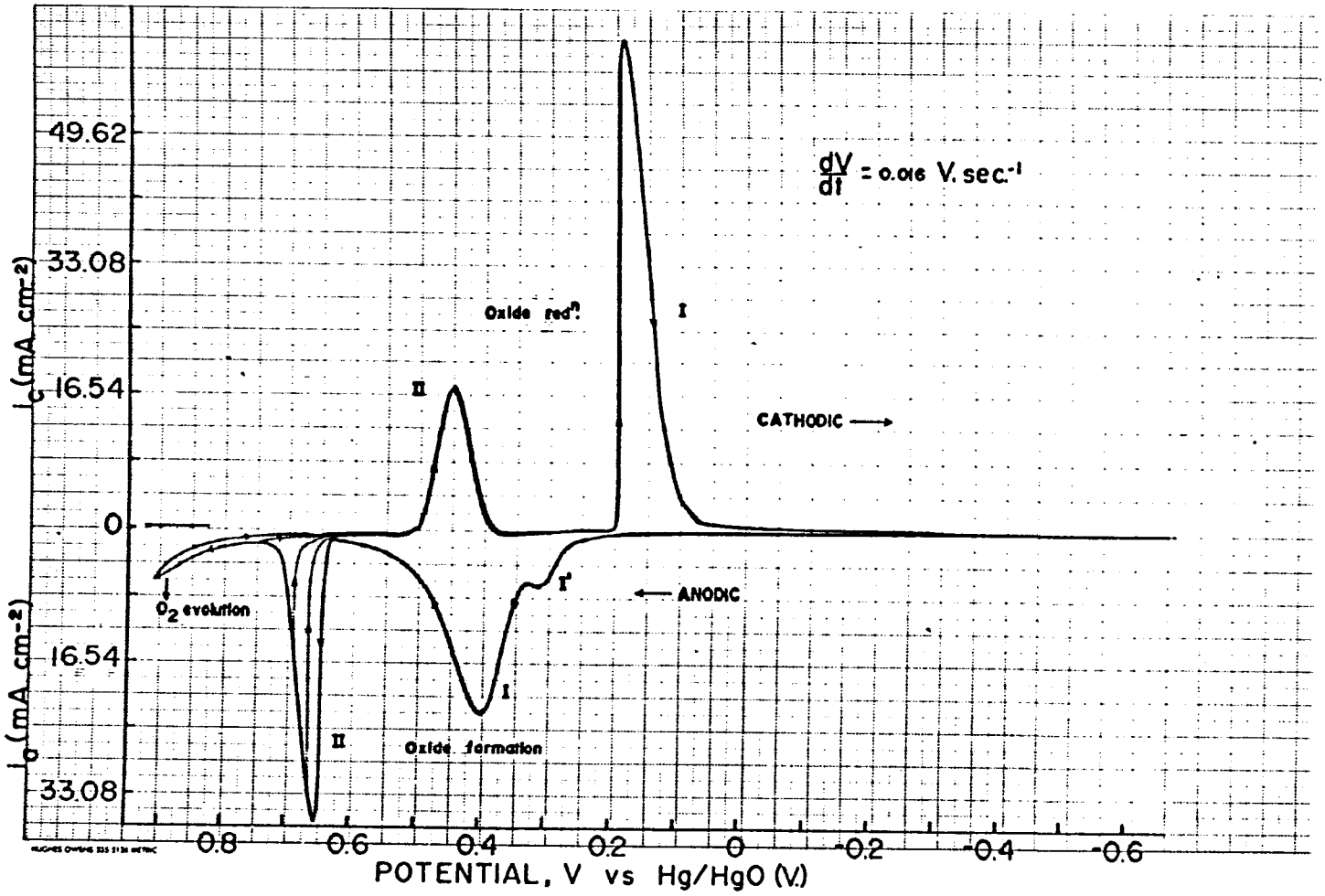
49.62
33.08
16.54
0
16.54
33.08
I_c (mA cm^{-2})
I_a (mA cm^{-2})
$\frac{dV}{dt}$ = 0.016 V. sec^{-1}
Oxide red^n.
II
I
CATHODIC ⟶
O_2 evolution
I'
⟵ ANODIC
I
II
Oxide formation
0.8
0.6
0.4
0.2
0
-0.2
-0.4
-0.6
POTENTIAL, V vs Hg/HgO (V.)

(b)

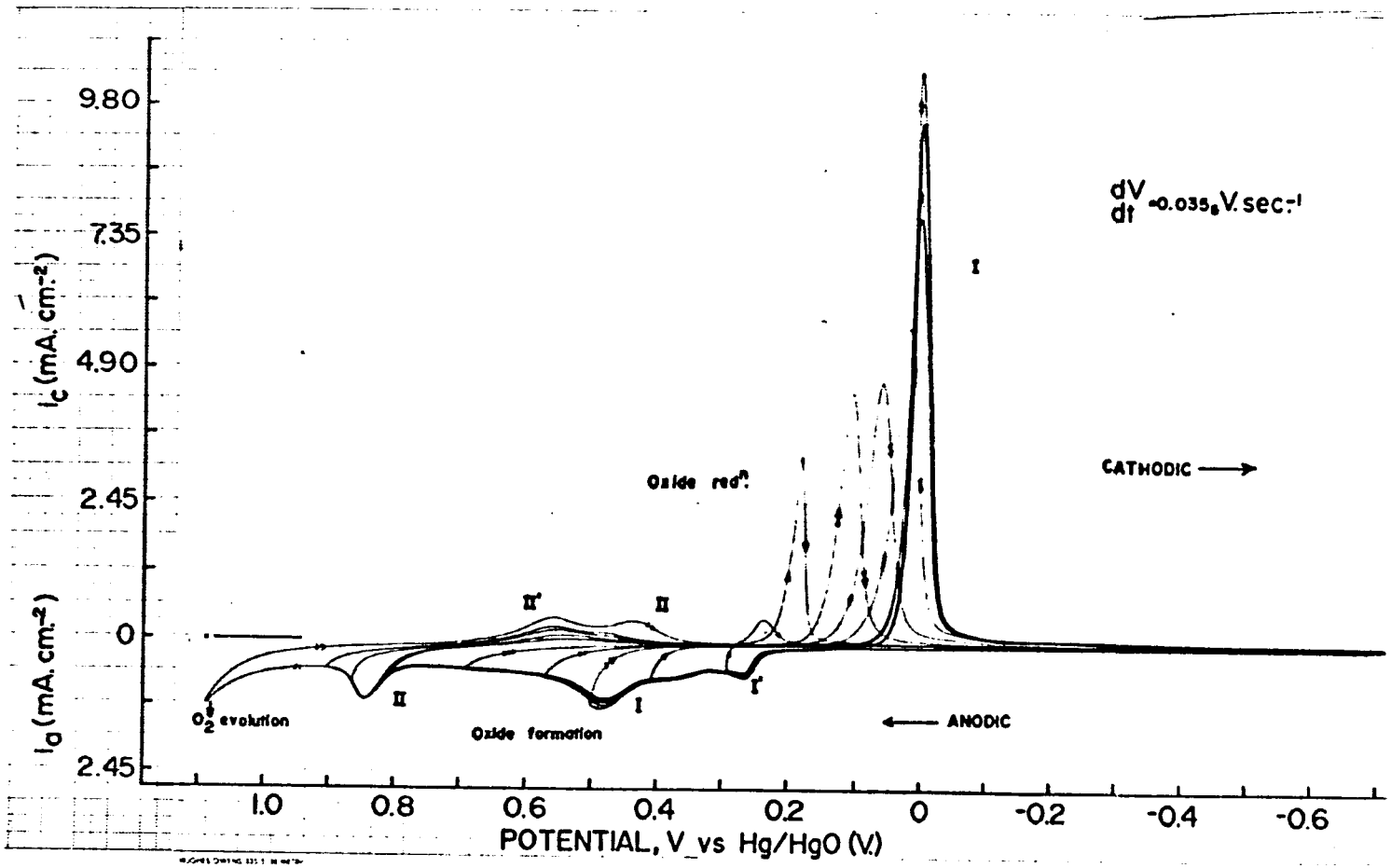
9.80
7.35
4.90
2.45
0
2.45
i_c (mA. cm.$^{-2}$)
i_a (mA. cm.$^{-2}$)
$\frac{dV}{dt}$ =0.035 V. sec.$^{-1}$
I
Oxide red^{n}.
CATHODIC ⟶
II'
II
I'
O_2 evolution
Oxide formation
⟵ ANODIC
1.0
0.8
0.6
0.4
0.2
0
-0.2
-0.4
-0.6
POTENTIAL, V vs Hg/HgO (V.)

(c)

II_{cath}, with hysteresis between the potentials for each of the corresponding charging and discharging peaks (cf. Fig. 36). In all cases studied, including Pt, the hysteretic effect is maintained down to the lowest practically useable sweep rates. The effects are not due to polarisation although the latter may tend to enhance the hysteresis (Figs. 44-46). The magnitudes of the hystereses in terms of the differences in charging peak potentials (ΔV_{peak}) are summarised in Table VII.

Since hysteresis phenomena can be characterised by so-called "scanning curves" (167 cf. the magnetization of iron), attempts were made to obtain these "curves" at nickel and silver electrodes in KOH solutions. The results are given in Fig. 48. It is observed that a family of systematic ascending and descending scanning curves exists within the main or "boundary loop". Similar "scanning curves" were also observed by Conway et al. (171) at platinum electrodes in H_2SO_4 solution.

3. RESULTS OF CHEMICAL ANALYTICAL EXPERIMENTS

The general procedures based on stripping by complexation and reduction have been described in Chapter II. Calibration data and results will now be considered.

Table VII

Hysteresis effects in Formation and Reduction of Surface Oxides At Nickel, Silver and Platinum (based on potentials of charging current maxima)

Metal, Solution and temperature	$V_{max.}$ (V)	
Nickel, 2M KOH, 22°C	0.080±0.02 (dV/dt=0.025V.sec^{-1});	0.120±0.01 (dV/dt=0.20V.sec^{-1})
Nickel, 2M KOH, 30°C	0.130±0.02 (dV/dt=0.50V.sec^{-1});	0.275±0.04 (dV/dt=4.5V. sec^{-1})
Nickel, 7M KOH, -30°C	0.11* (dV/dt=0.321V.sec^{-1});	
Bulk nickel oxide (battery plaque, ref. 7)	0.11 at 50% charge	
Silver, 2M KOH, 25°C	Peak I 0.250±0.02 (dV/dt=0.025V.sec^{-1});	Peak II 0.185±0.02 (dV/dt=0.025V.sec^{-1})
	Peak I 0.310±0.02 (dV/dt=0.20 V.sec^{-1});	Peak II 0.235±0.02 (dV/dt=0.020V.sec^{-1})
Silver, 2M KOH, 60°C	Peak I 0.160±0.02 (dV/dt=0.05 V.sec^{-1});	Peak II 0.180±0.02 (dV/dt=0.05V.sec^{-1})
	Peak I 0.195±0.02 (dV/dt=0.20V.sec^{-1});	Peak II 0.195±0.02 (dV/dt=0.20V.sec^{-1})
Pt. 1M H_2SO_4, 25°C	0.45** approximately	

* Wide charging and discharging region; non-symmetrical peaks
**Wide anodic charging region (figure based on middle of anodic oxidation region)

Magnitude of effects usually depends on maximum anode potential attained and the time spent at that potential.

Figure 49. U.v. spectrum of $[Ni(CN)_4]^{2-}$ from direct KCN stripping of surface oxide and from Ni complexed initially with hydrazine; graphs are for identical Ni concentrations and ref. solution is 0.5% aq. KCN.

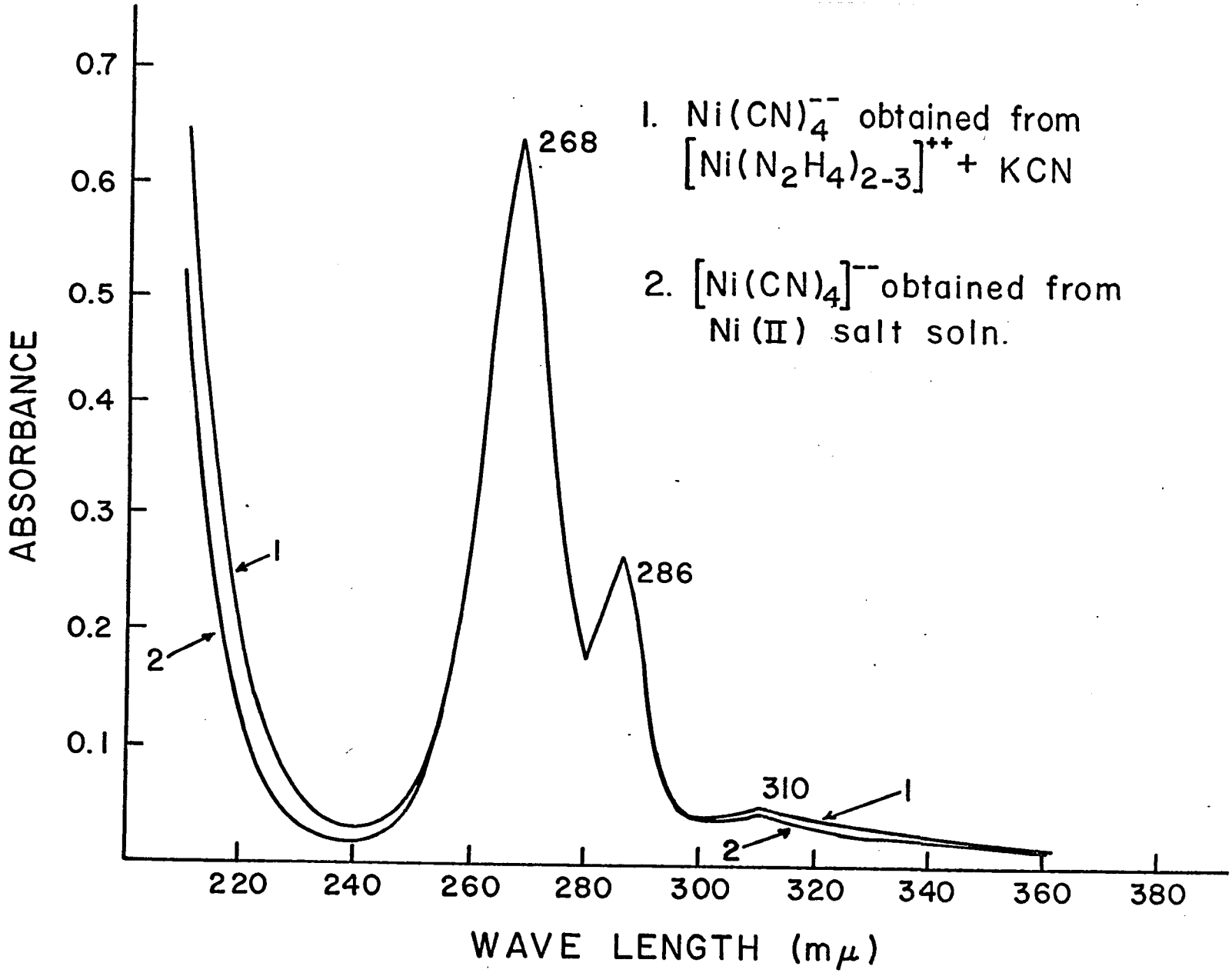
0.7
0.6
0.5
0.4
0.3
0.2
0.1
ABSORBANCE
1. Ni(CN)$_4^{--}$ obtained from [Ni(N$_2$H$_4$)$_{2-3}$]$^{++}$ + KCN
2. [Ni(CN)$_4$]$^{--}$ obtained from Ni(II) salt soln.
268
286
310
1
2
220
240
260
280
300
320
340
360
380
WAVE LENGTH (mμ)

Figure 50. Beer-Lambert calibration plot for $[Ni(CN)_4]^{2-}$ complex.

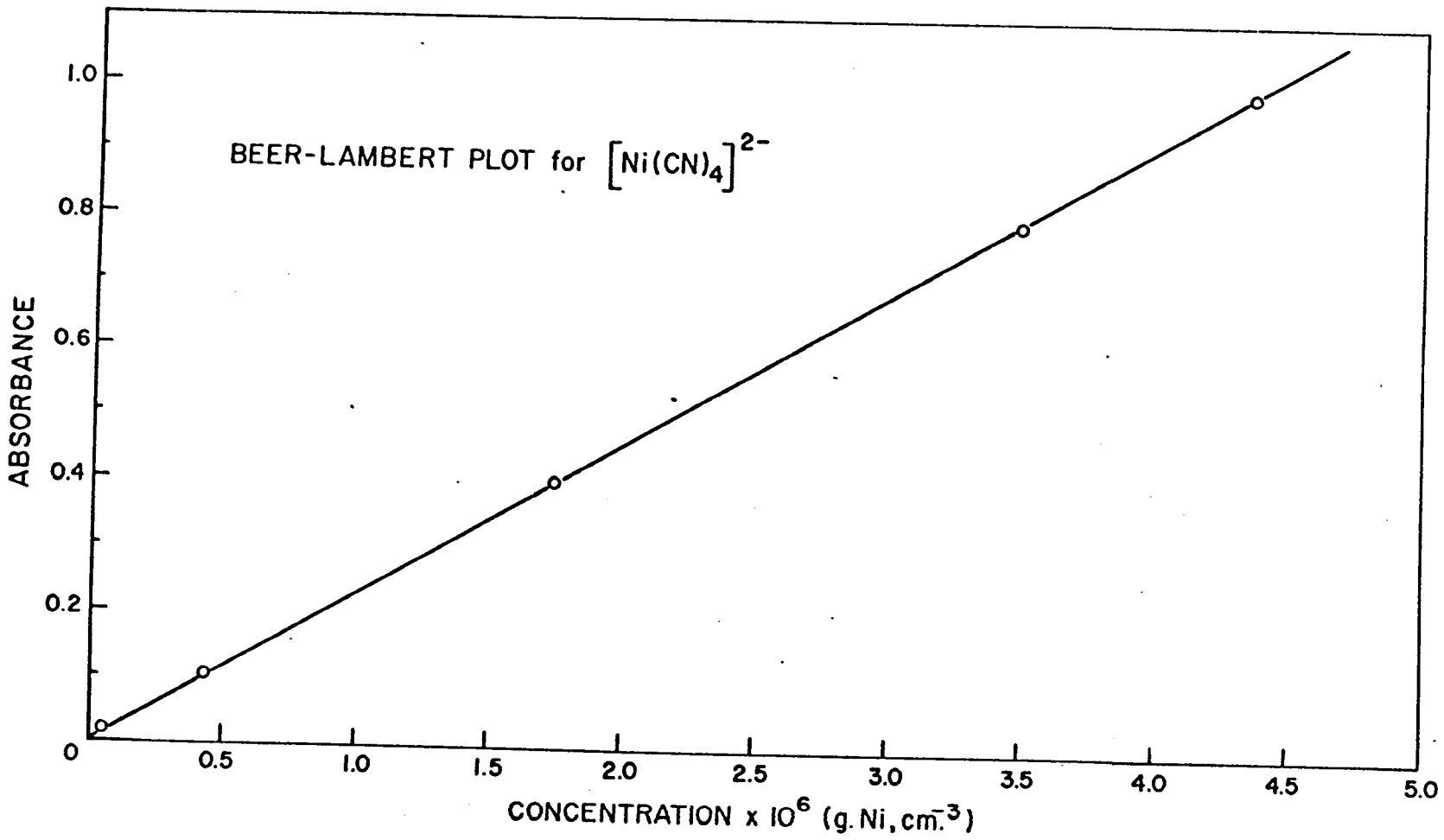
BEER-LAMBERT PLOT for $[Ni(CN)_4]^{2-}$
ABSORBANCE
0
0.2
0.4
0.6
0.8
1.0
0.5
1.0
1.5
2.0
2.5
3.0
3.5
4.0
4.5
5.0
CONCENTRATION x 10^6 (g. Ni, cm^{-3})

(a) The U.V. Spectrum of $[Ni(CN)_4]^{2-}$ Solution

Nickel in the oxide films was determined as the tetracyano complex. The u.v. spectrum of aq. $[Ni(CN)_4]^{2-}$ measured with respect to 0.5% aq. KCN as reference solution is shown in Fig. 49 and, for comparison, the spectrum of $[Ni(CN)_4]^{2-}$ prepared from $[Ni(N_2H_4)_{x=2,3}]^{2+}$ and measured against the same reference is superimposed.

(b) Beer-Lambert Plot for Analysis of Nickel as $[Ni(CN)_4]^{2-}$

By means of standard solutions of $NiSO_4$ diluted in 0.5% aq. KCN, a calibration plot for absorbance (at 268 mμ) vs concentration was prepared for the concentration range 10^{-8} to 5×10^{-6} g. nickel per ml. of solution. A Beckman DU or DB spectrophotometer was employed operating at a slit width of 0.1 mm. The calibration plot is shown in Fig. 50. The amount of nickel present in the sample was then calculated from the Beer-Lambert standardisation plot.

(c) Reliability of the Hydrazine Method

The hydrazine method for reductive oxide stripping (Chapter II, section 9(a), (ii)) was tested using precipitated nickelic oxide (NiO.OH) in order to determine both the Ni by the KCN method and the active oxygen by means of hydrazine. Nickel-hydroxy-oxide (NiO.OH) was precipitated quantitatively from a standard $NiSO_4$ solution by means of aq. KOH and Br_2

Figure 51. (a) Active O:Ni ratio from determinations on precipitated nickelic oxide (Ni by KCN, "O' by N_2H_4) as a function of reaction time up to 30 min.;
(b) Nickel:active O ratio from determination on precipitated nickelic oxide over a wider time range.

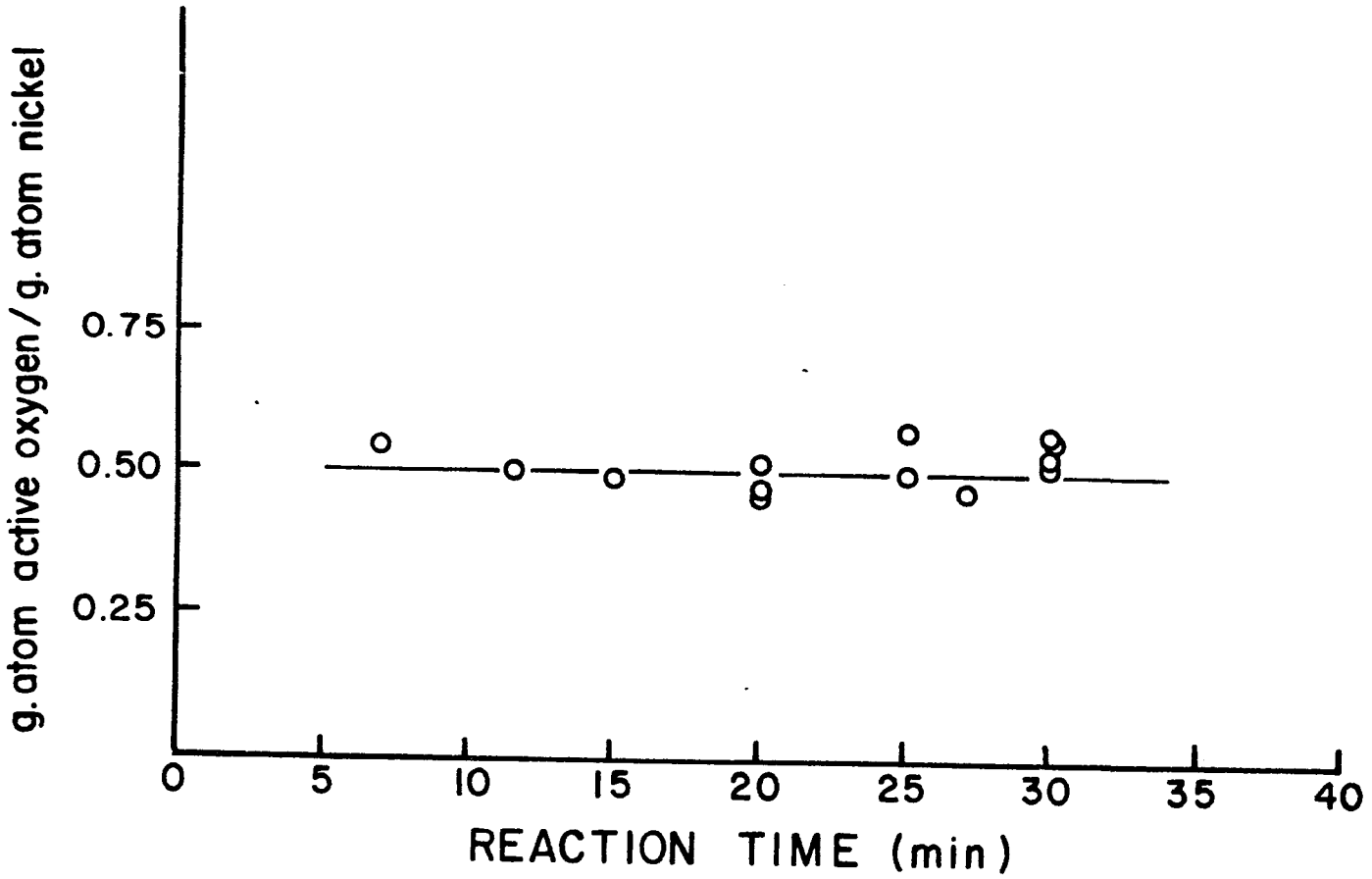
g. atom active oxygen / g. atom nickel
0.75
0.50
0.25
0
5
10
15
20
25
30
35
40
REACTION TIME (min)

(a)

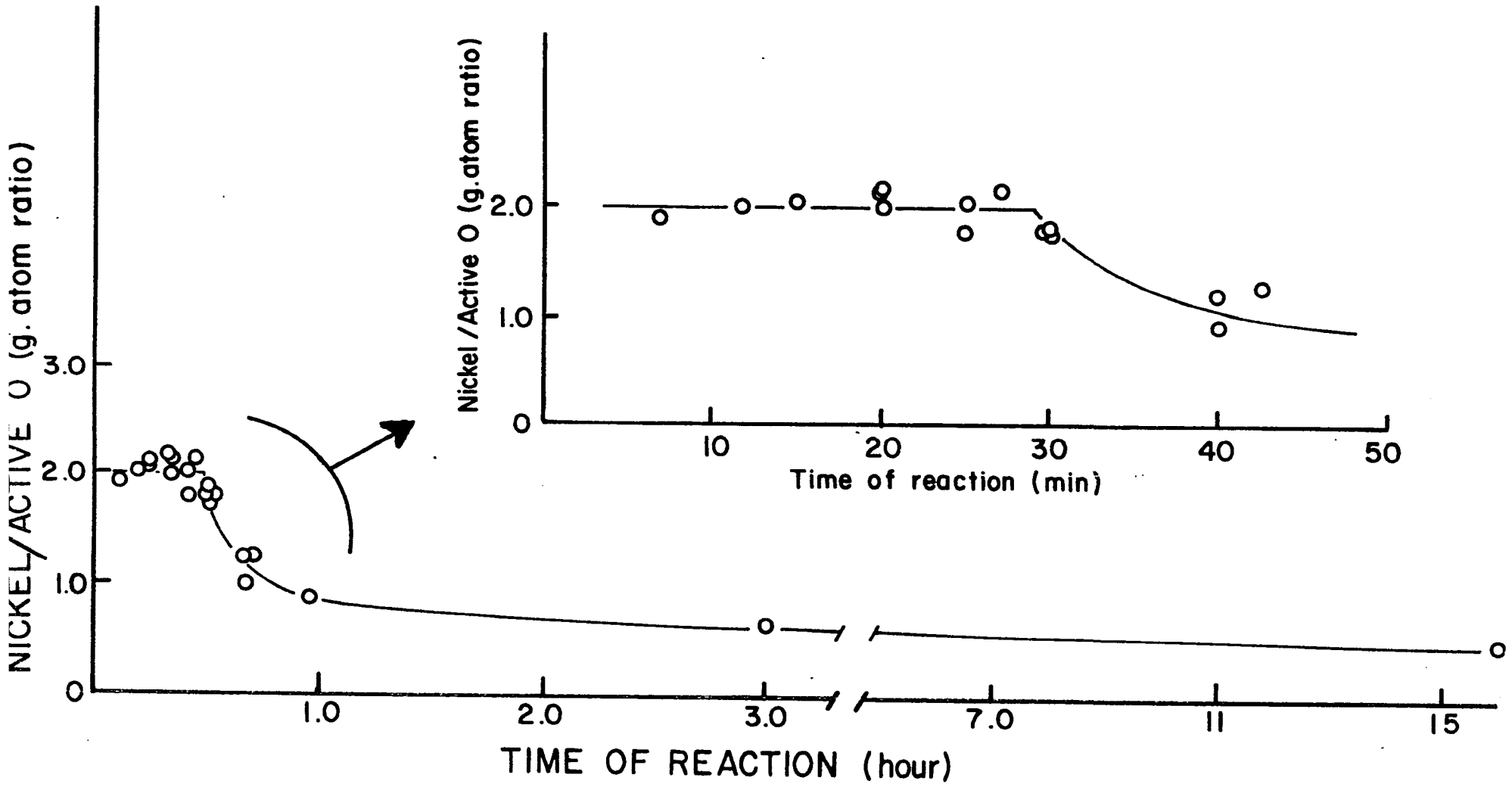
NICKEL/ACTIVE O (g. atom ratio)
3.0
2.0
1.0
0
1.0
2.0
3.0
7.0
11
15
TIME OF REACTION (hour)
Nickel /Active O (g.atom ratio)
2.0
1.0
0
10
20
30
40
50
Time of reaction (min)

(b)

(150). The results are shown in Fig. 51 and were regarded as encouraging in so far as for relatively short treatment times (up to 30 mins. Fig. 51a), a constant value of the active oxygen: nickel ratio (= 0.5, corresponding to "Ni_2O_3" or NiO.OH) was obtained. However, after longer times (Fig. 51 b), a substantial increase of this value became evident.

(d) Results with Large Area Oxidized Nickel Gauze Electrodes

Since the results obtained with the hydrazine method using precipitated NiO.OH seemed to be satisfactory at the shorter times, the method was applied to large area oxidized nickel gauze electrodes in order to determine the stoichiometry of the oxide in thin film oxide layers. The oxide was stripped from the electrode surface for controlled treatment times in aqueous deoxygenated N_2H_4 (or ammoniacal hydrazine to complete the dissolution of the Ni in the film). The Ni dissolved from the oxide film by the reductive stripping was determined by the KCN method and the active oxygen was estimated both by the new hydrazine procedure and by the electrochemical method (based on cathodic reduction transients). The results are compared in Table VIII. It is observed that the chemically determined active oxygen, [O], is seen to be much larger than the electrochemically determined values.

Table VIII

Active Oxygen by Hydrazine and by Electrochemical Reduction

(Large Nickel gauze electrode, 2M KOH, 22°C)

Potential, V_E vs Hg/HgO (V)	Amount of nickel in the oxide film (spectrometry) (μg.atom)	Electrochemically reducible oxide charge (mc)	Active oxygen (electrochemical equivalent) (μg.atom)	Loss of hydrazine (μg.atom)	Active oxygen (equivalent to hydrazine loss (μg.atom)
0.6	2.236	6578*	34.08*	20.34	40.7
0.5	1.432	2154*	11.16*	10.39	20.8
0.4	0.8	178.75	0.93	5.15	10.3
0.3	0.805	100.86	0.523	18.98	38.0

* These data were obtained in the oxygen evolution region; they may hence include some charge for reduction of molecular O_2 which might have been entrapped in the gauze. However, N_2 was bubbled through the electrodes.

Figure 52. Dissolution (corrosion) of metallic nickel in 0.5% aq. KCN and in 0.02 M N_2H_4; at 22°C.

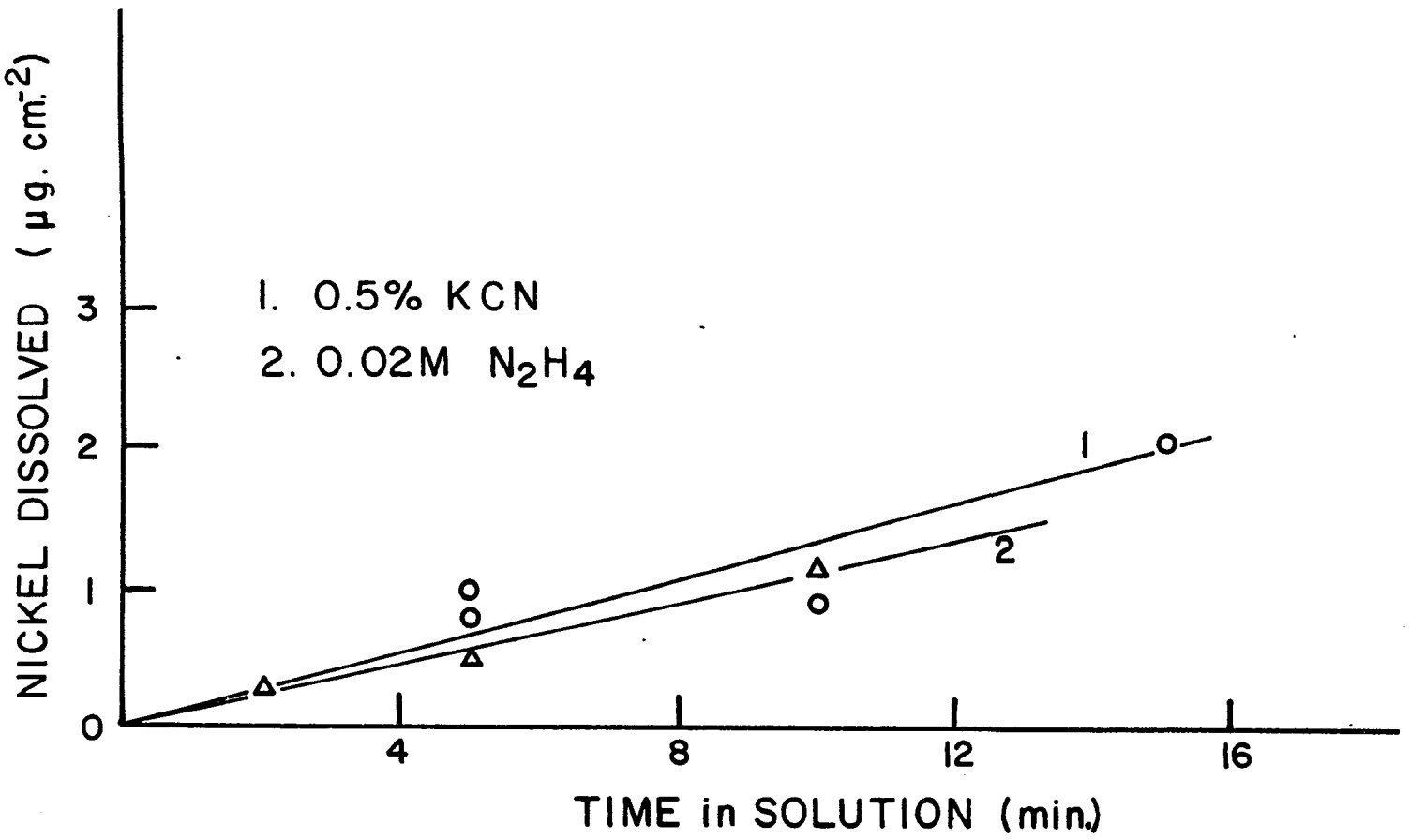
NICKEL DISSOLVED (µg. cm.-2)
0
1
2
3
1. 0.5% KCN
2. 0.02M N2H4
1
2
4
8
12
16
TIME in SOLUTION (min.)

This discrepancy, it seemed, might be due to some loss of N_2H_4 on account of catalytic decomposition by the underlying metal once the oxide film had been stripped. Hence, it was concluded that the oxidative loss of N_2H_4 in reductive stripping could not be reliably used as a method for determination of the active oxygen in thin films at nickel electrodes although for thicker or bulk material the method would be satisfactory. Cathodic reduction must therefore be the preferred method for the determination of active oxygen.

(e) Corrections for Loss of Nickel by Corrosion During the Analytical Stripping reaction

The necessity for corrections for loss of nickel from the metal by residual corrosion processes was pointed out in Chapter II, 9 (b), (v). The results are shown in Fig. 52 for various times of exposure $\tau_{dis.}$ to the stripping solutions.

(f) Extent of Reduction of Higher Valent Nickel Oxides In a Fast Galvanostatic Pulse

Experiments designed to determine if the higher nickel oxide becomes reduced in galvanostatic transients to the metallic state or only to the Ni(II) oxide were described in Chapter II, 9(b), (iii). The results are given in Table IX. It is seen that at all potentials, the amount of nickel in the film determined after charging

Table IX

Amount of Nickel in the Oxide Film after Charging the Electrode and that Remaining after Electrochemical Reduction of the Oxides

Time of polarization t (min.)	Potential, V_E vs Hg/HgO (V) in 2MKOH at 22°C	Amount of electrochemically reducible oxide (μg.atom "O" cm^{-2})	Amount of nickel in the oxide film after charge (μg.atom cm^{-2})	Amount of nickel in the oxide film after discharge (μg.atom cm^{-2})	Stoichiometry of nickel oxide in the film
2	0.2	0.004	0.462	-	$NiO_{1.01}$
2	0.2	0.004	-	0.465	$NiO_{1.01}$
2	0.5	0.031	0.245	-	$NiO_{1.13}$
2	0.5	0.035	-	0.181	$NiO_{1.19}$
2	0.8	0.119	0.325	-	$NiO_{1.37}$
2	0.8	0.098	-	0.256	$NiO_{1.38}$

Figure 53. Chemically determined nickel content in anodic oxide films in comparison with electrochemically determined charge for reduction; both quantities are shown as a function of prior anode potential held potentiostatically for 120 sec. (2M KOH, 30°C).

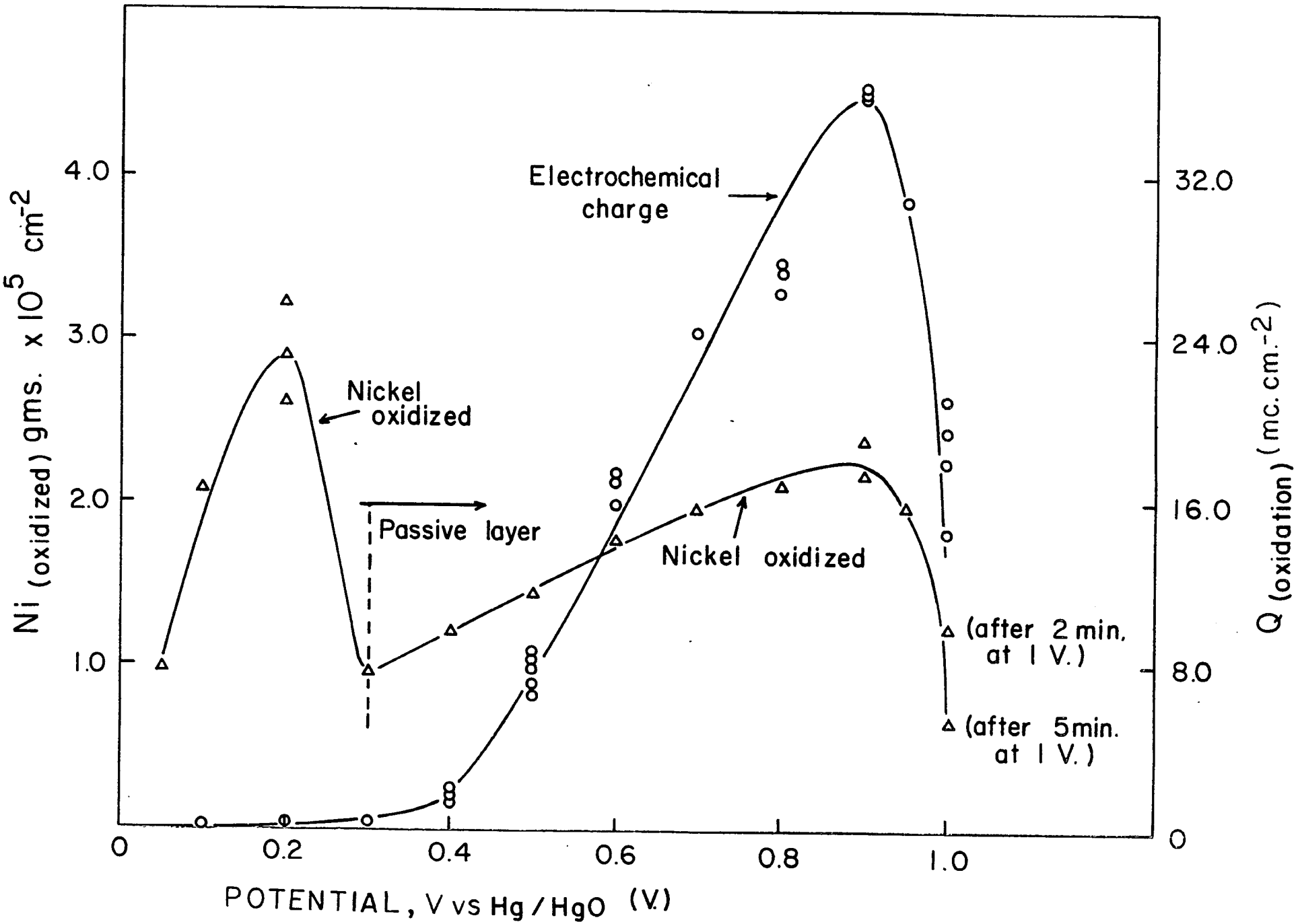
Electrochemical charge
Nickel oxidized
Passive layer
Nickel oxidized
(after 2 min. at 1 V.)
(after 5min. at 1 V.)
Ni (oxidized) gms. x 10^5 cm^-2
Q (oxidation) (mc. cm.^-2)
POTENTIAL, V vs Hg / HgO (V)
0
0.2
0.4
0.6
0.8
1.0
1.0
2.0
3.0
4.0
8.0
16.0
24.0
32.0

is approximately equal to that determined after discharging. This indicates that higher valent nickel oxides are reduced only to the Ni(II)-oxide (and not to the metal) in a fast galvanostatic pulse, at least when the oxide film is thicker than a monolayer or so. However, if cathodic hydrogen evolution is allowed to occur at the end of the cathodic pulse for some time, the Ni(II)-oxide becomes reduced by hydrogen to the metal, as in the first stage of the pretreatment programme (Fig. 14).

(g) Stoichiometry of Thin Film Nickel Oxide Layers

In the first set of experiments, nickel wire electrodes were used as working electrodes, and 0.5% KCN solution was used as the complexing agent for dissolving the oxides from the electrode surface. The amounts of electrochemically active oxygen (equivalent to the electrochemical "capacity" of the electrode in the sense used in battery terminology) and the corresponding amounts of nickel oxidized in the thin films of oxide are plotted in Fig. 53 as a function of electrode potential. These results, in terms of the stoichiometries of nickel oxide in the charged state of the electrode as a function of potential will be discussed further in Chapter IV.

An interesting maximum in the Q vs. V curve is apparent at a potential of ca. 0.9 V (cf. Fig. 53 for example). The maximum in the extent of oxide formation at ca. 0.9 V is reproducible and also corresponds to the inflections which are observed in the steady-state potentiostatic current

Figure 54. Active O:Ni ratio as a function of time period for which the electrode is held at 0.3 V (2M KOH, 30°C) prior to the application of a galvanostatic discharge pulse.

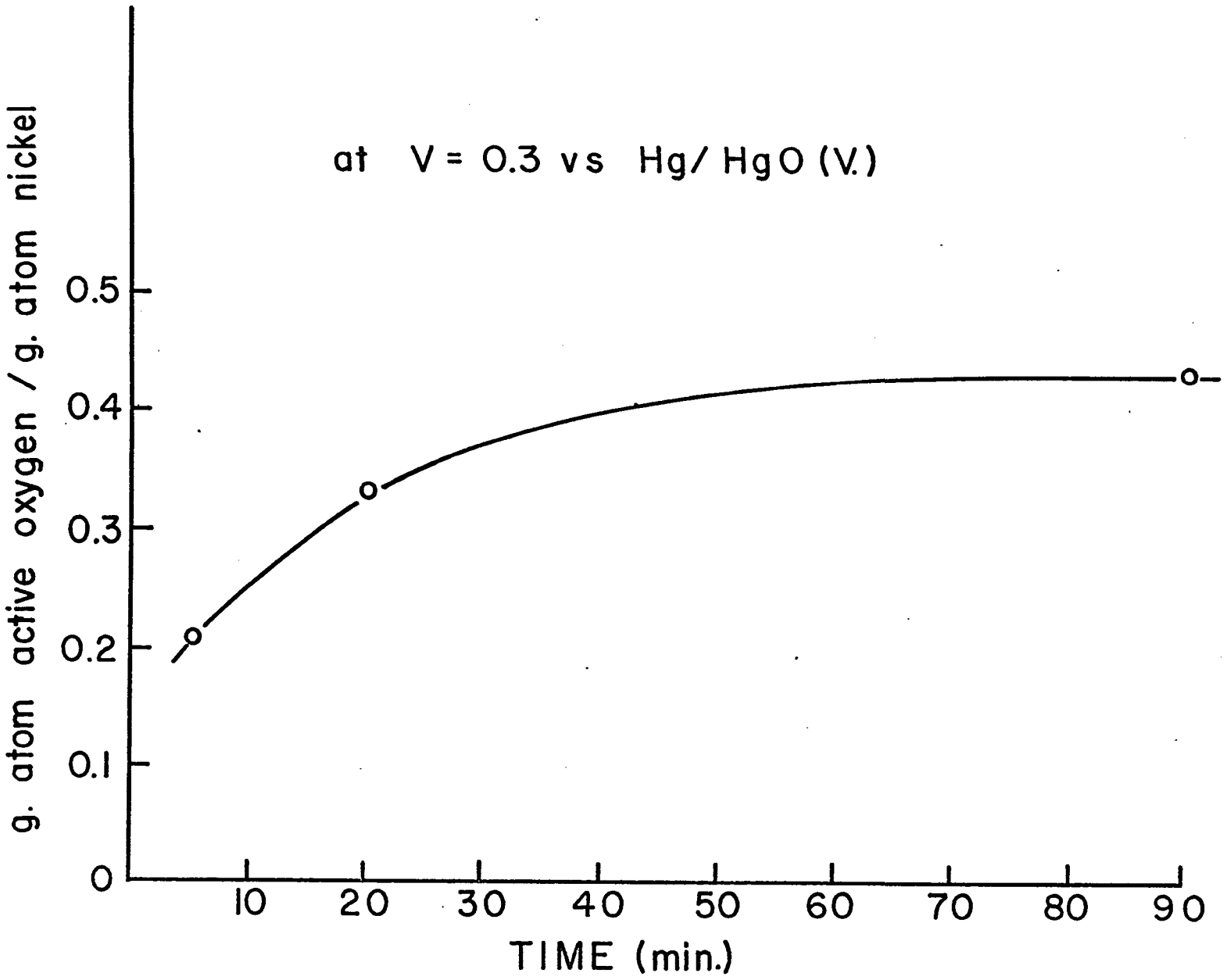
at V = 0.3 vs Hg/ HgO (V.)
g. atom active oxygen / g. atom nickel
0
0.1
0.2
0.3
0.4
0.5
10
20
30
40
50
60
70
80
90
TIME (min.)

potential relations for O_2 evolution on oxide-film Ni electrodes (cf. Fig. 40). It is evidently a real variation of the extent of Ni oxidation since a similar maximum occurs in the second curve in Fig. 53 for Ni content in the chemically stripped film. Another maximum in stripped nickel also arises at low potentials and is a real effect (based on a number of independent points) but this may correspond to a pre-passive, less consolidated film of the type also indicated by ellipsometry (54).

A second set of experiments was carried out using hydrazine in this case as the complexing agent for nickel and the nickel gauze as the electrode, and the stoichiometry of the oxide film was determined as a function of electrode potential. In this experiment, stoichiometries of the oxides at potentials above that for oxygen gas evolution were not investigated because at these potentials molecular oxygen is entrapped in the gauze and some can be reduced during the galvanostatic pulse as mentioned above. Results are given in Table X. Stoichiometries of the oxides are calculated on the basis that higher oxides of nickel are reduced only to Ni(II)-oxide.

It is also found in some experiments that as more time is allowed for formation of the higher oxide, a greater fraction of the lower valent oxide is oxidized to the higher valent state, and hence somewhat higher O:Ni stoichiometry tends to be attained (Fig. 54).

Table X

Stoichiometries of Thin Film Nickel Oxide (in 2M KOH)

as a function of Potential* based on

Chemical and Electrochemical determinations

Time of Polarization t (min.)	Potential, V_E vs Hg/HgO (V) in 2M KOH at 22°C	Amount of nickel in the oxide film (μg.atom)	Amount of electrochemically reducible surface oxide (μg.atom "O")	Stoichiometry of nickel oxide in the film
5	0.1	0.169	0.044	$NiO_{1.26}$
5	0.2	0.213	0.054	$NiO_{1.25}$
5	0.3	0.304	0.063	$NiO_{1.21}$
5	0.4	0.188	0.082	$NiO_{1.44}$
5	0.45	0.149	0.138	$NiO_{1.93}$ (-molecular O_2 evolution)

*Pretreatment programme: 2 min at 0.5 V ($E_{Hg/HgO}$), followed by potential step to 0.0 V for 2 min.; increase of potential to variable value V_E for variable time t followed by cathodic galvanostatic pulse.

This time-dependent overall valency change in the oxide film is also accompanied by time-dependent thickening of the film. However, the latter process must have been the principal one leading to the observed time-dependence of the active oxygen content in the thin oxide films (e.g. see Figs. 43 and 54).

CHAPTER IV

DISCUSSION

1. INTRODUCTION

First, the potentiostatic steady-state kinetics of oxygen evolution at oxidised nickel and silver electrodes will be discussed. After this, development of an original theory of the potentiostatic step charging method will be presented. Experimental results obtained by this method will then be compared with those obtained by other transient methods, e.g. the potentiodynamic sweep and fast galvanostatic discharging procedures. A concluding comparative discussion on these results will then be presented.

A simplified theory of the kinetics of growth of oxide films at nickel electrode surfaces will also be given. The kinetic results will be discussed in relation to the charges for oxide film reduction and the stoichiometry of the thin film oxide layers formed at the electrode surfaces during charging.

Finally a generalised discussion on hysteresis phenomena which are commonly observed in relation to charge and discharge processes at nickel, silver, platinum, palladium, etc. will be given.

2. POTENTIOSTATIC STEADY-STATE KINETICS: EVOLUTION OF OXYGEN AT NICKEL OXIDE ELECTRODE SURFACES

From the literature review given in Chapter I, it has been noted that there is no wide agreement amongst the kinetic results of various workers (e.g. 71-76,4,6). The apparent discrepancies between the conclusions of various workers undoubtedly arise because the electrode surfaces involved in various experiments are not in comparable states, or the electrodes were not pretreated in the same way. Similarly, the thicknesses of various oxides may not have been identical. Such differences in the chemical state of the surface oxides are almost certain to be reflected in differences in the oxygen evolution kinetics; such effects are indicated experimentally in the present work (see below).

It is therefore clear that further investigation of the differing kinetic results for the o.e.r. at Ni must involve:
(a) closer examination of the degree of surface oxidation of the nickel electrode in the steady-state at various anodic potentials in relation to the kinetics of the o.e.r.;
(b) attention to the role of surface preparation of the original nickel metal electrode that suffers surface oxidation in the anodic process of oxygen evolution, and
(c) consideration of time effects in the surface oxidation of the nickel. Potentiostatic procedures which have been

employed in the present work serve to provide a better characterisation of conditions under which (a) and (c) can be studied.

Potentiostatic steady-state kinetics of evolution of oxygen at silver electrodes were also investigated for comparative purposes. These results together with information obtained from potentiodynamic measurements will, however, be discussed in the later part of this Chapter (section 9). In the case of silver, it is known that various well-defined surface oxides of silver exist and oxygen evolution commences on the higher oxides (cf. ref. 85).

Comparison between the log[i]-V plots for 0.122 M aq. KOH prepared according to the standard method and the high purification technique (Fig. 18) for the nickel electrodes annealed in vacuum indicated no substantial difference in kinetic behaviour. This is probably because during pre-electrolysis depositable impurities which might affect a cathodic reaction are removed but these would usually not affect an anode surface and the reaction proceeding thereon. Anode depolarisers could, however, be removed as well. Anodic reactions are generally much less sensitive to impurities than cathodic ones. Based on this observation, the KOH solutions for all the subsequent measurements were therefore prepared according to the standard method (Chapter

II, section 2(a)).

Similarly no substantial difference in kinetic behaviour between the results obtained at electrodes annealed in vacuum and in hydrogen was noticed (Fig. 19): the kinetic results for these two types of electrodes were, in fact, more or less superimposible. However, electrodes prepared in purified oxygen gave results which were very irreproducible and exhibited variable Tafel slopes (Fig. 20). This indicated, as expected, that the surface preparation of the original metal electrodes plays an important role in the mechanism and kinetics of oxygen evolution (cf. ref. 152). It seems that electrochemically identical nickel surfaces are obtained when the electrodes are prepared by heating in vacuum or in hydrogen; on the other hand, surfaces of unknown and undefined nature (oxide) are produced if the electrodes are annealed in oxygen. That a very pure platinum metal surface is produced when that metal is annealed in hydrogen has been shown recently by electron microscopic study by Sewell et al. (177).

As mentioned previously in Chapter III, values of the Tafel slopes have been used in the present study as an indication of the mechanism(s) of evolution of oxygen at the nickel oxide electrode surface. In the linear log[i]-V parts of the kinetic curves for nickel, the Tafel slopes quite closely approximate to the values 2.3 (2RT/F) in the

Figure 55. Modified pH - potential diagram for the formation of various nickel oxides (ref. 203: T.S. de Gromoboy and L.L. Shreir).

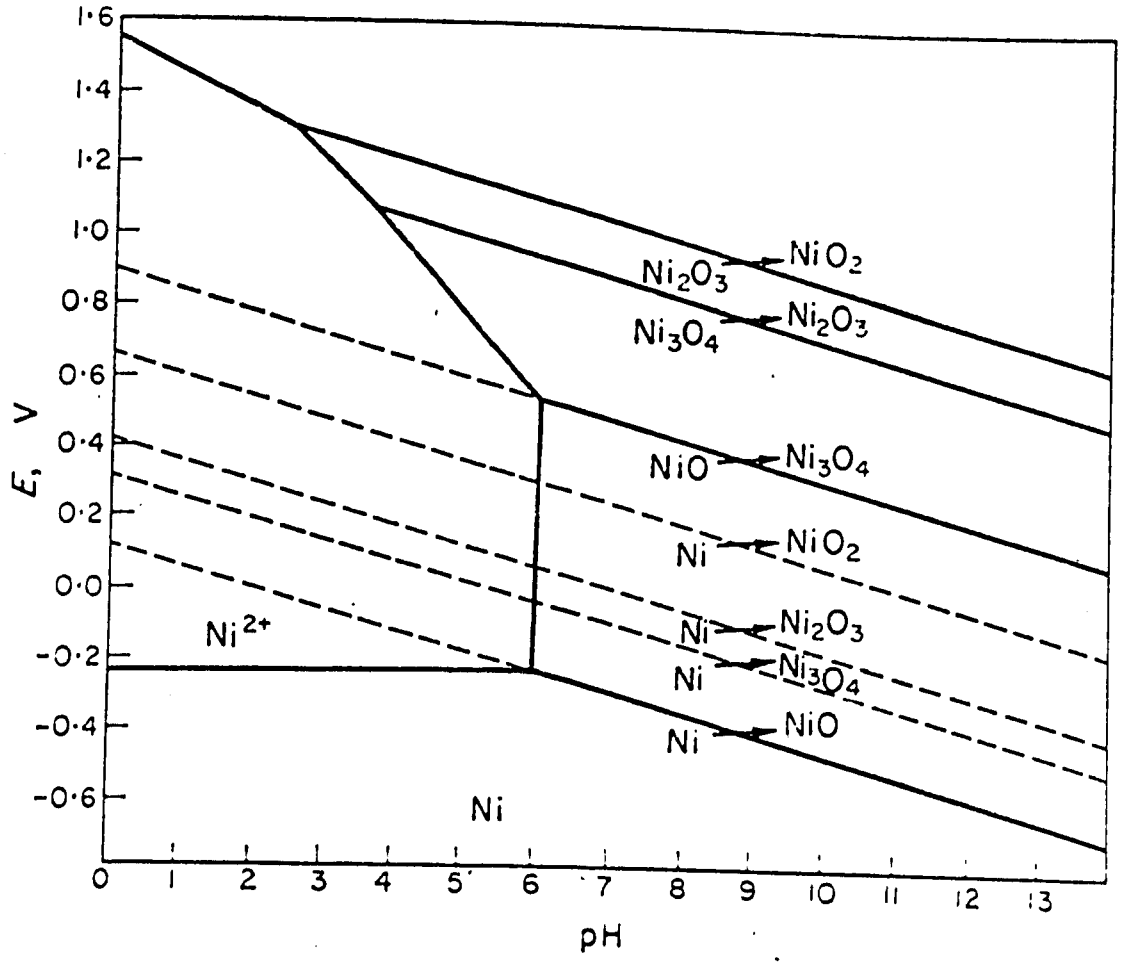
1·6
1·4
1·2
1·0
0·8
0·6
0·4
0·2
0·0
-0·2
-0·4
-0·6
E, V
0
1
2
3
4
5
6
7
8
9
10
11
12
13
pH
NiO2
Ni2O3
Ni2O3
Ni3O4
NiO
Ni3O4
Ni
NiO2
Ni2+
Ni
Ni2O3
Ni
Ni3O4
Ni
NiO
Ni

low potential regions (< 0.5 V) (except in the case of 14.3 M KOH at 60° and 89°C) and 2.3 (2RT/3F) in the high potential regions (> 0.5 V) for various temperatures and concentrations of the aq. KOH (see Table III), although there is some variation above and below these figures. However, the values of the Tafel slope in 14.3 M aq. KOH at 60° and 89°C were found to be close to 2.3 (RT/F) in both the high and the low potential regions (Table III).

Possible elementary reactions in the o.e.r. at bulk nickel oxide electrodes have been considered previously by Bourgault and Conway (4,6,7,172) and a generalized scheme for any metal was proposed by Bockris (77). It is evident from the oxide charge information given in Chapter III (e.g. Fig. 40), that the linear Tafel region for the o.e.r. at Ni commences when an appreciable rate of change of oxide formation charge Q with respect to potential begins to arise and when this charge already exceeds that for a monolayer of "OH".

Nickel is a weakly electropositive metal so that, according to the pH-potential diagram (203) (Fig. 55), when nickel metal is dipped in KOH solution, it becomes spontaneously covered with a thin layer of oxide, possibly the hydrated $Ni(OH)_2$ species (25) (E° for $Ni(OH)_2 + 2e \rightleftharpoons Ni + 2\ OH^-$ is -0.72 V vs NHE (178,181)). The elementary steps in the o.e.r. must therefore be considered as taking place (as in

the case of bulk nickel oxide electrodes) on a surface layer of oxide of thickness substantially greater than that for a monolayer. Experimentally, it is also observed that prior to oxygen evolution the bright electrode becomes dark. In the schemes to be considered below, S will therefore represent a site on the surface oxide rather than on the underlying metal.

From the schemes previously considered (4), the reaction sequence

$$S + OH^- \longrightarrow S.OH + e \qquad \text{I}$$

$$S.OH + OH^- \longrightarrow S.O + H_2O + e \qquad \text{II}$$

$$2S.O \longrightarrow 2S + O_2 \qquad \text{III}$$

will obviously give the observed Tafel slope of 2.3 (2RT/3F) in the potential region above 0.5 V when II is rate-controlling independent of whether ultimate oxygen evolution proceeds by III or by further elementary steps involving (77) species such as S.O.OH. Some deviations from the limiting value of b = 2.3 (2RT/3F) for step II can occur, as pointed out by Conway and Gileadi (173), when intrinsic heterogeniety of surface sites is considered in relation to a Temkin-Frumkin type of electrochemical isotherm for the potential dependence of coverage by "OH" species. However, the experimental values of b seem sufficiently near to the limiting value mentioned

above for such effects not to require further detailed consideration in this case.

The Tafel slopes of the linear regions of the log[i]-V relation became 2.3 (RT/F) for 14.3 M aq. KOH at 60° and 89°C. Such a slope could arise for the same mechanism with step II as rate-determining at intermediate coverage by "OH" species under Temkin conditions (6,173).

In the potential region below 0.5 V, at first a sharp ascent of the log[i]-V plot and then a very short linear region having an extrapolated Tafel slope of ca. 2.3 (2RT/F) is observed (see also ref. 18). This region corresponds to oxidation of metallic nickel with a possible initial step

$$Ni + OH^- \longrightarrow Ni/OH + e \qquad Ia$$

as rate-determining. It is this material in a higher oxidized state on which subsequent evolution of oxygen commences at more elevated potentials with increasing anodic polarisation, according to the reaction scheme I to III mentioned above.

An important aspect of the present results (Figs. 21-25, Chapter III) is the observation of anodic current-potential relations exhibiting regions of negative Tafel slope, i.e. reversal of the direction of the current-potential lines. It is clear that on the basis of a scheme of elementary steps such as I, II, III above, no explanation of a reversal of the

Tafel line could be given (115), since I and II will always increase in rate with increasing V and so will III since the coverage θ_O by "O" species will also tend to increase with increasing V.

However the following discussion, it will be seen, can provide a basis for these effects. Gilroy and Conway (115) have given a general treatment for cases of this type and an inhibiting species produced in the overall reaction sequence is required; they showed that the coverage by such a species must increase with potential at a greater rate than the reaction rate itself would otherwise increase due to the normal effect of potential on the activation energy. This species could be produced in an <u>alternative</u> mechanism (for the overall reaction) or in a step in which two sites are required for adsorption of the immediate product of that step for every one required by the reactant involved in that step, as in some organic oxidation reactions. Formally, step II could give the required behaviour if "O" required two sites for each one occupied by "OH", so that step II would be written as

$$S.OH + OH^- + S \longrightarrow \begin{matrix} S \\ \diagdown \\ O \\ \diagup \\ S \end{matrix} + H_2O + e \qquad \text{IIa}$$

with a rate equation given by*

$$i_{2a} = 2F\, k_{2a}\, C_{OH^-} \theta_{OH} (1 - \theta_{OH}) \exp[\beta VF/RT]$$

where θ_{OH} is potential-dependent through I if the latter step is at quasi-equilibrium (115,173).

Alternatively, if the parallel reaction pathway

$$S + OH^- \longrightarrow S.OH + e \qquad \text{I}$$

$$S.OH + OH^- \longrightarrow S.O + H_2O + e \qquad \text{II}$$

or

$$2S.OH \longrightarrow S.O + H_2O \qquad \text{IV}$$

were involved, followed by

$$S.O + OH^- \longrightarrow S.O.OH + e \qquad \text{V}$$

$$S.O.OH + OH^- \longrightarrow S.O_2 + H_2O + e \qquad \text{VI}$$

$$S.O_2 \longrightarrow S + O_2 \qquad \text{VII}$$

or with O_2 formed directly from V by

$$S.O.\,OH + OH^- \longrightarrow S + O_2 + H_2O + e \qquad \text{VIII}$$

the self-inhibition could arise as follows. If II were initially rate-determining, oxygen evolution and surface oxidation will proceed by the mechanism I, II, III so long as

---

*For such a case, Temkin adsorption conditions will probably apply and an exponential term in coverage will be required (173). However, this will not affect the general arguments to be developed below. A detailed analysis of inhibition effects under Temkin conditions has been given by Gilroy and Conway (115) elsewhere.

(on the above assumption) the rate constant k_3 for step III is sufficiently large compared with that for II, viz. $k_2 \exp[\beta VF/RT]$. However, if S.O can be further oxidised to S.O.OH (a type of oxidation state actually known in the series of nickel oxides) in a step such as V, at higher anodic potentials S.O.OH will tend to replace S.O, so that III could become inhibited both on account of surface coverage effects and changes of activation energy as discussed previously by Conway and Gileadi (173). As $\theta_{O.OH}$ became $\gg \theta_O$, the kinetics would no longer be mainly characterised by the pathway I → III but rather by I, II, V, VI, VII or through VIII. A further linear Tafel relation of normal sign of slope can then arise when $\theta_{O.OH} \gg \theta_O$ and the overall rate becomes limited by a step such as VI or VII.

More specifically for the above reaction steps, writing K's for quasi-equilibrium constants for elementary reactions prior to the rate determining step (cf. refs. 115,173), the coverages θ_{OH}, θ_O, $\theta_{O.OH}$ etc. will all go through maxima as the potential increases. This can be seen, for example, for θ_O which will be given by*

$$\theta_O = \frac{K_1K_2\exp[2VF/RT]}{1+K_1\exp[VF/RT]+K_1K_2\exp[2VF/RT]+K_1K_2K_5\exp[3VF/RT]}$$

$$\frac{}{+K_1K_2K_5K_6\exp[4VF/RT]} = f_1(V)$$

*Here it is assumed for convenience that constant OH^- concentration is involved and this can be regarded as included in the K terms. Only the exponential relationship between θ_O and V is of interest in this and other similar equations.

so that as the potential V becomes sufficiently large, the exponentials with larger arguments in V will predominate.

If O_2 evolution occurs through some alternate reaction from S.OH, S.O or S.O.OH in such a way that the species kinetically involved at the surface are maintained in quasi-equilibrium, then the Faradaic current for O_2 evolution will go through a maximum as potential increases. Possible alternative steps (cf. ref. 4) are formally

$$2S.OH + 2OH^- \longrightarrow 2S + O_2 + H_2O + 2e \qquad IIb$$

$$2S.O \longrightarrow 2S + O_2 \qquad IX$$

$$S.O.OH \longrightarrow S + O_2 + H^+ + e \qquad X$$

Then with step IX, for example,

$$i_9 = k_9\theta_O{}^2 = k_9[f_1(V)]^2$$

When the surface is characterised principally by states corresponding to "OH" species ($\theta_{OH} \longrightarrow 1$), a Tafel slope of 2.3 RT/2F results (cf. refs. 6,77) since the denominator of $[f_1(V)]$ reduces to $k_1 \exp VF/RT$. As the surface becomes more oxidised (S.OH $\longrightarrow$ S.O, S.O.OH) at higher potentials, and for $\theta_{O.OH} \simeq 1$, the denominator of $f_1(V)$ becomes $(K_1K_2K_5 \exp 3VF/RT)$ and the Tafel slope is -2.3 RT/2F, i.e. an inhibition reversal of slope will have occurred. Eventually in the final stages of surface oxidation, on the basis of the above

scheme, the steps $S.OOH \longrightarrow S.O_2$; $S.O_2 \longrightarrow S + O_2$ will pass the current and the current-potential relation will regain a normal positive slope.

Generally speaking, it is unlikely that the same reaction path can represent the kinetics throughout the course of the inhibition region, since once a reversal of the direction of the Tafel line has occurred, the effects which have led to this will continue to diminish the rate with increasing potential unless another step with normal sign of Tafel slope takes control and provides again increasing current with increasing anodic potential.

Incomplete reversal effects can manifest themselves in a slight inflection of the Tafel line or as a region of higher slope. In general such effects can be represented formally by the equation:

$$i = k \exp[V/b] \exp[-V/b']$$

when $\frac{1}{b'} > \frac{1}{b}$, reversal of the direction of the Tafel line will occur; if $\frac{1}{b'} = \frac{1}{b}$ a limiting current arises, while if $\frac{1}{b'} < \frac{1}{b}$ a change of slope of the Tafel line will arise.

A final possibility must be noted, viz. that at a certain critical composition of the electrode surface oxide layer, a weakly semi-conducting state might arise so that the electron affinity of the surface diminishes (insufficient density of p-states at the surface [cf. current limitation at cathodic

Figure 56. Log Q - potential plot for charging of the nickel oxide electrode in KOH solutions of various concentrations and temperatures by different methods:

(a) Fast galvanostatic reduction pulse; 1, 2 and 3 in 2.05 M KOH at 30°, 60° and 83°C respectively, and

(b) Fast galvanostatic reduction pulse; 1 and 2 in 6.7 M KOH at -30° and +30°C respectively.

(c) Potentiostatic step charging; 1 and 2 in 2.05 M KOH at 30° and 60°C and 3, 4 and 5 in 13.1 M KOH at 30°, 60° and 89°C respectively.

1-5 Electrochemically preconditioned; 6 in 2.05 M KOH, 30°C, vacuum annealed, no electrochemical pretreatment.

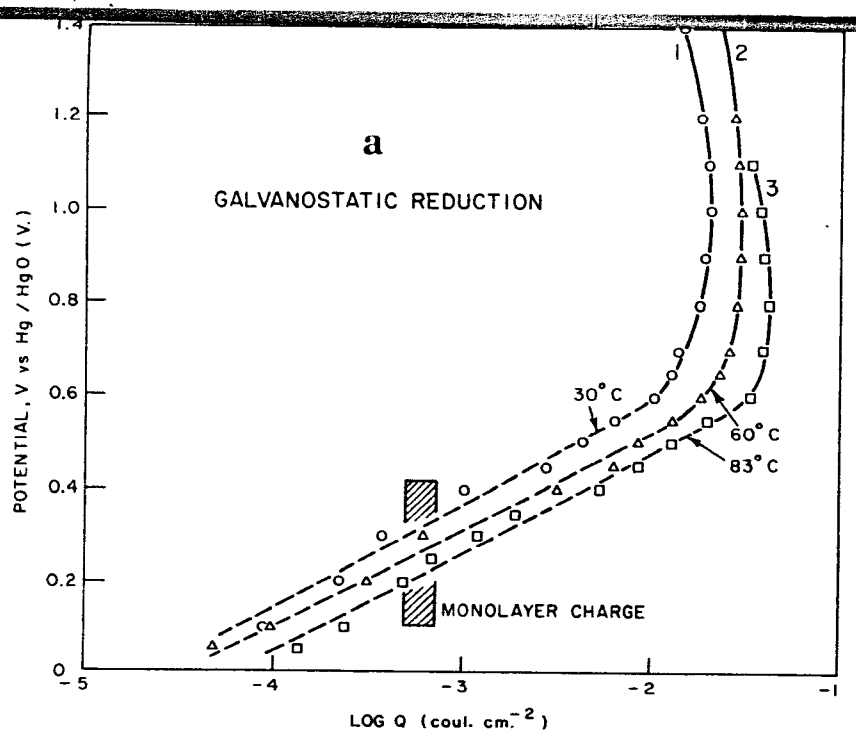
a
GALVANOSTATIC REDUCTION
POTENTIAL, V vs Hg / HgO (V.)
LOG Q (coul. cm.$^{-2}$)
1
2
3
30° C
60° C
83° C
MONOLAYER CHARGE

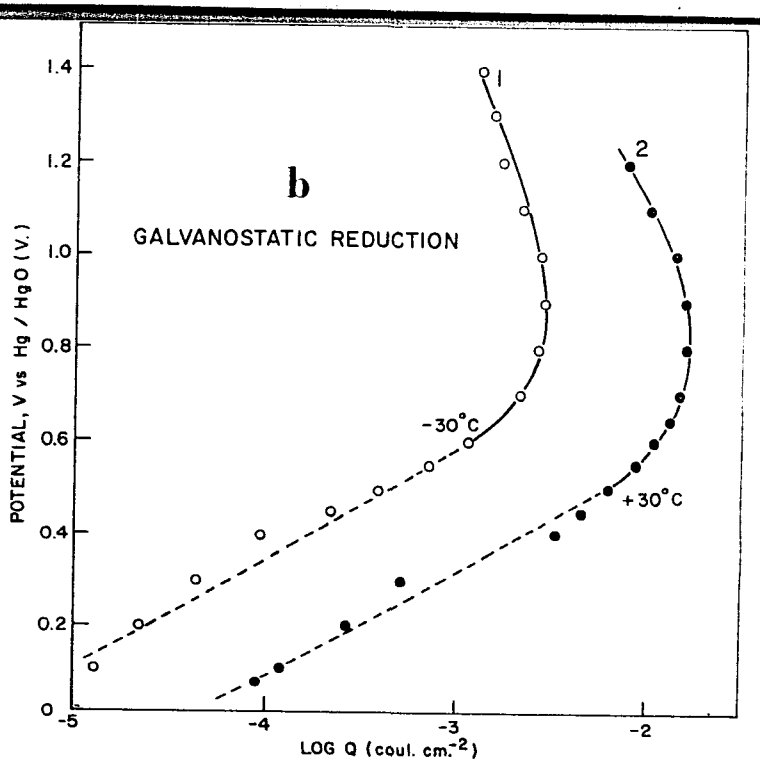
b
GALVANOSTATIC REDUCTION
POTENTIAL, V vs Hg / HgO (V.)
LOG Q (coul. cm.$^{-2}$)
1
2
-30°C
+30°C

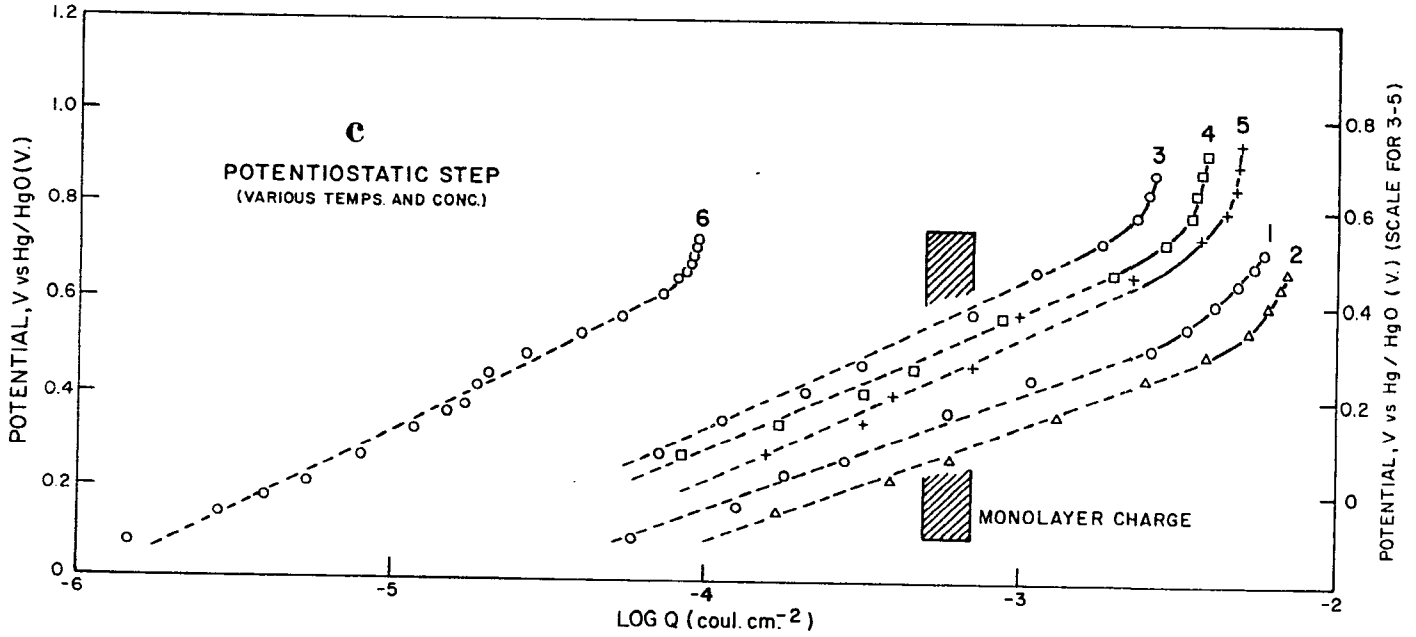
c
POTENTIOSTATIC STEP
(VARIOUS TEMPS. AND CONC.)
POTENTIAL, V vs Hg/HgO(V.)
POTENTIAL, V vs Hg / HgO (V.) (SCALE FOR 3-5)
LOG Q (coul. cm.$^{-2}$)
1
2
3
4
5
6
MONOLAYER CHARGE

Ge by low electron concentration] with a resulting fall of current). This could also be related to the diminished reducibility of the surface oxide layer beyond the critical potential corresponding to the maximum in the oxide reduction charge-potential plots (Fig. 53, Chapter III, and Fig. 56). The surface condition of the oxide film may thus directly influence the rate of the primary discharge process I over a certain range of potential. The fact that similar "self-passivation" effects have been observed in the o.e.r. kinetics at Pt in alkaline solution studied in this laboratory indicates that effects such as those mentioned above could not be the general reason for the inhibition behaviour. Thus, some special state of a thick oxide film is not necessary since at Pt the formal degree of surface oxidation hardly exceeds that corresponding to "PtO" in the region where self-inhibition occurs (62). In the case of silver, a close correlation does, however, exist between current maxima for the o.e.r. and the potentials for formation of various surface oxides of silver as shown in Fig. 27.

Taking into consideration the results of Fig. 56 for the nickel oxide electrode, it is clear that there is a definite logarithmic relation between charge and potential as is to be expected from the form of the above expression for θ_O. A slope (dV/dlog Q) of the value 2.3 RT/F would be

obtained if the condition of the surface oxide was such that $\theta_{OH} \longrightarrow 1$ since the expression for θ_O would then reduce to

$$\theta_O = K_2 \exp [VF/RT].$$

Although a logarithmic relationship is observed (Fig. 56), the experimental value of the slope (dV/dlog Q) is however, higher (ca. 0.220 - 0.250 V), a fact which at the moment seems difficult to interpret. It may arise on account of the growth of the oxide at the electrode surface, a factor which has not been taken into consideration in formulating the above relation for θ_O. It is to be noted that the oxygen evolution kinetics are related to the properties of the surface oxides through the type of surface sites available while in relation to charge determinations it is the total amount of reducible oxide at the surface which is involved as a function of potential. This exceeds a monolayer over part of the potential range in Fig. 56. Further discussion of this point will be deferred until a later section (section 4(d)).

The relation between the charge for oxide reduction and the potential reveals one very important fact: it seems that a close relationship between the self-passivation type of behaviour in the log[i]-V relations and the occurrence of maxima in the charge-potential plots exists. Both the "self-passivation" and the charge maxima occur at a potential

of ca. 0.9 V (e.g. Fig. 40). From the analytical results (Fig. 53), it is also observed that at potentials beyond ca. 0.9 V, the amount of nickel apparently oxidised during anodic polarisation is smaller than that at lower potentials. If the nature of the pre-treatment programme (Fig. 14) which precedes the reduction transients is recalled, then it is clear that the metal is polarised to the experimental potential in a rectangular step each time a galvanostatic determination of reduction charge is made. Under these conditions, when the metal is polarised at and beyond a potential of 0.9 V, it passivates too soon owing to the rapid formation of a more consolidated, electronically conducting oxide* film at the metal surface. Thus, as soon as the metal is covered with one or two layers of this type of oxide (viz. NiO.OH or NiO_2), the base metal virtually ceases to be oxidised further (54). This effect can hence produce maxima in the relations between potential and oxide reduction charge, and potential and the amount of nickel oxidised (e.g. Fig. 53).

This explanation is consistent with the kinetic results. At potentials beyond 0.9 V, when the higher oxide of nickel

---

*It is known that NiO.OH and NiO_2 are n-type semi-conductors having high electron densities. The density of conducting electrons in NiO_2 is such that this oxide has a greyish metallic lustre and behaves almost like a metal (e.g. 53,56).

(viz. NiO.OH or NiO_2) at the surface starts to become predominant, a reversal of the current-potential relation is observed as discussed above.

A kinetic hysteresis effect with respect to the ascending and descending current-potential curves is observed under most conditions over the higher range of potentials (Figs. 21-25). This effect becomes less apparent with increasing temperatures and more important with increasing concentration of KOH. As mentioned previously (Chapter I, section 2(c), (iv)), kinetic hysteresis is, in general, due to "sluggishness" of some step or steps in the ascending (change to more positive potentials) or descending polarization processes.

Addition of Li^+ ions to the KOH solutions had the following significant effects which are consistent with previous findings by other workers (17,55,56,60,61,200): the limiting (maximum) anodic current is somewhat diminished in comparison with that observed in 2.05 M KOH (25°C); the hysteresis between the ascending and descending curves is enhanced, i.e. it is maintained down to lower c.d.'s on the descending line indicating possibly an enhanced stability of the higher surface oxide species involved in the inhibition of the o.e.r. at these potentials (61) and the oxygen overvoltage is increased (55,56,200). The increase of oxygen overvoltage with the

incorporation of Li^+ ions into the lattice of "NiO_2" at the oxide/electrolyte interface has been explained (56) by considering that penetration of cations of lower valency (Li^+) into an oxide lattice having n-type conduction diminishes the concentration of free electrons, thus lowering its conductivity. As the conductivity through the oxide phase is lowered, the over-potential is increased. This has been experimentally verified by Lukovtsev et al. (56) by introducing, systematically, lower valent (viz. Li^+, Zn^{2+}, Al^{3+}, etc.) and higher valent (viz. Mo^{6+}, W^{6+}, etc.) cationic impurities into the nickel oxide lattice. With the higher valent cations, an opposite effect has been observed (56). According to another view (200), the higher oxygen overvoltage is due to the increase in the surface concentration of higher oxidation states at the electrode surface resulting from the inclusion of Li^+ ions in the oxide lattice (cf. ref. 53 and also 204*).

3. THEORY AND PRINCIPLES OF THE POTENTIOSTATIC STEP CHARGING TECHNIQUE

The charges, Q required for the formation and reduction

---

* Very recent results of Tuomi et al. (204) on the Li to Ni molar ratio (0.2 to 0.7) of the "β-phase" oxidation product (n-type semiconductor) and its Seebeck coefficient (ca. -100 $V/\mathring{K}$ at 1 mho/cm) hardly support the view that the electrochemical oxidation product is $LiNiO_2$. This latter compound is a p-type semiconductor and has a positive Seebeck coefficient.

of the oxides (or O-containing species) at the electrode surfaces were determined by the following transient methods:

(a) Potentiostatic step charging technique

(b) Potentiodynamic linear repetitive sweep method and

(c) Fast galvanostatic discharge method.

In this section, first the theory and principles of the potentiostatic step charging method as developed in the present work will be described.

It was previously mentioned (Chapter II) that the potentiostatic step charging method is similar, in principle, to Eigen's (133) relaxation methods for kinetic studies of very fast reactions. Gerischer and Mehl (117) were the first to apply a d.c. relaxation method to the study of activation controlled electrode processes and to develop the theoretical background for the potentiostatic step method for calculating kinetic parameters for the hydrogen evolution reaction.

According to Gerischer's calculation (117), the coverage in the steady-state can be evaluated from the <u>form</u> of the current-time transient observed, provided that the various assumptions made could be regarded as satisfactory. In his calculation the rate constants are first assigned and then by substituting these values into the equation for coverage, the latter quantity may be evaluated. This procedure is

applicable only when (i) the adsorbed intermediates formed electrochemically obey the Langmuir isotherm throughout the range of coverage studied; and (ii) any uncompensated resistance (iR) effect does not modify the shape of the transient and hence the values of the rate constants derived (140). However, in the range of intermediate values of coverage, the Temkin type of isotherm is rather generally applicable (173), and even a small variation in the apparent standard free energy of adsorption for the species concerned with their coverage, can affect significantly the rates (173).

In order to calculate the change of charge associated with adsorbed species at the electrode surface from a current-time transient arising from a rectangular potential jump, a rigorous theoretical calculation has been developed (cf. ref. 136) in the course of the present work. This approach is free from the objections which have been raised against Gerischer's calculations. It will be seen from the principle to be described below that the charge associated with change of coverage by the ad-species resulting from a rectangular change of potential can be determined by integrating the area under the relaxation curve after applying the appropriate corrections to be discussed below. It is to be noted that any errors which might be introduced into the calculation of change of charge on account of effects arising from any

uncompensated resistance (iR) in the circuit, and with respect to coverage effects under Temkin conditions, will be absent in so far as the area beneath the transient (even if it suffers some modification in shape) can still be evaluated.

In the present work, the method has been investigated from a kinetic point of view for determination of the charge associated with deposition of adsorbed species in activation controlled processes when the overall reaction is also proceeding at a significant rate, e.g., in the o.e.r. at potentials above the reversible potential. By considering two of the elementary steps (77) in the o.e.r. at an anode surface as model cases, a method is developed for calculating the charge associated with deposition of adsorbed intermediates at the electrode interface from the experimental current-time transients for potential jumps. In such cases, the potential step causes changes both in the quasi-equilibrium surface coverage by adsorbed O-containing species and in the steady-state velocity of the overall reaction which itself usually depends on the coverage of the ad-species. It is on account of the latter effect that this problem is complex and requires special treatment which is described in detail below.

In the potentiostatic step charging method (rectangular step), the potential of the electrode is controlled at a

Figure 57. Schematic diagram showing the principle of the potentiostatic step charging method.

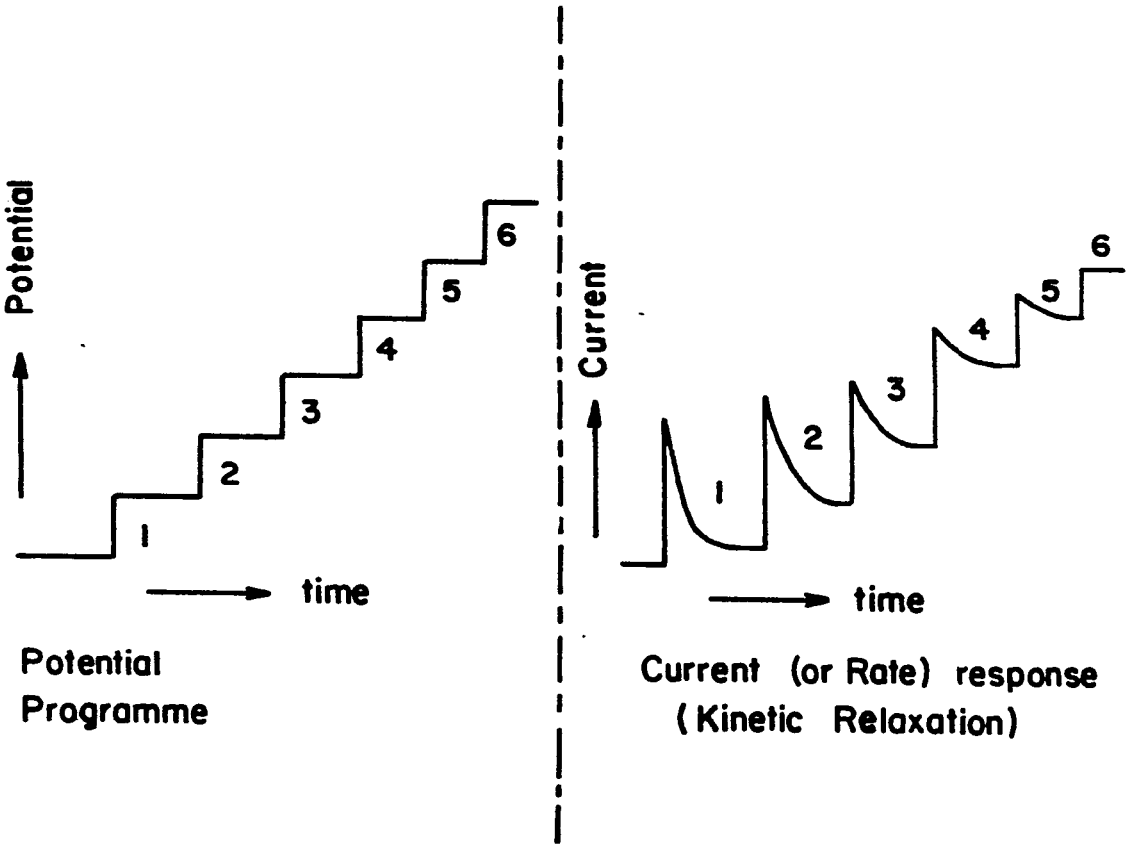
Potential
1
2
3
4
5
6
time
Potential
Programme
Current
1
2
3
4
5
6
time
Current (or Rate) response
(Kinetic Relaxation)

certain value say V_1 by a potentiostat and when steady-state conditions exist, the potential is instantaneously (of the order of several μ sec.) raised to a certain higher value say V_2 and kept constant, while the charge (proportional to the coverage) and the associated charging current are allowed to adjust themselves during a relaxation time τ to new values permitted by the kinetics of the reactions and the adsorption behaviour of the intermediates involved. After a certain lapse of time related to τ, the charging current effectively falls to zero, while the faradaic current gradually reaches a new value which ideally then remains constant. The effects involved are shown schematically in Fig. 57.

Calculation

The mechanism of evolution of oxygen at the electrode surface in alkaline medium may, in simple cases, be represented by (cf. ref. 77) the following schemes where "r.d." represents the rate-determining step, and k's are the rate constants.

(A) Volmer-Horiuti type of mechanism:

$$M + OH^- \underset{k_{-1}}{\overset{k_1}{\rightleftharpoons}} M/OH_{(ads.)} + e \qquad (A)I$$

$$M/OH_{(ads.)} + OH^- \xrightarrow[(r.d.)]{k_2} M/O_{(ads.)} + H_2O + e \qquad (A)II$$

$$2M/O_{(ads.)} \xrightarrow{fast} 2M + O_2(g) \qquad (A)III$$

(B) Volmer-Tafel type of mechanism:

$$M + OH^- \underset{k_{-1}}{\overset{k_1}{\rightleftharpoons}} M/OH_{(ads.)} + e \qquad (B)I$$

$$M/OH_{(ads.)} + M/OH_{(ads.)} \xrightarrow[(r.d.)]{k_2} M/O_{(ads.)} + H_2O \qquad (B)II$$

$$2M/O_{(ads.)} \xrightarrow{fast} 2M + O_2(g) \qquad (B)III$$

The reaction step I may be considered as being in a quasi-equilibrium condition if a subsequent step is a rate-determining one, thus leading to appreciable coverage of one or more intermediates (the case of interest here). Step III is assumed to have a relatively high rate constant and it removes the species $M/O_{(ads.)}$ as soon as it is formed.

In the subsequent discussion, we shall show how the charge associated with intermediates in these two important types of mechanisms for the o.e.r. can be calculated from the experimental current-time transients.

Case (A): Volmer-Horiuti type of Mechanism: The reaction under consideration is an activation controlled process and so the rate equations are written in the usual way in terms of potential; no diffusion effects are considered. The rate equation for the forward direction of reaction (A)I may be written in abbreviated form as

$$i_1 = k_1(1 - \theta)e^{\beta VF/RT} \qquad (1)$$

for a given constant concentration of KOH where V is the metal-solution potential difference and θ is the fractional coverage by $OH_{(ads.)}$ species, and β is the usual Brønsted-Volmer symmetry factor. Correspondingly the rate equation for the backward reaction in (A)I can be written as:

$$i_{-1} = k_{-1}\,\theta.e^{-(1 - \beta)VF/RT} \qquad (2)$$

and similarly for the other steps. In the present case, θ is a function of time t, so θ will be replaced in the above equations by θ_t, the coverage attained at a given time in the transient since we are concerned here with <u>the non-steady-state</u> kinetics in contrast to those in the steady-state more usually considered.

Here the charge required to produce a given coverage θ at the electrode will be proportional to the surface concentration of adsorbed OH on the electrode surface. The time-dependent net anodic charging current $i_{c(t)}$ is hence

$$i_{c(t)} = i_1 - i_{-1} - i_2$$

$$= k_1(1 - \theta_t)\, e^{\beta VF/RT} - k_{-1}\,\theta_t\, e^{-(1 - \beta)VF/RT} - k_2\,\theta_t\, e^{\beta VF/RT} \qquad (3)$$

Again, fractional coverage θ_t and charge q_t are related by

$$dq_t = K\, d\theta_t = i_{c(t)}\, dt \qquad (4a)$$

where K is the proportionality constant between charge and fractional coverage; hence

$$i_{c(t)} = K \frac{d\theta_t}{dt} \qquad (4b)$$

From equations (3) and (4b) we obtain

$$k_1(1-\theta_t)e^{\beta VF/RT} - k_{-1}\,\theta_t\, e^{-(1-\beta)VF/RT} - k_2\,\theta_t\, e^{\beta VF/RT} = K \frac{d\,\theta_t}{dt} \qquad (5)$$

If $\beta = 0.5$ and writing $\beta F/RT = \frac{1}{b}$ then equation (5) becomes

$$dt = K \frac{d\,\theta_t}{k_1\, e^{V/b} - (k_1\, e^{V/b} + k_{-1}\, e^{-V/b} + k_2\, e^{V/b})\,\theta_t} \qquad (6)$$

Let $A = k_1\, e^{V/b}$; $B = -(k_1\, e^{V/b} + k_{-1}\, e^{-V/b} + k_2\, e^{V/b})$

then

$$dt = K \frac{d\,\theta_t}{A + B\,\theta_t},$$

which, upon integration, gives

$$t = \frac{K}{B} \ln (A + B\,\theta_t) + I$$

where I is an integration constant, the value of which can be calculated by considering the boundary condition: $t = 0$, $\theta_t = \theta_i$, the initial value of coverage at the starting potential V_1.

$$\therefore \qquad I = -\frac{K}{B} \ln (A + B\,\theta_i)$$

$$\therefore \qquad t = \frac{K}{B} \ln \frac{A + B\,\theta_t}{A + B\,\theta_i}$$

or

$$e^{Bt/K} = \frac{A + B\,\theta_t}{A + B\,\theta_i} \qquad (7)$$

i.e.

$$\theta_t = e^{Bt/K} \left[\frac{A + B\,\theta_i}{B}\right] - \frac{A}{B} \qquad (8)$$

If Bt/K is quite small at low t, then $e^{Bt/K} \doteq 1 + \frac{Bt}{K}$, so that equation (8) simplifies to

$$\theta_t = \theta_i + \frac{t}{K} (A + B\,\theta_i) \qquad (9)$$

From the above equations (8) and (9) for fractional coverage θ as a function of time (t) and implicitly potential difference (V), through A and B, the fractional coverage θ_t can be deduced for two limiting conditions:

(α) When $t \to o$, from equation (9), $\theta_{t \to o} = \theta_i$ (10)

Figure 58. Variation of coverage (θ_t) as a function of time (t) for Volmer-Horiuti type mechamism. Values of θ_t are computed using equation 8, with values of $k_1 = 0.01$, $k_{-1} = 0.1$, $k_2 = 0.001$ and $K = 10^{-4}$ coul. cm^{-2}.

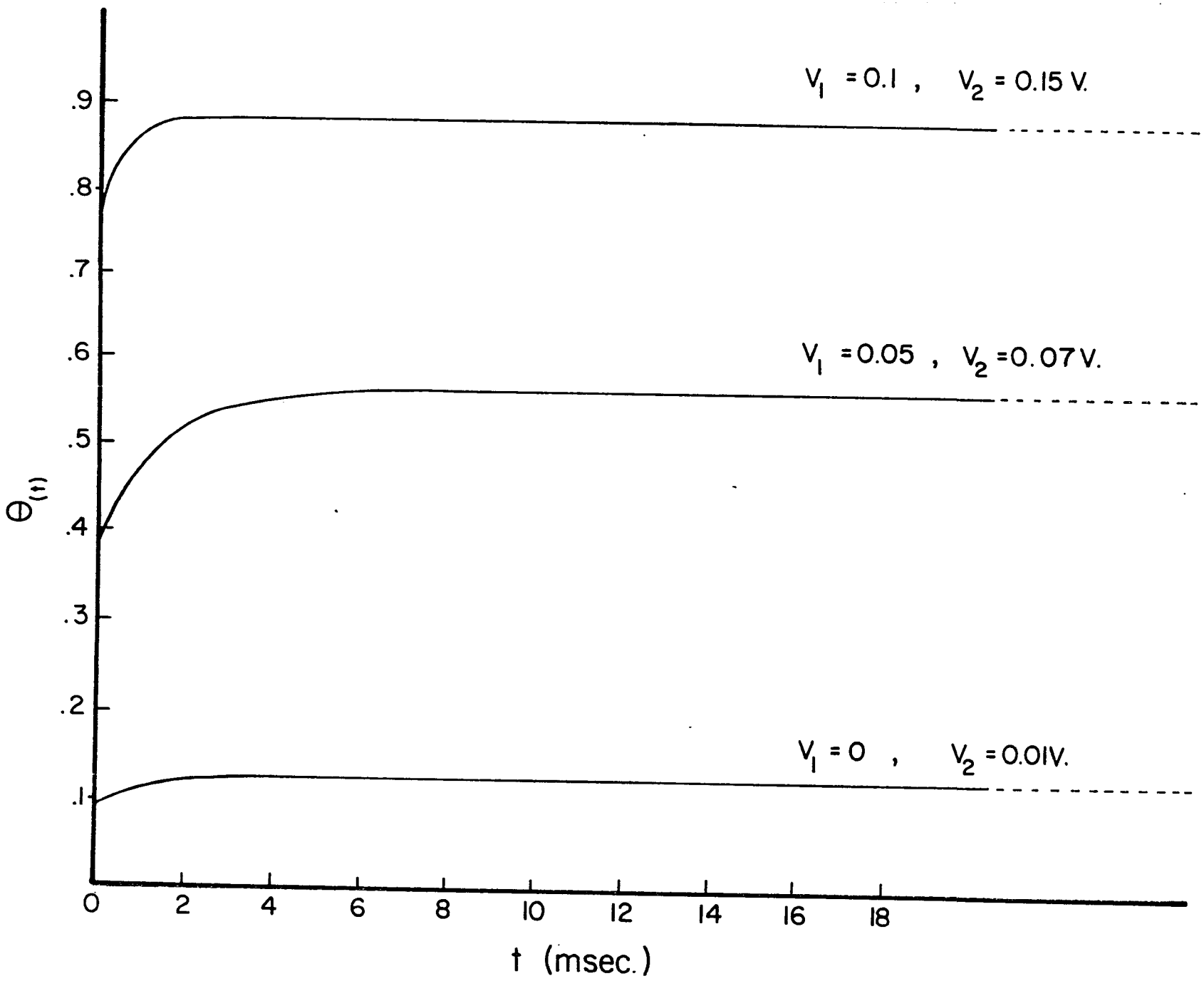
V_1 = 0.1 , V_2 = 0.15 V.
V_1 = 0.05 , V_2 = 0.07 V.
V_1 = 0 , V_2 = 0.01 V.
$\Theta_{(t)}$
.9
.8
.7
.6
.5
.4
.3
.2
.1
0
2
4
6
8
10
12
14
16
18
t (msec.)

Figure 59. Variation of steady-state coverage ($\theta_{t=\infty}$) as a function of potential (V) for

1. Volmer-Horiuti and
2. Volmer-Tafel type of mechanisms.

Values of $\theta_{t=\infty}$ are computed using equations 11 and 38 with values of $k_1 = 0.01$, $k_{-1} = 0.1$, $k_2 = 0.001$ and $K = 10^{-4}$ coul. cm^{-2}.

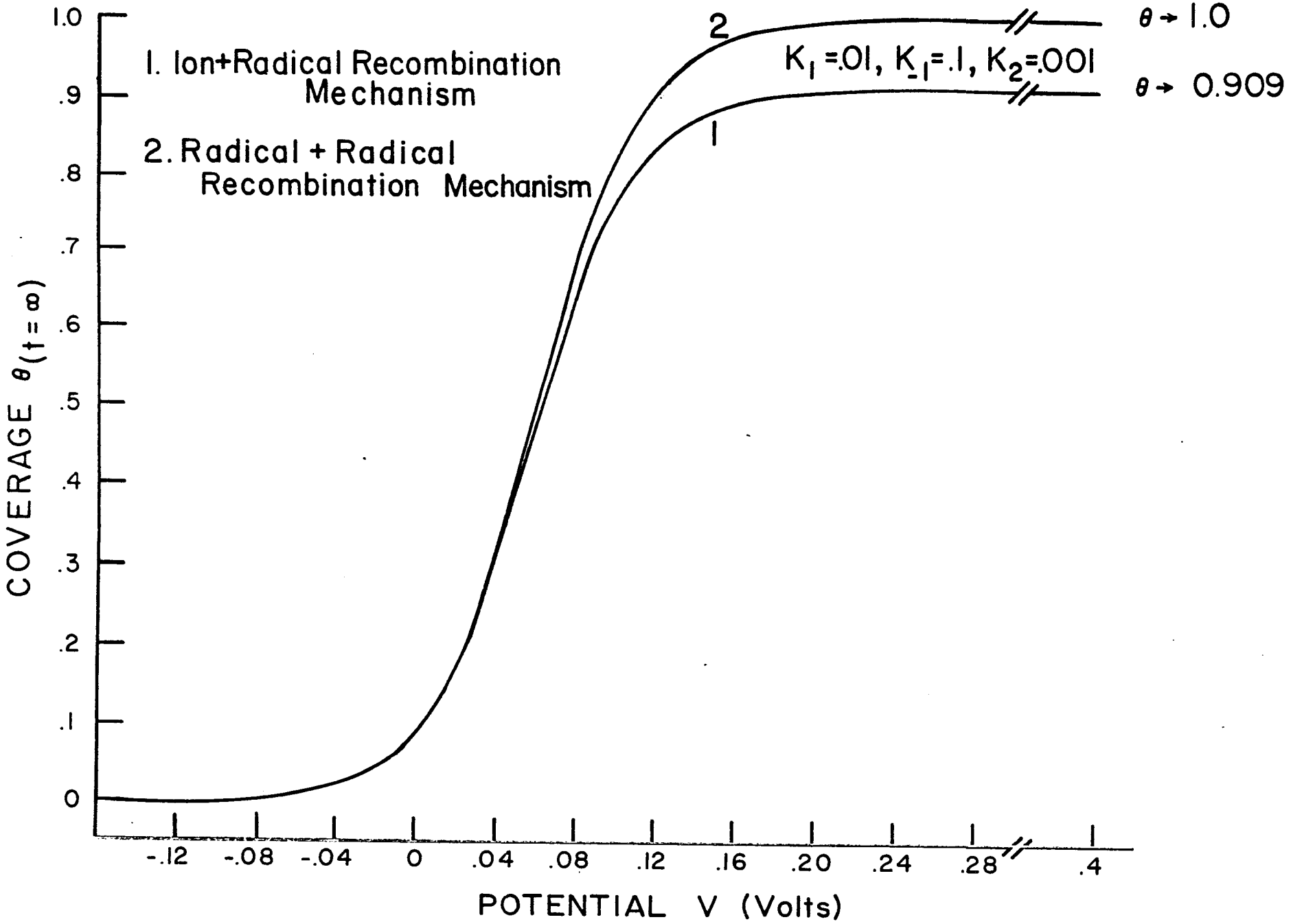
1. Ion+Radical Recombination Mechanism
2. Radical + Radical Recombination Mechanism
K_1 =.01, K_{-1}=.1, K_2=.001
$\theta \to 1.0$
$\theta \to 0.909$
2
1
COVERAGE $\theta_{(t=\infty)}$
1.0
.9
.8
.7
.6
.5
.4
.3
.2
.1
0
-.12
-.08
-.04
0
.04
.08
.12
.16
.20
.24
.28
.4
POTENTIAL V (Volts)

and

(β) When $t \rightarrow \infty$, from equation (8), $\theta_{t\rightarrow\infty} = \theta_{max.} = -\frac{A}{B}$

i.e.

$$\theta_{max.} = \frac{k_1 e^{V/b}}{k_1 e^{V/b} + k_{-1} e^{-V/b} + k_2 e^{V/b}}$$

$$= \left[1 + \frac{k_{-1}}{k_1} e^{-2V/b} + \frac{k_2}{k_1}\right]^{-1} \qquad (11)$$

$\theta_{max.}$ in the above equation is thus the steady-state coverage at the electrode surface at the end of the transient ($V = V_2$, $t = \infty$).

It is of interest to examine the form of the time dependence of θ and hence of the pseudo-faradaic charging current and the faradaic current for the overall reaction. From a numerical analysis, using selected values of the rate constants k_1, k_{-1}, k_2 and the constant K, the value of θ_t as a f(t) can be calculated for a potential jump from V_1 to V_2. The profiles of θ_t vs t for potential jump and $\theta_{t=\infty}$ vs V are shown in Figs. 58 and 59, respectively. From the nature of these model profiles we shall be able to show how the coverage $\theta_{t,V}$ can be obtained, in general, from experimental transients, using Fig. 60 and the procedure described below.

From knowledge of θ_t as a f(t), the charging current i_c, the time-dependent overall faradaic current i_F and the total

current i_T for a potential jump V_1 to V_2 can be calculated as functions of time using the following equations:

$$i_{c(t)} = A + B\,\theta_t \quad [\text{ from equation (3) }] \qquad (12)$$

$$i_{c,\text{initial}} = A + B\,\theta_i$$

$$i_{F(t)} = 2k_2\,\theta_t\,e^{V/b} \quad \text{(for step II)} \qquad (13)$$

and

$$i_{T(t)} = i_{F(t)} + i_{c(t)} + i_{d.l.}$$

$$\doteq i_{F(t)} + i_{c(t)} \qquad (14)$$

The latter approximation follows since the current for charging the double-layer for a small potential jump is negligible. Therefore,

$$i_{T(t)} = i_{F(t)} + i_{c(t)} = k_1\,e^{V/b} - k_{-1}\theta_t\,e^{-V/b} - k_1\theta_t\,e^{V/b} + k_2\theta_t\,e^{V/b}$$

$$= A - C\,\theta_t \qquad (15)$$

where

$$C = k_1\,e^{V/b} + k_{-1}\,e^{-V/b} - k_2\,e^{V/b}$$

Calculating θ_t, i_c, i_F and i_T all as functions of time for a potential jump from V_1 to V_2, a current-time transient can be

Figure 60. Profiles of charging current (i_c), faradaic current (i_F) and total current (i_T) as functions of time (t) computed, using equations 12, 13, and 14 with values of $k_1 = 0.01$, $k_{-1} = 0.1$, $k_2 = 0.001$ and $K = 10^{-4}$ coul. cm^{-2} for Volmer-Horiuti type mechanism.

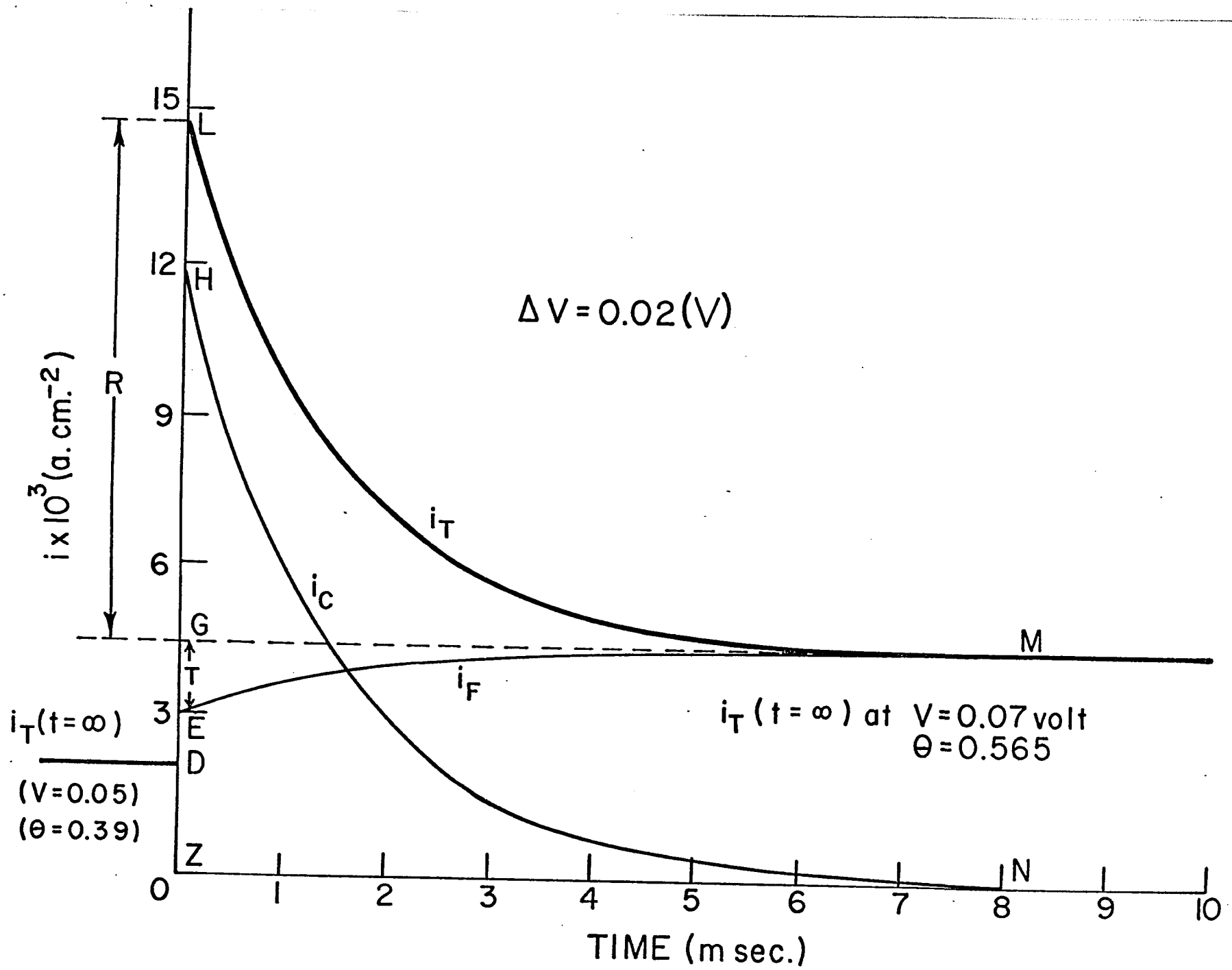
15
12
9
6
3
0
L
H
G
T
E
D
Z
R
$i \times 10^3$ (a. cm.$^{-2}$)
$\Delta V = 0.02$ (V)
i_T
i_C
i_F
M
N
$i_T(t=\infty)$
(V=0.05)
(θ=0.39)
$i_T(t=\infty)$ at V=0.07 volt
θ=0.565
1
2
3
4
5
6
7
8
9
10
TIME (m sec.)

constructed, as shown in Fig. 60.

As $t \rightarrow \infty$, $i_{c(t)} \rightarrow 0$ which can be seen easily by substituting the value of $\theta_{t \rightarrow \infty}$ in equation (12), and $i_{F(t)}$ becomes a steady new value measured on the ammeter. At lower coverage and at lower metal-solution potential difference, the faradaic current is very small and hence a relatively large relaxation charging current arises. At higher potentials, when full coverage is approached, the $i_{c(t)}$ for the potential jump tends to zero and hence the measured current which is the overall faradaic current attains its steady-state value, virtually instantaneously. Thus it can be shown that the "relaxation time" is a function of coverage, potential and the k-values.

The charge and hence change of coverage is an anodic current-time transient, for a potential jump V_1 to V_2, may be calculated as follows: The method of calculation of charge from the current-time transient, may be seen by considering Fig. 60. The current at point D (Fig. 60) is

$$i_{T_1}(t = \infty, V_1, \theta_1) \equiv i_{F_1}(t = \infty, V_1, \theta_1) \qquad (16)$$

Similarly, at M the current is

$$i_{T_2}(t = \infty, V_2, \theta_2) \equiv i_{F_2}(t = \infty, V_2, \theta_2) \qquad (17)$$

Now when the electrode is charged in a rapid potentiostatic step V_1 to V_2, the overall faradaic current momentarily shifts from point D to E (Fig. 60) but gradually changes from E to M exponentially, as the coverage changes with time since $i_{F(t)}$ involves θ_t. The charging current for the potential jump V_1 to V_2 momentarily rises from a zero value to H and then falls exponentially with time to zero. The total charge associated with the change of potential from V_1 to V_2 is then the area between the curve $i_{c(t)}$ and the base line. However, experimentally, the total current ($=i_{F(t)} + i_{c(t)}$) is measured and is represented by the curve LM. Therefore, the total charge associated with the change of potential from V_1 to V_2 would be given by the area under the curve LM less the area under the curve EM. Hence, the area ELM (Fig. 60) is the required change of charge (proportional to $\Delta\theta$) resulting from the potential step V_1 to V_2.

The same conclusions may also be reached as follows:

Since

$$i_{T(t)} - i_{F(t)} = i_{c(t)} = K \frac{d\,\theta_t}{dt}$$

or

$$i_{T(t)}dt - i_{F(t)}dt = K\,d\,\theta_t$$

Integrating

$$Q_T - Q_F = K\Delta\theta \qquad (18)$$

where Q_T = total charge and Q_F total faradaic charge passed for the overall reaction.

Experimentally, only the steady-state current at D (at potential V_1, coverage θ_1) (Fig. 60) and the total current LM as a f(t) for the potential jump from V_1 to V_2 are measured together with the steady-state current at M (potential V_2, coverage θ_2). Hence, for the calculation of charge, the value of current at the point E (Fig. 60) is required i.e., the faradaic current at potential V_2, coverage θ_1 and at $t = 0$, and the variation of faradaic current with time, i.e., the curve EM.

The current at E in Fig. 60 (i.e. $i_{F_2}(t = 0, \theta_1, V_2)$)is calculated as follows:

$$i_{F_2}(t=o, \theta_1, V_2) = 2k_2\, \theta_1(t=\infty, V_1) e^{V_2/b} \qquad (19)$$

and the current at D in Fig. 60 (i.e. $i_{T_1}(t=\infty, \theta_1, V_1)$) is

$$i_{T_1}(t=\infty, \theta_1, V_1) = 2k_2\, \theta_1(t=\infty, V_1) \cdot e^{V_1/b} \qquad (20)$$

Dividing equation (19) and (20), we obtain

$$i_{F_2}(t=o, \theta_1, V_2) = i_{T_1}(t=\infty, \theta_1, V_1) \cdot e^{\Delta V/b} \qquad (21)$$

$i_{T_1}(t=\infty, \theta_1, V_1)$ is an experimentally measured quantity and $e^{\Delta V/b}$ is known ($\Delta V = V_2 - V_1$); hence $i_{F_2}(t=o, \theta_1, V_2)$ can be calculated. Since the faradaic current for the overall reaction as a f(t) (i.e., curve EM) is not known, the change of charge for the change of potential may be calculated graphically as follows:

The horizontal line at M (Fig. 60) representing the steady-state faradaic current at θ_2, V_2 and $t = \infty$ is extended to meet EL at a point G. The area GLM is calculated, and is a fraction of the total change of charge for the potential jump, as shown below.

Since $i_{c(t=\infty)} = o$, the current represented by the horizontal line GM in Fig. 60 is

$$i_{F_2}(t=\infty, \theta_2, V_2) = i_{T}(t=\infty, \theta_2, V_2)$$

Therefore, from equation (15)

$$i_{T(t)} - i_{F_2}(t=\infty, \theta_2, V_2) = - C \left[\theta_t - \theta_{(t=\infty)}\right] \tag{22}$$

Since

$$K \frac{d\,\theta_t}{dt} = A + B\,\theta_t = i_{c(t)}$$

or

$$\theta_t = \frac{K\,(d\,\theta_t/dt) - A}{B} \quad \text{and} \quad \theta_{(t=\infty)} = - \frac{A}{B},$$

Equation (22) can be written as

$$i_{T(t)} - i_{F_2(t=\infty,\ \theta_2,\ V_2)} = -C\left[\frac{K\ (d\ \theta_t/dt) - A}{B} + \frac{A}{B}\right]$$

$$= -\frac{C}{B} K \frac{d\ \theta_t}{dt}$$

or

$$i_{T(t)}\ dt - i_{F_2(t=\infty,\ \theta_2,\ V_2)}\ dt = -\frac{C}{B} K\ d\ \theta_t$$

Integrating from t = o to a time t

$$\int_o^t \left[i_{T(t)} - i_{F_2(t=\infty,\ \theta_2,\ V_2)}\right]dt = -\frac{C}{B} K \int_{\theta_{t=o}}^{\theta_{t=\infty}} d\ \theta_t$$

$$= -\frac{C}{B} K\ \Delta\theta \qquad (23)$$

which is the area GLM. Hence we obtain the fraction $\frac{C}{B}$ of the required $\Delta\theta$, so that

$$K\Delta\theta = \text{change of charge} = -\frac{B}{C} \times [\text{area GLM}] \qquad (24)$$

The fraction $-\frac{B}{C}$ is estimated as follows: Again, from equation (22),

$$i_{T(t=o,\ \theta_1,\ V_2)} - i_{T(t=\infty,\ \theta_2,\ V_2)} = -C\left[\theta_{(t=o)} - \theta_{(t=\infty)}\right] \qquad (25)$$

and

$$i_{T(t=\infty,\ \theta_2,\ V_2)} - i_{F_2(t=o,\ \theta_1,\ V_2)} = -(B+C)\ \theta_{(t=\infty)} + (B+C)\ \theta_{(t=o)}$$

$$= (B+C)\left[\theta_{(t=o)} - \theta_{(t=\infty)}\right] \qquad (26)$$

where

$i_{T(t=o,\ \theta_1,\ V_2)}$ = momentary total current at L (Fig. 60),

$i_{T(t=\infty,\ V_2,\ \theta_2)}$ = current at G or M (Fig. 60)

and

$i_{F_2(t=o,\ \theta_1,\ V_2)}$=momentary faradaic current at E (Fig. 60)

(i.e. $i_{F_1(t=\infty,\ \theta_1,\ V_1)} \exp \Delta V/b$)

before θ has had time to change.

Dividing equation (26) by equation (25),

$$\frac{i_{T(t=\infty,\ \theta_2,\ V_2)} - i_{F_2(t=o,\ \theta_1,\ V_2)}}{i_{T(t=o,\ \theta_1,\ V_2)} - i_{T(t=\infty,\ \theta_2,\ V_2)}} = -\frac{B+C}{C} = -\frac{B}{C} - 1 \qquad (27)$$

Let

$$i_{T(t=\infty,\ \theta_2,\ V_2)} - i_{F_2(t=o,\ \theta_1,\ V_2)} = T \text{ (see Fig. 60)}$$

and

$$i_{T(t=o,\ \theta_1,\ V_2)} - i_{T(t=\infty,\ \theta_2,\ V_2)} = R \text{ (see Fig. 60)}$$

Then equation (27) becomes

$$\frac{T}{R} + 1 = -\frac{B}{C}$$

Substituting the value of $-\frac{B}{C}$ in equation (24), the change of charge for the potential jump is

$$K\Delta\theta = \frac{T+R}{R} \times [\text{area GLM}] \qquad (28)$$

T and R can be calculated from the transient as shown in Fig. 60; the area GLM can be directly measured and hence the change of charge $K\Delta\theta$, calculated.

Thus, the change of charge associated with the change of coverage by the adsorbed intermediate for each potential jump can be calculated, and by adding the increments $\Delta\theta$ for each ΔV, a profile of charge (or coverage) vs. potential can be constructed. Slopes of this profile give the differential pseudo-capacitance C_ϕ because

$$\frac{\Delta q}{\Delta V} \doteq \frac{dq}{dV} = C_\phi$$

The theoretical profile for the differential capacitance vs potential can be constructed for comparison with the experimental one. The capacitance is obtained by differentiating equation (11) with respect to potential, since

$$C_\phi = K \frac{d\,\theta_{(t=\infty)}}{dV}$$

Thus, from equation (11), (cf. ref. 175, q.v. for the shape of the profile under Langmuir conditions)

$$C_\phi = \frac{K}{b} \frac{2k_1 k_{-1}}{[k_1 e^{V/b} + k_{-1} e^{-V/b} + k_2 e^{V/b}]^2}$$

Case (B): Volmer-Tafel Type of Mechanism: Considering now the radical recombination step B(II) as the rate determining one in the o.e.r., we can write the time-dependent charging current $i_{c(t)}$ as above, in the form

$$i_{c(t)} = k_1(1-\theta_t)e^{V/b} - k_{-1}\,\theta_t\,e^{-V/b} - k_2\,\theta_t^2 \qquad (29)$$

which differs from equation (3) only in the last term. Again, using equation (4b) with equation (29), we obtain (cf. equation 6),

$$k_1\,e^{V/b} - \theta_t\,(k_1\,e^{V/b} + k_{-1}\,e^{-V/b}) - k_2\,\theta_t^2 = K\,\frac{d\,\theta_t}{dt} \qquad (30)$$

or

$$dt = K\,\frac{d\,\theta_t}{k_1\,e^{V/b} - \theta_t(k_1\,e^{V/b} + k_{-1}\,e^{-V/b}) - k_2\,\theta_t^2} \qquad (31)$$

Let $A = k_1\,e^{V/b}$, $B' = -(k_1\,e^{V/b} + k_{-1}\,e^{-V/b})$ and $C' = -k_2$; then equation (31) takes the form

$$dt = K\,\frac{d\,\theta_t}{A + B'\,\theta_t + C'\,\theta_t^2} \qquad (32)$$

Integrating equation (32),

$$t = \frac{K}{\sqrt{-q}}\,\ln\,\frac{2C'\,\theta_t + B' - \sqrt{-q}}{2C'\,\theta_t + B' + \sqrt{-q}} + I \qquad (33)$$

where $q = 4AC' - B'^2$ and I is an integration constant.

After evaluating I from the boundary condition $t = o$, $\theta_t = \theta_i$, equation (33) becomes

$$t = \frac{K}{\sqrt{-q}} \ln \left[\frac{2C'\theta_t + B' - \sqrt{-q}}{2C'\theta_t + B' + \sqrt{-q}} \times \frac{2C'\theta_i + B' + \sqrt{-q}}{2C'\theta_i + B' - \sqrt{-q}} \right] \tag{34}$$

or

$$\exp[t\sqrt{-q}/K] = \frac{2C'\theta_t + B' - \sqrt{-q}}{2C'\theta_t + B' + \sqrt{-q}} \times \frac{2C'\theta_i + B' + \sqrt{-q}}{2C'\theta_i + B' - \sqrt{-q}} \tag{35}$$

Solving equation (35) for θ_t,

$$\theta_t = \frac{1}{2C'} \left[\frac{\frac{2C'\theta_i + B' + \sqrt{-q}}{2C'\theta_i + B' - \sqrt{-q}} \times (B' - \sqrt{-q}) \times \exp[-t\sqrt{-q}/K] - (B' + \sqrt{-q})}{1 - \frac{2C'\theta_i + B' + \sqrt{-q}}{2C'\theta_i + B' - \sqrt{-q}} \exp[-t\sqrt{-q}/K]} \right] \tag{36}$$

Thus, equation (36) gives the variation of coverage in mechanism [B] as a function of time for a potential jump. From this equation two limiting cases can be usefully considered.

Limiting cases:

(α) When $t = o$, $\theta_t = \theta_i$; (37)

and (β) when $t = \infty$

Figure 61. Variation of coverage (θ_t) as a function of time (t) for Volmer-Tafel type mechanism. Values of θ_t are computed using equation 36 with values of $k_1 = 0.01$, $k_{-1} = 0.1$, $k_2 = 0.001$ and $K = 10^{-4}$ coul. cm^{-2}.

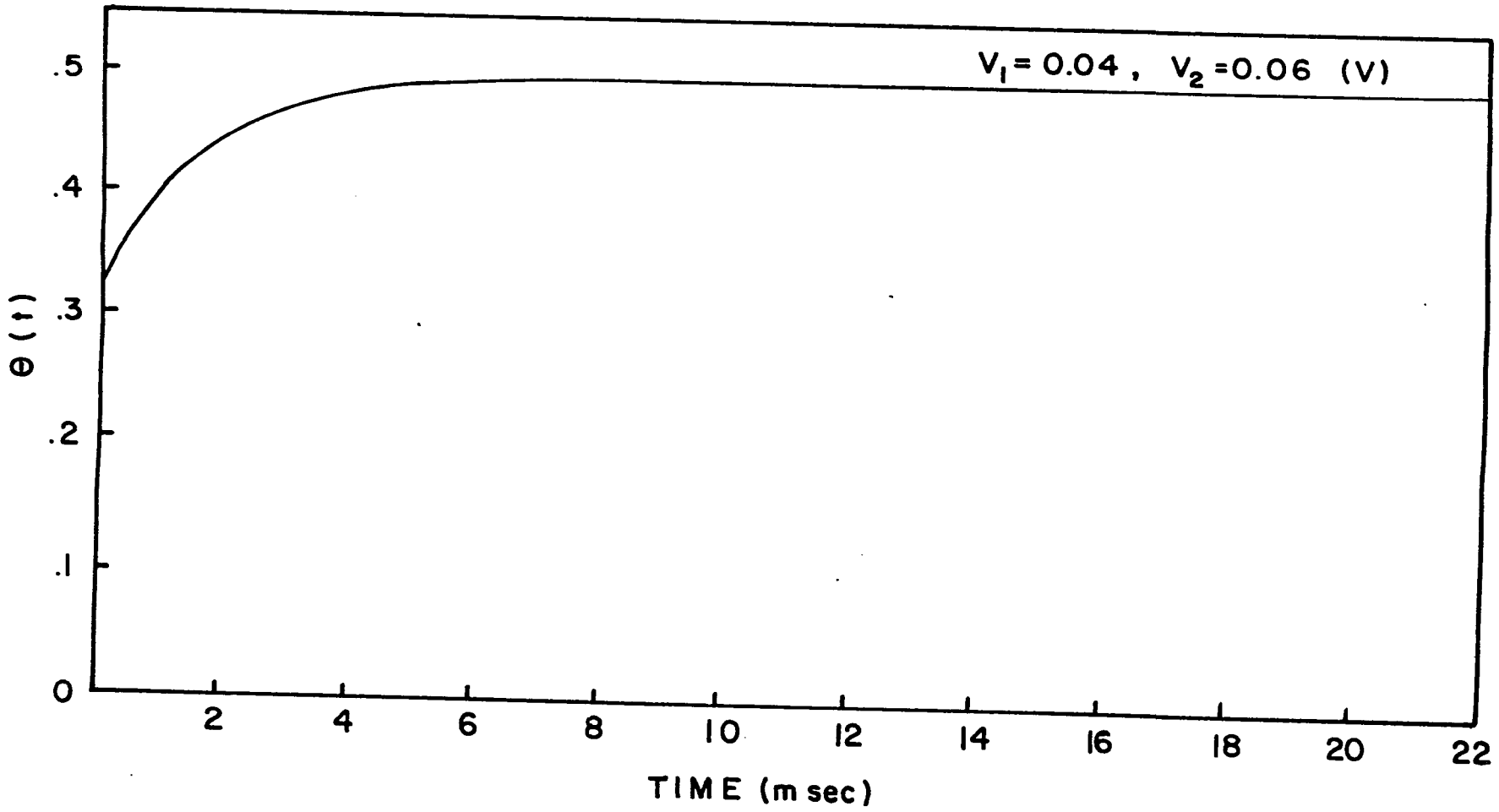
$V_1 = 0.04$, $V_2 = 0.06$ (V)
.5
.4
.3
.2
.1
0
θ(t)
2
4
6
8
10
12
14
16
18
20
22
TIME (m sec)

$$\theta_{(t=\infty)} = -(B' + \sqrt{-q})/2C'$$

$$= \frac{-k_1 e^{V/b} - k_{-1} e^{-V/b} + \left\{4k_1 k_2 e^{V/b} + [k_1 e^{V/b} + k_{-1} e^{-V/b}]^2\right\}^{\frac{1}{2}}}{2k_2} \qquad (38)$$

The steady-state coverage $\theta_{t=\infty}$ for this reaction can also be obtained by considering equation (30). Since $\theta_{t=\infty}$ is constant, $\frac{d\,\theta_{t=\infty}}{dt} = 0$. Therefore, the right hand side of the equation (30) is zero when θ_t is replaced by $\theta_{t=\infty}$ and so the quadratic equation

$$k_1 e^{V/b} - \theta_{(t=\infty)} (k_1 e^{V/b} + k_{-1} e^{-V/b}) - k_2 \theta^2_{(t=\infty)} = 0$$

is obtained having roots given by

$$\theta_{(t=\infty)} = \frac{-k_1 e^{V/b} - k_{-1} e^{-V/b} \pm \left\{[k_1 e^{V/b} + k_{-1} e^{-V/b}]^2 + 4k_1 k_2 e^{V/b}\right\}^{\frac{1}{2}}}{2\,k_2}$$

which is the same as equation (38) when the positive case in the third term is taken. $\theta_{(t)}$ as a f(t) and $\theta_{t=\infty}$ as a f(V) are shown in Figs. 61 and 59, respectively.

Thus, knowing θ_t as a f(t), the component currents as f(t) can be written down as follows:

$$i_{c(t)} = A + B' \theta_t + C' \theta_t^2 \qquad (39)$$

Figure 62. Profiles of charging current (i_c), faradaic current (i_F) and total current (i_T) as functions of time (t) computed using equations 39, 40 and 41 with values of $k_1 = 0.01$, $k_{-1} = 0.1$, $k_2 = 0.001$ and $K = 10^{-4}$ coul. cm^{-2} for Volmer-Tafel type mechanism.

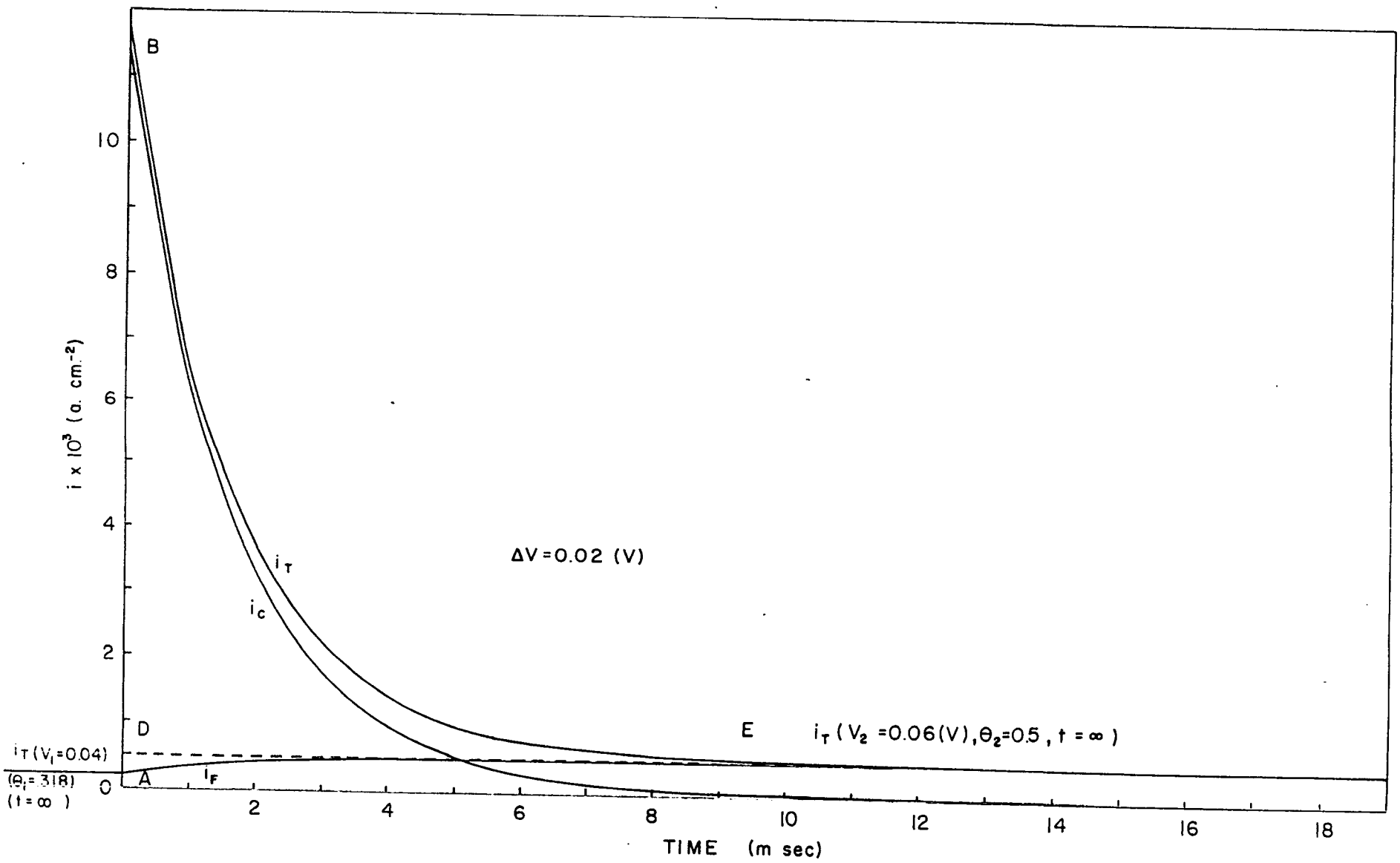
B
10
8
6
4
2
0
i x 10³ (a. cm⁻²)
ΔV=0.02 (V)
i_T
i_C
D
E
i_T (V₂ =0.06(V), θ₂=0.5 , t = ∞)
i_T (V₁=0.04)
(θ₁=318)
(t = ∞)
A
i_F
2
4
6
8
10
12
14
16
18
TIME (m sec)

$$i_{F(t)} = 2k_2\theta_t^2 = -2C' \theta_t^2 \qquad (40)$$

and

$$i_{T(t)} \doteqdot i_{c(t)} + i_{F(t)} = A + B' \theta_t - C' \theta_t^2 \qquad (41)$$

As in the case of the ion-radical recombination mechanism (A)II, we can construct the current-time profile for the potential step V_1 to V_2 assuming certain values of the k's (Fig. 62). In this reaction mechanism, the faradaic reaction step (B)II is only indirectly potential dependent. The area ABE (Fig. 62) is equal to the change of charge for the potential jump from V_1 to V_2, i.e.,

$$[\text{Area ABE}] = \int_o^t [i_{T(t)} - i_{F_2(t)}]dt = \int_o^t i_{c(t)}dt = k\Delta\theta \qquad (42)$$

Here also, since $i_{F_2(t)}$ as a f(t) is not known, the change of charge can be calculated by extending the horizontal portion of BE in Fig. 62 to meet AB at D, and then calculating the area.

Therefore

$$i_{T(t)} - i_{F_2(t=\infty)} = A + B' \theta_t - C' \theta_t^2 + 2C' \theta^2_{(t=\infty)} \qquad (43)$$

Again

$$i_{c(t)} = A + B' \theta_t + C' \theta_t^2 = K \frac{d\theta_t}{dt}$$

hence

$$A + B' \theta_t = K \frac{d \theta_t}{dt} - C' \theta_t^2 \qquad (44)$$

Combining equations (43) and (44)

$$i_{T(t)} - i_{F_2(t=\infty)} = K \frac{d \theta_t}{dt} - 2C' \theta_t^2 + 2C' \theta^2_{(t=\infty)}$$

which upon integration gives,

$$\int_o^t [i_{T(t)} - i_{F_2(t=\infty)}]dt = k\Delta\theta - 2C' \int_o^t [\theta_t^2 - \theta^2_{(t=\infty)}]dt$$

$$= [\text{area DBE}]$$

$$\text{Therefore the charge} = K\Delta\theta = [\text{Area DBE}] + 2C' \int_o^t [\theta_t^2 - \theta^2_{(t=\infty)}]dt$$

$$= [\text{Area DBE}] + 2k_2 \int_o^t [\theta^2_{(t=\infty)} - \theta_t^2]dt \qquad (45)$$

The integral in the equation (45) is positive and its solution is in this case very difficult; however, it can be neglected when the ΔV is small, the fractional coverage θ is low and k_2 is very small. Under these conditions, although the correction is positive, it can be neglected so that

$$K\Delta\theta \doteqdot [\text{Area DBE}] \qquad (46)$$

For the mechanism (B)II the error involved in the calculated charge for adsorbed species will not be quite negligible when the potential step is bigger and the coverage is higher. Under these conditions the integral in the equation (45) would have to be evaluated; for successive small steps, the error would be cumulative.

The capacitance can also be conveniently calculated by differentiating the charge vs potential profile. The theoretical value of the pseudo-capacitance C_ϕ under steady-state conditions can be evaluated by differentiating equation (38), and this profile can be compared with the experimental one. Thus (cf. ref. 175)

$$C_\phi = \frac{K}{2k_2 b}\left[-k_1 e^{V/b} + k_{-1} e^{-V/b} + \frac{2k_1 k_2 e^{V/b} + k_1^2 e^{2V/b} - k_{-1}^2 e^{-2V/b}}{[4k_1 k_2 e^{V/b} + k_1^2 e^{2V/b} + k_{-1}^2 e^{-2V/b} + 2k_1 k_{-1}]^{\frac{1}{2}}}\right]$$

The above treatment for the potentiostatic step charging method can, of course, also be used for direct experimental determination of pseudo-capacitance, C_ϕ, as a stepwise function of potential, V. Experimentally, the change of charge, Δq for the change of potential, ΔV, is determined over a number of successive changes of potential in the whole experimental potential range. If ΔV is very small, the change of charge in the short potential region can be assumed linear. Therefore,

the differential pseudo-capacitance, C_{ϕ}, at potential $V_1 + \frac{1}{2}\Delta V$ can be obtained approximately as

$$C_{\phi} = \frac{dq}{dV} \doteq \frac{\Delta q}{\Delta V}$$

From these values of pseudo-capacitance at various potentials, a pseudo-capacitance vs potential profile can be constructed.

The treatment given above for surface charging will obviously be more complex when a potential step produces a change of oxide film thickness in addition to a change of coverage by oxygen ad-species at the solution interface of the oxide layer. Since the correction for charge passed in Faradaic oxygen evolution processes will probably apply, however, as well to the electrochemical processes occurring on the surface of the conducting oxide (4) as they do to the initial processes occurring on the metal itself, it has seemed reasonable to use the analyses proposed above for the treatment of experimental results for such cases, particularly as only small correction terms are involved. The only complication may be the involvement of overshoots or undershoots (176) but it is unlikely that these will be significant with nickel oxide films which have appreciable electronic conductivity.

Results obtained by the step-charging method have been presented in Chapter III and will be discussed further below.

4. NON-STEADY-STATE MEASUREMENTS: CHARGE AND PSEUDO-CAPACITANCE BEHAVIOUR OF THE NICKEL OXIDE ELECTRODE

Applications of the potentiostatic anodic step charging method have been made to the study of the involvement of surface oxide species in the oxygen evolution reaction at nickel electrodes in alkaline solution. The potential range covered included a region where faradaic oxygen evolution can occur. Under these conditions, a method based on the principles described above must be adopted, since currents of both a faradaic (for the overall reaction) and a pseudo-faradaic (for the surface charging process) origin pass in a common range of potentials. The potential sweep method under these conditions yields results which are difficult to interpret. Comparison of the results obtained with those from the latter method and from the galvanostatic reduction method is made over appropriate ranges of potential. The formation of various oxide species at the electrode surface is indicated by studies on the stoichiometry of the oxide (to be discussed in a later section) as determined by chemical methods.

(a) Discussion of Potentiostatic Step Charging Results

(i) Development of Surface Oxides: From the potentiostatic measurements of the steady-state anodic log[i]-V relations for nickel electrodes, the Tafel slopes observed

(below the self-passivation region) indicate that the ion-discharge or the ion-radical type of recombination mechanism might be operative for the metal oxidation process as well, depending on the potential region.

From this indication of mechanism of the o.e.r. on the oxidized nickel surface in alkaline solutions, the appropriate method of calculation of the charge associated with adsorbed intermediates was applied using the potentiostatic step procedure described above. It should be mentioned that in the absence of any appreciable faradaic reaction associated with production of final reaction product (O_2), the potentiostatic step charging method can also be used for the determination of the charge associated with change of coverage by adsorbed species involved in the overall reaction, irrespective of the detailed mechanism, since for this condition, the area between the current-time transient curve and the final steady-state current line then represents quite accurately the charge passing for surface oxidation of the metal (or for the formation of ad-species) for the potential jump ΔV (see Fig. 28 a). When oxide continues to grow beyond the monolayer stage as is the case here (see Fig. 56), the potentiostatic step charging method can still, of course, be used. The corrections for faradaic oxygen evolution current are then relatively small and a simple approximation for

estimation of the charge passed due to co-evolution of oxygen can be made by a geometrical procedure on the records of the charging transients with an accuracy of ca. 4-5%.

On the above basis, the charge for formation of the surface oxide film was calculated for each potential jump from the experimental current-time transients. Addition of the charge increments gave the charge, Q vs. potential, V profile shown in Figs. 29, 31 and 32. Differentiation gave the pseudocapacitance (dQ/dV) profile (Figs. 30 and 33), which is almost symmetrical about a potential of ca. 0.5 V (= 1.43 V vs H_2H^+); the exact value depends on temperature and concentration (Fig. 30). The Q-V profile may represent (cf. ref. 179) progressive oxidation between oxide states represented by

$$Ni(II) \longrightarrow Ni(III) + e \qquad I$$

or

$$Ni(II) \longrightarrow Ni(IV) + 2e \qquad II$$

The standard reversible potential* for oxide formation in alkaline solution by a reaction such as I was found (7) to be

---

*The E^o value for reaction I seems to be higher than the E^o value for reaction II. However, E^o for reaction II may be quite uncertain because the value for the free energy of formation of "NiO_2" is not well known since such material is not well characterised chemically. Foerster's experimental data may refer rather to the formation of "NiO.OH" than to "NiO_2" (see p. 34).

0.425 V vs Hg/HgO and that for reaction II is recorded (12, 178,64) as 0.49 V vs NHE (i.e. E^o = 0.392 V vs Hg/HgO). Except initially, the thickness of oxide layers on anodized Ni is sufficient for such potentials to be chemically meaningful so that below this potential (i.e. E^o = 0.5 V vs Hg/HgO), Ni(II) species predominate in the surface oxide layer. Also from the thermodynamic potentials, it is clear that as soon as the electrode is dipped into KOH solution, $Ni(OH)_2$ will tend to be formed on the metallic surface; thus, Weininger and Breiter (25) observed by electron microscopy that $Ni(OH)_2$ was formed spontaneously in KOH solution, without the application of an external field, to the extent of at least 1 or 2 layers on single- and on poly-crystalline nickel. Above this potential (E^o = 0.5 V vs Hg/HgO) oxygen evolution therefore occurs (cf. ref. 7) through the formation and removal of NiO.OH species or some other species corresponding to a higher state of oxidation.

Various pathways may be proposed for the initial stages of oxidation of metallic nickel involving states such as $Ni(OH)_2$, NiO.OH or NiO_2 (47) which may also be involved in O_2 evolution. Since the E^o values for the oxidation processes I and II are close together, both processes may occur simultaneously in anodization (cf. ref. 30). In the case of O_2 evolution on the oxide surface, surface oxide species

must provide the sites at which OH^- ions are oxidised liberating O_2. In representations of such sites by chemical formulae (cf. ref. 77) it is not intended to imply that species of such stoichiometries are typical bulk substances nor that the surface layer has necessarily a homogeneous composition of such stoichiometry. Even with impregnated nickel oxide electrodes, the experimental evidence (4-7) indicates that the surface layer may have a higher degree of oxidation (56,87) than the bulk under anodic charging conditions.

(ii) Electrochemical Charging Behaviour: The charge Q associated with formation of the species on the electrode surface was determined by the potentiostatic step method also starting from -0.92 V (i.e. 0.006 V vs. H_2/H^+) using a fresh electrode annealed in purified dry hydrogen. The Q vs. V and C vs. V profiles are shown in Figs. 32 and 33, respectively. The first small peak (Fig. 33) at -0.6 V, it seems, may be due to dissolution of any atomic hydrogen ab- or adsorbed during the preparation of the electrode and the second peak at 0.5 V to the oxidation of the metal to $Ni(OH)_2$ and on to NiO.OH and higher oxides (cf. ref. 25,26). The estimated charge corresponding to the peak at -0.6 V is too small to be realistically considered as being connected with the metal oxidation except perhaps at active regions.

Supporting information was obtained from the non-steady-state current-potential profile resulting from the application of a repetitive linear sweep (cf. refs. 25,26) at the nickel electrode in KOH solution (Fig. 34) (see below). Since the current-time relationship obtained by the potential-sweep method can be transformed into a capacitance-potential plot by simply changing the units on both coordinates (163,164), the non-steady-state current-potential relationship shown in Fig. 34 also represents the capacitance-potential profile analogous to Figs. 30 and 33 obtained by the potentiostatic step method. This conversion can only be made, of course, in ranges of potential where a negligible current for the overall faradaic reaction passes. The first small peak in Fig. 34 a,c (near -0.6 V) is similar to that in Fig. 33.

The total charge for anodization of a fresh electrode by the potentiostatic step method was found to be appreciably smaller than that for an electrochemically preconditioned electrode (see Figs. 29,31 and 32) but the Q vs. V profile was similar. This effect may be connected with the possibility that the thermally annealed metal has different crystal face exposure (cf. ref. 180) at the surface than that at the electrochemically preconditioned electrode. Thermally annealed nickel has larger grain size than electro-deposited material which normally has a characteristic

dendritic structure (180) (except when prepared from special bright plating baths). This discrepancy may also be due to the fact that the thermally annealed metal passivates more quickly by forming 1 or 2 layers of relatively conducting oxide film at active regions on the surface, whereas the electrochemically preconditioned electrode is probably initially covered with a prepassive film of $Ni(CH)_2$ which takes more charge for its oxidation or becomes more active after pre-conditioning (cf. Fig. 8).

In a series of comparative measurements, the results from the step charging method were compared with those from the fast galvanostatic reduction method (Table IV, Chapter III) in order to assess the reliability of the step method. From the results (Table IV), it is seen that the maximum charge for oxide reduction at the highest potential, estimated in a galvanostatic transient, was about 20% more than that determined by successive anodic potential-step charging transients. This discrepancy may arise because oxide was continuing to grow slowly but significantly between consecutive potential steps. In a separate set of experiments at various constant potentials, the charge for oxide reduction was, in fact, found to increase approximately logarithmically with time (87) as shown in Fig. 64. Similar behaviour is even observed at platinum (63). The growth of surface oxides

as a logarithmic function of time was also recently observed by Makrides (182) at gold and by Sato et al. (183) at iron electrodes. Since the growth rate will obviously be slower at low (e.g. -30°C) than at high temperatures, the discrepancy between the charges determined by the above mentioned methods is smaller for the measurements conducted at low temperatures than for those made at higher temperatures.

(b) Discussion of Potentiodynamic Linear Repetitive Sweep Results

A typical potentiodynamic i-V profile obtained at a nickel electrode in aq. KOH has two significant peaks in the charging (anodic) direction and one oxide reduction peak in the discharging (cathodic) direction of scanning. As mentioned in the section above, the first small charging peak at about -0.6 V can be associated with both the dissolution of ad- or absorbed atomic hydrogen as in the step measurements (Fig. 33). This is supported by the fact that when measurements were made for the scanning potential ranges under such conditions that no hydrogen evolution occurred, (i.e. only NiO.OH could reduce to $Ni(OH)_2$) the small peak at -0.6 V disappeared (Fig. 34, b,d). Unlike the case of platinum, no H adsorption peaks are observed for nickel electrodes. This is probably because hydrogen already starts being evolved on $Ni(OH)_2$ itself (54) and hence there is no sharp boundary between the processes of (eventual) reduction of $Ni(OH)_2$ to metal and the adsorption of hydrogen

at the metal surface.

The second anodic oxide formation peak, which occurs at a potential of ca. 0.5 V, represents mainly direct oxidation of $Ni(OH)_2$ to NiO.OH (16,29,35) or via NiO_2 (12,13,47) or to both simultaneously (30) and oxidation of more metallic nickel as well (film growth). These processes are usually accompanied, to some extent, by the overall faradaic reaction* of oxygen evolution because the reversible potential for this latter process (E^o = 0.401 vs NHE) is close to that for the former process(es) ($E^o \doteq 0.5$ vs NHE).

The peak corresponding to the reduction of NiO.OH to $Ni(OH)_2$ occurs at a potential of ca. 0.35 V. Appreciable hysteresis between the processes of oxidation of and reduction to the lower valent oxide species (viz. $Ni(OH)_2$) at the electrode surface therefore exists. The potentials at which the peaks occur, however, depend significantly on the sweep-rate (87,163,164), the scanning potential range**,

---

* The Faradaic oxygen evolution reaction may, of course, have different overvoltages on different kinds of oxide species.

**This is probably related to the varying oxide film thicknesses developed at the electrode surfaces in different scanning potential ranges through the ohmic overpotential (iR) effect within the film.

and concentration and temperature of the KOH solutions (Fig. 44).

The charges Q passed during a linear anodic sweep oxidation of the lower valent nickel oxide ($Ni(OH)_2$) to higher valent oxides, and during reduction of higher valent oxides to the lower valent one, are given in Table V. The Q values are in fairly good agreement with those measured by galvanostatic reduction pulses provided the proper potential ranges are considered. It is observed, as expected, that the slower is the sweep-rate, the greater is the charge for surface oxidation, and that at low temperature (-30°C) much smaller charges are involved. An important point is that the oxides of nickel are not reduced to the metal unless the oxide electrode is kept potentiostatically in the cathodic potential region for some time (cf. Section 3 (f), Chapter III and ref. 54). Thus, it has been shown indirectly (Chapter III, section 3 (f)) that under galvanostatic conditions, hydrogen gas can be evolved on the lower valent oxide surface itself, as observed previously in ellipsometric experiments (54).

The formal change of valency for the oxidation and reduction processes (for example, 1 in the oxidation of $Ni(OH)_2$ to NiO.OH or 2 for $Ni(OH)_2$ to NiO_2) in the sweep experiments cannot be deduced simply from knowledge of the charges corresponding to the different peak areas because

complications due to oxide film thickening and change of degree of oxidation in the film usually arise in the case of nickel.

The significance of oxidation or reduction charges determined in sweep and other electrochemical experiments must be elucidated by complementary chemical experiments. In the next section some aspects of this approach will be discussed.

(c) Discussion of Fast Galvanostatic Discharge Results

The charges associated with reduction of oxygen-containing species at the electrode surface in KOH solution at various concentrations (2.0 M to 14.0 M) and temperatures (from -30°C to +90°C) were determined by fast galvanostatic reductions from controlled anodic potentials at 0.05 V intervals and the charge (Q) vs. potential (V) profiles were constructed (Fig. 39). The Q vs. V profile has a maximum at ca. 0.8 V or 0.9 V. Comparison with the steady-state log[i]-V plots (e.g. Fig. 40) shows that in the region where self-passivation occurs, the quantity of cathodically reducible oxide gradually decreases, and the chemically determinable (Fig. 53) amount of nickel oxidised also decreases.

Up to the potential at which the charge maximum occurs, the Q vs. V profile has the same shape as that observed in a V - t transient (Fig. 38 a) from a galvanostatic pulse,

as would be expected in the absence of an appreciable faradaic current for O_2 evolution.

The apparent decrease of charge with increase of potential (cf. Fig. 39) (beyond the maximum) may be due to the fact that (i) a self-discharge process occurs at high potentials simultaneously with the electrochemical reduction during determination of oxide charge in a galvanostatic cathodic pulse and/or (ii) metallic nickel is oxidised insufficiently rapidly during the fast charging producing only a relatively thin film of oxide (perhaps NiO_2*) having electronic conductivity comparable to that of the metal, i.e. a passive oxide film is formed directly. The self-discharge process may correspond to an electrochemical decomposition of "NiO_2" at the surface of the thin film oxide as discussed previously by Conway and Bourgault (4-6) or to chemical decomposition (cf. ref. 71) of "NiO_2" on account of its instability at the surface of the oxide film (see Fig. 63). Both processes will lead to a lower valent compound, viz. "Ni_2O_3" or $Ni(OH)_2$:

$$4\text{"}NiO_2\text{"} \longrightarrow 2\text{"}Ni_2O_3\text{"} + O_2 \qquad \text{I}$$

$$2\text{"}NiO_2\text{"} + 2H_2O \longrightarrow 2Ni(OH)_2 + O_2 \qquad \text{II}$$

---

*See footnote on p. 154.

In order to account for this loss of electrochemically active oxide material, experiments were performed in which the electrode was polarized potentiostatically to a certain potential for a definite period of time after the usual pre-conditioning programme (Fig. 14): the electrode was then kept on open-circuit for various known periods of time (τ_D), after the lapse of which a fast galvanostatic cathodic pulse was automatically applied (see Fig. 38 b). From the plot of charge remaining vs. τ_D (Fig. 42 a), it is observed that the extent of loss of charge due to a surface self-discharge process is ca. 20% or less. It is also found, as expected (4,5,6), that the extent of loss of cathodically reducible material is potential-dependent (Fig. 42 b). A similar effect arises in the cathodic transients themselves (Fig. 41); as cathodic c.d. is decreased, the cathodic reduction charge Q decreases presumably for the same reason, since the transition time is longer. This latter observation also supports the view that the galvanostatically determined charge does not include the charge contribution due to reduction of molecular oxygen dissolved in the solution: since this process is a diffusion-controlled one, more charge rather than less would have been measured in a slow galvanostatic transient than in a fast one.

However, since the loss of charge arising in the self-discharge process is only 20%, it cannot alone account for the appearance of a maximum in the Q vs. V profile (Fig. 39). Therefore a relatively smaller quantity of metallic nickel must have been oxidised during the fast galvanostatic charging process. This seems quite probable because in the pre-treatment programme (Fig.14) the electrode was usually polarised immediately to the experimental potential in a single rectangular step and then kept at this potential for 2 mins. before the galvanostatic discharging pulse was applied. Under these conditions, at potentials beyond ca. 0.8 V or 0.9 V, the electrode metal becomes rapidly oxidised (cf. p. 192) to such an oxidation state that the surface oxide acquires good electronic conductivity and hence passivation of the metal oxidation process (cf. ref. 54) sets in. Consequently, smaller quantities of charge are required to form and hence reduce the film at potentials exceeding ca. 0.8 V so that a maximum in the Q vs. V profile results. These conclusions are consistent with the analytical results (Fig. 53) in which a maximum in the plot of the amount of nickel oxidised vs. potential is also observed at the same potential as the maximum in the charge for oxide reduction.

From this information, it can be deduced that the higher oxidation states of nickel, viz. Ni(III)O.OH and

$Ni(IV)O_2$ predominate in this potential range giving the oxide film at the surface good electrical conductivity (one of the conditions for passivity). Both these oxides are n-type semi-conductors and have high density of conduction electrons (cf. refs. 56,53). This view is again consistent with the experimentally determined stoichiometries of the thin film oxide material: the mean oxidation state of nickel in the oxide film exceeds + 3 at potentials higher than 0.8 or 0.9 V. (Table XI and Fig. 63, section 5). This matter will be discussed in more detail in section 5. The fact that the exact potential at which the maximum in a Q vs. V profile occurs depends on the experimental temperature also supports the above proposals.

From Figs. 29 and 39, or 56, it is seen that when the electrode is oxidized in a potentiostatic step, much less oxidation charge is taken up. This apparent difference may be explained by the fact that in step charging, owing to the progressive application of higher potential differences to the electrode (in addition to any previously existing potential difference) the passive oxide layer already formed at the electrode surface cannot grow appreciably during the short duration of the pulse, whereas in the fast galvanostatic reduction pulse method, the electrode has been initially polarized potentiostatically at a potential for 2 mins.

during which period, under the influence of high field, the prepassive oxide ($Ni(OH)_2$) layer which has been formed initially by metal oxidation grows and hence takes further charge for oxidation to a greater thickness and/or higher state of oxidation.

(d) Form of Oxidation Charge-Potential Relation: Logarithmic Behaviour with respect to Charge

From the determination of Q as f(V), it was considered of interest in relation to the kinetics (section 2) to investigate if any logarithmic region of the oxidation isotherm existed. The resulting plots are shown in Fig. 56. The Q values were determined independently by galvanostatic reduction and potential-step oxidation. At various temperatures and KOH concentrations, there is evidently quite generally a logarithmic relation ($Q \sim f(\exp[kVF/RT])$ as proposed in section 2 of this Chapter. However, the slopes (dV/dlog Q) are in the range 0.220 - 0.250 V, i.e. ca. $2.3(4RT/F)$. Within experimental uncertainty, dV/dlog Q for the fresh electrode, surprisingly enough, has the same value up to the monolayer region as for multilayer formation at preconditioned electrodes, although there is some indication of two populations of points in the galvanostatic reduction data for the preconditioned electrodes (Figs. 56). The continuity of the log plots and the similarity of their slopes for fresh and

preconditioned surfaces suggests that the oxide may be laid down in patches or domains (cf. the circular and hemispherical growth behaviour which has been considered previously (184,185)) prior to attainment of nominal geometrical "full coverage". At higher potentials and/or for Q > ca. 20 mc. cm^{-2}, a limiting degree of oxidation is reached as discussed earlier. This limit of Q at the end of the log region is, however, much greater than the charge for a monolayer even allowing for uncertainities of real area and valence state of Ni in the oxide film.

The observed slopes* dV/dlog Q cannot be combined (4-6) with any normal activation energy factor $\beta VF/RT$ in a kinetic equation to give the Tafel slopes found in section 2, so it must be presumed that any variation of surface concentration of electrochemically active sites (e.g. M/O, M/OH; see p. 149) with potential is not the same as the overall variation of log Q with potential. This supports the view taken above that chemical species written in kinetic equations for oxygen evolution on oxide surfaces should refer to local sites on the oxide rather than to individual M/O or M/OH species when the oxide is more than a monolayer in thickness.

---

*However, these slopes arise predominantly in the region of metal oxidation and hence below the region of oxygen evolution but, of course, eventually correspond to extension into this latter region.

5. STOICHIOMETRY OF THIN FILM NICKEL OXIDE LAYERS

The analytical results which characterise the stoichiometry (i.e. active oxygen to nickel ratio) of the thin surface oxide films have been described in Chapter III and shown in Fig. 53 for various potentials. These results were based on combined chemical and electrochemical procedures. A maximum in the extent of charge for surface oxide reduction and two maxima in the plots for the nickel content in the chemically stripped film were observed (Fig. 53). In the low potential region, the oxide film consists mainly of $Ni(II)(OH)_2$ and hence the electrochemically determinable charge is small (Fig. 53).

In order to determine the stoichiometries of the oxides in the charged state of the electrode, the results are expressed in g. atom units and the observed stoichiometries are calculated on the basis (see section 3 (f), Chapter III) that higher oxides of nickel are reduced only to Ni(II)-oxide. Corrections for the losses of reducible oxide charge due to self-discharge process on open-circuit were also made for several electrode potentials (Chapter III, p. 123). The results are shown in Table XI for various potentials. A plot of the dependence of the ratio of active oxygen to nickel vs. electrode potential, which reflects the stoichiometry of the nickel oxide in the thin film oxide layers as a function

Table XI

Apparent Stoichiometries and Stoichiometries Corrected for Self-discharge in Thin Film Nickel Oxide

Time of polarization t (min.).	Potential V_E vs Hg/HgO (V) in 2M KOH at 25°C	Amount of nickel in the oxide film(μg.atom cm^{-2})	Amount of electrochemically reducible oxide (μg.atom "O" cm^{-2})	Stoichiometry of nickel oxide in the film	Corrected* electrochemically reducible oxide (μg.atom "O" cm-2)	Corrected stoichiometry of nickel oxide in the film
2	0.05	0.165	0.0003	$NiO_{1.002}$		
2	0.20	0.546	0.0012	$NiO_{1.002}$		
2	0.20	0.441	0.001	$NiO_{1.002}$		
2	0.30	0.162	0.002	$NiO_{1.012}$		
2	0.40	0.203	0.009	$NiO_{1.044}$		
2	0.50	0.245	0.041	$NiO_{1.17}$	0.044	$NiO_{1.18}$
2	0.60	0.299	0.090	$NiO_{1.30}$		
2	0.70	0.332	0.126	$NiO_{1.38}$	0.133	$NiO_{1.40}$
2	0.80	0.324	0.136	$NiO_{1.42}$		
2	0.90	0.372	0.186	$NiO_{1.50}$	0.224	$NiO_{1.61}$
2	0.90	0.406	0.187	$NiO_{1.46}$	0.225	$NiO_{1.55}$
2	0.95	0.338	0.159	$NiO_{1.47}$		
2	1.0	0.207	0.101	$NiO_{1.49}$	0.119	$NiO_{1.58}$
5	1.0	0.111	0.075	$NiO_{1.68}$	0.088	$NiO_{1.79}$

* Corrected for self-discharge during the time τ_G.

Figure 63. Active O:Ni ratio, based on the data in Table XI, as a function of potential, V.

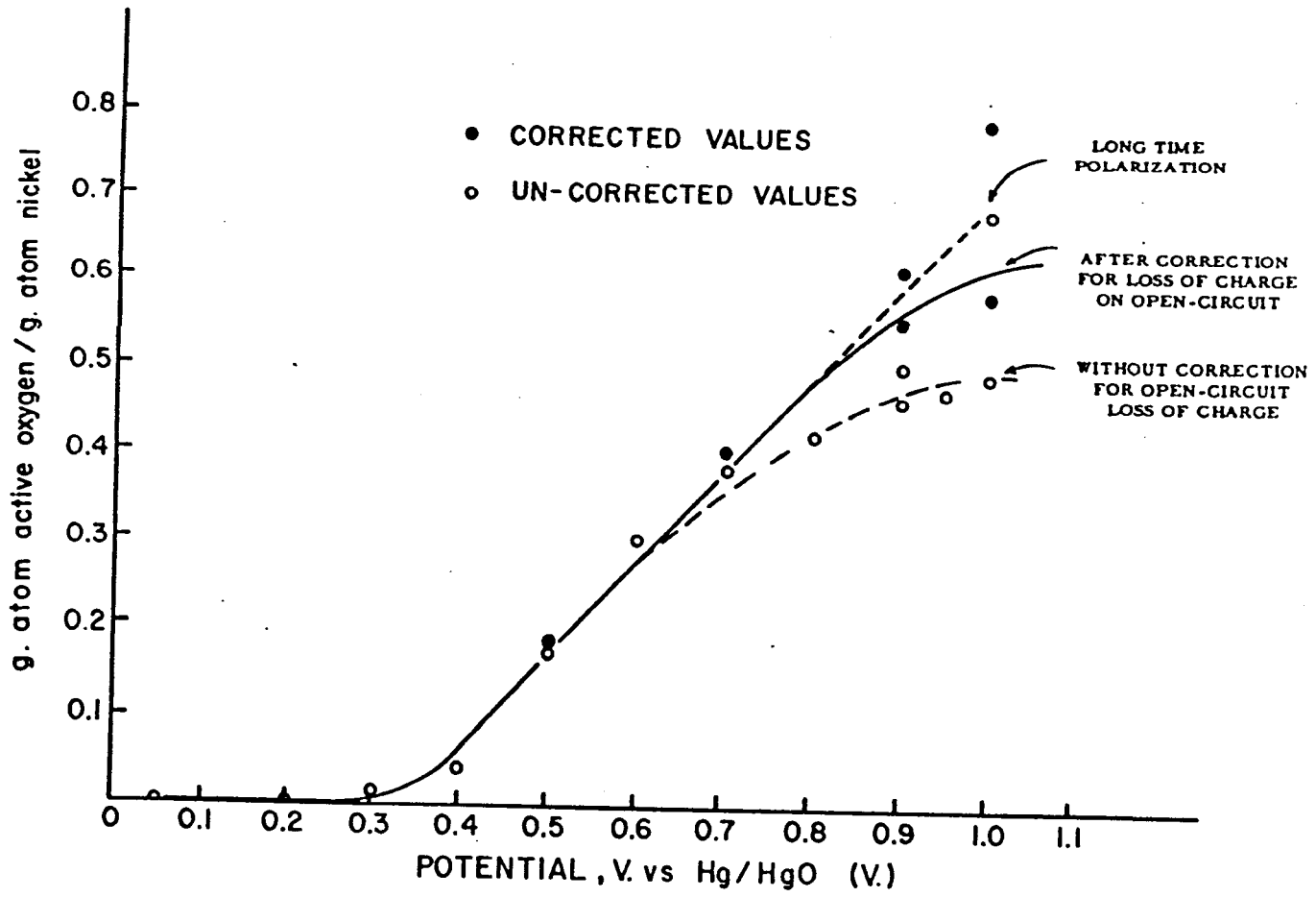
g. atom active oxygen / g. atom nickel
0.8
0.7
0.6
0.5
0.4
0.3
0.2
0.1
0
0.1
0.2
0.3
0.4
0.5
0.6
0.7
0.8
0.9
1.0
1.1
POTENTIAL, V. vs Hg/HgO (V.)
CORRECTED VALUES
UN-CORRECTED VALUES
LONG TIME POLARIZATION
AFTER CORRECTION FOR LOSS OF CHARGE ON OPEN-CIRCUIT
WITHOUT CORRECTION FOR OPEN-CIRCUIT LOSS OF CHARGE

of electrode potential, was also constructed (Fig. 63).

Although maxima are observed both in the active oxygen and the Ni content of the thin films (Fig. 53), the [O]:Ni ratio plotted in Fig. 63 is a continuously increasing function of potential so that the maxima in Fig. 53 simply reflect a smaller film thickness (see below) at higher potentials ("tight", thin and probably more passive films). From Fig. 63 it is also evident that during the self-discharge process, nickel oxide in which the oxidation state of nickel exceeds +3 undergoes decomposition.

The highest formal oxidation state of nickel observed in the present work is in fair agreement with that found by Conway and Bourgault (4), Wynne-Jones et al. (29) and Aia (32) using thicker (or bulk) oxide material, but these degrees of oxidation are only attained at quite high potentials of ca. 1.0 V, with thin films.

In the present experiments, the electrode was polarized potentiostatically for periods of only 2 min. in which time only a fraction of the lower valent oxide present may have been converted to the higher valent state; hence [O]:Ni ratios are observed which are lower than those found by other workers at corresponding potentials. In one set of experiments chemical and electrochemical determinations of stoichiometries of the oxides formed anodically for controlled times at

constant potential (0.3 V), showed that the degree of oxidation (active "O" to Ni ratio) increases with time (see Section 3(g) of Chapter III and Fig. 54); this result presumably requires that at any time the oxide species at the electrode surface is not homogeneous with respect to valency state of nickel ions. Thus, it seems likely that a gradient of decreasing state of oxidation of nickel from the electrolyte/oxide interface [Ni(IV)] to the oxide/metal interface [Ni(II)] would be involved (see also section 8 of this Chapter and ref. 56).

6. EXTENT OF FORMATION OF SURFACE OXIDE OF NICKEL

Both from the electrochemical charging and the chemical stripping experiments, the approximate film thicknesses attained in these experiments have been estimated. The thickness developed depends, of course, on prior anodic polarisation time (or on the sweep rate and potential range in potentiodynamic experiments) which must be controlled in longer period experiments.

The average charge for a z-electron oxidation of nickel (face-centred cubic structure with 3.499 $\mathring{A}$ lattice length (197)) to form a surface monolayer is 260z $\mu c.\ cm^{-2}$, so that the number of layers, n, of the surface oxide formed (or reduced) at a given potential at 30°C is given by Q/260zR where Q is the charge in $\mu c.\ cm^{-2}$ for electrochemical reduction

of the film and R is the initial real to apparent area factor. With R=2 and z=1 [for Ni(III) $\longrightarrow$ Ni(II) in the discharging process] for an observed value of $Q \doteqdot 36000\ \mu c.\ cm^{-2}$ at 0.9 V, n will be of the order of 69 layers.

The amount of nickel present in the oxide film at 0.9 V determined by chemical stripping was $\sim 23\ \mu gm.\ cm^{-2}$; this quantity corresponds to a thickness of 145 layers of oxide if R=1 and 72.5 layers if R=2.

At 0.2 V, the amount of nickel determined in the oxide film was ca. $29\ \mu gm.\ cm^{-2}$: the equivalent thickness of the oxide is 183 layers when R=1 or 91.5 layers if R=2. This would closely correspond to the pre-passive film of the type indicated by ellipsometry (54).

The thicknesses determined by the analytical method are somewhat greater than the figure obtained by Weininger and Breiter (25,26) in potentiodynamic sweep experiments but nearer to that obtained by Bockris et al. (54) using ellipsometry in acid solution and much smaller than that obtained by Wynne-Jones et al. (29) in some experiments. In the work on passivation in acid solutions lower anodic potentials were, however, involved so that comparisons are difficult to make quantitatively. In some of the experiments of Wynne-Jones, specially thick oxide films were deposited by hypochlorite etching.

Figure 64. Increase of oxide charge for nickel oxide electrodes (determined by galvanostatic reduction) with the logarithm of time at various indicated potentials in aq. KOH solutions of various concentrations and at temperatures (based on the data in Fig. 43): (a) 2.0 M KOH, 30°C; (b) 2.0 M KOH, 60°C; (c) 13.1 M KOH, 30°C and 60°C.

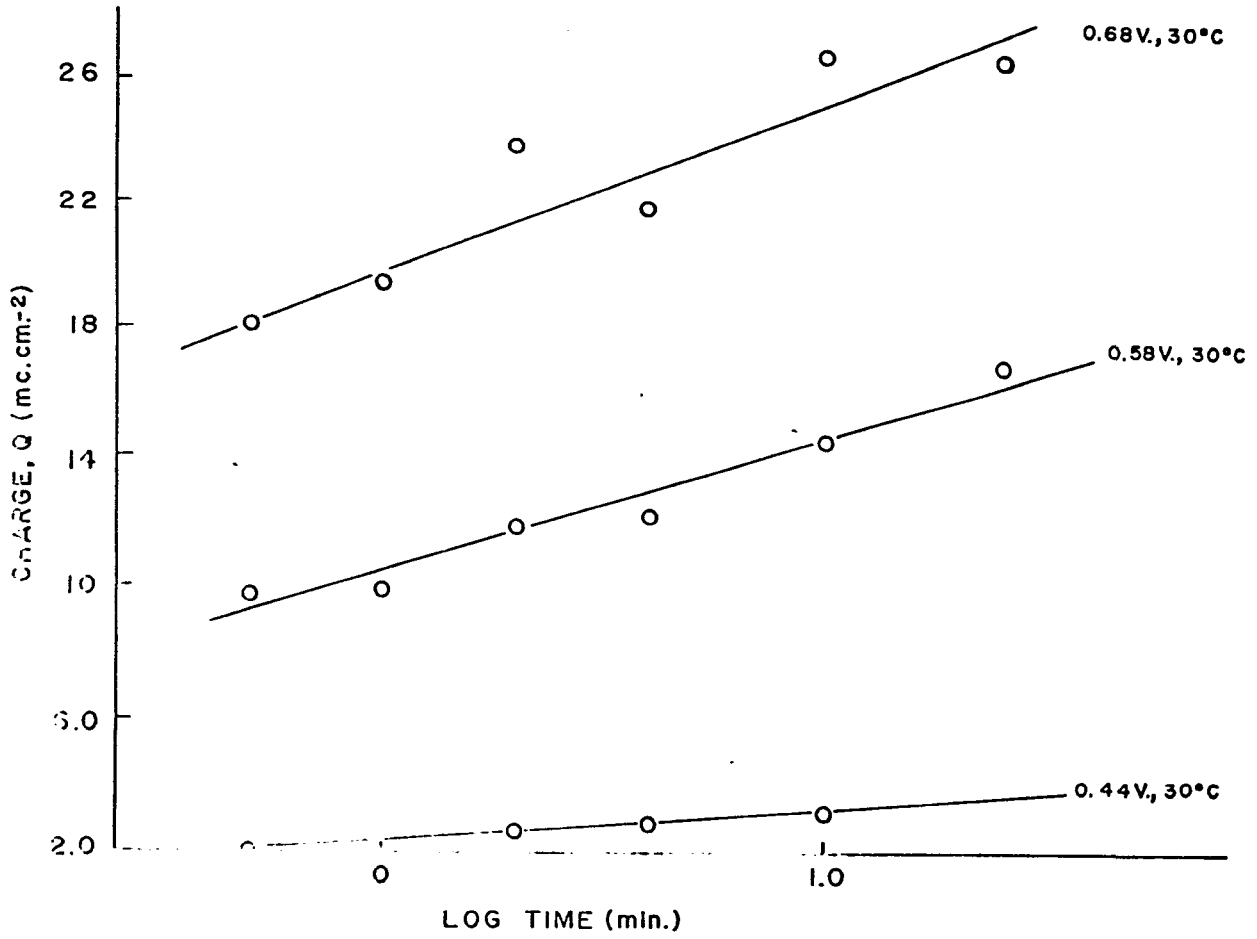
0.68V., 30°C
0.58V., 30°C
0.44V., 30°C
26
22
18
14
10
6.0
2.0
CHARGE, Q (mc.cm.-2)
0
1.0
LOG TIME (min.)

(a)

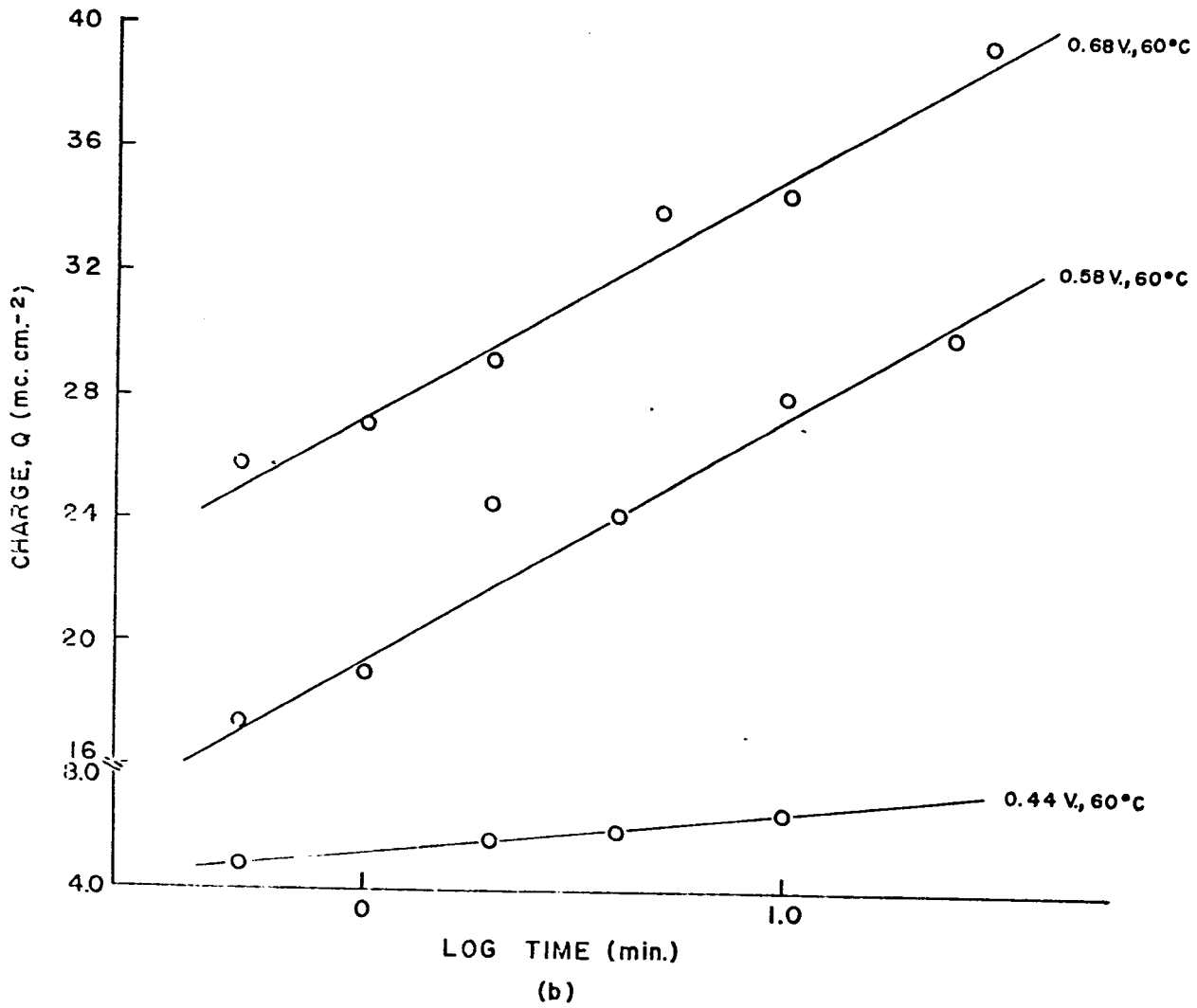
40
36
32
28
24
20
16
3.0
4.0
CHARGE, Q (mc. cm.-2)
0.68 V., 60°C
0.58 V., 60°C
0.44 V., 60°C
0
1.0
LOG TIME (min.)

(b)

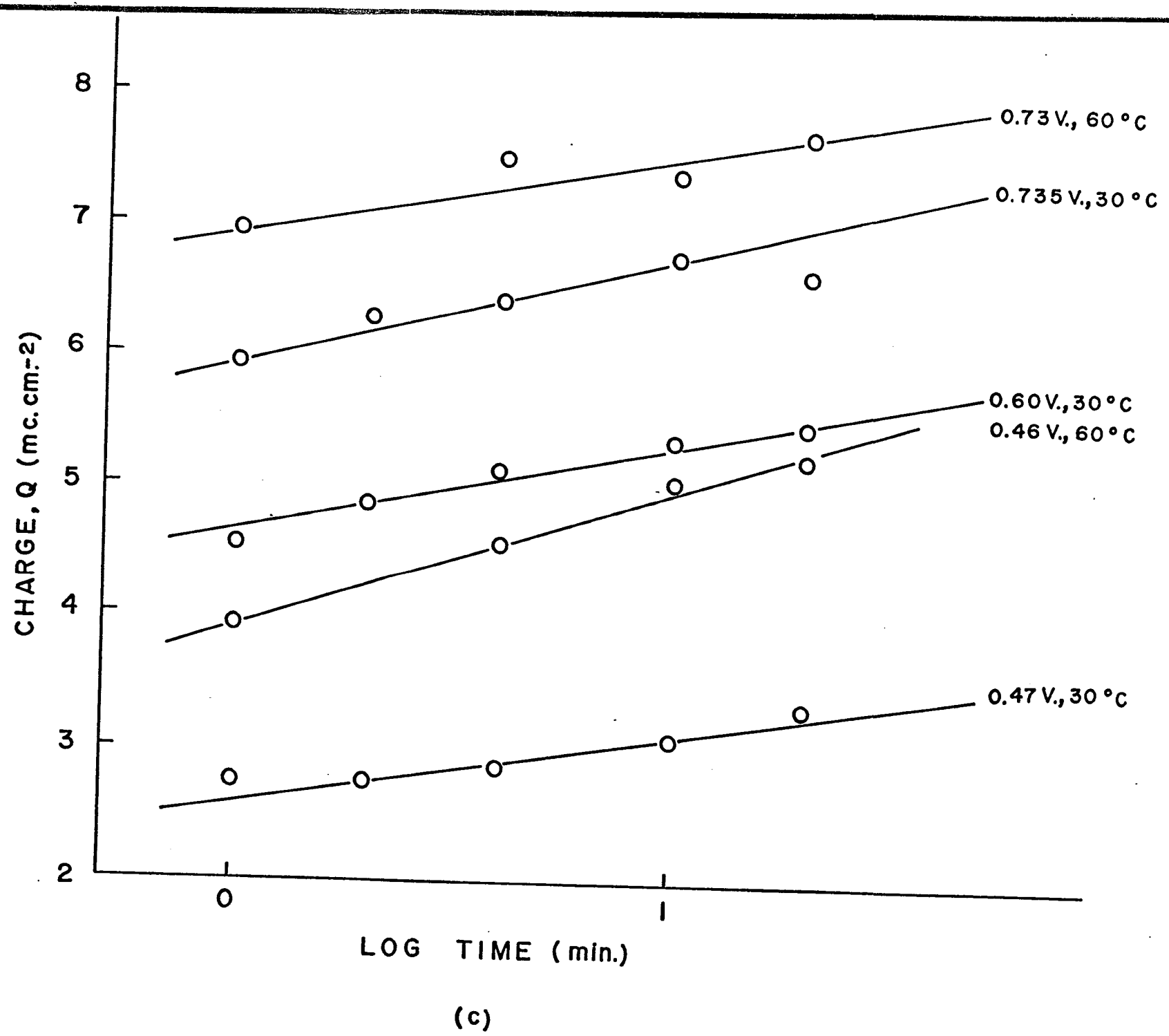
8
7
6
5
4
3
2
CHARGE, Q (mc.cm.-2)
0.73 V., 60 °C
0.735 V., 30 °C
0.60 V., 30 °C
0.46 V., 60 °C
0.47 V., 30 °C
0
1
LOG TIME (min.)

(c)

Figure 65. Increase of oxide charge for nickel oxide electrodes as a logarithmic function of charge (based on the data in Fig. 43): 2M KOH, 30°C.

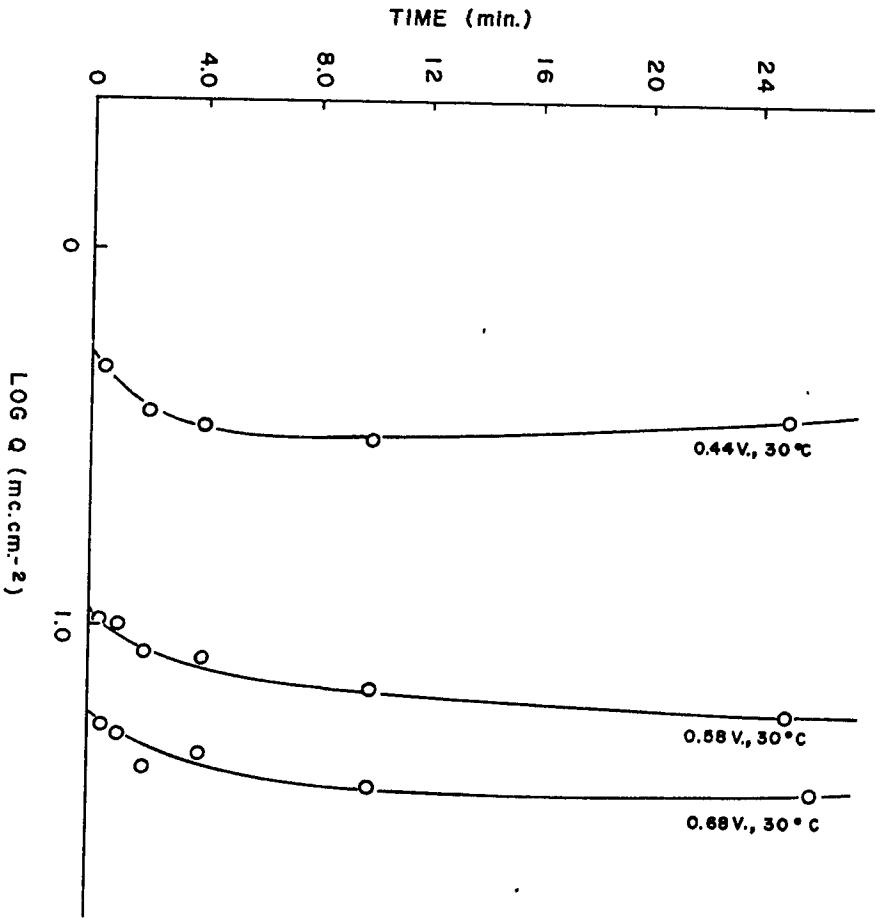
TIME (min.)
0
4.0
8.0
12
16
20
24
0
1.0
LOG Q (mc.cm.⁻²)
0.44V., 30°C
0.58V., 30°C
0.68V., 30°C

7. KINETICS OF GROWTH OF NICKEL OXIDE AT THE NICKEL METAL ELECTRODE SURFACE

The extent of "growth" of oxide at the nickel oxide electrode surface, in terms of the charge Q required for its electrochemical reduction was determined at 30°C and 60°C in aq. KOH (2.05 M and 13.1 M concentrations) by successive galvanostatic transients, each at the same c.d. The oxide films were grown potentiostatically at selected potentials for various period of time (Figs. 43). Linear relations are obtained when these results are plotted with respect to the logarithm of the time (Figs. 64). This type of growth behaviour is similar to that found by Makrides (182) at gold and Sato et al. (183) at iron electrode surfaces. In the present work, other relations (e.g. log Q vs t) were tested but did not give linear plots (Fig. 65). As in Makrides' work, a kinetic account of this behaviour cannot be given in terms of previous well known theories of oxide growth and the same difficulties arise here as in that work in regard to a mechanistic explanation of the observed growth kinetics. However, the following new theory* may tentatively be offered

---

* A similar theory leading to a direct log t dependence was independently given by Sato et al. (183) and published in June 1967. The present theory was submitted as a full paper in March 1967 to the Advisory Group for Aerospace Research and Development and presented at its meeting in Liège, June 1967. It appears in the published Proceedings of that meeting (87).

which leads to a kinetic growth law directly in log t for films significantly thicker than a monolayer.

It is supposed that (a) a potentiostatically controlled constant potential difference V is available at the nickel-solution interface and leads to anodic oxidation at a rate i a. cm^{-2} which is a function of time t; and also (b) that at $t > 0$, an oxide film is formed to a thickness δ corresponding to a formation charge q. It will now be of interest to investigate the consequences of supposing that the formation of the layer to a thickness δ in time t is associated with the development of a small p.d. ΔV across the film layer (cf. ref. 186) in proportion to its thickness as measured by q in a reduction transient (see equation 2 below). This p.d. can arise on account of a gradient of extent of oxidation (Ni^{2+}/Ni^{3+}) in the oxide layer. At the nickel oxide layer on nickel electrodes, ΔV is unlikely to be more than a moderately small fraction of V since the oxide film is a fairly good conductor (cf. the discussion of Ammar and Darwish (186) on passive films at Ni, and the ellipsometric evidence (54)). The p.d. will, for example, presumably be much less than that involved in oxide growth at Al, Zr, U or Ta studied in various papers by Vermilyea, by Young and by Leach et al. (103).

On this basis, the anodic current density for film growth could be written in the form

$$i = k \exp (V - \Delta V)/b \qquad (1)$$

where k is a rate constant and b is the slope of the current-potential relation for oxide growth. On the above model,

$$\Delta V = a \int i \, dt \qquad (2)$$

where a is another constant related to the ohmic resistance of the film (assumed electrically homogeneous over most of its thickness). From (1) and (2),

$$\frac{d \ln i}{dt} = - \frac{a}{b} i \qquad (3)$$

which upon integration, noting that $d \ln i = \frac{1}{i} di$, gives

$$1/i = \frac{a}{b} t - A \qquad (4)$$

where A is an integration constant equal to $- 1/i_o$, the reciprocal of the initial oxidation current at $t = 0$ that would pass if there were no change of mechanism as $t \rightarrow 0$ and $q \rightarrow 0$. The latter assumption is probably not justifiable for development of the subsequent layers in relation to the development of the first (and second?) layer, but this will not affect the form of the resulting growth law (see below) for

most of the time of development of the film where $\delta \gg$ monolayer.

Now for the charge q associated with the formation of the film during time t of anodisation, equations (1) and (2) also give

$$\ln i = \ln k + \frac{V}{b} - \frac{a}{b}(q) \qquad (5)$$

since $q = \int_o^t i\, dt$. At constant V, $\ln k + \frac{V}{b}$ is a constant equal to $\ln i_o$ when $t = o$ and $i = i_o$. Rearrangement of equation (4) (after replacing A by $-\frac{1}{i_o}$) to

$$i = \frac{b}{a} \frac{1}{t + \frac{b}{ai_o}} \qquad (6)$$

together with substitution for i as a f(t) from equation (6), gives from equation (5) upon elementary rearrangement

$$\frac{a}{b}(q) = \ln [i_o a/b] + \ln[t + b/ai_o] \qquad (7)$$

which is the required growth rate law for q as f(t); it will be seen that equation (7) is consistent with initial conditions since $q = 0$ when $t = 0$. Equation (7) gives a <u>direct log</u> law in the quantity <u>time</u> modified by addition of a constant term b/ai_o which becomes a relation in time alone for longer periods of anodisation. The observed kinetic growth behaviour can thus be accounted for. The derived relation (7) will

not be expected, as mentioned earlier, to apply to the first one or two layers of oxide since different electrochemical processes and local potential differences may then be operative. Moreover, complications due to simultaneous growth of the oxide layer thickness and changes of valency in the existing oxide material can arise at a constant potential and these effects may cause the Q vs. log(t) plot to deviate from a simple linear relation such as that deduced above.

8. HYSTERESIS IN ANODIC OXIDE FORMATION AND REDUCTION: ORIGIN OF THE EFFECTS

A characteristic of the formation and reduction of thin film oxide layers on electrodes is the hysteresis between the formation and reduction processes, which may be characterised in suitable cases by the difference between the potentials for the current maxima in linear potentiodynamic charging and discharging, or the difference in the inflection potentials of transients taken under anodic and cathodic galvanostatic conditions. Hysteresis between the oxide formation and reduction processes has been observed (section 2(b) of Chapter III) to occur at Ni and Ag electrodes and also at Pt (171) and Pd (153) electrodes. It therefore appears that the hysteresis is an intrinsic "thermodynamic" effect of the kind discussed by Everett (167-170) in adsorption and

sorption processes involving the formation of metastable surface domains and is not a kinetic polarisation effect, although the latter effects may tend to enhance the apparent hysteresis. The magnitudes of the hysteresis can be expressed in terms of the difference, ΔV_{peak}, in charging and discharging peak potentials and have been summarised in Table VII (Chapter III). They correspond to free energy differences of ca. 2 to 7 kcal. per Faraday in the oxidation or reduction processes. This free energy loss for the hysteresis loop is likely to be due to change (production) of entropy ($T\Delta S>0$) arising from the recrystallization and re-orientation of the oxides.

As mentioned in Chapter I, the views of Foerster (12-14), Glemser and Einerhand (47) and of Wynne-Jones et al. (29) are not quite adequate for explaining the phenomenon of hysteresis at the nickel oxide electrodes. Labat (30) showed that in the electrochemical oxidation of $Ni(OH)_2$ both the NiO.OH and NiO_2 were formed simultaneously.

Both silver and nickel oxides are semiconductors and their electronic conductivities can hence be increased by raising the experimental temperature, by irradiation or by doping with lithium ions. Therefore, by one or more of these processes, the internal resistance (iR) arising within the oxide film (cf. ref. 29) which could contribute to the apparent

hysteresis can be reduced. However, it is observed that by increasing the operating temperature of the silver oxide electrode (Fig. 45), by irradiating it (187) or by doping the nickel oxide electrode with Li^+ (188), hysteresis between the charging and discharging peak potentials is reduced only slightly (see Table VII). Therefore it seems again that the hysteresis is an intrinsic thermodynamic effect and not one due to internal resistance effects alone.

In the case of silver, it is of interest to note that the anodic peak (I) is appreciably photosensitive (187) and the charge associated with its formation can be increased by ca. 25% under u.v. irradiation; the potential of its formation and reduction is, however, very little affected by illumination.

The origin of the hysteresis may therefore be considered to be connected with a rearrangement of recrystallisation of the immediately electrodeposited species, produced in the anodic charging process, into a more stable form reducible only over a range of lower cathodic potentials. The effect is evidently quite general. The recrystallisation or rearrangement may be analogous to the kind considered by Rhead (189) in regard to oxide film formation on metals at the gas-solid interface (cf. 190) where surface diffusion processes are involved leading to the build up of consolidated centres of oxide. The hysteresis is evidently not connected only

with the build-up of the first layer of oxide (as, for example, in the case of Pt*) since (a) at Ni and Ag quite thick layers are involved and most of the charge passed must go to form layers beyond the first monolayer and (b), of greater cogence, similar hysteresis occurs with respect to the formation and reduction of the second (peaks $II_{an.}$ and $II_{cath.}$) oxide at silver, i.e. with regard to the further oxidation of an already existing surface oxide (peak $I_{an.}$) and the corresponding reduction (peak $II_{cath.}$) back to the lower surface oxide. Here the hysteresis is no less than that for the first peak ($I_{an.}/I_{cath.}$) where formation of the oxide from, or reduction of the oxide to, the basis metal is involved.

In the more familiar case of adsorption and desorption, hysteresis can arise (167-170)** when the adsorbate is laid down in a metastable state or in metastable domains (167,169) and undergoes some thermodynamically irreversible (in this case "2-dimensional") phase change (190) to a condition of lower free energy. In such a case, desorption then proceeds at lower chemical potentials of adsorbate in the bulk phase

---

* At Pt, the hysteresis may be due to a transition between a Pt-OH or Pt-O dipole ad-layer and a two dimensional Pt-O-Pt-O.... layer having a lower standard free energy (63).

**Another more trivial cause of hysteresis in adsorption and desorption arises for kinetic reasons when the adsorption is exothermic so that the activation energy for the desorption process is usually greater than that for the adsorption process.

(with which the surface is in "equilibrium") than those chemical potentials required to reach the same respective degrees of accommodation in the adscrption process. Similarly, in the present electrochemical case, the electrochemical "desorption" (reduction) of the oxide proceeds at lower electrochemical potentials than those required for formation of the oxide. In the case of sorption, this kind of intrinsic hysteresis can arise when attractive potentials characterise the intermolecular forces in the absorbate layer at the surface (63).

Most systems exhibiting hysteresis involve, it has been suggested, a distribution of states of varying effective metastability so that the greater the breadth of variation of the intensive variable (temperature, magnetic field, or electric potential in the present case) the larger is the hysteresis loop. Within this "loop", smaller scans of the intensive variable lead to correspondingly smaller hysteresis loops (the so-called scanning curves (167)). With the anodisation of Ni, Ag, Pt or Pd, a very similar situation exists as shown in Fig. 48. If oxide formation and reduction scans are made over small potential ranges, the hysteresis between the potentiodynamic charging and discharging peaks is small; if larger potential ranges are involved in the formation of the oxide, correspondingly larger ranges are

Figure 66. (a) Schematic potentiodynamic scanning curves for an oxidation and reduction process exhibiting hysteresis; (b) corresponding integral charging and discharging curves showing hysteresis loops; (c) hysteresis loops in charging and discharging bulk nickel oxide electrodes (ref. 7: B.E. Conway and E. Gileadi).

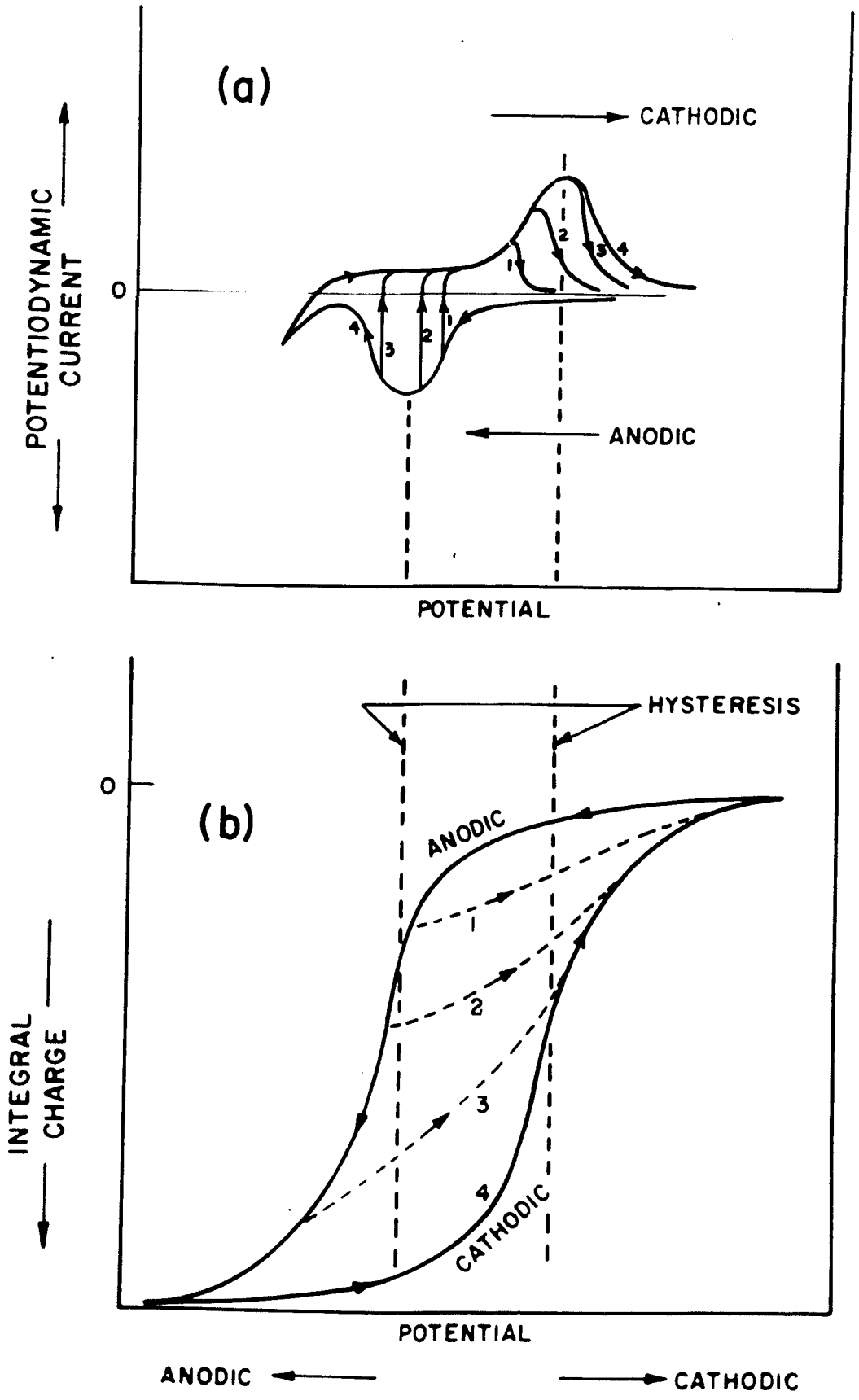
(a)
CATHODIC
POTENTIODYNAMIC CURRENT
0
1
2
3
4
ANODIC
POTENTIAL
(b)
HYSTERESIS
0
ANODIC
1
2
3
4
CATHODIC
INTEGRAL CHARGE
POTENTIAL
ANODIC
CATHODIC

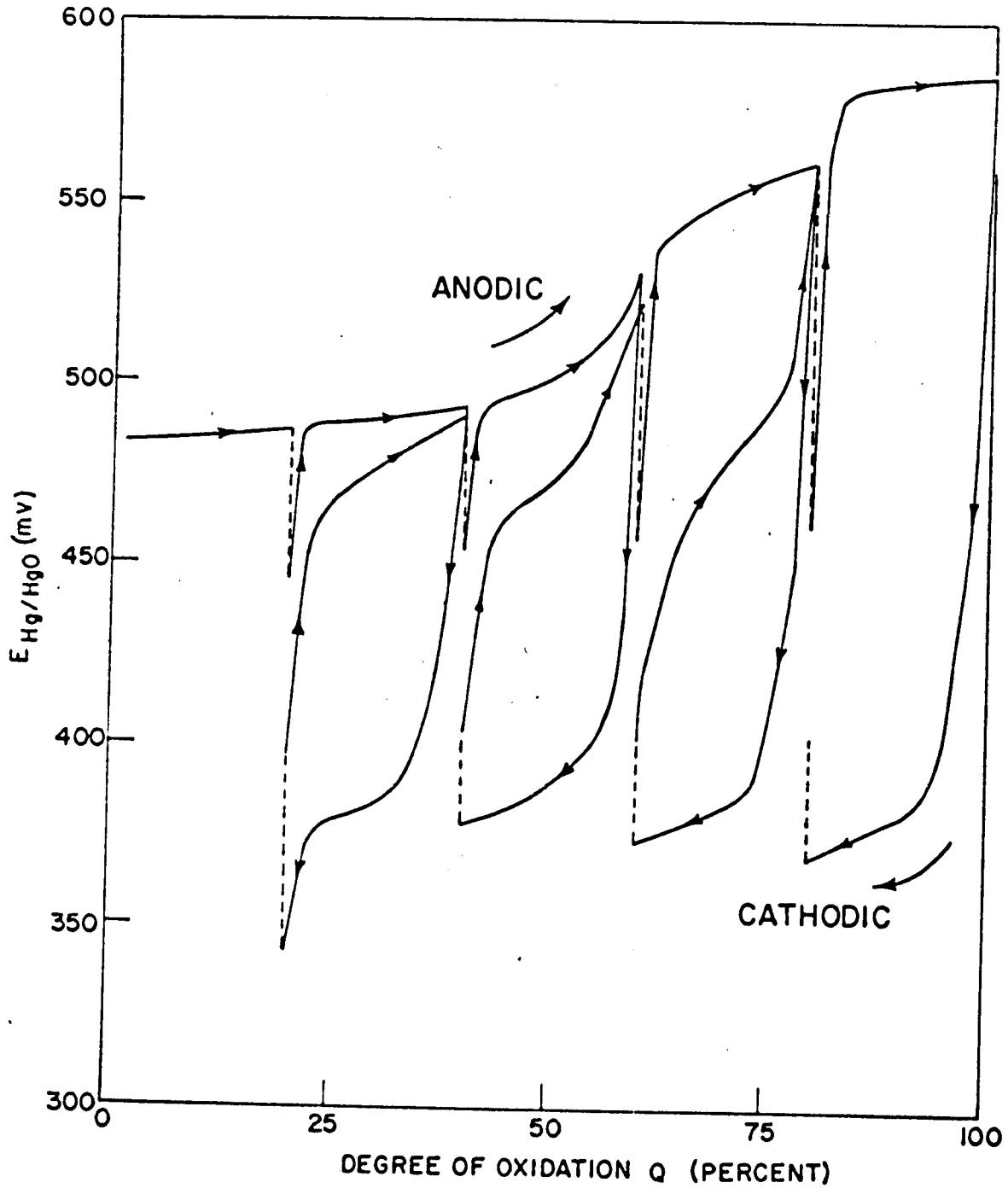
600
550
500
450
400
350
300
$E_{Hg/HgO}$ (mV)
ANODIC
CATHODIC
0
25
50
75
100
DEGREE OF OXIDATION Q (PERCENT)

(c)

required for reduction: thus, that fraction of the surface oxide which requires the highest anodic potentials for its formation, requires, when formed, descent to the lowest cathodic potentials for its reduction. The relation to more familiar hysteresis scanning curves (e.g. in magnetisation) is shown in Fig. 66 where the situation for the charging and discharging curves is shown (cf. electrochemical adsorption isotherms) schematically for different degrees of charging. In the present cases, the following mechanism for the origin of these effects may be suggested.

With thicker film and bulk material, a different type of effect may be involved and give rise to hysteresis. Thus, in earlier work with bulk nickel oxide impregnated plaques, some evidence has been given (e.g. 4,6) for a charge and self-discharge process involving a surface region of the oxide having formally a higher state of oxidation than that in the bulk. The charging process, and in the present case, the oxide growth, is regarded as proceeding by a solid state diffusion process (e.g. 16,19) involving effective migration of Ni^{2+} and Ni^{3+} ions (by electron transfer) coupled with proton diffusion experimentally indicated by Lukovtsev and Slaidin (16). Thus, at all times in the anodic oxidation process, it may be suggested that a potential is required which is sufficiently positive to generate a higher valent surface layer (Ni^{4+}) on the oxide film which then enables, by a solid state diffusion process, the remainder of the sub-surface

oxide to be grown and/or charged to a progressively higher average degree of oxidation. The supposed requirement of a surface layer having a certain minimum higher-than-average degree of oxidation is analogous to the usual requirement of supersaturation (a metastable condition) for chemical or electrochemical crystal growth*. Once the oxide has been formed, and reduction commences in a following cathodic transient, the requirement for a more highly oxidized surface layer on the oxide is presumably no longer necessary (and in fact the reverse condition may be required) and the bulk material can then be reduced over its normal (or a lower) potential range which will tend to be lower** than that required for formation of the oxide layer through the development of the "superoxidised" surface layer. An intrinsic hysteresis will then result.

---

* The situation is also similar to that involved in the magnetically biassed, bi-metallic switch model discussed by Everett (167,169).

**Higher anodic potentials are usually required to form thicker layers (greater Q) which then require lower cathodic potentials for complete reduction. This, it may be suggested, is the result of the necessity for establishment of a minumum gradient of degree of oxidation (186) or of degree of reduction across the oxide layer to enable the charging or the discharging process, respectively, to take place at finite rates.

9. ELECTROCHEMISTRY OF THE SILVER OXIDE ELECTRODE

(a) Charge-Discharge Mechanism

The electrochemical work on the silver oxide electrode was initiated mainly for the purpose of comparing the behaviour of the nickel oxide electrode with that of silver where at least two distinguishable surface oxidation states can be observed. The results have been given in Chapter III. In this section, only a brief preliminary discussion of the present findings will be presented. A complete discussion must await results from other investigations in progress in this laboratory, e.g. in regard to the behaviour of the silver electrode under u.v. irradiation and the determination of stoichiometry and impedance of the silver oxide in the thin films.

As mentioned in Chapter I (section 4), there is disagreement in the literature concerning the reactions which take place on silver anodes. Partly in order to clarify this mechanism of oxidation of silver but mainly for the comparative purposes mentioned above, potentiostatic and potentiodynamic linear sweep studies were carried out. From the steady state log[i]-V plots (Fig. 27) it is seen that self-passivation (cf. the effects at Ni) occurs at a potential of ca. 0.20 V to 0.30 V and a second, smaller effect, arises at 0.46 V. In the potentiodynamic i-V

profiles, three oxide formation peaks (one of them is small and ill-defined) and two corresponding oxide reduction peaks are observed. In the low temperature work (-30°C), a third oxide reduction peak (which may correspond to the reduction of Ag_2O_3) has been observed (Fig. 36d).

From thermodynamic data, the standard electrode potentials for the following reactions have been given (178, cf. also ref. 191) as follows:

$Ag_2O + H_2O + 2e = 2\,Ag + 2OH^-$ $\quad E^\circ = 0.345$ V vs. NHE I

$2\,AgO + H_2O + 2e = Ag_2O + 2OH^-$ $\quad E^\circ = 0.607$ V vs. NHE II

$Ag_2O_3 + H_2O + 2e = 2\,AgO + 2OH^-$ $\quad E^\circ = 0.739$ V vs. NHE III

The experimental values of E° for reaction (I) are 0.338 $\pm$ 0.001 V vs. NHE at 25°C determined by Dirkse (192) and 0.342 V vs. NHE by Hammer and Craig (128); that for reaction (II) is 0.599 $\pm$ 0.001 V vs NHE at 25°C determined by Dirkse (193) and 0.604 V vs. NHE by Bonk et al. (194).

Thus, using these thermodynamic electrode potentials and comparing them with the characteristics of the current-potential relations, the following oxidation and O_2 evolution mechanisms may tentatively be proposed:

$2\,Ag + 2OH^- = Ag_2O + H_2O + 2e$ I

$Ag_2O + 2OH^- = 2\,AgO + H_2O + 2e$ II

$2\,AgO + 2OH^- = Ag_2O_3 + H_2O + 2e$ III

$2\,Ag_2O_3 = 4\,AgO + O_2\,(g)$ IV

However, it may be supposed on the basis of the potentiodynamic i-V relations that Ag_2O can be derived from Ag-OH. Thus, the first small and ill-defined peak (I') which appears prior to the first main oxide peak (I) (Fig. 36) may correspond to this process.

When a silver electrode is polarised anodically at controlled potentials in alkaline solutions, then it appears that Ag is first oxidised to Ag_2O possibly via AgOH at a potential of 0.2 V and the current increases; the oxidation process continues until the surface of the electrode is completely covered by Ag_2O at 0.3 V. Under these conditions, since electrochemically deposited Ag_2O is an n-type semiconductor* (201, also cf. ref. 202), the electrode surface becomes passivated (cf. ref. 54) and the current falls with further increase of potential. The current again increases very slowly when the second process (oxidation of Ag_2O to AgO) can commence at a potential of ca. 0.4 V. When Ag_2O is "completely oxidised" to AgO, a third process of evolution of oxygen, through the formation and decomposition of Ag_2O_3, occurs at a potential of ca. 0.6 V and above.

When the polarising current is switched off, some self-discharge of the oxides (AgO, Ag_2O_3) takes place. These

---

*Dry Ag_2O is however a p-type semiconductor (199, see also ref. 201).

higher oxides are unstable in alkaline solution because their reversible potentials are much higher than that for the oxygen evolution process (E° = 0.401 V *vs.* NHE in KOH). Under open-circuit conditions, they therefore decompose to Ag_2O liberating oxygen (195,196): for example,

$$4\ AgO \longrightarrow 2Ag_2O + O_2 \qquad V$$

It is well known that when the Ag-Zn alkaline battery is left on open-circuit for a considerable period of time a certain amount of "available charge" is lost, although no loss in weight of the material is observed. This has been explained in terms of the discharge of part of the AgO by reaction with metallic Ag formed at the surface (79,195,196) of the oxide, according to

$$AgO + Ag = Ag_2O \qquad VI$$

Metallic Ag atoms from the basis metal can also diffuse through the oxides (199) and react as above. This reaction can occur because if an electrode contains both metallic Ag and AgO, a local action mechanism must proceed (79) with a driving force of 0.262 V according to the equations

$$2\ Ag + 2OH^- = Ag_2O + H_2O + 2e,\ (E^{\circ} = 0.345) \qquad I$$

$$Ag_2O + 2OH^- = 2\ AgO + H_2O + 2e\ (E^{\circ} = 0.607) \qquad II$$

with the first reaction proceeding in the forward direction and the second in the backward direction.

This has been substantiated with the results obtained by the potentiodynamic sweep method in the present work (Table VI). Thus, it was observed that the anodic charge for the formation of Ag_2O (peaks I and I') is smaller than the charge required for the reduction of Ag_2O while the charge for the formation of AgO (peak II) is higher than that obtained for its reduction. Thus, after charging, although the oxide film contains mostly AgO, the peak for its reduction is relatively small (Fig. 36) due to covering of AgO by Ag_2O at the surface of the former oxide (79). As the passivating layer of Ag_2O is converted to Ag corresponding to the next peak, further AgO can be discharged by formation of more Ag_2O, itself produced by reaction between AgO and Ag.

There is some evidence for the formation of an oxide higher than AgO (viz. Ag_2O_3) at the silver electrode surface during charging, at least, under low temperature conditions ($< -30^{\circ}C$, Fig. 36d) (cf. refs. 99,198): a third peak (II') in the higher potential region of the potentiodynamic i-V curves corresponding possibly to reduction of Ag_2O_3 (stable only at low temperatures) appears. If AgO had been a mixture of Ag_2O and Ag_2O_3 as proposed (97), then only two oxide reduction peaks in the potentiodynamic i-V profiles at

low temperatures (Fig. 36 d) would be expected, but three distinct reduction peaks are observed. In the charging process, because of overlapping of the oxidation regions, all the steps cannot be identified. "iR"-effects within the Ag_2O oxide film are increased as the temperature is lowered and this effect eventually shifts the peak position as well. However, AgO has been observed to be diamagnetic even at liquid helium temperature (97 and see also 96); hence, evidently Ag(II)($4d^9$) which is paramagnetic cannot occur, as such, in the solid AgO oxide phase. Neutron diffraction results (97) have shown that there are two types of Ag atoms in the crystal lattice (having Ag-O bond distances of 2.18 Å and 2.03 Å), one with linear co-ordination to two oxygen atoms (Ag(I)) and the other square planar with respect to oxygen (Ag(III)). Another suggestion (96) has been that there is a mutual saturation of the unpaired electrons to form covalent or metallic bonds in the AgO crystal lattice: thus Ag in AgO has three valences and of the three valences two are used for binding oxygen atoms and the third for binding another Ag atom (thus resulting in Ag_2O_2*). The high electronic conductivity is also in accord with this conclusion (96).

---

*This is not a peroxide because H_2O_2 is not obtained by treatment with acids (96).

The present potentiodynamic sweep results are, however, observed to be in agreement with the latter interpretation i.e. AgO (with possible mutual saturation of the unpaired electrons in the lattice) does form at the electrode surface.

One final point to be mentioned here is that the observed anodic/cathodic charge ratio ($Q_{an.}/Q_{cath.}$) (Table VI) is in most cases slightly less than unity. This is definitely not related to any error arising from possible asymmetry in the wave-form, but it could be suggested that it originates from a possible shift in the "zero current" line due to the presence of evolved oxygen. The higher cathodic charge cannot, however, arise for this reason since the O_2 reduction process is a diffusion-controlled one. Hence, smaller ratios should be expected at lower than at higher sweep rates; results contrary to this are obtained.

(b) Extent of Formation of Surface Oxide at Silver

In terms of the number of layers, n, of surface oxide involved, only an approximate estimate can be given. The treatment of this problem follows that in the case of nickel (p. 201). The average charge for a z-electron oxidation of silver (a face-centred cubic structure with lattice spacing 4.079 Å (197)) in a surface monolayer is 191z μc. cm^{-2}, so that the value of n attained at a potential of ca. 0.93 V at 25°C will vary from 158080/191zR to

216202/191zR, where R is the initial real to apparent area factor. When z=2 [Ag(II) $\longrightarrow$ Ag(I) $\longrightarrow$ Ag(0)] and R=10 (79), the average value of n would vary from 41 to 57. This is in agreement with the thicknesses (50-100 layers) obtained by Cahan et al. (79).

From the above figures, it is seen that the thickness of the surface oxide layer depends, as expected, significantly on the sweep rates; for example, a 57 layer thickness is obtained for a sweep-rate of 0.009 V. sec^{-1} and a 41 layer film is indicated for a sweep-rate of 0.0924 V. sec^{-1}. For the sweep-rate of 0.006 V. sec^{-1}, a thickness of 60 layers of oxide is obtained.

10. CLAIMS TO ORIGINAL RESEARCH

The early stages of electrochemical oxidation of nickel metal electrode surfaces have been investigated and the thin oxide films so formed have been characterised with respect to stoichiometry, oxidation and reduction behaviour and involvement in the oxygen evolution process in anodic electrolysis. The following original contributions connected with these investigations have been made:

(a) The mechanism('s) and kinetics of oxygen evolution at nickel oxide surfaces have been studied. (i) It has been confirmed that an ion-radical recombination type of process is the rate-determining step in the o.e.r. which occurs at oxide sites on the nickel oxide surface. (ii) A "self-passivation" effect in oxygen evolution kinetics analogous to those found in anodic organic oxidations at the noble metals has been observed for the first time. A kinetic theory of the "self-passivation" effect has been presented for various supposed oxidation states of the surface region. The "self-passivation" effect has also been shown to be related to valency changes within the nickel oxide phase. (iii) The kinetic hysteresis that arises between curves for anodic and cathodic charging processes at nickel has been treated for the first time. The extent of the effect is found to be dependent on temperature and concentration of alkali, and on cationic impurity ions (viz. Li^+).

(b) An experimental technique and its theoretical basis has been developed for a potentiostatic step charging method. Rigorous calculations based on kinetic equations for two simple (activation controlled) mechanisms have been given as a basis for the application of the method to the study of formation of thin oxide films. The method developed allows close and progressive examination of the valency changes occurring in the electrode film forming reactions, and a quantitative characterisation of film growth.

(c) Growth of nickel oxide films at various electrode potentials, concentrations of KOH and temperatures has been studied and it has been shown that the kinetics of growth of nickel oxide films are logarithmic in time.

(d) A new simple mathematical derivation of a direct logarithmic growth law for oxide film formation has been given.

(e) For the determination of micro-quantities of nickel in thin film oxide layers, a new spectrophotometric method based on the principle of reductive stripping of the oxide by aq. hydrazine has been developed. The possibility of using this method for estimating "active" oxygen content in the thin film oxide layers was also investigated.

(f) Stoichiometries of nickel oxide in thin film oxide layers have been determined by the combination of

chemical and electrochemical methods. It has been shown that the stoichiometry is not only potential dependent but also characterised by the time of anodic potentiostatic polarisation. In other words, it has been shown indirectly that at any time, there is always a gradient of degree of oxidation of nickel within the oxide film.

(g) It has been shown that higher valent nickel oxides are reduced with facility in a galvanostatic pulse but only to $Ni(OH)_2$ and not to the metal. On this basis, it has been proposed that thin nickel oxide film material may form a useful battery cathode material for pulsed drain and pulsed charge systems. The thin film material does not suffer the disadvantage of isolation of some of the active material on discharge, which arises with bulk oxide electrodes on fast (high c.d.) discharge.

(h) Formation of a pre-passive layer of $Ni(OH)_2$ prior to anodic passivation of nickel has been confirmed by analytical film-stripping experiments.

(i) The spontaneous fall in degree of oxidation of nickel oxide on open-circuit has been investigated and its dependence on potential and time has been characterised. The initial losses of active "O" are due to self-decomposition of oxides higher than that of stoichiometry "Ni_2O_3".

(j) Oxidation of silver has been studied by the potentiostatic steady-state method mainly for the purpose of comparison with the behaviour of nickel. A "self-passivation" type of effect has also been observed in this case. It is proposed that this effect is related to the oxidation of less conducting Ag_2O to a more electronically conducting oxide species (AgO). Oxygen evolution occurs presumably on AgO through the formation of Ag_2O_3.

(k) Appearance of a new peak in the potentiodynamic i-V relations at silver electrodes in KOH solution at low temperatures (viz. -30°C) confirms the formation of a higher oxide (Ag_2O_3) of silver during anodization. Thus new evidence for the existence of Ag_2O_3 has been obtained.

(l) A generalised theory of the origin of hysteresis effects which arise in charge-discharge processes has been considered for the cases of nickel and silver oxide electrodes. It has been proposed that hysteresis is due to an intrinsic thermodynamic effect associated with rearrangement or recrystallisation of surface oxides within the solid oxide surface phase. The extent of hysteresis may, however, be enhanced by resistance effects within the film and by kinetic polarization in the surface oxidation and reduction processes.

REFERENCES

1. E.M. Kuchinskii and B.V. Ershler, Zhur. Fiz. Khim., 14, 985 (1940).
2. J.O'M. Bockris and S. Srinivasan, J. Electroanal. Chem., 11, 350 (1966).
3. P.L. Bourgault, Ph.D. Thesis, University of Ottawa, (1961).
4. B.E. Conway and P.L. Bourgault, Can. J. Chem., 37, 292 (1959).
5. P.L. Bourgault and B.E. Conway, ibid., 38, 1557 (1960).
6. B.E. Conway and P.L. Bourgault, ibid., 40, 1690 (1962).
7. B.E. Conway and E. Gileadi, ibid., 40, 1933 (1962).
8. A. Fleischer, Trans. Electrochem. Soc., 94, 289 (1948).
9. J. Zedner, Z. Elektrochem., 11, 809 (1905).
10. J. Zedner, ibid., 12, 463 (1906).
11. J. Zedner, ibid., 13, 752 (1907).
12. F. Foerster, ibid., 13, 414 (1907).
13. F. Foerster, ibid., 14, 17 (1908).
14. F. Foerster, ibid., 14, 285 (1908).
15. S.U. Falk, J. Electrochem. Soc., 107, 661 (1960).
16. P.D. Lukovtsev and G.I. Slaidin, Electrochim. Acta, 6, 17 (1962).
17. E.J. Casey, A.R. Dubois, P.E. Lake and W.J. Moroz, J. Electrochem. Soc., 112, 371 (1965).
18. P.D. Lukovtsev and G.Ya. Slaidin, Russ. J. Phys. Chem., 36, 1227 (1962).
19. E. Jost and F. Rufenacht, J. Electrochem. Soc., 113, 97 (1966).
20. F.P. Kober, ibid., 112, 1064 (1965); 114, 215 (1967).

21. H. Bode, K. Dehmelt and J. Witte, Electrochim. Acta, 11, 1079 (1966).

22. G.W.D. Briggs, E. Jones and W.F.K. Wynne-Jones, Trans. Faraday Soc., 51, 1433 (1955).

23. H.K. Embaby and A.A. Moussa, J. Chem. Soc., 4027 (1958).

24. G.W.D. Briggs and W.F.K. Wynne-Jones, Electrochim. Acta, 7, 241 (1962).

25. J.L. Weininger and M.W. Breiter, J. Electrochem. Soc., 110, 484 (1963).

26. J.L. Weininger and M.W. Breiter, ibid., 111, 707 (1964).

27. M.L. Kronenberg, J. Electroanal. Chem., 13, 120 (1967).

28. P.C. Milner and U.B. Thomas, "The Nickel-Cadmium Cell", A Chapter in Adv. in Electrochemical Engineering and Technology, Edited by P. Delahay, Intersc., in Press.

29. E. Jones and W.F.K. Wynne-Jones, Trans. Faraday Soc., 52, 1260 (1956).

30. J. Labat, Thesis Univ. Bordeaux; Ann Chim. (Paris), 9, 399 (1964); also A. Pacault and J. Labat, Compt. Rend., 258, 4963 (1964).

31. J. Labat, J. Chim. Phys., 60, 1253 (1963).

32. M.A. Aia, J. Electrochem. Soc., 114, 418 (1967).

33. O. Glemser and J. Einerhand, Z. anorg. u. allgem. Chem., 261, 43 (1950).

34. A.J. Salkind and P.F. Bruins, J. Electrochem. Soc., 109, 356 (1962).

35. G.W.D. Briggs and W.F.K. Wynne-Jones, Trans. Faraday Soc., 52, 1272 (1956).

36. F.A. Cotton and G. Wilkinson, "Advanced Inorganic Chemistry", Interscience Publishers (1962), p.732.

37. S.J. Teichner and J.A. Morrison, Trans. Faraday Soc., 51, 961 (1955).

38. I. Shimomura, I. Tsubokawa and M. Kojima, J. Phys. Soc. Japan, 9, 521 (1954).

39. G. Brauer (Editor), "Hand Book of Preparative Inorganic Chemistry" Vol. II, Acad. Press (1965) p. 1548.

40. G.F. Hüttig and A. Peter, Z. Anorg. u. allgem. Chem., 189, 183, 190 (1930); C.A. 24, 3188 (xxiv, xxv) (1930).

41. A. Merlin and S. Teichner, Compt. Rend., 236, 1892 (1953).

42. R.W. Cairns and E. Ott, J. Am. Chem. Soc., 55, 527; 534 (1933).

43. O.R. Howell, J. Chem. Soc., 123 (II), 1772 (1923).

44. O. Glemser and J. Einerhand, Z. Anorg. Chem., 261, 26, 43 (1950).

45. L. Dede and H. Zieriacks, Z. Anal. Chem., 124, 25 (1942); C.A. 37, 5305 (1943).

46. J. Besson, Compt. Rend., 222, 390 (1946).

47. O. Glemser and J. Einerhand, Z. Elektrochem., 54, 302 (1950).

48. S. Okada, T. Shiraishi, K. Watanabe and T. Yasuhara, J. Chem. Soc. Japan, Ind. Chem. Section, 51, 129, 130 (1948); 52, 37 (1949); 53, 5 (1950).

49. S. Okada and T. Shiraishi, J. Chem. Soc. Japan, Ind. Eng. Chem. Section, 52, 32 (1949).

50. T. Seiyamo, M. Abe and W. Sakari, J. Chem. Soc. Japan, Ind. Eng. Chem. Section, 57, 343 (1954).

51. W. Feitknecht, H.R. Christen and H. Studer, Z. anorg. u. allgem. Chem., 283, 88 (1956).

52. W.H. Beck, R. Lind and W.F.K. Wynne-Jones, Trans. Faraday Soc., 50, 147 (1954).

53. D. Tuomi, J. Electrochem. Soc., 112, 1 (1965).

54. J.O'M. Bockris, A.K.N. Reddy and B. Rao, J. Electrochem. Soc., 113, 1133 (1966); see also J. Chem. Phys., 42, 2246 (1965).

55. G.I. Slaidin and P.D. Lukovtsev, Dokl. Akad. Nauk. SSSR, 142, 1130 (1962).

56. P.D. Lukovtsev and G.Ya.Slaidin, Russ. J. Phys. Chem., 38, 299 (1964).

57. J.P. Hoare, J. Electrochem. Soc., 112, 1129 (1965).

58. E.M. Kuchinskii and B.V. Ershler, Zhur. Fiz. Khim.,20, 539 (1946).

59. A.L. Pitman and G.W. Work, U.S. Naval Res. Lab. Report 4845 (1956); 5031 (1957); and also 4852 (1956).

60. S. Okada, T. Shiraishi and T. Yasuhara, J. Chem. Soc. Japan, Ind. Eng. Chem. Section, 53, 378 (1950); 54, 16 (1951).

61. Yu.I. Golovkin, N.P. Vasilistov and N.A. Fedotov, Elektrokhimiya, 3, 805 (1967).

62. B.E. Conway, M.A. Sattar and D. Gilroy, Electrochim. Acta, accepted for publication.

63. D. Gilroy and B.E. Conway, Can. J. Chem., 46, 875 (1968).

64. W.M. Latimer,"Oxidation Potentials", 2nd Edition, Prentice-Hall, Inc.(1953)p.202.

65. P. Bro and D. Cogley, J. Electrochem. Soc., 113, 521 (1966).

66. L.D. Dyer, B.S. Borie (Jr.) and G.P. Smith, J. Am. Chem. Soc., 76, 1499 (1954).

67. N.Yu. Uflyand, A.M. Novakovskii, S.V. Mendeleva and S.A. Rozentsveig, Elektrokhimiya, 3, 785 (1967); C.A., 67, 70051z (1967).

68. F.P. Kober and P. Lublin, J. Electrochem. Soc., 113, 396 (1966).

69. B.V. Ershler, G.S. Tyurikov and A.D. Smirnova, Zhur. Fiz. Khim., 20, 539 (1946).

70. F. Kornfeil, Proc. 127 U.S. Army Battery Res. and Development Conference (1958).

71. L.M. Elina, T.I. Borisova and Ts.I. Zalkind, Zhur. Fiz. Khim., 28, 785 (1954); C.A., 48, 12588c (1954).

72. S.A. Gantman and P.D. Lukovtsev, Trudy Soveshchaniya Elektrokhimi Izd. Akad Nauk SSSR., Otdel Khim. Nauk, 1950, 504 (1953); C.A., 49, 12159h (1955).

73. N. Sato and G. Okamoto, Electrochim. Acta, 10, 495 (1965).

74. V.N. Fiseiskii and Ya.I. Tury'an, Zhur. Fiz. Khim., 24, 567 (1950); C.A., 44, 8798h (1950).

75. L.M. Volchkova and A.I. Krasil'shchikov, Zhur. Fiz. Khim., 23, 441 (1949).

76. A.I. Tsinman, Russ. J. Phys. Chem., 37, 714 (1963).

77. J.O'M. Bockris, J. Chem. Phys., 24, 817 (1956).

78. A.I. Krasil'shchikov, Russ. J. Phys. Chem., 37, 273 (1963).

79. B.D. Cahan, J.B. Ockerman, R.F. Amlie and P. Rüetschi, J. Electrochem. Soc., 107, 725 (1960).

80. T.P. Dirkse, J. Electrochem. Soc., 106, 453 (1959).

81. A. Hickling and D. Taylor, Discuss. Faraday Soc., No. 1, 277 (1947);

82. D.M.Yost, J. Am. Chem. Soc., 48, 152 (1926).

83. T.P. Dirkse and G.J. Werkema, J. Electrochem. Soc., 106, 88 (1959).

84. P. Jones, H. Thirsk and W.F.K. Wynne-Jones, Trans. Faraday Soc., 52, 1003 (1956).

85. T.P. Dirkse, J. Electrochem. Soc., 106, 920 (1959).

86. T.P. Dirkse and D.B. DeVries, J. Phys. Chem. 63, 107 (1959).

87. B.E. Conway and M.A. Sattar, Proceedings of the AGARD, June Meeting, 1967 Liège, Belgium, (Published June, 1968).

88. S. Yoshizawa and Z. Takehara, Denki Kagaku, 32, 27 (1964), C.A. 61, 11607c (1964).

89. V. Scatturin, P.L. Bellon and R. Zannetti, Ricerca Sci., 27, 2163 (1957); C.A., 52, 35b (1958).

90. H. Göhr and E. Lange, Z. Physik. Chem., Frankfurt, 17, 100 (1958).

91. D.I. Leikis, G.L. Vidovich, L.L. Knoz, and B.N. Kabanov, Z. Physik. Chem., (Leipzig), 214, 334 (1960).

92. C.P. Wales and J. Burbank, J. Electrochem. Soc., 106, 885 (1959); 112, 13 (1965).

93. R.G. Barradas and G.H. Fraser, Can. J. Chem., 42, 2488 (1964).

94. W. Klemm, Z. Anorg. Chem., 201, 32 (1931).

95. A.A. Noyes, K.S. Pitzer and E.L. Dunn, J. Am. Chem. Soc., 57, 1229 (1935).

96. A.B. Neiding and I.A. Kazarnovskii, Dokl. Akad. Nauk, SSSR, 78, 713 (1951); C.A. 45, 8385h (1951).

97. V. Scaturin, P.L. Bellon and A.J. Salkind, J. Electrochem. Soc., 108, 819 (1961).

98. Yu.S. Gorodetskii, Sov. Electrochemistry, 1, 600 (1965).

99. E.J. Casey and W.J. Moroz, Can. J. Chem., 43, 1199 (1965).

100. U.R. Evans, Z. Elektrochem., 62, 619 (1958).

101. M. Faraday, "Experimental Researches in Electricity", 2, 244 London (1844).

102. J.S. Llewelyn Leach and A.Y. Nehru, Corrosion of Reactor Materials Vol. I, p.58, International Atomic Energy Agency (Vienna) (1962).

103. J.S. Llewelyn Leach and A.Y Nehru, J. Electrochem. Soc., 111, 781 (1964).

104. J.S. Llewelyn Leach and A.Y. Nehru, Corrosion Science, 5, 449 (1965).

105. A. Hickling, Trans. Faraday Soc., 41, 333 (1945); 42, 518 (1946); see also A. Hickling and J.E. Spice, ibid., 43, 762 (1947) and A. Hickling and D. Taylor, ibid., 44, 262 (1948).

106. B.N. Kabanov, Trudy Soveshchaniya po Elektrokhimii, Akad. Nauk SSSR, Otd Khim. Nauk, p.138 (1953).

107. H.H. Uhlig, Z. Elektrochem., 62, 626 (1958).

108. K.G. Weil, Z. Elektrochem., 62, 638 (1958).

109. K.J. Vetter, Z. Elektrochem., 62, 642 (1958); 58, 230 (1954).

110. W.A. Mueller, J. Electrochem. Soc., 107, 157 (1960).

111. W.J. Müller, Z. Elektrochem., 30, 401 (1922).

112. N. Sato and G. Okamoto, Trans. Japan Inst. of Metals, 2, 113 (1961).

113. N. Sato and G. Okamoto, J. Electrochem. Soc., 110, 605 (1963).

114. Y.M. Kolctyrkin, Z. Elektrochem., 62, 664 (1958); see also First International Congress on Metallic Corrosion, Butterworth, London p.10, (1961).

115. D. Gilroy and B.E. Conway, J. Phys. Chem., 69, 1259 (1965).

116. E.J. Casey, Proceedings of the meeting of the Advisory Group of Aerospace and Development, June 1967, Liège, Belgium, (Published June, 1968).

117. H. Gerischer and W. Mehl, Z. Elektrochem., 59, 1049 (1955).

118. F.G. Will and C.A. Knorr, Z. Elektrochem., 64, 258, 270 (1960); see also F.G. Will, J. Electrochem. Soc., 112, 451 (1965).

119. M.W. Breiter, Trans. Faraday Soc., 60, 1445 (1964).

120. H. Angerstein-Kozlowska and B.E. Conway, J. Electroanal. Chem., 7, 109 (1964).

121. E.C. Potter, Ph.D. Thesis, London University (1950).

122. A. Damjanovic, A. Dey and J.O'M. Bockris, Electrochim. Acta, 11, 791 (1966).

123. A.C. Makrides and M.T. Coltharp, J. Electrochem. Soc., 107, 472 (1960).

124. J.O'M. Bockris and B.E. Conway, J.Sc. Instr. 19A, 23 (1948); see also J.O'M. Bockris and B.E. Conway, Trans. Faraday Soc., 48, 724 (1952).

125. Ming Chow, J. Am. Chem. Soc., 42, 488 (1920).

126. S. Mujamoto, Sci. Papers, Inst. Phys. Chem. Res. (Tokyo), 1, 31 (1922).

127. G.N. Lewis and M. Randall, "Thermodynamics" p.408, McGraw-Hill, New York (1923).

128. W.J. Hamer and D.N. Craig, J. Electrochem. Soc., 104, 206 (1957).

129. W.M. Latimer, "Oxidation Potentials", 2nd Edn.,Prentice-Hall Inc. New York, (1953) p.179; see also D.J.G. Ives and G.J. Janz, "Reference Electrodes", Academic Press, N.Y. (1961) p.336.

130. N.V. Sidgwick, "The Chemical Elements and Their Compounds", Oxford University Press, London (1950) p.292.

131. A.M. Azzam, J.O'M. Bockris, B.E. Conway and H. Rosenberg, Trans. Faraday Soc., 46, 918 (1950).

132. J.J. MacDonald and B.E. Conway, Proc. Roy. Soc. (London), A269, 419 (1962); see also B.E. Conway, Proc. Roy. Soc. (London), A256, 128 (1960).

133. M. Eigen, Disc. Faraday Soc., 17, 194 (1954); 24, 25 (1957).

134. L. Roe, Trans. Symp. On Electrode Processes, The Electrochemical Society, Philadelphia (1959), p.217 in discussion. J. Wiley and Sons, N.Y. (1960).

135. N. Pangarov, I. Christova, M. Atanasov and V. Kertov, Electrochim. Acta, 12, 717 (1967).

136. B.E. Conway and E. Gileadi, "Modern Aspects of Electrochemistry", Vol. III, Chap. V p.359, Eds. J.O'M. Bockris and B.E. Conway, Butterworths Publications (1964), London.

137. S. Gilman, Electrochim. Acta, 9, 1025 (1964).

138. H. Gerischer and W. Vielstich, Z. Physik. Chem. (Frankfurt), 3, 16 (1955); 4, 10 (1955).

139. J.H. Christie, G. Lauer and R.A. Osteryoung, J. Electroanal. Chem., 7, 60 (1964); see also J.H. Christie and J.J. Lingane, ibid., 10, 176 (1965).

140. K.B. Oldham, J. Electroanal. Chem., 11, 171 (1966).

141. A. Sevčik, Coll. Czech. Chem. Comm., 13, 349 (1948).

142. P. Delahay and G. Perkins (Jr.), J. Phys. Coll. Chem., 55, 586, 1146 (1951).

143. F.P. Bowden and E.K. Rideal, Proc. Roy. Soc., 120A, 59, 80 (1928).

144. A.N. Frumkin and A.I. Shlygin, Izv. Akad. Nauk. SSSR, Chem. Series, p.773 (1936); see also V.I. Niesterova and A.N. Frumkin, Zhur. Fiz. Khim., 26, 1178 (1952).

145. A.N. Frumkin and A.I. Shlygin, Acta Phys. Chim. SSSR, 3, 791 (1935).

146. A.I. Shlygin and B.V. Ershler, ibid., 11, 45 (1939).

147. J.D. Pearson and J.A.V. Butler, Trans. Faraday Soc., 34, 1163 (1938).

148. B.D. Brummet and R.M. Holweg, Anal. Chem., 28, 887 (1956).

149. L.F. Audrieth and Betty Ackerson Ogg, "The Chemistry of Hydrazine, J. Wiley & Sons. Inc., N.Y. p.159; see also, W.C. Bray and E.J. Cuy, J.Am. Chem. Soc., 46, 858 (1924); I.M. Kolthoff, ibid., 46, 2009 (1924), E.C. Gilbert, ibid., 46, 2648 (1924).

150. G. Brauer, (Editor) "Handbook of Preparative Inorganic Chemistry" Academic Press (1965), p.1549; see also, F.A. Cotton and G. Wilkinson, "Advanced Inorganic Chemistry", Interscience Publ. (1962), p.743.

151. Yu- Mei Huang, N.P. Keier and S.Z. Roginskii, Dokl. Akad. Nauk SSSR, 133, 413 (1960).

152. J.O'M. Bockris, I.A. Ammar and A.K.M.S. Huq, J. Phys. Chem., 61, 879 (1957).

153. B.E. Conway, N. Marincic, D. Gilroy and E. Rudd, J. Electrochem. Soc., 113, 1144 (1966).

154. J.O'M. Bockris, A.K.M.S. Huq, Proc. Roy. Soc, A237 , 277 (1956).

155. J. Horiuti and M. Ikusima, Proc. Imperial Acad., Tokyo, 15, 39 (1939).

156. J. Horiuti, J. Res. Inst. Catalysis, Hokkaido Univ., 1, 8 (1948).

157. P.C. Milner, J. Electrochem. Soc., 111, 228 (1964).

158. R. Parsons, Trans. Faraday Soc., 47, 1332 (1951).

159. J.O'M. Bockris, "Modern Aspects of Electrochemistry", Vol. I, Edited by J.O'M. Bockris and B.E. Conway, Butterworth Publications, London (1954) p.187 and 188.

160. B.E. Conway and M. Salomon, Electrochim. Acta., 9, 1599 (1964).

161. K.J. Vetter, Trans. Symp. Electrode Processes, Philadelphia, Pa., (1959) p.47, J. Wiley & Sons, N.Y. (1960).

162. S. Barnartt, J. Electrochem. Soc., 106, 991 (1959).

163. B.E. Conway, E. Gileadi and H. Angerstein-Kozlowska, J. Electrochem. Soc., 112, 341 (1965).

164. S. Srinivasan and E. Gileadi, Electrochim. Acta, 11, 321 (1966).

165. J.M. Hale and R. Greef, Electrochim. Acta, 12, 1409 (1967).

166. B.E. Conway and A.K. Vijh, J. Phys. Chem., 71, 3637 (1967); see also, A.K. Vijh and B.E. Conway, Zeit. anal. Chem., 224, 160 (1967).

167. D.H. Everett and W.I. Whitton, Trans. Faraday Soc., 48, 749 (1952).

168. D.H. Everett and M. Nordon, Proc. Roy. Soc., (London), A259, 341 (1960).

169. D.H. Everett and F.W. Smith, Trans. Faraday Soc., 50, 187 (1954); see also D.H. Everett, ibid., 50, 1077, (1954); 51, 1551 (1955).

170. D.H. Everett, "The Solid-Gas Interface", Vol. II, Edited by E.A. Flood, Publ: Marcel Dekker, Inc., New York (1967) p. 1055.

171. B.E. Conway and P. Stonehart, in course of publication.

172. B.E. Conway and P.L. Bourgault, Trans. Faraday Soc., 58, 593 (1962).

173. B.E. Conway and E. Gileadi, Trans. Faraday Soc., 58, 2493 (1962).

174. A.M. Shams el Din, L.A. Kamel and F.M. Abd el Wahab, J. Electroanal. Chem., 15, 21 (1967).

175. E. Gileadi and B.E. Conway, J. Chem. Phys., 39, 3420 (1963).

176. L. Young, "Anodic Oxide Films", Academic Press, London (1961), p.7.

177. P.B. Sewell, M. Cohen and D.F. Mitchell, "Surfaces and Interfaces", Vol. I, Chemical and Physical Characteristics" Eds. J.J. Burke, N.L. Reed and V. Weiss, Syracuse Univ. Press (1967), p.53.

178. A.J. de Bethune and N.A.S. Loud, "Standard Aqueous Electrode Potentials and Temperature Coefficients at 25°C", (1964), Clifford A. Hampel, Skokie, Ill.

179. B.E. Conway, "Theory and Principles of Electrode Processes" p.143, (1965), Ronald Press, New York.

180. G.A. Di Bari and J.V. Petrocelli, J. Electrochem. Soc., 112, 99 (1965).

181. W.M. Latimer, "Oxidation Potentials", Second Edition, Prentice-Hall, Inc., N.Y. (1953), p.200.

182. A.C. Makrides, J. Electrochem. Soc., 113, 1158 (1966).

183. N. Sato and T. Notoya, J. Electrochem. Soc., 114, 585 (1967).

184. G.W.D. Briggs and M. Fleischmann, Trans. Faraday Soc., 62, 3217 (1966).

185. M. Fleischmann and H.R. Thirsk, "Advances in Electrochemistry and Electrochemical Engineering" (Ed. P. Delahay), 3, 123 (1964), Interscience (London).

186. I.A. Ammar and S. Darwish, Electrochim. Acta, 11, 1541 (1966).

187. R.S. Perkins and B.E. Conway, in course of publication.

188. T.O. Rouse and J.L. Weininger, J. Electrochem. Soc., 113, 184 (1966).

189. G.E. Rhead, Trans. Faraday Soc., 61, 797 (1965).

190. R. Kikuchi, J. Chem. Phys., 47, 1646; 1653; 1664 (1967).

191. W.M. Latimer, "Oxidation Potentials", Second Edition, Prentice-Hall, Inc., N.Y. (1953), p.192.

192. T.P. Dirkse, J. Chem. and Eng. Data, 6, 538 (1961).

193. T.P. Dirkse, J. Electrochem. Soc., 109, 173 (1962).

194. J.F. Bonk and A.B. Garret, J. Electrochem. Soc., 106, 612 (1959).

195. R.F. Amlie and P. Rüetschi, J. Electrochem. Soc., 108, 813 (1961).

196. T.P. Dirkse, J. Electrochem. Soc., 107, 859 (1960).

197. "International Critical Tables", Vol. I, p.340, Publ: McGraw-Hill, N.Y. for NRC of U.S.A.

198. Yu.V. Pleskov, Dokl. Akad. Nauk, SSSR., 117, 645 (1957); C.A., 52, 1958g (1958).

199. N.D. Rozenblyum, N.S. Bubyreva, V.I. Bukhareva and G.Z. Kazakevich, Russ. J. Phys. Chem., 40, 1324 (1966).

200. Y.I. Tur'yan and A.I. Tsinman, Russ. J. Phys. Chem., 36, 212 (1962).

201. A.A. Yakovleva, T.I. Borisova and V.I. Veselovskii, Russ. J. Phys. Chem., 36, 763 (1962).

202. A.V. Byalobzheskii and V.D. Val'kov, Dokl. Akad. Nauk SSSR, 134, 121 (1960).

203. T.S. De Gromoboy and L.L. Shreir, Electrochim. Acta, 11, 895 (1966).

204. D. Tuomi and G.J.B. Crawford, J. Electrochem. Soc., 115, 450 (1968).